Università degli Studi di Napoli Federico II
Facoltà di Ingegneria

Maria Rosaria Grippa

STRUCTURAL IDENTIFICATION OF ANCIENT TIMBER CONSTRUCTIONS BY NON-DESTRUCTIVE TECHNIQUES

Tesi di Dottorato
XXII ciclo

Il Coordinatore
Prof. Ing. Federico M. MAZZOLANI

Dottorato di Ricerca in Ingegneria delle Costruzioni

Acknowledgements

At the end of the three years of my PhD Course, I would like to thanks all the people who helped and supported me, allowing the elaboration of this work.

First of all, I would like to express my deep gratitude to my tutor Prof. Federico Massimo Mazzolani for having welcomed me in important research activities developed for this thesis. His invaluable guidance, teaching, experience and competence have been extremely significant for my studies and both personal and scientific growth.

I am very grateful to Dr. Beatrice Faggiano, who guided me during the whole Doctoral period. Her competence, determination and enthusiasm have represented a clear reference for my activity. I have for her affection and admiration for giving me constructive feedback and suggestions that directed this work forward.

I would like to thank Dr. Anna Marzo for her participation and contribution in the development of the numerical analysis and experimental activity presented in the thesis.

Special thank to the staff of the DIST Laboratory of the University of Naples “Federico II”, Eng. Marco Cocca, Eng. Giuseppe Campanella and all laboratory technicians: Livia Montella, Antonio Lanzotti, Emanuele Scaiella, Giuseppe Costagliola, Luigi Frascogna and Giovanni Manetta for their technical assistance during the experimental campaign. In particular, I wish to express my deep acknowledge to technician and friend Giovanni Belfiore for his competence and technical support. His collaboration and patience has made possible the execution of several tests. Thanks Gianni!!!

In the frame work of my research activity I respectfully acknowledge the financial support given by the International research project PROHITECH "*Earthquake Protection of Historical Buildings by Reversible Mixed Technologies*", Prof. Federico Massimo Mazzolani coordinator, and the National research project PRIN 2006 "*Diagnosis techniques and totally removable low invasive strengthening methods for the structural rehabilitation and the seismic improvement of historical timber structures*", Prof. Maurizio Piazza coordinator, research unit UNINA "*Experimental evaluation of the mechanical properties of wood by means of non-destructive compared techniques for the characterization of existing wooden structures*", Dr. Beatrice Faggiano scientific responsible. Moreover I would like to thank the research centre BENECON of the Region of Campania (Scientific Director Carmine Gambardella) for providing the ultrasonic device needed for the experimental investigations.

I am very grateful to Engineers who shared with me the experience in laboratory work for their active contribution to the experimental tests end data elaboration, which have been the subject of their degree thesis. I wish to thank my dear friends, Gelsomina Pacchiano, Letizia Esposito, Francesco Grasso and Andrea Rocci.

I extend my acknowledgements to my fellow Engineers, Daniela De Gregorio, Brando & Matteo, Giulio Martire, Carmine Castaldo, Pierpaolo Di Feo, Luisa Alterio, Fabio Nardone, Francesco Campitiello, Mario D'Aniello, Emilia Cordasco, Gaetana Pacella and Costantino Giubileo.

I also thanks Dr. Antonello Formisano, Dr. Gaetano Della Corte and Dr. Luigi Fiorino for the useful teachings provided me during the PhD Course.

I would like to thanks my dear friends Antonella and Domenico for having supported me with care, time and energy while I completed this thesis.

Last but no least, an immense gratitude is devoted to the members of my wonderful family, for their affection and sacrifices proved me during these years. They believed in me every day of my life.

To my family

Contents

Chapter 2

THE ANCIENT TIMBER STRUCTURES OF THE ROYAL PALACE OF NAPLES: DIAGNOSIS, ANALYSIS AND RESTORATION

Chapter 5

NON-DESTRUCTIVE TESTS (NDT)

Chapter 6

DESTRUCTIVE TESTS IN COMPRESSION (DT)

Chapter 7

DESTRUCTIVE TESTS IN BENDING (DT)

Chapter 8

NDT-DT CORRELATIONS FOR THE MECHANICAL CHARACTERIZATION OF TIMBER

Introduction

MOTIVATIONS AND GOALS

The refurbishment and enhancement of the existing building heritage held a very important rule in all the Europe Countries, where the belief that historical constructions should be preserved and restored, confirming their initial static function by means of appropriate interventions in harmony with the pre-existent structural configuration, is deeply rooted. In this field, conservative restoration principles developed for the protection of monuments are currently applied in the structural upgrading of traditional existing constructions in order to preserve their cultural heritage.

In many ancient buildings located in historical centres of Italy and more widely of the Mediterranean area, the horizontal load-bearing structures, such as roof and floor, are made of timber, which is one of the oldest structural material, together with masonry and stone. In particular, most ancient complex systems are composed by two main superimposed units, such as beam floor and vaulted ceiling or light vault, often connected each other, which are an evidence of the past applications and technologies and, at the same time, the ancestors of the modern framed systems.

These timber structures often require an assessment of the actual safety conditions and monitoring, together with conservation and remedial measures. Generally, their restoration consists in the total or partial substitution of deteriorated elements or in reinforcing interventions. It can be carried out with

two different aims: improvement and rehabilitation of the existing structures by preserving the original structural configuration or renovation by changing the original structural configuration due to safety lacks or change of destination or upgrading to current safety codes. In particular, for the floors, it is also often the case that higher live loads are applied due to a change of use, which requires structural analysis and, if necessary, strengthening.

The current practice is often affected by strong difficulty in evaluating the deterioration condition of the basis material and, consequently, in defining of the actual residual load bearing capacity and efficiency degree of the structural elements. This leads to frequently irrational and harmful interventions, mainly characterized by the substitution of timber with other structural material, causing an irreversible alteration of the original configuration and, sometimes, yielding unsatisfactory results in terms of structural behaviour.

Actually, the analysis of ancient structures, made of timber, is very cumbersome for all the inherent difficulties to be faced at both material and structural behaviour characterization. In particular, due to its nature, wood presents natural defects and structural anomalies, moreover it suffers a biological deterioration, closely connected to the environmental conditions.

Therefore, the static behaviour of the whole structures and of each component, together with the state of conservation of single members and their complete characterization should be identified after an accurate *in situ* evaluation of the condition of the standing structures. Preliminary diagnostic inspections are needed to evidence any damage and decay situations, to find and eliminate their causes, and the same time to characterize the structure as respect to the mechanical properties, for determining the actual load-bearing performance and capacity.

In this context, non-destructive evaluation (NDE) methods are excellent to achieve a good level of knowledge in the structural analysis, diagnosis and restoration. The visual inspection is the most simple and oldest non-destructive method, which is traditionally used to grade wood in end-use categories. Furthermore it allows the evaluation of the wood original quality, species and main features of the element, natural defects, such as spiral grain, knots, ring shakes, cracks the identification of biodeterioration through the presence of biological agents, fungi and insects in order to assess the residual section of damaged elements.

Actually, in Italy the diagnostic activity of timber elements is based on UNI 11119 (2004) standard, which establishes objectives, procedures and criteria in order to evaluate the state of conservation and assess the performances of timber members in load-bearing ancient timber structures by means of *in situ* inspection and the use of non-destructive techniques or methods. According to this standard, the structural grade of the timber elements is based on the visual inspection, through the individualization of the critical area, defects and decay. However, the estimation of the serviceability properties of new and/or ancient timber constructions by means of the visual grading method is not entirely reliable due to the many factors influencing the mechanical properties of timber and, further, the biased influence of the human factor. Moreover, the information is mostly qualitative.

Recently, instrumental non-destructive techniques have evolved as a means for evaluating physical and mechanical properties of wood and detecting internal defects and decay. Sonic stress wave is one of the most popular NDT global method used for wood. This techniques is usually employed in two different ways using either the speed of sound or the vibration spectrum. Stress wave speed is often used to evaluate the dynamic modulus of elasticity. Local methods, as electronic penetrometers and superficial hardness systems, are typically used to support visual grading of timber structures.

Generally, NDT methods present several advantages such as their practical utilization, transport and efficiency, however up to now, although they allow to gather a lot of useful information about the state of conservation of the timber members, these are only qualitative and do not lead to the determination of the mechanical properties, necessary to estimate the strength and stiffness capabilities of the structural systems. The efficiency and reliability of NDT methods can be increased if laboratorial tests are used to study the variability of the mechanical characteristics of the wooden elements. In this way, experimental results could provide important information for the execution, design, safety verification and the retrofitting design of structures.

Different type of laboratory tests are by now standardized to give physical and mechanical properties of each material, but only non-destructive tests are compatible with the demand of conservation. Therefore, it is fundamental to provide new methods for *in situ* mechanical characterization of timber

elements and structures, by means of recognized correlations between non-destructive and destructive test results.

The general aim of this thesis is the structural identification of ancient timber constructions, including several aspects and applications, summarized in three main topics, as follow:

- *Analysis of historical timber structures*. The attentions is focused on studies case which are the complex roofing structures of the Royal Palace of Naples. The detailed geometrical and mechanical surveys are presented, as preliminary phase for the structural identification. On the basis of the results of the numerical analysis, by means of 3D FEM models, the safety checks, according to Eurocode 5 provisions, have allowed the identification of capacity of the structures in terms of strength and deformation and then the necessity of their retrofitting. Details of the adopted and proposed restoration interventions, based on the mixed technologies, are presented.
- *Study of an innovative system for r.c.-timber floor.* The new connector between the timber beam and the concrete slab consists of a steel collar, composed by two or more parts, bolted together at appropriate folded wings. Monotonic push-out tests and bending test on a full-scale composite floor are presented as they being part of a more comprehensive experimental campaign, aimed at the system performance evaluation and optimization. The experimental activity has been developed within the international research project PROHITECH "*Earthquake Protection of Historical Buildings by Reversible Mixed Technology*", Prof. F.M. Mazzolani coordinator.
- *Mechanical characterization of timber by means of NDT-DT correlations.* A research activity has been developed by means of an extensive experimental campaign, including non-destructive investigations (NDT) and destructive tests (DT) on structural elements and defect-free specimens, made of old chestnut wood. Experimental results are discussed and statistically analyzed in order to calibrate novel correlations between NDT and DT parameters, based on linear regression model. In particular, NDT combined methods for the estimation of both physical and mechanical properties of chestnut timber are provided as a methodological

procedure for *in situ* mechanical identification of existing ancient structures. The research activity has been developed in the framework of the Italian project PRIN 2006 "*Diagnosis techniques and totally removable low invasive strengthening methods for the structural rehabilitation and the seismic improvement of historical timber structures*", prof. M. Piazza coordinator; research unit UNINA "*Experimental evaluation of the mechanical properties of wood by means of non-destructive compared techniques for the characterization of existing wooden structures*", prof. B. Faggiano scientific responsible, M.R. Grippa and A. Marzo research team.

All experimental tests have been carried out at the Laboratory of the Department of Structural Engineering (DIST) of the University of Naples "Federico II".

OUTLINE

Chapter 1 provides the main physical and mechanical properties of wood and structural timber. It is a traditional construction material and, over the years, considerable knowledge has been gained on its important characteristics which have effects on structural design and service behaviour. The mechanical characterization of timber cannot be derived with any reliability from the properties of clear wood, free from faults. In fact, the presence and character of knots and other defects and alterations, affect the performance and properties of timber elements, together with other strength reducing-factors, such as moisture content and time-dependent effects. Furthermore, it should be kept in mind that, unlike some structural materials such as steel or concrete, the behaviour of timber is very sensitive to environmental conditions. Under proper conditions, wood will give centuries of service. However, if conditions exist that permit the development of wood-degrading organisms, protection must be provided during processing, merchandising, and use. Wood is also the only building material that is subjected to destruction by biological agencies, such as fungi and insects. Nevertheless, due to anatomical structure, wood material shows a good structural efficiency for stress conditions along the grain direction, represented by a high strength/density ratio. This is one of the inherent advantages of using timber in constructions.

Chapter 2 deals with a methodology for the analysis of complex historical timber structures. Firstly, an overview of the European and Italian existing codes is introduced, emphasizing the lack of regulations about ancient timber constructions. Moreover a procedure for restoration intervention is presented with reference to the covering structures of the Historical Apartment of the Royal Palace of Naples, datable between the XVII and the XVIII centuries, which are representative of the past applications and technologies in monumental buildings. After an overview of the identified structural configurations, the attention is focused on three case studies, which are the complex roofing systems of the Diplomatic Hall (II), Third Anteroom (V) and Guard Room (XXIX). Both the geometrical and mechanical surveys are preliminary presented. Therefore the capacity in terms of resistance and deformation, evaluated on the basis of purposely set-up 3D FEM models, is discussed. According to the results of the structural analysis, the more appropriate retrofitting interventions are proposed. They are based on the use of the so-called mixed technologies, consisting in the combination of techniques, which use different material (in the specific case new timber, steel, reinforced concrete, rubber) for realizing global and local strengthening and stiffening systems of the existing constructions.

Chapter 3 presents experimental investigations on an innovative system for r.c.-timber composite floor. The stiffening and strengthening of ancient timber floors by a thin collaborating concrete slab is a common suitable technique used in the restoration of historical buildings. It generally consists of a concrete thin slab connected to the wooden beams by means of devices, like screws, nails, and studs, inserted in the beam, in ad hoc drilled holes. In order to avoid any strength reduction of the existing wooden beams due to perforation, which is necessary for the installation of traditional connectors, an innovative type of connector has been conceived. It is a steel collar surrounding the timber stock, which is composed by two parts bolted together at appropriate folded wings; the function of connector is held by the superior wings. A rubber layer is interposed at the wood-steel interface, for guaranteeing the complete adherence between elements. Due to the bolt tightening, the collar also provides a transversal ringing action on the beam. Therefore, monotonic push-out tests on several circular shaped configurations

of the innovative connection system are presented, together with bending test on full-scale r.c.-timber floor, which have been carried out for studying the global performance of the composite system and the local behaviour of the connectors in terms of both stiffness and strength.

Chapter 4 introduces a wide research activity aiming at providing a methodological process for *in situ* mechanical identification of timber elements using compared non-destructive techniques. A deep experimental campaign has been developed on both full-scale and small defect-free specimens, made of old chestnut wood (*Castanea sativa* Mill.), including non-destructive investigations (NDT), such as hygrometric, ultrasonic, sclerometric and resistographic, and destructive tests (DT) in compression and in bending. Other several phases have been involved in the research activity, such as data processing and interpretation, mechanical characterization of timber by means of combined NDT-DT correlations. In this chapter, the attention is focused on the features of the tested specimens, visual inspection and on the NDT methods for wood, commonly used in place for non-destructive diagnosis and structural assessment of timber members.

Chapter 5 deals with the experimental investigations based on NDT methods which have been employed in the research activity. They are: hygrometric tests, for the evaluation of the moisture content of wood, which severely affects its mechanical properties and its susceptibility to degradation by decay; ultrasonic investigations, through which a direct relationship between the stress wave speed and the elastic properties of the material can be defined, based on the theory of acoustic wave propagation; sclerometric tests, based on the wood test hammer system, through which the quality and hardness of superficial layers of wood are estimated by the penetration depth of a blunt pin, fired into the wood; resistographic measurements, for the evaluation of the wood density by measuring the drilling resistance along the path of a small needle inserted into the wood with a regular advancing speed. Testing equipment and experimental set-up, together with the applied methodology for data processing and interpretation, are illustrated. The obtained results are presented and statistically analyzed.

Chapter 6 concerns the laboratory activity based on destructive tests in compression carried out on elements made of old chestnut wood, taking into account the methods specified in UNI and ISO specific codes. The mechanical characterization is analyzed by comparing the overall behaviour of structural elements with the same one of small and clear specimens, in terms of modulus of elasticity, strength and failure modes, pointing out on the influence of defects and deteriorations in timber structural behaviour. Furthermore, the orthotropic nature of the chestnut wood is investigated by means of compression tests on defect-free specimens in both parallel and perpendicular direction to the grain, taking into account the orientation of the annual rings with respect to the direction of the applied load. In this chapter, the characteristics of the specimens are given, and testing apparatus and set-up are illustrated. Destructive tests results are discussed and compared with the mechanical properties reported in European and Italian codes.

Chapter 7 provides the experimental results of bending destructive tests (DT) on full-scale chestnut timber beams, which have been performed according to UNI EN 408 standard. The main features of the specimens, testing equipment and set-up are described and the local and global modulus of elasticity, flexural strength are determined. The collapse mechanisms under bending stress condition are examined taking into account the influence of knots location respect to the loading direction, the tensile side as well as to the middle cross-section of the specimens.

Chapter 8 presents the last phase of the whole research activity, concerning the mechanical characterization of chestnut timber based on statistical NDT-DT correlations. The following relationships have been analyzed by means of linear regression model: correlation between NDT parameters, relating the longitudinal and transversal measures by ultrasonic, sclerometric and resistographic tests; correlations between DT parameters, for the determination of the mechanical behaviour in compression and bending of old chestnut timber; simple and multiple NDT-DT correlations, for a non-destructive estimation of density, modulus of elasticity and strength of the material, based on combined methods. Scatter plots among the variables involved in the model, coefficients of determination, together with the

estimated regression lines and equations, are reported. In addition, the quality of the correlations are evaluated by means of statistical tests, such as *Student's t-test* and *F-test* or ANOVA (ANalysis Of VAriance), using SPSS v. 17 program.

Chapter 1
Timber as structural material

1.1 GENERAL

Timber has always been one of the more plentiful natural resources available and consequently is one of the oldest known materials used in constructions. It is a material that is used for a variety of structural forms, such as beams, columns, trusses, girders and is also used in building systems such as piles, deck members, railway foundations and for temporary forms in concrete.

Basically, there are two types of lumber for carpentry: softwoods and hardwoods. The first ones generally come from trees with needle-like leaves (conifers); they are “evergreens”. Hardwoods comprise the broad-leaved trees, mostly deciduous, although there are many broad-leaved trees that are evergreen in certain climates. Generally, the hardwoods are harder and stronger than the softwood.

In structural engineering, the term “wood” is usually reserve for small clear elements, free from defects and irregularities on the macro level. Instead, the term “timber” is used to describe elements with structural dimensions, characterized by the presence of macro defects which influence its mechanical behaviour.

Wood is an organic and anisotropic material derived from trees. Its cellular structure is composed of longitudinally arranged fibres which confer to wood a good structural efficiency, represented by a high strength/density ratio,

especially in tension. Due to the complex anatomical structure, the strength and stiffness properties of wood in parallel to grain direction are very large in relation to the same ones in transversal orientation.

Because timber structural members are cut from trees rather than being formed from a human-made material, they will have some strength-reducing characteristics, defects and biological alterations, such as knots, cross grain, checks, shakes, compression wood, wane and decay. Thus the presence of faults should be considered in the design of structural members. Other factors which affect the mechanical properties of timber are the moisture content, which has a direct effect on both strength and swelling or shrinkage, the creep effect and duration of load.

This chapter provides the basic information of the structure and properties of wood and the main features of timber as structural material in constructions, essential in engineering design.

1.2 BASIC STRUCTURE OF WOOD

Wood material is biologically "produced" in the growing tree to meet the needs of the tree itself. In this respect, the wood is a high quality fibre composite, optimally designed to resist loads acting on the tree, but also to provide transport of water and nutritional agents. The stem and branches of the tree are designed to resist gravity loads and wind loads. The wood structure is adapted to create maximum strength in stressed directions, whereas in other directions the strength is quite low.

Wood is composed of long thin tubular cells, which are predominantly oriented in one direction, called the fibre direction or grain direction. This is the strong direction, generally parallel with the longitudinal axis of the stem. This aspect imparts wood characteristics, as physical and mechanical properties, which are determined by also other factors, such as species, growing conditions and wood quality.

Wood cell

Wood, in general, is composed of long thin hollow and tubular cells (Fig. 1.1). They are approximately rectangular shape in cross section and have

unsymmetrical tapered ends that overlap, in staggered position, with the cells above and below. The cell walls consists principally of cellulose and lignin. Cellulose accounts for 45-50% of the weight of completely dry wood, and lignin for about 20-30%. Another ingredient, hemicellulose, amounts to 20-25%. Minor components, which vary from species to species, include natural resins, oils, tannin, and alkaloids. Often, it is these minor components that make a species suitable or unsuitable for some particular application.

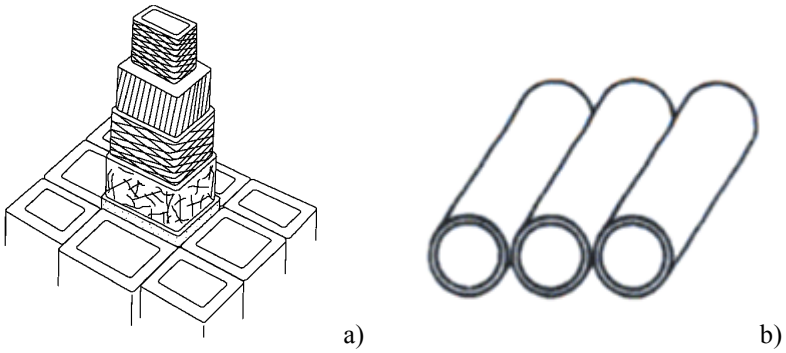

a) b)

Figure 1.1. Basic structure of wood: a) Cell; b) Tubular arrangement.

Cellulose gives the wood its strength, being the load-carrying material, whereas the lignin is the "glue" that cements cellulose fibres together, filling the spaces between fibres and stiffening the fibres. The tube width as well as the wall thickness can vary, but the wall material properties are very similar in all species. In fact, the wall material density, due to cellulose-lignin combination, is about 1500 kg/m^3 (Kollmann *et al.*, 1968). However, wood cells are hollow so that the specific gravity of whole wood ranges from 150 to 1000 kg/m^3 for most woods used in construction. This means that wood material properties such as modulus of elasticity and strength along the grain and density are strongly linked to the cell or tube wall thickness.

Figure 1.2 shows typical cross-sections of wood, focusing on its structure, which is characterized by the arrangement and shape of wood cells. Notice that most of the hollow, tubular cells are in longitudinal position, that is, their long dimension is vertical, parallel to the trunk (stem) of the tree. A few cells, in localized bundles, run radially, that is, parallel to a radial line from the center of the tree trunk to the outside.

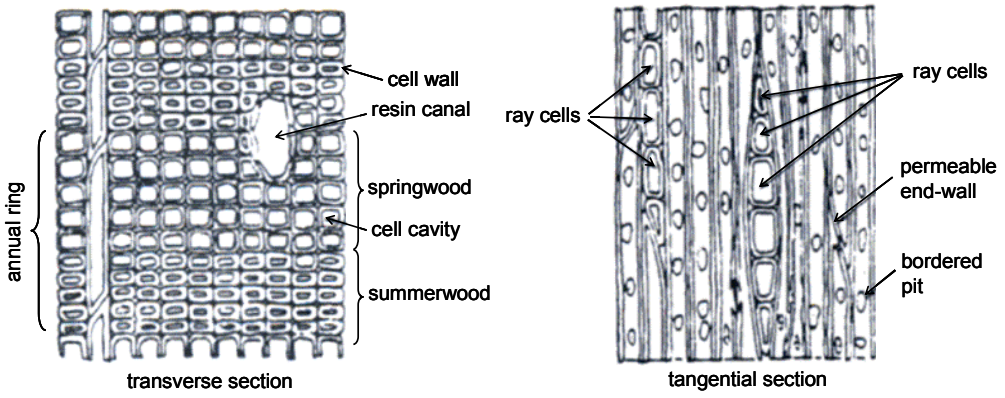

Figure 1.2. Basic structure of wood: softwood cross-sections.

Because the wood cell is a hollow tube, it is very efficient for resisting a compressive force parallel to its length. For this reason, wood under longitudinal compression has a rather high ratio of strength to weight. However, compression forces normal to the length of the cells easily crush the cells, bending their walls. Thus, the strength of wood is poor under compression perpendicular to the cell length, called compression perpendicular to the grain.

Longitudinal shear strength of wood is limited by the strength of the lignin that binds adjacent cells together, or by the shear strength of the cell wall, whichever is lower. Longitudinal shear strength of wood is lower than its compression strength in any direction and also lower than its longitudinal tensile strength. The only strength that is lower than longitudinal shear strength is the transverse tensile strength.

Interestingly, the hollow-cell arrangement has a good effect on both longitudinal compressive strength and bending strength. Given a specified weight of wood in the form of either a beam or a column, its strength is higher than it would be if all void spaces were eliminated and the wood substance moved together to form a solid member of lesser cross-sectional area.

Cambium

New wood cells, formed by cell division, are produced by the cambium layer (Fig. 1.3). As new cells are added on the inner side of the cambium, the

diameter of the tree increases. At the same time, the cambium adds new cells to the inner bark, just outside of the cambium layer. Immediately, the newly created cell begins to grow in both length and diameter. During this growth the cell wall is thin and pliable, but after growth ceases a secondary layer is added to the cell wall, thickening it. At this stage the cell wall is primarily cellulose. After wall thickening ceases, lignin is deposited, cementing the fibres together in a process called lignification. The cell now has structural strength that enables it to help carry the weight which later is added to the tree.

Earlywood and latewood

During springtime, growth is rapid and the newly create cells have relatively large cell openings (cavities) and thin walls. Portions of new wood created during this season are known as earlywood (or springwood; Fig. 1.2). New cells created later in the year, when less moisture is available, have smaller cavities and thicker walls. This portion of the wood is called latewood (or summerwood; Fig. 1.2). Latewood contains more cellulose per unit of cross-sectional area that earlywood; consequently, latewood is stronger than earlywood.

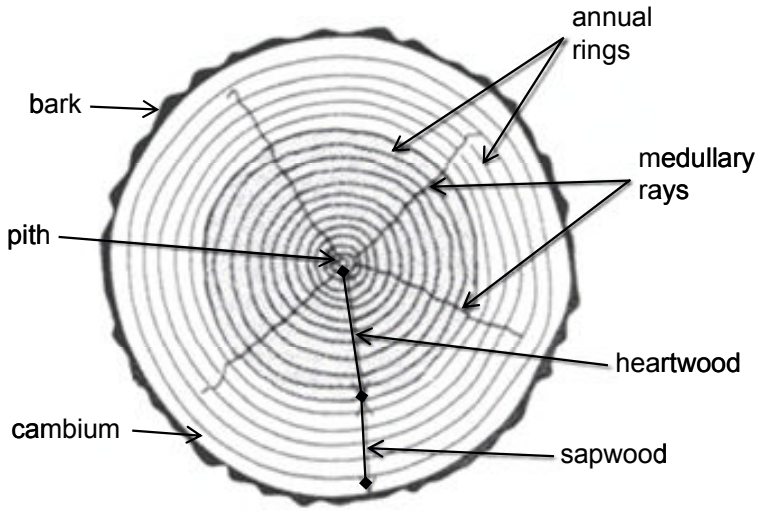

Figure 1.3. Basic structure of wood: tree cross-section.

Annual rings

Each year a band of earlywood and then a band of latewood are added to the tree. Together, these two bands comprise an annual ring or growth ring (Figs. 1.2 and 1.3). Generally, the latewood portion of the annual ring in darker than the earlywood. In some tropical woods, grown where differences between season are not marked, annual rings may be either obscure or absent.

Medullary rays

Medullary rays are ribbonlike bundles of cells arranged in a radial direction in the tree (Fig. 1.3). This is, they are perpendicular to the annual rings, running from the center (pith) toward the bark. The rays serve a useful structural function: they brace the longitudinal cells so that their buckling strength is higher. Tensile strength perpendicular to the annual rings may be benefited a little, but tangentially (in a direction parallel to the rings and perpendicular to the rays) tensile strength may actually be reduced by the rays.

Heartwood and sapwood

The annual band of cross-section nearest to the bark is called sapwood. The central core of the wood which is inside the sapwood is heartwood (Fig. 1.3). The sapwood is lighter in colour compared to heartwood. It acts as medium of transportation for sap from the roots to the leaves, while the heartwood functions mainly to give mechanical support or stiffness to the trunks. In general, the moisture content, strength and weights of the two are nearly equal. Sapwood has a lower natural resistance to attacks by fungi and insects and accepts preservatives more easily than heartwood.

1.3 SOFTWOODS AND HARDWOODS

Trees and commercial timbers are divided into two groups: softwoods and hardwoods. This classification is not based upon the hardness or density of the wood, rather upon the taxonomy of the tree. In fact, softwoods, or coniferous, are generally evergreen with needle-like leaves comparing single cells called tracheids, which are like straws in plan, and they fulfil the functions of

conduction and support. Rays, present in softwood, run in a radial direction perpendicular to the growth rings. Their function is to store fool and allow the convection of liquids to where they are needed. The main characteristics of the softwoods are:

- Quick growth rate; trees can be felled after 30 years, resulting in low density timber with relatively low strength.
- Generally poor durability qualities, unless treated with preservatives.
- Due to speed of felling, they are readily available and comparatively cheap.

Hardwoods, or deciduous, are generally broad-leaved trees that lose their leaves at the end of each growing season. The cell structure of hardwoods is more complex that that of softwoods, with thick walled cells, called fibres, providing the structural support and thin walled cells, called vessels, providing the medium for food conduction. Due to the necessary to grow new leaves every year the demand for sap is high and in some instances larger vessels may be formed in the springwood – these are referred to as rig porous woods. When there is no definite growing period the pores tend to be more evenly distributed, resulting in diffuse porous woods. The main characteristics of hardwoods are:

- Hardwoods grow at a slower rate than softwood. This generally results in a timber of high density and strength which takes time to mature – over 100 years in some instances.
- There is less dependency on preservatives for durability qualities.
- Due to time taken to mature and the transportation costs of hardwood, as most are tropical, they tend to be expensive in comparison to softwood.

1.4 ANISOTROPIC NATURE OF WOOD

Due to its complex biological structure, wood is a anisotropic material, which means that its appearance, as well as its properties, are significantly influenced by the surface orientation relative to its location in the tree stem. Wood has different orientations relative to the growth rings and longitudinal

fibre arrangement. The cross section is perpendicular to the longitudinal direction of the fibres. The surface from the center of the stem outward is the radial surface. The outer surface, parallel to the growth rings, is called the tangential surface. Wood properties are significantly influenced by the direction relative to the fibre and growth ring orientation.

Concerning the mechanical model of wood, it may be described as an orthotropic material, so that it has unique and independent mechanical properties in the directions of three mutually perpendicular axes: longitudinal, radial and tangential (Fig. 1.4).

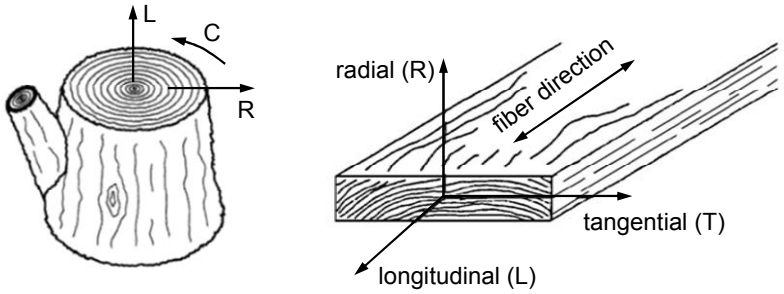

Figure 1.4. Anisotropic nature of wood: three principal axes of wood with respect to grain direction and growth rings.

The longitudinal axis *L* is parallel to the grain; the radial axis *R* is normal to the growth rings (perpendicular to the grain in the radial direction); and the tangential axis T is perpendicular to the grain but tangent to the growth rings.

Following the deformation matrix for orthotropic material is reported, using the engineering parameters, such as elasticity moduli (E), shear moduli (G) and Poisson's ratios (ν).

Twelve constant, of which nine are independent, are needed to describe the elastic behaviour of the material: three moduli of elasticity *E*, three shear moduli *G*, and six Poisson' ratios *ν*. The moduli of elasticity and Poisson's ratios are related by the following expressions:

$$\frac{\nu_{RL}}{E_R} = \frac{\nu_{LR}}{E_L}; \quad \frac{\nu_{TL}}{E_T} = \frac{\nu_{LT}}{E_L}; \quad \frac{\nu_{TR}}{E_T} = \frac{\nu_{RT}}{E_R}$$

$$\begin{bmatrix} \varepsilon_L \\ \varepsilon_R \\ \varepsilon_T \\ \gamma_{LR} \\ \gamma_{RT} \\ \gamma_{LT} \end{bmatrix} = \begin{bmatrix} \frac{1}{E_L} & -\frac{\nu_{RL}}{E_R} & -\frac{\nu_{TL}}{E_T} & 0 & 0 & 0 \\ -\frac{\nu_{LR}}{E_L} & \frac{1}{E_R} & -\frac{\nu_{TR}}{E_T} & 0 & 0 & 0 \\ -\frac{\nu_{LT}}{E_L} & -\frac{\nu_{RT}}{E_R} & \frac{1}{E_T} & 0 & 0 & 0 \\ 0 & 0 & 0 & \frac{1}{G_{LR}} & 0 & 0 \\ 0 & 0 & 0 & 0 & \frac{1}{G_{RT}} & 0 \\ 0 & 0 & 0 & 0 & 0 & \frac{1}{G_{LT}} \end{bmatrix} \begin{bmatrix} \sigma_L \\ \sigma_R \\ \sigma_T \\ \tau_{LR} \\ \tau_{RT} \\ \tau_{LT} \end{bmatrix}$$

The Poisson's ratios are denoted by ν_{LR}, ν_{RL}, ν_{LT}, ν_{TL}, ν_{RT}, ν_{TR}. The first letter of the subscript refers to direction of applied stress and the second letter to direction of lateral deformation. Typical average values of Poisson's ratios for softwoods and hardwoods are given in Table 1.1. It is possible to notice that the values for ν_{RL} and ν_{TL} are less precisely determined than are those for the other Poisson's ratios.

Table 1.1. Anisotropic nature of wood: Poisson's ratios for various species at approximately 12% moisture content (Bodig and Jayne, 1982).

Poisson's ratio	Softwoods	Hardwoods
ν_{LR}	0.37	0.37
ν_{LT}	0.42	0.50
ν_{RT}	0.47	0.67
ν_{TR}	0.35	0.33
ν_{RL}	0.041	0.044
ν_{TL}	0.033	0.027

The three moduli of elasticity, which are denoted by E_L, E_R and E_T, respectively, are the elastic moduli along the longitudinal, radial and tangential axes of wood (Fig. 1.5). These moduli are usually obtained from compression tests; however, data for E_R and E_T are not extensive.

The three moduli of rigidity, also called shear moduli, denoted by G_{LR}, G_{LT} and G_{RT} are the constants in the *LR*, *LT* and *RT* planes, respectively (Fig. 1.5). For example, G_{LR} is the modulus of rigidity based on shear strain in the *LR* plane and shear stresses in the *LT* and *RT* planes.

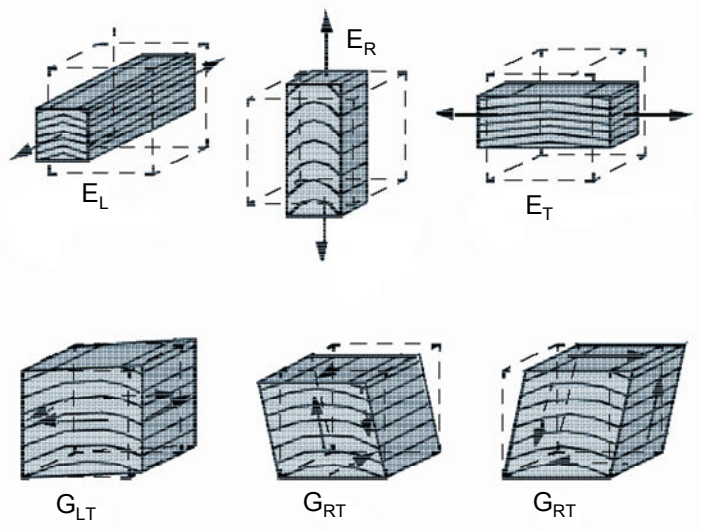

Figure 1.5. Anisotropic nature of wood – Orthotropic behaviour: elasticity and shear moduli.

Average values of elasticity and shear moduli for samples of a few species are given in Table 1.2, in comparison with other common materials used in constructions, such as concrete, steel and aluminium (Piazza *et al.,* 2005). It is worth noticing that, they vary within and between species and with moisture content and specific gravity.

Table 1.2. Anisotropic nature of wood – Elasticity moduli and shear moduli for various species at approximately 12% moisture content (Bodig and Jayne, 1982).

	Elasticity modulus E [GPa]			**Shear modulus G [GPa]**		
Species	E_L	E_R	E_T	G_{LR}	G_{LT}	G_{RT}
Douglas fir	14.50	0.96	0.09	0.83	0.76	0.08
Fir, red	11.71	0.83	4.94	0.70	0.66	0.07
Larch	14.13	1.05	0.69	0.84	0.78	0.09
Poplar	10.76	0.76	0.33	0.59	0.42	0.13
Pine	11.52	1.00	0.65	0.81	0.75	0.25
Beech	13.06	1.31	0.68	1.01	0.75	0.25
Oak	13.82	1.28	0.66	0.99	0.74	0.25
Birch	15.25	1.26	0.64	0.97	0.72	0.24
Balsa	3.30	0.27	0.08	0.21	0.14	0.03
		E [GPa]			G [GPa]	
Concrete (mean)		25			11	
Steel		207			79	
Aluminium (alloy 7000)		70			26	

For the most wood species, although the many variations between the stiffness properties, the following ratios between moduli can be considered (Bodig e Jayne, 1982):

$E_L : E_R : E_T \approx 20 : 1.6 : 1$

$G_{LR} : G_{LT} : G_{RT} \approx 10 : 9.4 : 1$

$E_L : G_{LR} \approx 14 : 1$

In engineering, the values for the mechanical properties of wood may allow further simplification that hypothesis is to consider, apart the longitudinal direction (0), only one transversal one (90), confusing the anatomical transversal directions *R* and *T*. In this way the assumption of cylindrical orthotropic can be made (Fig. 1.6), assuming as follow:

$E_L = E_0 ; \; E_R = E_T = E_{90}$

$G_{LR} = G_{LT} = G_{0,90} ; \; G_{RT} = G_{90}$

$\nu_{LR} = \nu_{LT} = \nu_{0,90} ; \; \nu_{RT} = \nu_{TR} = \nu_{90}$

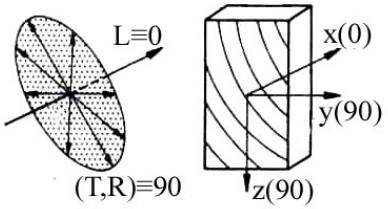

Figure 1.6. Anisotropic nature of wood: cylindrical orthotropic assumption.

For softwoods, the following ratios between the mechanical properties can be assumed:

$G_{0,90} = E_0/16$

$E_{90} = E_0/30$

1.5 WOOD AND MOISTURE

Similar to other organic materials, wood is hygroscopic in that it absorbs or loses moisture to reach equilibrium with the surrounding environment. Wood can naturally hold large quantities of water. Understanding the effects of water in timber is important because it influences many properties of wood and engineered wood products. The measure of water in wood is called the moisture content (MC) and it is reported as the weight of water of over-dry, or moisture-free, wood. The moisture content of freshly cut wood can exceed 100% because the weight of water in a given volume of wood can exceed the weight of the oven-dry wood.

Moisture may be absorbed by the cell walls, or after the walls are saturated, it may be occupy the void space within the cell cavities. The first type is called “bound water” and the second “free water”. When wood is dried, the free water disappears first, and at around 30% moisture content almost all of the remaining water is bound in the cell wall. This moisture state is called the “fibre saturation point” (FSP). It varies among species, as illustrated in Table 1.3.

Table 1.3. Wood and moisture: fibre Saturation Point (FSP) of different wood species.

Species	FSP [%]	Species	FSP [%]
Ask, white	24.0	Pine, loblolly	21.0
Basswood	32.0	Pine, longleaf	25.5
Birch, yellow	27.0	Pine, red	24.0
Cedar, Alaska	28.5	Pine, slash	29.0
Cedar, western red	22.0	Pine, shortleaf	30.0
Douglas fir	26.0	Poplar, yellow	31.5
Fir, red	30.0	Redwood	22.5
Hemlock, western	28.0	Spruce, Sitka	28.5
Larch, western	28.0	Spruce, red	27.0
Oak, white	32.5	Tamarack	24.0
Oak, swamp	31.0	Teak	22.0

Wood is dimensionally stable when the moisture content is greater than the FSP, whereas it changes dimensions as it gains or loses moisture below that point. Moisture affects the size of a piece of wood, and, perhaps its shape. With increasing MC (again, only up to the fibre saturation point), the cell

walls swell and all dimensions of the piece become larger. With reduction MC, all dimensions became less, that is, the wood shrinks.

Therefore, another manifestation of wood anisotropy is moisture-induced strain, i.e. shrinkage and swelling. Wood shrinks most in the direction of the annual growth rings (tangentially), about half as much across the rings (radially), and only slightly along the grain (longitudinally). The combined effects of radial and tangential shrinkage can distort the shape of wood pieces because of the difference in shrinkage and the curvature of annual rings. The major type of distortion as a result of these effects are illustrated in Figure 1.7.

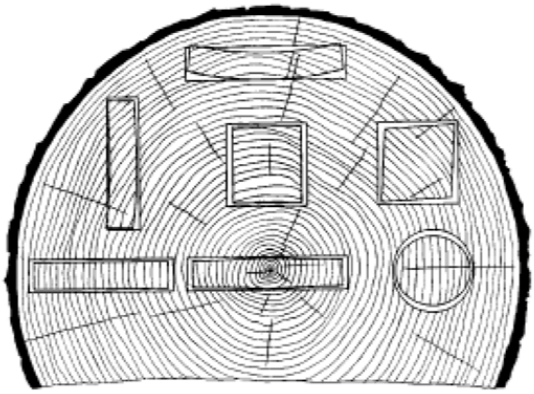

Figure 1.7. Wood and moisture: characteristics shrinkage and distortion of flat, square, and round pieces as affected by direction of growth rings.

Swelling and shrinkage are very small in the longitudinal direction, varying from 0.1% to 0.2% as green wood is completely dried. However, they are considerably more in the radial direction and highest of all tangentially. The expansion/shrinkage across the grain is a function of wood species and other variables. Generally, there is greater shrinkage with wood with higher density.

1.6 BIODETERIORATION OF WOOD

Wood is a natural plant material, and as such, is made up of a host of organic compounds, many of which represent a food source for the attacking agents. The principal organisms that can degrade wood are fungi and insects.

Decay-producing fungi may, under conditions that favour their growth, attack either heartwood or sapwood in most wood species. The results is a condition designated as decay, rot, dote or doze (Fig. 1.8).

Figure 1.8. Biodeterioration of wood: rotten wood.

The growth of fungi depends on suitably mild temperatures, moisture and air. Two kinds of major decay fungi are recognized: brown rot and white rot. (Fig. 1.9a, b) With brown-rot fungi, only the cellulose is extensively removed, the wood takes on a browner colour, and it can crack across the grain, shrink, collapse and be crushed into powder. With white-rot fungi, both lignin and cellulose usually are removed, the wood may lose colour and appear “whiter” than normal, it does not crack across the grain, and until severely degraded, it retains its outward dimensions, does not shrink or collapse, and often feels spongy. With white-rot fungi, both lignin and cellulose usually are removed, the wood may lose colour and appear “whiter” than normal, it does not crack across the grain, and until severely degraded, it retains its outward dimensions, does not shrink or collapse, and often feels spongy. Brown-rot fungi commonly colonize softwoods, and white-rot fungi commonly occur on hardwoods, but both brown-and white rot fungi occasionally colonize both types of wood. A third and generally less important kind of decay is known as soft rot. Soft rot typically is relatively shallow; the affected wood is greatly degraded and often soft when wet, but immediately beneath the zone of rot, the wood may be firm.

Insects also may damage wood, and in many situations must be considered in protective measures. In particular, termites are the main source of destruction of wood by insects (Fig. 1.9c).


a)

b)

c)

Figure 1.9. Biodeterioration of wood – Wood decay by fungi and insect attacks: a) Brown rot; b) White rot; c) Holes caused by termites.

1.7 STRUCTURAL TIMBER

1.7.1 *From clear wood to timber material*

Generally, in structural engineering, the term “wood” is usually reserve for small clear wood elements more or less free from defects and irregularities on the macro level. Instead, the term “timber” is used to describe elements on a structural scale, where the influence of macro defects on the performance is important. Therefore, “timber is different from wood as concrete is from cement” (Borg Madsen, 1999).

Clear straight-grained wood is used for determining fundamental mechanical properties, which are very important for a basic understanding of

the key problems in timber engineering. However, because of natural growth characteristics of trees, wood products vary in specific gravity, may contain cross grain, or may have knots and localized slope of grain. These wood characteristics must be taken into account in assessing actual properties or estimating the actual performance of timber elements.

Timber engineering deals with the properties and performance on levels above clear wood, from timber elements to structural systems.

In Figure 1.10 the chain from micro level to macro level for wood is illustrated. Wood, being a biological material means that there is a considerable variability at all levels.

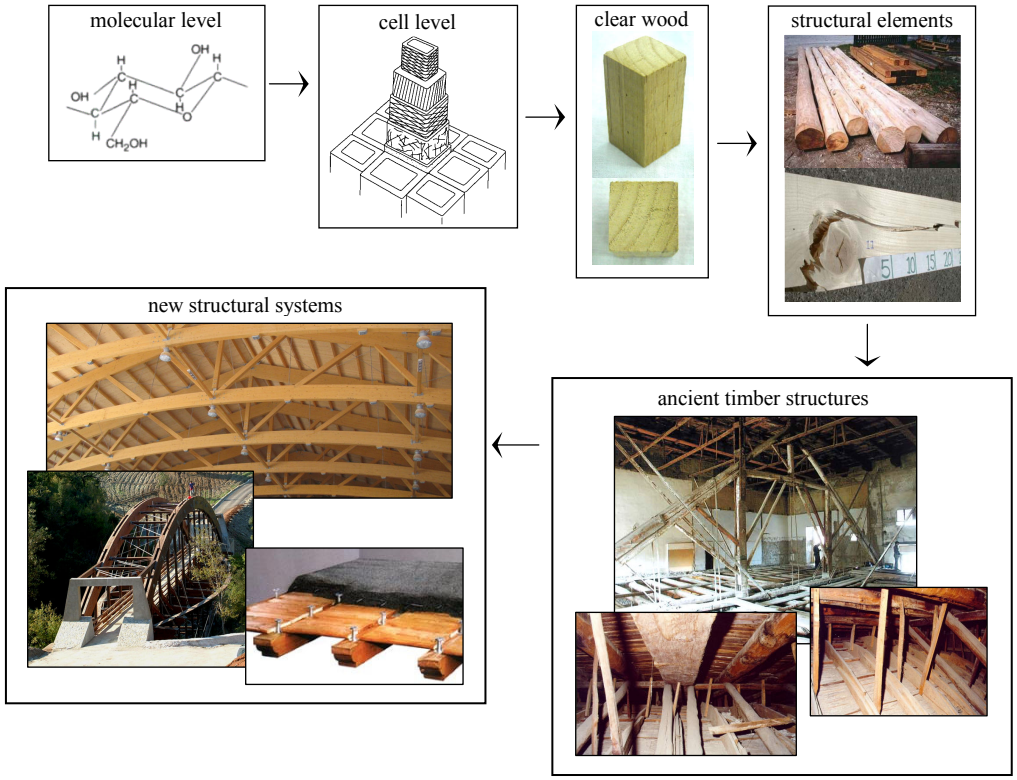

Figure 1.10. Structural timber: the wood chain: from micro level to macro level.

1.7.2 *Mechanical properties*

Typical stress (σ) – strain (ε) curves for clear wood are shown in Figure 1.11 (Piazza *et al.,* 2005). In particular, it is worst noticing that, the tensile strength of clear, straight-grained timber is much higher than its compressive strength when evaluated parallel to the grain, since compression causes buckling or plastic crushing of the fibres. Furthermore, higher stiffness and strength properties are provided in parallel to grain direction than the perpendicular one.

However, in structural timber containing knots and distorted grain, the opposite is the norm. Failure in tension is mainly due to shear failure between fibres or cells. Bending stresses are very commonly applied to timber in service and, as would be expected, flexural strength, as measured between tensile and compressive strength.

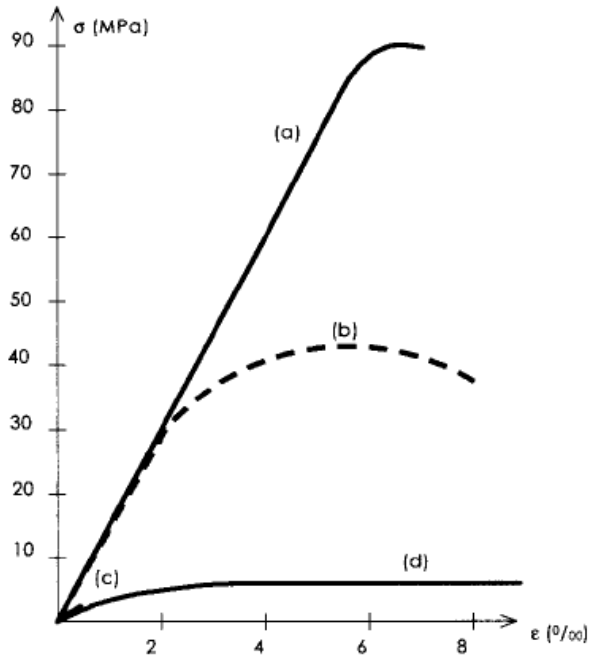

Figure 1.11. Mechanical behaviour of clear wood – Typical σ–ε curves: a) Tension parallel to grain; b) Compression parallel to grain; c) Tension perpendicular to grain; d) Compression perpendicular to grain.

The comparison between strength values of clear wood and structural timber, for parallel stress conditions, is provided in Table 1.4.

Table 1.4. Strength values for clear wood and structural timber.

Stress conditions [N/mm^2]	**Clear wood**	**Structural timber**
Tension // to grain	80-100	15-40
Tension ⊥ to grain	0.5-0.6	<0.5
Compression // to grain	40-70	20-40
Compression ⊥ to grain	5-10	<5

The mechanical properties of timber not only depend by natural defects but also by other several factors, including physical properties, density, moisture content, duration of the applied load, as it is illustrated in the following sections.

1.7.3 *Factors affecting strength*

1.7.3.1 Density and specific gravity

The density, or weight per volume, of wood varies considerably between and within wood species. Density of wood is always reported in combination with its moisture content due to the significant influence moisture content has on overall density. To standardize comparisons between species or products, it is common to report the specific gravity, or density relative to that of water, on the basis of oven dry weight of wood and volume at a specified moisture content. In general, the greater the density or specific gravity of wood, the greater its strength, expansion and shrinkage and thermal conductivity.

Density is the best single indicator of the properties of a timber and is a major factor determining its strength. Basic specific gravity of commercial timber ranges from 0.29 to 0.81, most falling between 0.35 and 0.60.

Approximate relationships between various mechanical properties and specific gravity for clear straight-grained wood of hardwood and softwood are given in Table 1.5 as power functions.

Table 1.5. Mechanical properties as a function of specific gravity for wood (G) at 12% moisture content (Woodhandbook, 1999).

	Wood at 12% moisture content	
Property	*Softwood*	*Hardwood*
Static bending		
MOR (kPa)	$170.7\ G^{1.01}$	$171.3\ G^{1.13}$
MOE (kPa)	$20.5\ G^{0.84}$	$16.5\ G^{0.7}$
Compression parallel (kPa)	$93.7\ G^{0.97}$	$76.0\ G^{0.89}$
Compression perpendicular (kPa)	$16.5\ G^{1.57}$	$21.6\ G^{2.09}$
Shear parallel (kPa)	$16.6\ G^{0.85}$	$21.9\ G^{1.13}$
Tension perpendicular (kPa)	$6.0\ G^{1.11}$	$10.1\ G^{1.30}$

(*) Compression parallel to grain is maximum crushing strength; compression perpendicular to grain is fibre stress at proportional limit. MOR is modulus of rupture (bending strength); MOE is modulus of elasticity.

The average data vary around the relationships, so that the relationships do not accurately predict individual average species values or an individual specimen value. In fact, mechanical properties within a species tend to be linearly, rather than curvilinearly, related to specific gravity; where data are available for individual species, linear analysis is suggested.

1.7.3.2 Natural defects

Sawn timber in structural dimensions normally contains defects of various kinds, such as knots, slope of grain, shakes and checks, compression wood, decay, bark pockets, wane and resin pockets (Fig. 1.12). The seriousness of these defects is not only a matter of how much each individual defect reduces the strength, but also how often they occur. In particular, knots are regarded as very serious defects as they can greatly reduce strength and are almost always present in large numbers in a piece of timber.

a) b) c) d)

Figure 1.12. Structural timber – Natural defects: a) Knot; b) Ring shakes; c) Crack; d) Fungi decay.

Knots

Knots are formed by the change of wood structure that occurs where limbs grow from the main stem of the tree. The limb, extending approximately radially in the main trunk, has its own annual rings and rays, and this local arrangement of cells interrupts the normal pattern for the main portion of the tree.

Most mechanical properties are lower in sections containing knots than in clear straight-grained wood because: the clear wood is displaced by the knot; the fibres around the knot are distorted, resulting in cross grain, the discontinuity of wood fibre leads to stress concentrations and checking often occurs around the knots during drying. Hardness and strength in compression perpendicular to the grain are exceptions, where knots may be objectionable stress distributions at contact surfaces.

Knots have a much greater effect on strength in axial tension than in axial short-column compression, and the effects on bending are somewhat less those in axial tension. For this reason, in a simply supported beam, a knot on the lower side (subjected to tensile stresses) has a greater effect on the load the beam will support than does a knot on the upper side (subjected to compressive stresses).

The knot has a weakening effect on stresses, as it is illustrated in Figure 1.13. The grain direction changes severely as the wood fibres pass around the knot (cross grain). In this region, the applied load causes tensile stress components normal to the grain of the knot. Since tensile strength normal to the grain is very low, the knot weakens the member significantly. Tensile strength is affected most by the knot, but compressive strength is reduced also. Bending strength is reduced too, the amount of reduction depending on where the knot is located on the beam cross section. In drying, wood shrinks more radially than longitudinally, so knots frequently become loose and may even fall out. Then, obviously, they are as damaging to bending, compressive, or shear strength as they are to tensile strength.

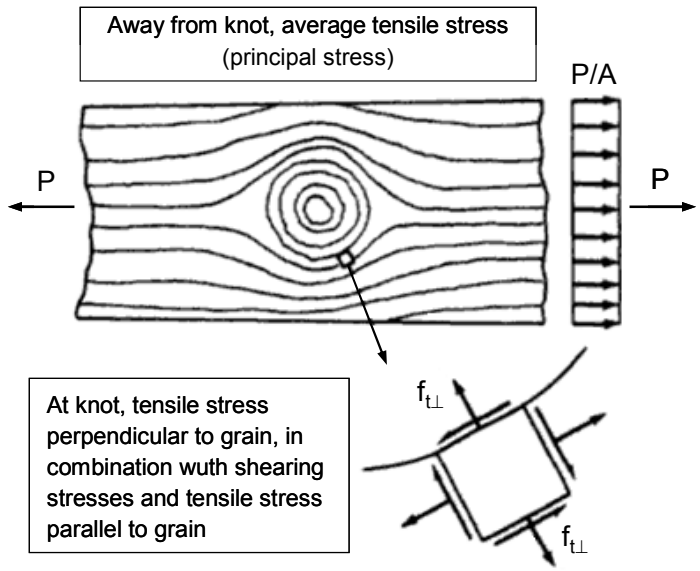

Figure 1.13. Structural timber – Natural defects: effect of knot on stresses.

Slope of grain

Grain is the longitudinal direction of the main elements of timber, these main elements being fibres or tracheids, and vessels in the case of hardwoods. In many instances the angle of the grain in a cut section of timber is not parallel to the longitudinal axis. It is possible that this variation is due to poor cutting of the timber, but more often than not the deviation is due to poor cutting of the timber, but more often than not the deviation in grain angle is due to irregular growth of the tree. This effect is of lesser consequence when timber is axially loaded, but leads to a significant drop in bending resistance. The angle of the microfibrils within the timber also affects the strength of the timber, as with the effects of the grain, if the angle of deviation increases the strength decreases.

The relationship between grain angle and properties has been empirically described by Hankinson equation:

$$N = \frac{PQ}{P\sin^n\theta + Q\cos^n\theta}$$

where N is strength at angle θ from fibre direction, Q strength perpendicular to grain, P strength parallel to grain, and n an empirically determined constant. This formula has been used for modulus of elasticity as well as strength properties. Values of n and associated ratios of Q/P are given in Table 1.6.

Table 1.6. Constants for calculating effect of grain angle on strength of wood.

Property	***n***	***Q/P***
Tensile strength	1.5-2	0.04-0.07
Compression strength	2-2.5	0.03-0.40
Bending strength	1.5-2	0.04-0.10
Modulus of elasticity	2	0.04-0.12

Shakes and checks

Sometimes the generic term splits is used to cover both shakes and checks. Shakes and checks are longitudinal planes of separation (cracks) in the wood (Fig. 1.14). They may be in the longitudinal/radial plane, in which case they are called heart shakes or rift cracks. When they are in the longitudinal/tangential plane they are called ring shakes, the plane of the break being parallel to the annual rings. Ring shakes are thought to be caused by shear due to wind.

Checks occur as the wood season after the tree is felled. They are longitudinal cracks, usually in the longitudinal/radial plane but occasionally in the longitudinal/tangential plane. They occur because of stresses resulting from differential shrinkage in the tangential and radial directions during drying, or from uneven drying in different portions of the lumber. Thus, checking can be reduced by careful attention to drying procedures during lumber production. The major structural effect of checks is to reduce longitudinal shear strength, often the deciding factor in designing timber beams.

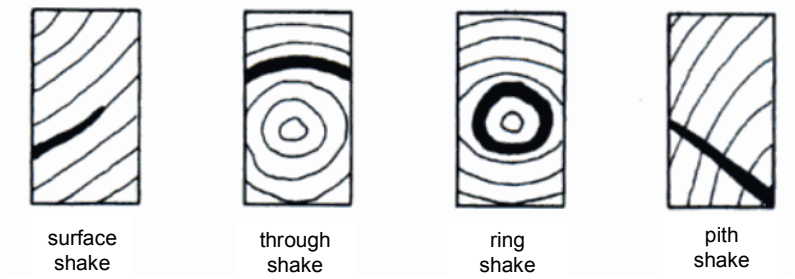

Figure 1.14. Structural timber – Natural defects: type of shake.

1.7.3.3 Moisture content

Many mechanical properties are affected by changes in moisture content below the fibre saturation point (FSP). In fact, most properties increase with decrease in moisture content (Fig. 1.15). In fact, if the adsorbed water softens the cellulose/lignin material of the cell wall, weakening the wood properties, the free water within the cell cavity has no effect whatever, except to increase the weight of the wood members.

Wood is hygroscopic, which means that its moisture content adjusts to reach equilibrium with the temperature and relative humidity of the atmosphere in which it is used. The moisture content that remains constant under a given atmospheric condition is called the "equilibrium moisture content", sometimes abbreviated EMC. In the present European standards, the "normal ambient condition" corresponds to 20±2 °C of temperature and 65±5 % of humidity. For softwood elements, this condition implies a moisture content of 12 %.

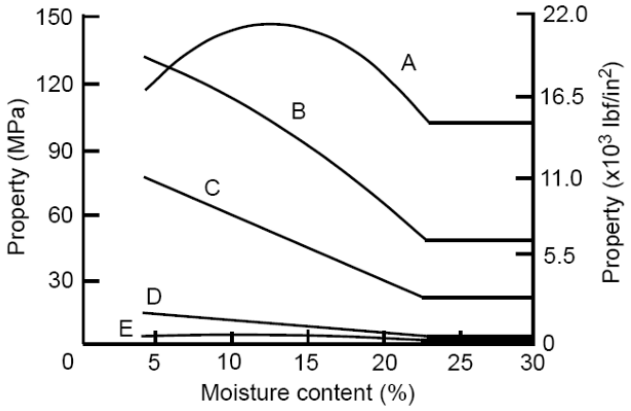

Figure 1.15. Effect of moisture content on wood strength properties: a) Tension parallel to grain; b) Bending; c) Compression parallel to grain; d) Compression perpendicular to the grain; e) Tension perpendicular to grain (Woodhandbook, 1999).

Concerning the strength and stiffness properties variations, due to the values of the moisture content, they mainly depend by wood species and by mechanical parameter which is considered. For softwoods, the ratios between the values of these parameters measured in "normal conditions" and beyond the fibre saturation point, can be assumed equal to as follow (Woodhandbook, 1999):

- Modulus of elasticity parallel to the grain: 1.1-1.3;
- Bending strength: 1.4-2.0;
- Compression strength parallel to the grain: 1.7-2.3;
- Shear strength: 1.1-1.7.

This increase in mechanical properties with drying assumes small, clear specimens in a drying process in which no deterioration of the product (degrade) occurs. For 51 mm thick lumber containing knots, the increase in property with decreasing moisture content is dependent upon timber quality. Straight-grained timber may show increases in properties with decreasing moisture content that approximate those of small, clear specimens. However, as the frequency and size of knots increase, the reduction in strength resulting from the knots begins to negate the increase in property in the clear wood portion of the lumber. Very low quality timber, which has many large knots,

may be insensitive to changes in moisture content. Figures 1.16a, b show the effect of moisture content on the properties of lumber as a function of initial lumber strength.

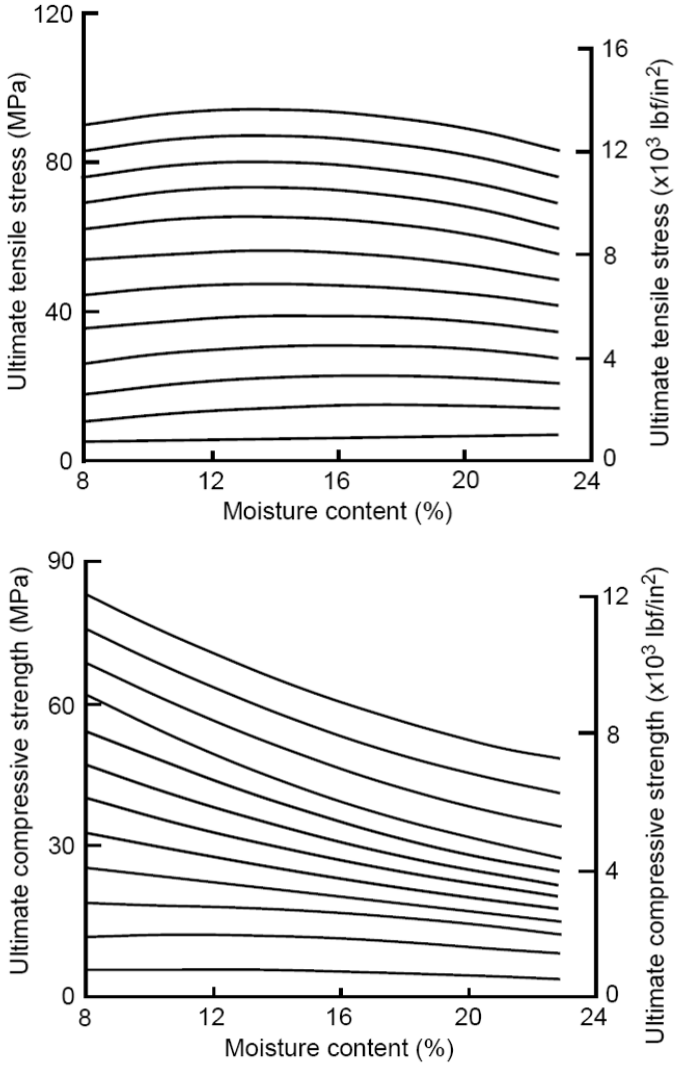

Figure 1.16. Effect of moisture content on timber strength properties: a) Tension parallel to grain; b) Compression parallel to grain (Woodhandbook, 1999).

1.7.3.4 Time-dependent behaviour of timber

In this section the time-under-load effects on the mechanical property of wood and structural timber are discussed, focusing on the following aspects: rate of loading, creep and duration of load.

Rate of loading

Mechanical properties values are usually referred to as static strength values. Static strength tests are typically conducted at a rate of loading or rate of deformation to attain maximum load in about 5 min. Higher values of strength are obtained for wood loaded at a more rapid rate and lower values are obtained at slower rates. For example, the load required to produce failure in a wood member in 1 s is approximately 10% higher than that obtained in a standard static strength test. Over several orders of magnitude of rate of loading, strength is approximately an exponential function of rate.

Figure 1.17 illustrates how strength decrease with time to maximum load. The variability in the trend shown is based on results from several studies pertaining to bending, compression and shear.

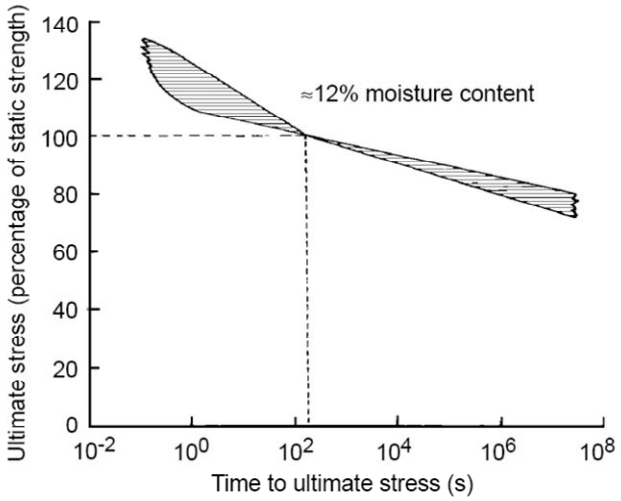

Figure 1.17. Relationship of ultimate stress at short-time loading to that at 5-min loading, based on composite of results from rate-of-load studies on bending, compression and shear parallel to grain. Variability in reported trends is indicated by width of band (Woodhandbook, 1999).

Creep

When initially loaded, a timber member deforms elastically. If the load is maintained, additional time-dependent deformation occurs. This is called creep. It occurs at even very low stresses and continues over a period of years.

At typical design level and use environments, after several years the additional deformation caused the initial, instantaneous elastic deformation.

For illustration, a creep curve based on a creep as function of initial deflection at several stress levels is plotted in Figure 1.18. As it is shown, the creep is greater under higher stresses than under lower ones.

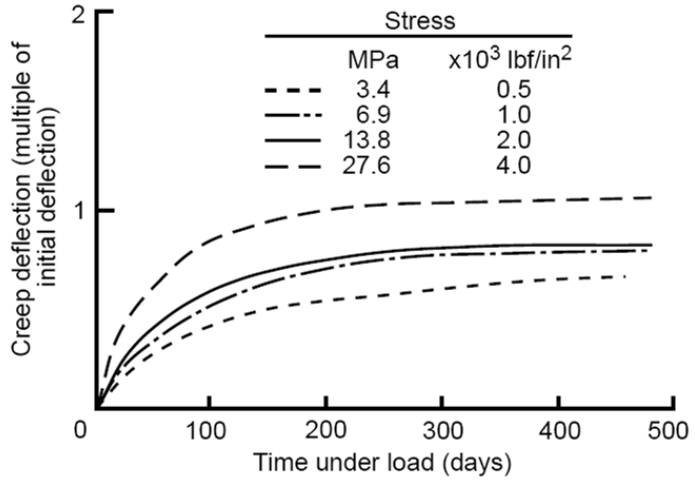

Figure 1.18. Influence of four levels of stress on creep (kingston, 1962).

Duration of load

The duration of load or the time during which a load acts on a wood member either continuously or intermittently, is an important factor in determining the load that the member can safely carry. The duration of load may be affected by changes in temperature and relative humidity.

The constant stress that a wood member can sustain is approximately an exponential function of time of failure, as illustrated in Figure 1.19. This relationship is a composite of results on small, clear wood specimens, conducted at constant temperature and relative humidity.

For a member that continuously carries a load for a long period, the load required to produce failure is much less than that determined from the strength properties. Based on Figure 1.19, a wood member under the continuous action of bending stress for 10 years may carry only 60% of the load required to produce failure in the same specimen loaded in a standard bending strength test of only a few minutes duration. Conversely, if the duration of load is very short, the load-carrying capacity may be higher than that determined from strength properties.

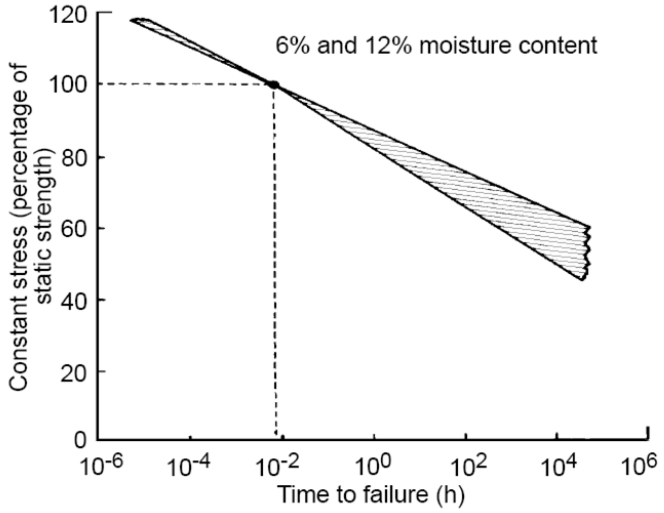

Figure 1.19. Relationship between stress due to constant load and time to failure for small clear wood specimens, based on 28 s at 100% stress. Variability in reported trends is indicated by width of band (Woodhandbook, 1999).

Furthermore, duration of load tests are commonly performed under constant load acting until failure occurs, or alternatively with some type of ramp loading applied at different rates. For a timber structure in practice, a significant part of the load will vary in a random manner over the life-time of the structure. It is still an open question as to how results from duration of load tests should be interpreted and used for arbitrary time variations of loads.

1.7.4 *Advantages of timber as structural material*

Timber principal advantages respect to the other common structural materials are its economy, appearance, ease of working and reworking, durability (for some application) and an excellent thermal insulating properties.

Concerning the mechanical behaviour, for stress conditions along the grain direction, the wood material shows a good structural efficiency, represented by a high strength/density ratio. It is due to the fact that, when wood is used for all components of a structure, the total weight is often less than for a structure of other materials. This is particularly true in comparison to reinforce concrete. The strength/density ratio of wood is advantageous wherever dead load is an appreciable part of the total load. Table 1.7 shows a comparison of strength/density ratios for some structural materials. It is worth noticing that, for clear wood this ratio is significantly higher than for concrete material. Also, in the case of structural timber, where natural defects reduce strength, the strength in relation to weight is of the same order of magnitude as ordinary structural steel and aluminium.

Table 1.7. Strength/density ratios for some structural materials.

Material	**Density** [kg/m^3]	**Strength** [MPa]	**Strength/density** 10^{-3} MPa · m^3/kg
Clear wood, tension //	~550	80-100	160-180
Clear wood, compression //	~550	40-70	70-130
Structural timber, tension//	~550	15-40	30-70
Structural timber; compression //	~550	20-40	35-70
Concrete, compression	2500	20-120	8-50
Structural steel	7800	400-1000	50-130
Aluminium	2700	100-300	40-110

Chapter 2

The ancient timber structures of the Royal Palace of Naples: diagnosis, analysis and restoration

2.1 GENERAL

The analysis of ancient timber structures shows some difficulties related to several factors, like the high features variability due to the material nature, the inaccessibility to carry out in depth surveys, the insufficient information about the used past technologies. Nevertheless during time wooden structures are exposed to some degradations, which often cause structural anomalies, such as splitting, shakes, cracking. Therefore their study requires a suitable knowledge of the conservation state and the actual load-bearing performance, aiming at the definition of the appropriate reinforcing interventions for the preservation or restoration of structural integrity and serviceability (Faggiano *et al.*, 2008).

The current conservation trend requires developing criteria for interventions and implementing operative procedures complying with modern structural safety requirements and satisfying conservative restoration principles. Research progress is also being made in understanding the behaviour of traditional timber joints and elements in service conditions and at the limit state under exceptional actions, as well as the effectiveness of different types of reinforcement. Actual cases of restoration of buildings that

included conservation of timber structures have proven to be economically competitive with the choice of substitution (Parisi and Piazza, 2007).

After an overview of the European and Italian current roles for timber constructions design and restoration, this chapter presents the study of the ancient timber structures of the Royal Palace of Naples, which are an evidence of the past ability of workmanship in timber carpentry applications and techniques. The roofing structures at the top floor are generally made of trusses and tiles. All the trusses were originally made of chestnut wood, but some of them, due to the weather degradation have been recently substituted by trusses made of either reinforced concrete, steel, composite and glued laminated timber. At the second level of the building, there are generally false ceiling, which reduce the significant height of the hall. These are realized by both vault or in plane wooden structures suspended to the floor above. At the first floor, almost all the wooden structures are located at the northern-west part of the Palace, datable between the XVII and the XVIII centuries, covering the Halls of the Historical Apartment. Two main structural units were realized: the beam floor, whose function is to bear vertical loads, and the light vault or vaulted ceiling, as the supporting skeleton of the reed laths, lined at the intrados with a coat of lime and plaster, as a base of the stucco. Wherever the spans between the perimeter masonry walls are small, the false ceilings were erected as self-bearing vaults. In the other cases the vaults were connected and partially suspended to the upper floor structures by means of wooden links. After all, during the survey, three different structural typologies have been detected: 1) the self-bearing vault, it leaning on the perimeter masonry walls only; 2) the vault linked to the beam floor above; 3) the vault linked to an ad-hoc supporting structure independent from the floor.

The applied study methodology of the timber structures of the Royal Apartment has led to a comprehensive knowledge of the systems. The geometrical and photographic surveys, through *in situ* investigations, have allowed to detect the configuration of the component structural units, the connection between them, the shape and size of each singular element. Moreover the wooden species have been identified, together with the location and extent of defects and alterations, such as knots, shakes, fibre deviation, biological and mechanical damages, like rots and insect attacks. Subsequent phases of the structural life, from the construction up to the present state of

use, according to different load conditions which the structure is supposed to have undergone, are recognised. Corresponding to each phase, 3D FEM models are set up. It is worth noticing that the wood degradations and working lacks are accounted for as a stiffness reduction of the structural members. The analysis of the structural behaviour emphasizes the weaknesses in terms of resistance and deformation capacities. In particular, the actual deflection state is evaluated considering also the effects of wood creep and moisture. Safety checks are carried out according to Eurocode 5. The supplied indications about any critical part of the structure have allowed the identification of the appropriate restoration interventions, based on the so-called mixed technologies, which consist in the combination of techniques, using different materials, like new wood, steel, reinforced concrete, whose prerogatives are reversibility, lightness, ductility, easiness of supply, transportation and erection (Mazzolani *et al.*, 2005).

The attentions is focused on three case studies, which are: 1) the complex roofing structure of the Diplomatic Hall (II); 2) the covering structure of the Third Anteroom (V); 3) the vaulted ceiling of the Guard Room (XXIX).

2.2 EUROPEAN CODES FOR TIMBER STRUCTURES DESIGN

2.2.1 *Design and safety checks*

As the European level for the design of timber structures reference can be made of Eurocode 5 (EN 1995-1-1) “Design of timber structures – Part 1-1: Common rules and rules for buildings”, which was published by CEN (European Committee for Standardisation) in November 2004.

EN 1995-1-1 is a limit state design code which requires structural stability to be in accordance with two specifically defined state, within which the structure complies in relation to particular performance criteria. These limit states are:

- *Ultimate limit state*, associated with collapse or with other forms of failure which include loss of equilibrium, excessive deformation, transformation into a mechanism, rupture or loss of stability;

- *Serviceability limit state*, associated with deformation which affects the appearance or effective use of the structure, vibrations which cause discomfort to people or damage to the structure, damage or cracking which is likely to adversely affect the durability of the structure.

EC5 is intended to be used in conjunction with:

- EN 1990 (2004): *Eurocode* "Basic of design", which sets out the principles and requirements for safety, serviceability and durability of structures", which described the design and verification procedures and provides guidelines for related aspects of structural reliability;
- EN 1991 (2002): *Eurocode 1* "Actions on structures", which provides design guidance and actions for the structural design of buildings and civil engineering works, including data for densities of construction materials and stored material, self-weight of construction elements and imposed loading for buildings;
- EN 1998 (2004): *Eurocode 8* "Design of structures for earthquake resistance – Part 1: General rules, seismic actions and rules for buildings", which provides general requirements for assessment of seismic actions and combinations with other actions, together with general rules for earthquake-resistant design of buildings and specific rules for buildings and elements constructed with each of the various structural materials;
- *EN Standards*: in respect of construction products relevant to timber structures.

At National level, the following standards can be used for structural design in timber:

- *German National Standard*, DIN 1052 (2004): "Entwurf, Berechnung und Bemessung von Holzbauwerken – Allgemeine Bemessungsregeln und Bemessungsregeln für den Hochbau"; Deutsches Institut Fur Normung E.V.;
- *British Standard*, BS 5268 (2001): "Structural use of timber"; British Standard International;

- *French Norms*, NF P21 (1993): "Structures en bois"; Association Francaise de Normalisation);
- *Austrian Norms*, ÖNORM B 4100-2: "Holzbau – Holztragwerke – Teil 2: Berechnung und Ausfuhrung".

In Italy, until a few years ago, the structural codes do not officially include structural timber design. Recently, a proposal code, so-called N.I.CO.LE., acronym of Italian role for the wooden constructions (Norma Italiana per le COstruzioni in LEgno), has been approved in draft form by a special CNR committee (National Research Council), but actually this document does not exist in official version. At present state, a CNR document (CNR-DT 206, "Istruzioni per la progettazione, esecuzione e controllo delle strutture in legno", 2007) has been approved as technical guide for design of timber structures. However both European codes and the existing Italian codification refer to new wood constructions. Therefore, the use of such provisions to the ancient timber requires appropriate consideration based on the results of experimental investigations.

2.2.2 *Rules for timber grading*

A pre-requisite for the use of timber in load bearing constructions is that the strength and stiffness properties are known and can be controlled to stay within desirable limits. Therefore strength properties are the key to structural design although other attributes may well come into consideration when assessing the overall performance of a component or structure. However, as far as the mechanical properties of wood are concerned, the only realistic way of obtained quality within desired limits is grading. The present grading systems allow to determine the strength class of the timber to satisfy the design requirements. Strength grading takes into account timber defects, such as slope of grain, existence and extent of knots and fissures, etc.

All timber used for structural applications needs to be strength graded by either visual inspection or by an approved strength grading machine, aiming at assigning the elements to "Strength Classes", defined in European standard EN 338 (2003) "Structural timber. Strength classes". There are a total of 16 strength classes, C14 to C40 for softwoods and D30 to D70 for hardwoods. The number in each strength class refers to its "characteristic bending

strength" value; for example, D40 timber hardwood has a characteristic bending strength of 40 N/mm^2 (Table 2.1). This is a value intended for use with the limit state Eurocode 5 (EN 1995-1-1, 2004).

Table 2.1. Strength classes for structural timber (hardwoods; EN 338, 2003).

		D30	*D35*	*D40*	*D50*	*D60*	*D70*
Strength properties [N/mm^2]							
Bending	$f_{m,k}$	30	35	40	50	60	70
Tension // to grain	$f_{t,0,k}$	18	21	24	30	36	42
Tension ⊥ to grain	$f_{t,90,k}$	0.6	0.6	0.6	0.6	0.6	0.6
Compression // to grain	$f_{c,0,k}$	23	25	26	29	32	34
Compression ⊥ to grain	$f_{c,90,k}$	8.0	8.4	8.8	9.7	10.5	13.5
Shear	$f_{v,k}$	3.0	3.4	3.8	4.6	5.3	6.0
Stiffness properties [kN/mm^2]							
Elasticity modulus // to grain (mean)	$E_{0,mean}$	10	10	11	14	17	20
Elasticity modulus // to grain (5-percentile)	$E_{0.05}$	8.0	8.7	9.4	11.8	14.3	16.8
Elasticity modulus ⊥ to grain (mean)	$E_{90,mean}$	0.64	0.69	0.75	0.93	1.13	1.33
Shear modulus (mean)	G_{mean}	0.60	0.65	0.70	0.88	1.06	1.25
Density [kg/m^3]							
Density (5-percentile)	ρ_k	530	560	590	650	700	900
Density (mean)	ρ_{mean}	640	670	700	780	840	1080

The visual method is a manual process carried out by an approved grader, which examines each piece of timber to check the size and frequency of specific physical characteristics or defects, as knots, slope of grain, rate of growth, wane, resin pockets and distortion. EN 518 (1995) "Structural timber – Grading – Requirements for visual strength grading standards" provides the principles for visual grading that national standards should achieve.

Machine strength grading relies essentially on the relationship between the modulus of elasticity and the modulus of rupture (bending strength) of a particular species of timber. This relation is evaluated on a statistical population of pieces. The European standard EN 519 (1995) "Structural timber – Grading – Requirements for machine strength graded timber and grading machine" provides the required specifications for strength grading machine.

For Italian structural timber, the required specifications for visual grading are given in UNI 11035-1 (2003) "Structural timber – Visual strength grading for Italian structural timbers: terminology and measurements of features" and UNI 11035-2 (2003) "Structural timber – Visual strength grading rules and characteristics values for Italian structural timber population" (Table 2.2).

Table 2.2. Strength classes for Italian structural timber (hardwoods; UNI 11035-2, 2003).

		Chestnut	*Deciduous oak*	*Poplar and alder*	*Other hardwoods*
Strength properties [N/mm^2]					
Bending	$f_{m,k}$	28	42	26	27
Tension // to grain	$f_{t,0,k}$	17	25	16	16
Tension ⊥ to grain	$f_{t,90,k}$	0.5	0.8	0.4	0.5
Compression // to grain	$f_{c,0,k}$	22	27	22	22
Compression ⊥ to grain	$f_{c,90,k}$	3.8	5.7	3.2	3.9
Shear	$f_{v,k}$	2.0	4.0	2.7	2.0
Stiffness properties [kN/mm^2]					
Elasticity modulus // to grain (mean)	$E_{0,mean}$	11.0	12.0	8.0	11.5
Elasticity modulus // to grain (5-percentile)	$E_{0.05}$	8.0	10.1	6.7	8.4
Elasticity modulus ⊥ to grain (mean)	$E_{90,mean}$	0.73	0.8	0.53	0.77
Shear modulus (mean)	G_{mean}	0.95	0.75	0.5	0.72
Density [kg/m^3]					
Density (5-percentile)	ρ_k	465	760	420	515
Density (mean)	ρ_{mean}	550	825	460	560

2.3 ITALIAN STANDARDISATION ACTIVITY IN THE FIELD OF CONSERVATION OF ANCIENT TIMBER STRUCTURES

2.3.1 *Methodological standards*

The standardisation activity in the field of cultural heritage started in Italy in 1996, following an agreement between the Ministry of Cultural Heritage and U.N.I (Italian standardisation body). The aim of the agreement was to activate a collaboration, which would help in developing common technical

standards valid on a national level and suitable for proposal on a European level (Macchioni and Piazza, 2009)

The agreement consequently gave birth to the UNI / NORMAL Technical Committee whose activity is unique in the world in developing specific standards in the conservation of artefacts that constitute the cultural patrimony of every country. Several Working Groups were established during times, dealing with different materials. Last year the Working Groups of UNI-Normal were reorganised in order to mirror the organisation within CEN.

The activity was organized through the institution of ad hoc groups on a series of standard projects. Work Group 20 (Wood and wood based products) of the UNI -NORMAL TC was established in 1999, with the aim of studying and producing standards focused on the approach to material. The final product is a set of published standards that indicates a correct approach towards wooden material and deteriorated wooden artefacts, including criteria to follow in their restoration, conservation and maintenance. More than 40 experts belonging to diverse fields were invited to contribute their varied activities of study in the restoration of wooden artefacts in order to obtain the widest possible shared documents.

Concerning the load-bearing timber structures, the following two standards are already approved:

- UNI 11119 (2004) “Cultural Heritage – Wooden Artefacts – Load bearing Structures of Buildings – On site inspection for the diagnosis of timber members”, aiming to establish objectives, procedures and criteria in the execution of *in situ* inspection and the use of non-destructive techniques, in order to evaluate the state of conservation and assess the performances of timber members in load-bearing ancient timber structures.
- UNI 11138 (2004) “Cultural Heritage – Load bearing structures of buildings – Criteria for the preliminary evaluation, design and execution of works”, which deals with the design and execution of restoration interventions in ancient timber structures that belong to our cultural heritage with the principle aim of the standard being the conservation of above said timber structure typologies.

2.3.2 *UNI 11119*

2.3.2.1 Objectives of the inspection

The inspection should evaluate the original characteristics of each timber member and the eventual modifications which each member underwent during its service life. The information which can be collected are as follows:

- Wooden species;
- Moisture content of wood and eventual moisture gradients;
- Class of biological risk of wood, according to EN 335-1 (1992) and EN 335-2 (1992);
- Geometry and morphology of the timber member indicating the position and extension of main defects, decay and damage;
- Position, shape and dimension of the critical area and critical section;
- Strength grading of the timber elements as a whole and/or in single critical parts.

For the execution of an inspection the following preliminary conditions must be fulfilled: accessibility, cleaning, lighting. If these preliminary conditions are absent or insufficiently met they can impede inspection or else limit the quantity and quality of accessible information.

2.3.2.2 Procedures

The procedure obviously involves the identification of wooden species, the determination of wood moisture content with non destructive methods, and the determination of the level of biological risk according to the EN 335-1 and 2 standards. These procedures can be carried out on any kind of wooden artefact.

More specifically, the structures must undergo geometric surveys; surveys that take into account the original characteristics of the wooden member (such as position of the pith, growth irregularities); type, length and position of main defects and any other information that will allow one to obtain all the necessary information about the mechanical characteristics of the timber members.

In order to evaluate the mechanical performance of each timber member it is of fundamental importance to identify the so called “critical area”, defined as “part of a wooden element with longitudinal axes no less than 150 mm, which is considered to be relevant because of defects, position, state of conservation and also stress conditions which are determined by static analysis”.

Through the individualization of the critical area and based on the presence of defects and decay, it is possible to execute a structural grading of the timber elements. This classification derives from a type of analysis which is visual and therefore is only practicable on the parts which are directly visible. Where and when the presence of non visible alterations is suspected it is necessary to carry out actions by means of proper instrumentation that prove the presence and extension of alterations, in order to determine the efficient section, “the cross section of a wooden member (including defects) where the critical section is excluded from analysis and where actual wood degradation and/or damage are determined”. It is important to note that the surveys to be executed must not only be non destructive but also consider the impact on other relevant aspects of the structure (e.g. decorations). The results from the survey must be validated for each timber member and for each area of a member.

Concerning the strength grading by means of visual inspection, the standard provides the grading table in which three categories are defined on the basis of defects characteristics (Table 2.3).

During the grading phase it is fundamental to observe with great care the following general criteria:

- Classify the entire wooden member and if necessary, identify each critical area separately;
- Take into consideration the limitations that derive from the conditions of accessibility and visibility of the wooden member’s surface;
- If an alteration occurs due to mechanical damage or localized biological decay (rot, insect attacks found on the surface) refer the classification only to the efficient section.

Table 2.3 Regulations for visual grading of timber members (UNI 11119, 2004).

Features	**On-site grading**		
	I	*II*	*III*
Wanes	1/8	1/5	1/3
Various damages	absent	absent	only limited
Frost cracks	"	"	"
Ring shakes	"	"	"
Single knots	≤1/5 ≤50 mm	≤1/3 ≤70 mm	≤1/2
Group of knots	≤2/5	≤2/3	≤3/4
Slope of grain (rd section) (inclination %)	≤1/14	1/8	1/5
Slope of grain (tg section) (inclination %)	≤1/10	1/5	1/3
Shrinkage checks	admissible if not passing the pith		

The standard also includes a table which gives the maximum values of stresses that can be used applying the admissible stress design methods and average elasticity moduli in bending for each category and species of timber, traditionally used in Italian constructions (Table 2.4). Some research laboratories are undergoing surveys to define and update the criteria for grading and resistance profiles.

2.3.3 *UNI 11138*

2.3.3.1 Field of application

The standard establishes the technical-scientific principles to be followed during an operation involving restoration of timber structures of historical and cultural interest (Macchioni and Piazza, 2009). Furthermore, it indicates the steps that any restoration project in this field must follow:

a) Preventative evaluation of the state of the artefact;
b) Planning possible intervention, if required;
c) Criteria for controlling the efficiency of an intervention;
d) Methodology and techniques in the execution of an intervention;
e) Periodic inspections.

Table 2.4. Admissible stresses and elasticity modulus for each category and timber species [N/mm^2] (UNI 11119, 2004).

		Compression		*Bending*	*Tension*	*Shear*	*Elasticity*
Species	**Category**	// to grain	⊥ to grain		// to grain		*modulus*
Fir white	I	11	2.0	11.5	11	0.9	13000
	II	9	2.0	10.0	9	0.8	12000
	III	7	2.0	7.5	6	0.7	11000
Fir red	I	10	2.0	11.0	11.0	1.0	12500
	II	9	2.0	9.0	9.0	0.9	11500
	III	6	2.0	7.0	6.0	0.8	10500
Larch	I	12.0	2.5	13.0	12.0	1.1	15500
	II	10.0	2.2	11.0	9.5	1.0	14500
	III	7.5	2.0	8.5	7.0	0.9	13500
Pine	I	11.0	2.0	12.0	11.0	1.0	13000
	II	9.0	2.0	10.0	9.0	0.9	12000
	III	7.0	2.0	8.0	6.0	0.8	11000
Chestnut	I	11.0	2.0	12.0	11.0	0.8	10000
	II	9.0	2.0	10.0	9.0	0.7	9000
	III	7.0	2.0	8.0	6.0	0.6	8000
Poplar	I	10.0	1.5	10.5	9.0	0.6	9000
	II	8.0	1.5	8.5	7.9	0.5	8000
	III	6.0	1.5	6.5	4.5	0.4	7000
Oak	I	12.0	3.0	13.0	12.0	1.2	13500
	II	10.0	2.5	11.0	10.0	1.0	12500
	III	7.5	2.2	8.5	7.0	0.9	11500

(*) The admissible stress in perpendicular tension is conventionally assumed equal to zero.

2.3.3.2 Preventative evaluation of the actual conditions

The aim of a preventative evaluation is to understand the performance of the overall static suitability of a building and the role of the timber structure within the building. Keeping this in mind, its single purpose is to serve as knowledge and does not necessarily mean that the execution of a restoration intervention must be carried out.

Preventative evaluation must be based on a series of preliminary operations which can be more or less thoroughly examined or not shown at all, depending on the major or minor complexity of the problem and the level of detail requested for the structure.

Historical analysis is a very important phase which reveals the chronological events of a building such as its structural typology and its evolution, its construction characteristics and traumatic events. A

dendrochronological analysis of the timber members (UNI 11141, 2004) can also play an important role in this documentation area.

Characterization of materials is carried out according to the UNI standards 11118 (2004) and 11119 (2004), in that it follows the absolutely necessary informative role of the diagnosis.

The geometric survey should be carried out on the structure and on each timber member, including its state of deformation, the defects of the wood and its particular shape, which can reach levels that cannot be neglected in cases dealing with ancient structures.

Characterization of decay helps to analyze the interaction between biotic decay and microclimates that have established around the wooden member or a part of it. Decay may have established by non biotic causes; therefore, this type of analysis must also keep in mind the state of stress and the interaction between the timber members.

The structural analysis must always be considered compulsory even though the different levels of detail can vary depending on the complexity of the problem and the entity of the proposed intervention. The structural scheme must refer to the situation of the building as a whole, including all non wooden parts, and defining their contribution to the whole wooden structural scheme, including single timber structural units. Particular attention must be paid when verifying the joints of single timber members pertaining to the heads of beams.

2.3.3.3 Planning intervention

The section regarding the planning of an intervention is the most detailed of the entire standard and indicates at each step informative criteria for planning choices, defines actions and the criteria to follow during a restoration intervention, gives indications regarding the definition of a maintenance and inspection program and gives information about the essential requirements of a project.

Because of space limitations, we cannot go into detail about each point listed below. It must be high-lighted the importance of preliminary studies through a multidisciplinary approach, which precisely defines the characteristics of the material (and its interaction with other materials) and the typology of decay/damage found.

The definition of an intervention plan must go through an analysis of compatibility with itself and other materials and with the future function of the actual structure. With this in mind the plan must define:

- The specific aim of every work and its necessity, meaning a statement that demonstrates an absence of necessary levels of safety of the structure;
- The location of the intervention;
- The materials that one intends to use;
- The methodology of application;
- The preliminary evaluation of the effectiveness of an intervention;
- Verification during the execution phase and at the end of the intervention, as well as those that should take place periodically.

What makes the approach to this standard so innovative is probably in the last two clauses of the list.

Clause e) states that it is obligatory to control the efficiency of an intervention when carried out, in a laboratory or during the realization of the project it-self, therefore through direct physical experimentation or through experimental simulation but there is also the possibility of extending similar known results to the case in object.

The following clause f) states that it is required to clearly indicate the type and the time intervals of periodic maintenance carried out on the artefact that has undergone intervention as well as the methodology of efficiency control of an intervention through the course of time.

The most significant criteria pertaining to project choices are listed as indications to be followed whenever possible, within the limits of imposed criteria considered more important such as the stability of a building or levels of safety.

Also stated is that all interventions that have been designed and realized should leave a trace that should not be hidden but, rather, pleasantly included within the actual structural context. In addition, operations involving the removal of past interventions are to be generally avoided.

The overall performance of the static model must be maintained and respected during the restoration intervention, in the same way that pre-existing

joints and restraints must be restored maintaining their original stiffness values.

Care must be taken, when designing an intervention, in order to guarantee the possibility of a variation of a timber member's dimension which can be caused by variations of its moisture content: therefore, interventions where the longitudinal cracks caused by shrinkage have been tampered with or interventions which impede in any way the transversal swelling and shrinkage of wood are not admissible.

2.3.3.4 Criteria for controlling the efficiency of an intervention

The evaluation of the efficiency of an intervention is an integral part of an actual intervention plan, and therefore is obligatory. It can be carried out generically or through direct physical experimentation or through numeric experimentation, (in other words on a laboratory scale sample) based on trusted and proven mathematical models.

Special attention must be paid assuming the results of laboratory simulations, with regard to the scale adopted for the specimens and to the time parameter.

The standard also imposes that the interventions are carried out by personnel with proven experience in works involving ancient timber restoration.

2.3.3.5 Periodic inspection

Documentation must also contain a Maintenance Plan, which should clearly indicate the typology and time intervals of periodic inspections as well as the type of periodic ordinary maintenance. Indeed it has been demonstrated that, more often than not, the de-cay of a wooden structure is due to the lack of ordinary maintenance, periodic inspections, as well as the bad planning and execution of recent interventions of restoration.

Therefore, periodic inspections should execute an attentive visual examination in order to ascertain if single members show possible new or accentuated dangerous conditions which may be caused by excessive load bearing or environmental conditions.

2.4 THE ROYAL PALACE OF NAPLES

2.4.1 *Historical background*

The Royal Palace of Naples is located in the historical centre of the town, in Plebiscito square (Fig. 2.1). It, at the beginning of the VVII century, was designed by Domenico Fontana (1543-1607), one of the most famous architects of that time. The Palace foresaw a square body with a court in its centre. Subsequently a new *L* shaped body was realized at the back of the Paladin Chapel of the building. The principal central court is the Honour Court; on its left there is the Royal Garden and on its right there are the Coach Court and the Belvedere Court (Fig. 2.2).

The original design of the Palace committed to Domenico Fontana has undergone several transformations during time, due to both the royal needs and static demands.

The construction works started in 1600 and in 1613 the three levels of the principal body, looking on to San Luigi square (the actual Plebiscito square), were completed. In 1631 the Palace become the viceroy residence, but it was not complete, lacked the Royal Chapel and all the part looking on to park.

a)

b)

Figure 2.1. The Royal Palace of Naples: a) Bird's eye view; b) Main façade on Plebiscito Square.

The main entrance to the Royal Apartment at the first floor, so called "Scalone D'Onore", was erected in 1649 and some vaults were rebuilt (Fig. 2.3a).

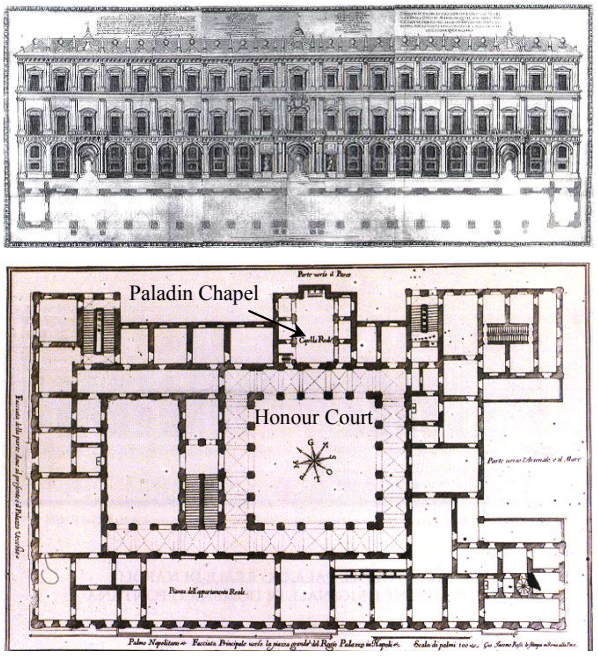

Figure 2.2. The Royal Palace of Naples – Drawing of Domenico Fontana (1606):
a) Front view; b) Plan view.

In 1724 the effects of a subsiding, which affected the side of the Palace facing San Luigi square, required a consolidation intervention on some arcades and pillars. In the XVIII century, Luigi Vanvitelli was charged to design and work up a further consolidation intervention for the reinforcement of the foundations of the "portico" as well as to wall up eight arcades of the façade (Fig. 2.3b). In 1734 a raised section was built on the southern wing of the Palace destined to stables.

The part of the Palace, now occupied by the National Library, was erected in 1737 and it was completed in the second middle of 1700. In 1735, under the reign of Carlo di Borbone, the vaults of the Royal Apartment were painted. Unfortunately only one original decoration resisted until today: the fresco of the vault of the Body Guards Hall (now the Diplomatic Hall). A large restoration intervention for extending and regularizing the building was done in 1837, after a fire broke. That is the reason why the Palace was subsequently restored by Gaetano Genovese. It was damaged also during the last war and then it was removed once again.


a)

b)

Figure 2.3. The Royal Palace of Naples: a) “Scalone D’Onore”; b) “Portico”.

For three centuries the Royal Palace has been connected, in the northern part, to the Old Palace, which was demolished in 1848 (Fig. 2.4). At present state, part of the northern wing is connected to the structure of the San Carlo theatre, which was erected in 1736.

From 1600 to 1946 the Royal Palace was a Royal Residence, but since 1919 the building houses the Museum of the Royal Apartment and the National Library.

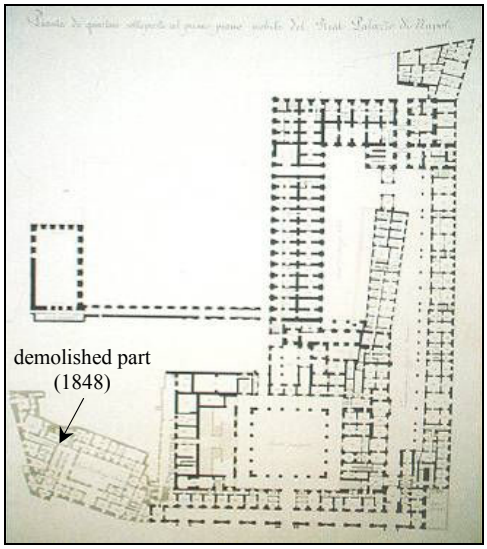

a)


b)

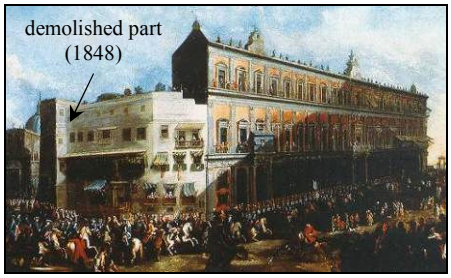

c)

Figure 2.4. The Royal Palace of Naples in the XVIII century: a) General layout; b) Main view in 1696; c) Main view in 1735.

2.4.2 *Structural layout*

The Palace is distributed on three levels (Fig. 2.5): the ground floor, which in the past was used for the services related to the royal activities and at present it houses the offices of the Superintendence; the first floor, where the Royal Apartment at the northern-west part and the National Library at the northern-east part are located; the second floor, which in the past was used as servants' accommodations and now it houses the National Library.

Two significant sections of the Palace are plotted in Figure2.6.

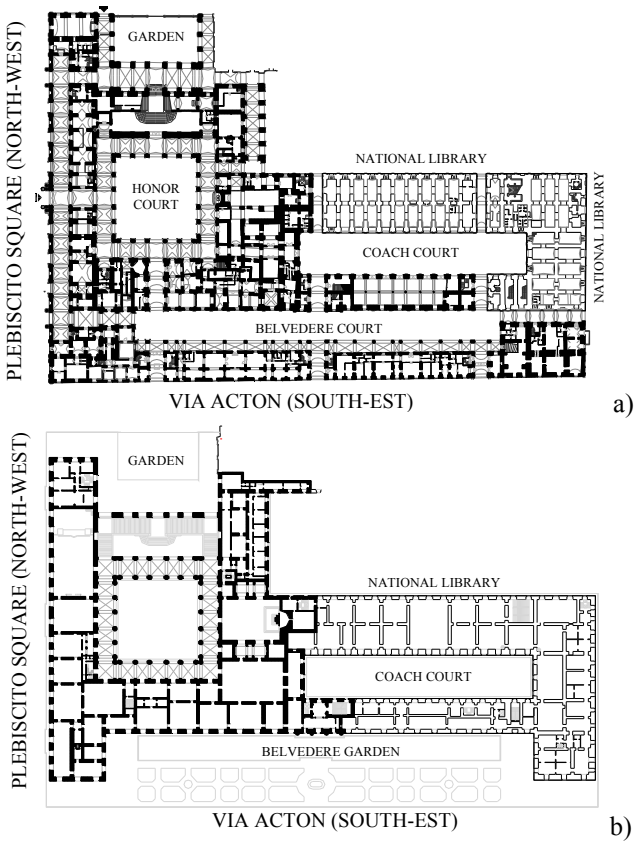

Figure 2.5. The Royal Palace of Naples – Horizontal sections: a) Ground floor; b) First floor; c) Second floor. (continues)

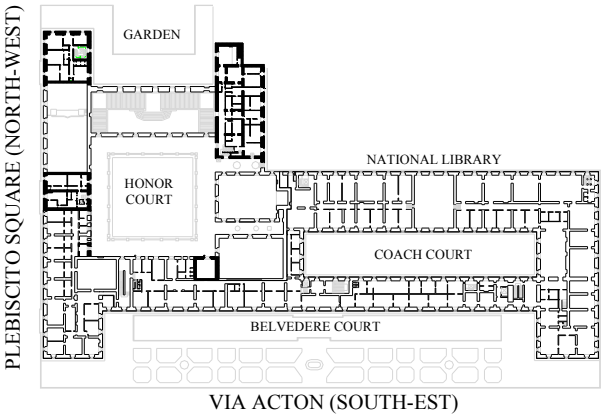

c)

Figure 2.5. The Royal Palace of Naples – Horizontal sections: a) Ground floor; b) First floor; c) Second floor.

Figure 2.6. The Royal Palace of Naples: transversal sections.

The main vertical structures are made of tuff masonry walls, whereas the horizontal structures are made of either wood (beam floors and vaulted ceilings) and tuff masonry (vaults).

The roofing structures are generally made of trusses and tiles. All the trusses were originally made of timber, but some of them, due to the weather degradation and some accidents occurred during time, have been recently substituted by trusses made of either reinforced concrete, steel or laminated timber (Fig. 2.7).

At the 3rd level the horizontal floor are timber beam floors, whereas between the 3rd and 2nd floors there are generally false ceiling, which reduce the significant (about ten metres) high of the hall. They are realized by both vault or in plane wooden structures suspended to the floor above (Fig. 2.8).

Both masonry vaults, realized by barrel shape and complex timber structures, composed by beam floors and false vaults connected each other, are located at the 2nd level of the building (Fig. 2.8). In particular, almost the timber systems cover the halls of the Historical Apartment, which will be object of an in depth description in the next sections of the present work.

At the ground floor the horizontal structure are made of tuff masonry crossing vaults. With regard to the foundations, according to the constructional practice of the age relating to the tuff masonry buildings, vertical walls basements were simply obtained by tuff rock blocks, rising at the basement with very large width. In some cases, where caves were situated, arch and vaults masonry structures were realized for horizontally connecting and stiffening the vertical walls each other.

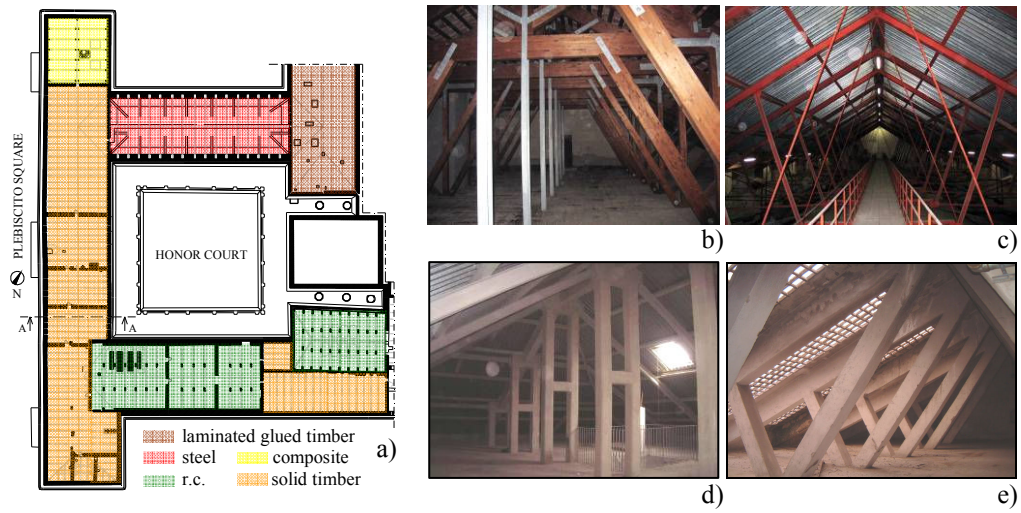

Figure 2.7. The Royal Palace of Naples – Roofing structures: a) Laminated glued timber; b) Steel; c) Composite; d) R.c.

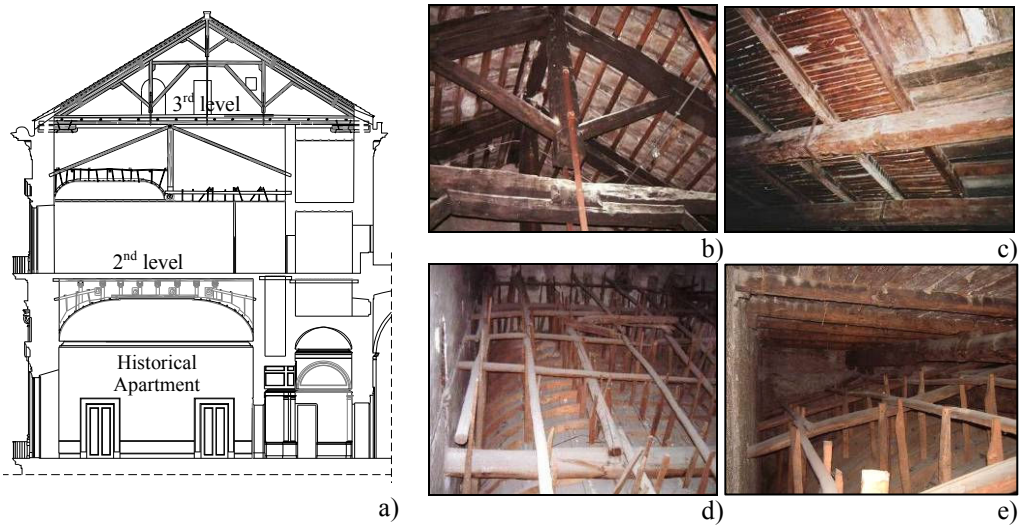

Figure 2.8. Royal Palace of Naples – Timber structures: a) Section A-A; b) Roof trusses; c) Beam floor at 3rd level; d) Vaulted ceiling at 3rd-2nd level; e) Complex structure at 2nd level.

2.5 THE TIMBER STRUCTURES OF THE HISTORICAL APARTMENT

2.5.1 *Structural identification*

The Museum of the Historical Apartment of the Royal Palace of Naples is housed in the noble nucleus of the building, located at the first floor, around the Honour Court (Fig. 2.9a). The original pictorial and sculptural works, paints, statues and tapestries decorate the historical halls.

Most of the timber covering structures of the halls are complex systems, datable between the XVII and the XVIII centuries, which are an evidence of the past construction applications and technologies in monumental buildings.

The timber structures were generally realized by means of a composition of two different sub-structures, such as the floor beam, whose function is to bear vertical loads, and the light vault or vaulted ceiling, as the supporting skeleton of the reed laths, lined at the intrados with a coat of lime and plaster, as a base of the stucco. The vault structure is made of timber grid elements, ribs and splines, shaped as a reversal boat keel. Generally ribs are composed by three parts, placed side by side, with variable heights, nailed together. The rib curvature is conferred by connecting elements of different length, so that they realize a broken line. Four main ribs are placed at the vault corners.

Wherever the spans between the perimeter masonry walls are small, the false ceilings were erected as self-bearing vaults. In the other cases, the vaults were connected and partially suspended to the upper floor structures by means of wooden links.

After all, during the survey, three different structural typologies have been detected (Fig. 2.9b, c): 1) the self-bearing vault, it leaning on the perimeter masonry walls only; 2) the vault linked to the floor beam above; 3) the vault linked to an ad-hoc supporting structure independent from the floor.

With reference to the surveyed covering systems of the Historical Apartment, only the behind rooms structures (XXVI, XXVII, XXVIII, so-called Queen Passage Halls) belong to the first typology. The roofing structures of both Diplomatic Hall (II) and Throne Hall (VI) belong to the second type, while all other timber coverings belong to the third one. Peculiar case is the vaulted ceiling of the Guard Room (XXIX).

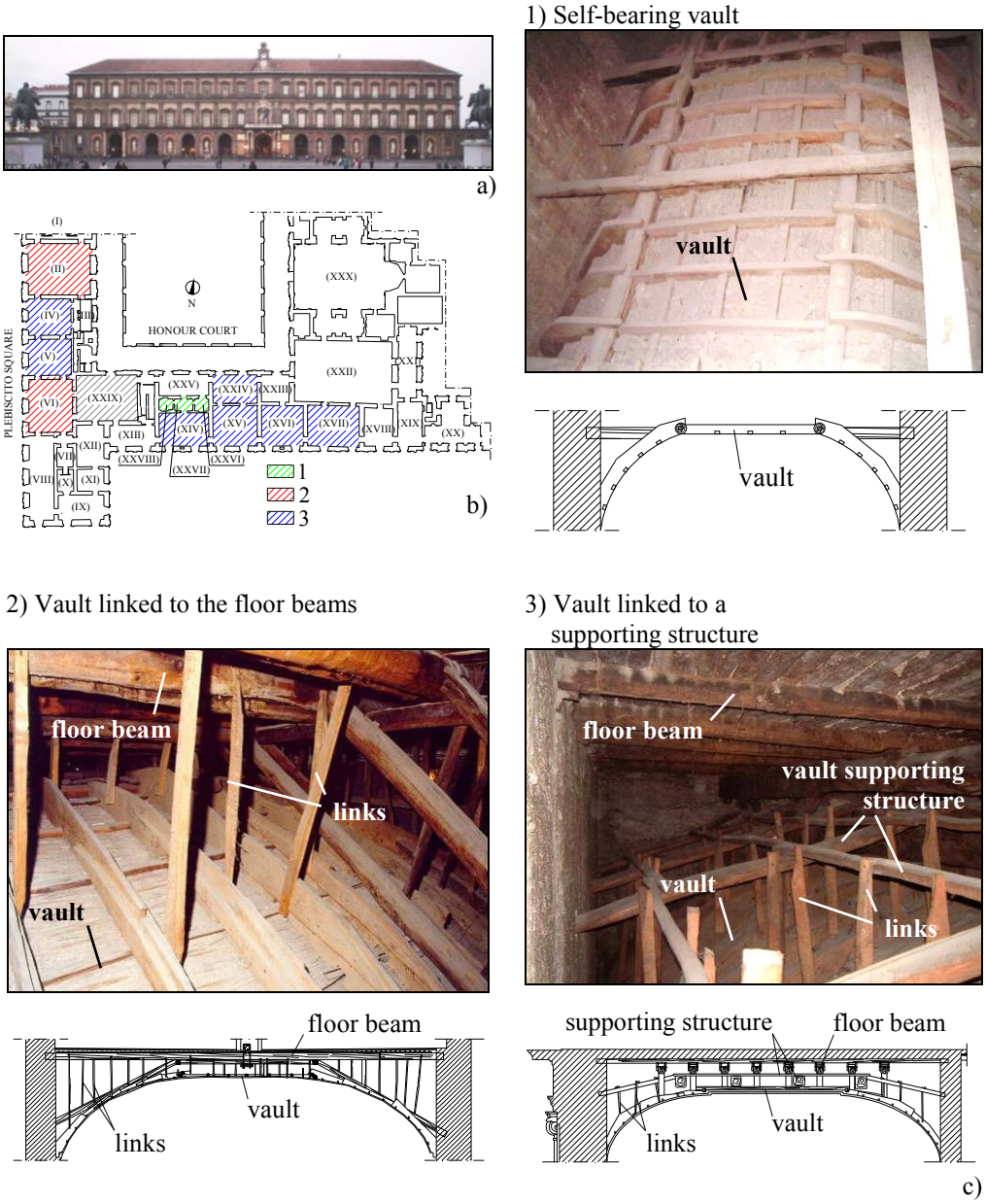

Figure 2.9. Historical Apartment: a) Main façade on Plebiscito Square; b) Plan layout; c) Typologies of the covering timber structures.

2.5.2 *Methodology of analysis*

2.5.2.1 Foreword

In the restoration field of the ancient timber structures, universally recognized procedures do not exist, but it can be made reference to common methodologies. With regards to the timber structures of the Historical Apartment of the Royal Palace of Naples, retrofitting interventions have been identified on the basis of a wide analysis which has developed through the following steps:

1. *Geometrical survey*, including the identification of the structural scheme by means of *in situ* inspections;
2. *Failure diagnosis*, for the evaluation of material defects and deterioration degrees, together with the mechanical properties of old timber elements by means of *visual grading*;
3. *Structural modelling*, for the definition of geometrical, mechanical and loading model;
4. *Numerical analysis*, for the evaluation of the structure capability, carried out according to the current codes;
5. *Identification of the appropriate retrofitting intervention* among the possible ones, considering the characteristics of the existing systems and the required performance after the restoration.

In the next sections, the attentions is focused on three cases study, which are: 1) the complex roofing structure of the Diplomatic Hall (II); 2) The covering structure of the Third Anteroom (V); 3) The vaulted ceiling of the Guard Room (XXIX; Fig. 2.9a).

2.5.2.2 Geometrical survey

Essential aim of this first analysis is the identification of the kind of hierarchic organization existing between the structural systems, the units, the members and the connections, as well as the relations between the same components and the other parts of the building. Furthermore, a great importance is given to the detection of the changes in the behaviour of the

structure, such as alterations, which have been introduced to the initial configuration, the degradation occurred, the consolidation interventions.

By means of *in situ* investigations the geometrical survey has allowed to identify the peculiar configuration of the timber structures under study and to recognize the shapes, sizes and position of each structural element and members components (beams, links, vault grid elements, etc.), which occupy a defined part of the tri-dimensional space. Concerning the joists and connections, it was essential to determine design, nature, degree of movement freedom they allow to the concurring members, effectiveness and efficiency.

The investigations have been integrated by means of photographic survey, which helped to clarify the structural identification of the detected complex systems.

2.5.2.3 Failure diagnosis and visual grading

Preliminary *in situ* diagnostic inspections were carried out in order to evaluate the environment conditions of the timber structures, to evidence the presence on the members of natural defects, damage and decay situations and, at the same time, to characterize the elements as respect the wooden species and mechanical properties by means of visual grading.

Concerning the environment conditions, several factors, which have great influence on the conservation of the structure, have been detected. Humidity in the bearing walls at timber beams supports, the lack of aeration and ventilation at the blank between the ceiling vaults and the above sub-structures, occasional factors, as condensations, exposure and malfunctioning of the gutters, have often damaged the base material and, in same cases, caused water infiltrations in diffuse zones of the vaults stucco. Therefore, some elements are locally rotten or subjected to biological attacks and, in any case, degradations of the decorations at the vaults intrados are visible.

Furthermore, the location and extent of defects and alterations, such as knots, shakes, fibre deviation, insect attacks and biological damage, together with typical failure patterns due to structural anomalies, such as cracking for overstress, large deformations induced by long duration loads or structural imperfections, connection degradation, have been identified.

By means of visual inspection, the structural elements were classified by species and by mechanical properties, according to Italian codes (UNI 11118

and UNI 11119, 2004). In particular, with regards to the wooden species identification, the beam floors and the vault supporting structures elements are predominantly made of chestnut, which is an hardwood largely used in the South of Italy; whereas the timber skeleton of the vault and the links are made of poplar, which is a lighter wood.

2.5.2.4 Structural modelling

On the basis of the acquired knowledge of the structures obtained during the geometric and mechanical survey, three-dimensional FEM models have been set-up aiming at evaluating the bearing capacity of each structural component and its contribution to the behaviour of the whole structure.

The structural modelling has included the definition of the geometrical model, the loading conditions and the material mechanical properties.

Generally, due to high level of variability and irregularity, which is peculiar of the ancient timber systems, the geometrical models are necessary affected by some approximation, in particular relating to the elements shapes and connection types. It simplifies the structural rendering without preserving the real mutual contribution of each sub-structure to the overall behaviour of the complex. 3D models have been implemented by using the software for structural calculation SAP 2000 v. 9.1.6 (Wilson, 1998).

In order to go along the stress and strain states during the service life of the structures from the beginning until today, it was necessary to analyzed different load conditions, which the structure was supposed to have undergone, starting from the ones corresponding to the successive erection stages until the service load condition. In this perspective, different phases and corresponding structural models have been identified.

With regards to the load analysis, for the vault the permanent load is due to the contribution of the lathing, the stucco and the plaster. The total thickness of the layer is about 7 cm. Altogether the unit weight can be considered as equal to 16 kN/m^3, corresponding to 1.12 kN/m^2. Such load has been applied as a distribution of forces concentrated at the grid nodes, adopting the criterion of the influence area enclosed between the spanning of ribs and splines.

For the beam floors, considering that the rooms above the Diplomatic Hall (II) had a residential use destination and the rooms at the second floor above the other Halls of the Historical Apartment have a office use destination, the

permanent load on the frames of timber beams is due to the contribution of the structural and non-structural weights, including the partition walls. The floor slab is composed by planks with a semi-circular cross-section, so-called "panconcelle", over which a layer of lapilli and cement lime mortar, so-called "caldana", is cast. The thickness of this layer was measured at the upper side of the floor slab during the phase of demolition of the non-structural parts of the covering structure of the Diplomatic Hall (II), in view of its consolidation intervention. For the covering structure of the Guard Room (XXIX), on the floor beams, located above the vaulted ceiling and below the r.c. roofing structure of the Palace, the permanent actions are due to both the dead load of the elements and the plank.

The variable actions are determined on the basis of Eurocode 1 specifications (EN 1991-1-1, 2002). In Table 2.5 the loading analysis is given for unit dead load (G_1), permanent (G_2) and variable actions (Q). In addition, vertical seismic actions are considered according to OPCM 3431 (2005), which was the Italian reference code at the time of the performed analysis of the timber structures under study.

Table 2.5. Structural modelling – Load analysis: vault and floor.

Load	**Vault**	kN/m^3	kN/m^2	**Floor**	kN/m^3	kN/m^2
Dead (G_1)	Poplar timber	4.7		Chestnut timber	5.5	
Permanent (G_2)	Stucco and plaster (7 cm thick)	16	1.12	Planks (4 cm thick)	6	0.24
				"Caldana" (20 cm thick)	20	4.00
				Floor rough (2 cm thick)	18	0.36
				Tiled floor (2 cm thick)	20	0.40
				Partition walls		1.00
Variable (Q)				Hall II and V		2.00
				Hall XXIX		1.00

Concerning the mechanical characterization, timber is modelled as cylindrical orthotropic material. As it is usual, the elastic modulus along the parallel to the grain direction is considered equal in tension and in compression. The assumed mechanical properties are summarized in Table

2.6, where γ is a mean value of wood density (UNI 11035-2), E_0 and E_{90} are the longitudinal and transversal moduli of elasticity, $G_{0,90}$ and G_{90} are, respectively, the shear moduli in the parallel-perpendicular to grain planes and in transverse plane, ν_0 and ν_{90} are, respectively, the Poisson's ratio in longitudinal and transverse direction, according to technical literature (Giordano, 1996).

It is worth noticing that, for the structural models related to the erection phases of the structure the material is modelled as "new timber", assuming the mechanical properties according to Italian standard (UNI 11035-2, 2004). Whereas, considering that the timber could be affected by degradation and working lacks during the service life of the structure, the material is modelled as "ancient timber" in the phases related to the present state. Therefore, the consequent stiffness reduction of the structural members has been considered by assuming the mean modulus of elasticity in longitudinal direction (E_0) corresponding to the strength class of third category, according to UNI 11119. For ancient timber the other moduli, E_{90}, $G_{0,90}$, G_{90}, are determined considering the same ratios between each modulus and the longitudinal one (E_{90}/E_0; $G_{0,90}/E_0$; G_{90}/E_0) as for new timber. In this way the mechanical properties of ancient wood correspond to about a 25% reduction as respect to the new material.

Table 2.6. Structural modelling: mechanical properties of "new timber" and "ancient timber".

Species	**Timber**	**γ**	**E_0**	**E_{90}**	**ν_0**	**ν_{90}**	**$G_{0,90}$**	**G_{90}**
		kg/m^3	N/mm^2				N/mm^2	
Chestnut	New timber	550	11000	730	0,37	0,46	950	250
Poplar	(UNI 11035-2)	470	8000	530	0,38	0,47	500	180
Chestnut	Ancient timber	550	8000	530	0,37	0,46	690	182
Poplar	(UNI 11119, III)	470	7000	464	0,38	0,47	438	156

2.5.2.5 Numerical analysis

The analysis of the structural behaviour has evidenced the weaknesses of the structure in terms of resistance and deformation capabilities. The Ultimate and Serviceability Limit States safety checks have been performed according to Eurocode 5 (EN 1995-1-1, 2004), combining the permanent (G) and variable (Q) actions according to Eurocode 1 (EN 1991-1-1, 2002).

The first step of the structural analysis is devoted to evaluate the overall deformation, deriving from the complete erection of the whole timber structure or of each structural unit, such as vault and floor beam. As a consequence, the analysis at each erection stage has been performed, so that the evolution of deflections from the beginning to the end of the installation can be followed. In this first step the material is modelled as "new timber", this assumption being reasonable at the time of the original erection. Aiming at evaluating the actual deflection state, three effects have been considered: 1) the reduction of the elastic modulus due to the degradation typical of ancient timber; 2) the creep, such as the material strain at constant load; 3) the moisture content of the material. In particular, the increment of deformation, during the service life of the structure, due to the combined effect of material degradation and creep, has been taken into account by amplifying the instantaneous deformation, according to EC5 for the worst climatic condition.

As example, the expressions for deformations calculation at the erection phases and at the present state of the timber structures are following reported.

Erection phases (new timber):

- *Complete structure*:
  $u = u_{inst,G}^{N}$
- *Complete structure in service conditions (new timber)*:
  $u = u_{inst,G}^{N} + u_{inst,Q}^{N}$

where:

- $u_{inst,G}^{N}$ and $u_{inst,Q}^{N}$ are the instantaneous deformations due to permanent (G) and variable actions (Q) respectively, evaluated using the mean value of stiffness modulus of new timber (N).

Phases at the present state (ancient timber):

- *Complete structure*:
  $u_{fin} = u_{inst,G}^{N} + k_{def}(u_{inst,G}^{A} + \psi_2 u_{inst,Q}^{A})$
- *Complete structure in service conditions (ancient timber)*:
  $u_{fin} = u_{inst,G}^{N} + k_{def}(u_{inst,G}^{A} + \psi_2 u_{inst,Q}^{A}) + u_{inst,Q}^{A}$

where:

- $u^{A}_{inst,G}$ and $u^{A}_{inst,Q}$ are the instantaneous deformations due to permanent (G) and variable actions (Q) respectively, evaluated using the mean value of stiffness modulus of ancient timber (A);
- k_{def} takes into account the increment of deformations, during the service life of the structure, due to the combined effect of moisture and creep. In fact, it is associated to the service class of the structure which is characterised by the moisture content in the material and the climatic conditions (EN 1995-1-1, 2004; Table 2.7);
- ψ_2 is the factor for the quasi-permanent value of variable actions (EN 1991-1-1, 2002).

Table 2.7. Service classes and corresponding k_{def} values for solid timber (EN 1995-1-1, 2004).

Service class		**k_{def}**
1	It is characterised by a moisture content in the materials corresponding to a temperature of 20°C and the relative humidity of the surrounding air only exceeding 65% for a few weeks per year.	0.60
2	It is characterised by a moisture content in the materials corresponding to a temperature of 20°C and the relative humidity of the surrounding air only exceeding 85% for a few weeks per year.	0.80
3	It is characterised by a climatic conditions leading to higher moisture contents than in service class 2.	2.00

On the basis of the climatic condition, evaluated measuring the relative humidity and temperature, the structures under study were assigned to the third service class; therefore the factor k_{def} is assumed equal to 2.

Concerning the Serviceability Limit State (SLS) safety checks, according to EC5, the deflections (w_{fin}) of the beams on two supports should be limited within the value (w_{lim}) equal to L/350, where L is the beams span.

The structural analysis at each erection stage has been performed, in order to reproduce the stress state of each structural complex. Therefore, the evolution of stresses from the beginning to the end of the installation has been analyzed.

The duration of the load and the moisture content of wood influence the material strength properties. This effect is considered by assuming a reduction

factor k_{mod} for the determination of the design strength, calculated using the following equation, according to EC5:

$$f_d = k_{mod} \frac{f_k}{\gamma_m}$$

where:

- f_k is the characteristic value of the strength property;
- γ_m is the partial factor for the material property, equal to 1.3 for solid timber;
- k_{mod} is the reduction factor defined as a function of the load duration class and of the service class of the structure. For load combinations including loads of different duration, the k_{mod} corresponding to the shorter duration should be assumed (Table 2.8).

Table 2.8. Values of k_{mod} for solid timber (EN 1995-1-1, 2004).

Service	**Load-duration class**				
class	*Permanent*	*Long term*	*Medium term*	*Short term*	*Instantaneous*
1	0,60	0,70	0,80	0,90	1,10
2	0,60	0,70	0,80	0,90	1,10
3	0,50	0,55	0,65	0,70	0,90

For strength and stability checks according to Ultimate Limit State (ULS), the k_{mod} factor is assumed equal to 0.50 in the *complete structure* phases, when only permanent load (G) are considered, and to 0.65 in *complete structure in service conditions* phases, when both permanent and variable action (G+Q) are applied. With reference to the relevant stress conditions, the characteristic and design strength values for chestnut and poplar timber are listed in Table 2.9 and 2.10 respectively, according to UNI 11035-2 standard.

Table 2.9. Characteristic and design strength values for chestnut timber (EN 1995-1-1, 2004).

Stress condition	**Characteristic strength** [N/mm^2]		**Design strength** [N/mm^2]	k_{mod} = 0.50	k_{mod} = 0.65
Compression // to grain	($f_{c,0,k}$)	22	($f_{c,0,d}$)	8.5	11
Tension // to grain	($f_{t,0,k}$)	17	($f_{t,0,d}$)	6.5	8.5
Bending	($f_{m,k}$)	28	($f_{m,d}$)	10.8	14
Shear	($f_{v,k}$)	2	($f_{v,d}$)	0.8	1

Table 2.10. Characteristic and design strength values for poplar timber (EN 1995-1-1, 2004).

Stress condition	**Characteristic strength** [N/mm^2]		**Design strength** [N/mm^2]	k_{mod} = 0.50	k_{mod} = 0.65
Compression // to grain	($f_{c,0,k}$)	22	($f_{c,0,d}$)	8.5	11
Tension // to grain	($f_{t,0,k}$)	16	($f_{t,0,d}$)	6.2	8
Bending	($f_{m,k}$)	26	($f_{m,d}$)	10	13
Shear	($f_{v,k}$)	2.7	($f_{v,d}$)	1	1.4

2.5.2.6 Restoration interventions

Generally, the consolidation systems of the timber structures can be grouped in two main typologies:

1. Upgrading the structural behaviour through strengthening and stiffening;
2. Restoring of static function due to biological or structural degradation, required for insect and/or fungi attacks, joint failure, cracks for overstress, etc.

Moreover, the intervention can be local or global; in the first case it concerns a single element or its part, while, in the second case, it concerns the whole structural complex.

Examples of local interventions are the following ones:

- *Stiffened impregnation*, which consists of introducing binder substance in the timber element with the purpose to increase the mechanical characteristics. Te used materials are natural, polyurethane or acrylic resins.
- *Injection of fluid resin* at opportune pressure until the saturation of the cavities. This local intervention aims at repairing cracks and discontinuities

within timber members and improve their mechanical properties. The injections are done in fit holes realized perpendicular or parallel to grain, because of the permeability along the grain. The used resins are epoxidic bi-component or acrylic in solvent dispersion. During the application the forming of air bubbles should be avoid.

- *Metallic or wooden plats*, which consist of applying metallic plates or wooden planks underneath the damaged beam for increasing the member strength and stiffness. The added elements can be glued by resins or nailed to the existing beam.
- *Realization of prosthesis* by epoxidic resin or by glued timber, which are used, for example, in the case of joints completely damaged by fungi or insect attacks. It is realized by resin conglomerate casted in fit frameworks or by a new wood element, which reproduce the substituted part, connected to the healthy part by means of fiber glass reinforced rebars fixed in the predisposed holes by resin.

Examples of global interventions on the whole structure are:

- *Substitution of existing elements with new ones*, preferably of the same species;
- *Increment of both stiffness and strength*, introducing new constraints between elements. For the beam floor, as an example, it is possible to add one or more transversal secondary beam (metallic or wooden beam) in the middle span, for reducing the span of the primary floor beams.
- *Realization of a composite timber-concrete system for the floors*, when the existing structure has both inadequate stiffness, with consequent unacceptable deformations, and inadequate strength, or when the beam floor does not accomplish the function of a rigid diaphragm in its plane late when subjected to horizontal forces. In composite slab the timber beam is connected to a concrete slab, so that the timber mainly resists to tensile forces and the concrete to compressive ones, generated by flexure. The common used connectors are screws, nails, studs or special device ad hoc conceived.
- *Stiffening of the nodal joints,* which consist of both placing metallic elements at both sides of the joint and nailed each other, and substituting damaged parts aiming at restoring the functionality and the required stiffness.

The surfaces must be smooth and the elements concurrent in the joint must be coplanar. Often this intervention is covered by paint or wooden elements for aesthetic reasons.

With regards to the timber structures of the Historical Apartment under study, the supplied indications by numerical analysis, about the critical parts of the units, have allowed the identification of the appropriate restoration interventions, whose design was subjected to the achievement of predetermined objectives, including:

- *Maximise the retention of original material*, limiting the changes in order to respect the authenticity and preserve the historical and cultural value of the ancient structures;
- *Allow the original form to be seen*, due to the fact that the significance of the structure lies in the material and its configuration;
- *Upgrading and retrofitting* of the structures according to the current regulations;
- *Consider reversible remedial interventions,* which should leave the existing structures essentially unmodified, removing or replacing the repairs if required and allowing the control, monitoring and maintenance of the whole work in the time. In this way, the interventions should be based on the use of the so-called mixed technologies, consisting in the combination of techniques, which use different materials, such as new wood, steel, reinforced concrete, etc., for realizing local strengthening systems of the existent structures. The prerogatives of such retrofitting technologies are the reversibility of materials, the lightness, the ductility, the easiness of supply, transportation and erection.

2.6 THE COMPLEX ROOFING STRUCTURE OF THE DIPLOMATIC HALL (II)

2.6.1 *Geometrical survey*

The roofing structure of the Diplomatic Hall (II), is composed by a complex floor slab-vault structural system and belongs to the second structural typology (see chapter 2.5.1). Therefore, the timber vault elements are connected and partially suspended to the upper floor by means of wooden links. In particular, the structure is composed by three main units (Fig. 2.10): 1) vaulted ceiling (V); 2) floor beam (F); 3) truss (T).

It is worth noticing that at present a structural restoration has been required by the noticeable state of damage of the frescos at the vault intrados, which has an important artistic value it being painted by Francesco De Mura (1696-1782) (Mazzolani *et al.,* 2009).

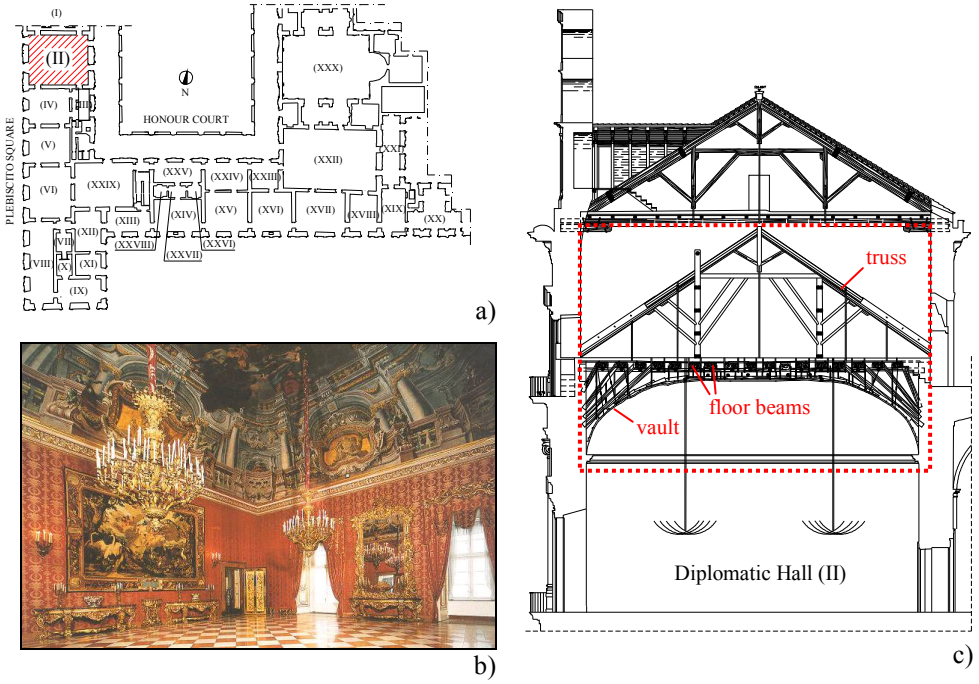

Figure 2.10. Diplomatic Hall (II) – Geometrical survey: a) Plan layout; b) Internal view; c) Structural section of the Royal Palace at the Hall II location.

V: Vaulted ceiling (Fig. 2.11)

The vaulted ceiling covers a rectangular surface 16.80×14.20 m^2 sized. The structure skeleton is made of a grid of timber elements, ribs and splines, which constitute the ceiling skeleton of the hall. Ribs have rectangular sections, 4 cm thick and 5 to 20 cm high and are located at variable span. They simply abut to the perimeter masonry walls, whereas they are nailed at the ends at the vault crown. Splines (3×4-6 cm^2) are orthogonal to ribs, with the same span as the ribs in order that they form a square grid. The horizontal part at the vault crown is realized by a rectangular grid of timber elements with circular section (8-12 cm diameter), which are nailed one each other at the intersection points and enclosed in a perimeter rectangle. The wooden links are nailed at both ends, upside to the primary floor beams and downside to the ribs. In view of the retrofitting intervention, the vault was propped up by provisional supports.

F: Floor beam (Fig. 2.12)

The primary frame of timber beams is arranged along the minor span and almost equally spaced. Each beam is composed by two wood stocks placed side by side at the mid-span for about 5 m superposition length, connected one each other by four 1.50 m equal spaced nails. Only one large beam is shaped with a rectangular cross-section 48×38 cm^2, being a single member along the whole span. The floor beam is stiffened by means of three different systems: 1) longitudinal secondary beams set under the primary beams (12 cm diameter), parallel to them and connected to longitudinal inclined struts (12 cm diameter), forming a supporting portal frame, which the wooden links of the vault are connected to; they are placed at the beams, with the exception of three alignments of beams near the perimeter masonries; 2) two transversal secondary beams (12 cm diameter), orthogonal to the primary beams; 3) a system of three series of four transversal inclined struts arranged in planes perpendicular to the primary beams axes, located at their central part near the transversal secondary beams and the tie beam of the truss. Near the façade wall, at the middle span of the floor there's a system of five secondary beams, equally spaced about 0.50 m and spanning from the masonry wall to the second primary beam. The connection between the primary beams and the

secondary ones is done by means of metallic stirrups. Probably such system has been installed for the need to locally stiffen the floor.

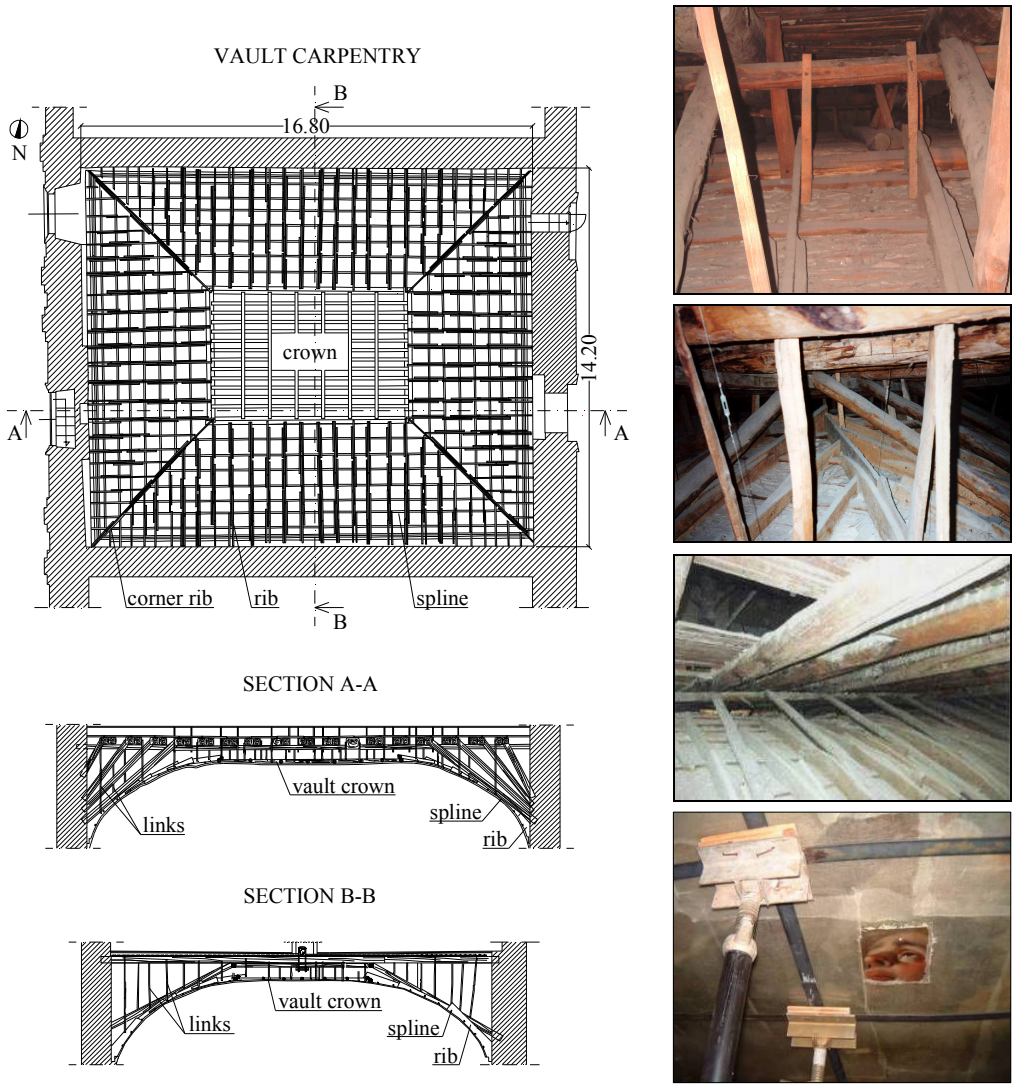

a) b)

Figure 2.11. Diplomatic Hall (II) – Geometrical survey – Vault structure: a) Carpentry and structural sections [m]; b) Photographic survey.

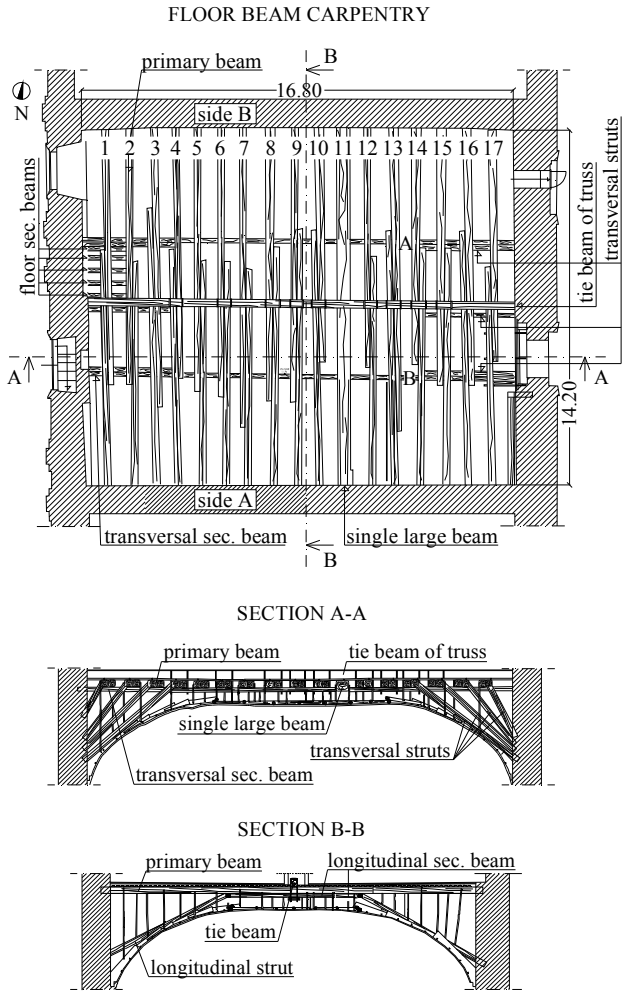

a)

b)

Figure 2.12. Diplomatic Hall (II) – Geometrical survey – Floor beam structure: a) Carpentry and structural sections [m]; b) Photographic survey.

T: Truss (Fig. 2.13)

The truss was discovered after the demolition of the partition walls in which the structure was enclosed. It close to he middle span of the floor slab,

orthogonal to the primary floor beams. Its struts are composed by different wooden stock' parts, placed side by side and nailed one each other, with a variable cross section along the element axis. The tie beam is connected to some floor beams by means of metallic U shaped stirrups. The structure is composed by two queen posts with a composite cross-section, whose parts are connected to the queen posts, a central king post with one order of connected struts. Two heavy chandeliers of the Diplomatic Hall are hung to the tie beam.

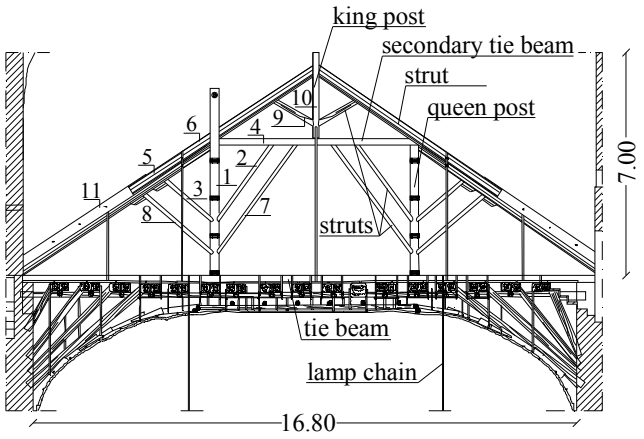

Sections [cm]			
n.	Type	n.	Type
1		6	
2		7-8	
3		9	
4		10	
5		11	

a)

b)

Figure 2.13. Diplomatic Hall (II) – Geometrical survey – Truss structure: a) Section A-A [m]; b) Photographic survey.

2.6.2 *Failure diagnosis and visual grading*

A structural identification of all elements of the vault, beam floor and truss was carried out by means of visual inspection (Level I), aided by non-destructive evaluation (Level II), using resistographic technique, only for the floor elements. The diagnostic analysis was performed by IVALSA (Istituto per la VAlorizzazione del Legno e delle Specie Arboree; CNR).

The members were classified by species and mechanical properties, according to UNI 11118 and UNI 11119, respectively.

As a result, the vault elements are made of poplar; the floor beam are in chestnut wood, apart from the beams n. 11 and n. 17 which are made of pine and white fir, respectively; the truss elements are in chestnut wood.

The Level I inspection of the vault and the truss elements highlighted the inefficiency of some connections at the vault crown location and the complete deterioration of the truss strut, supported by the façade wall, due to water seepage (Fig. 2.13b).

For the beam floor elements, the Level I and II inspection has evidenced what follows:

- The length of the beams support at the masonry wall is about 10-15cm only, causing for the beams n. 4, 5, 6, 7, 8 the overstress of the supporting walls (Fig. 2.14a);
- Some previous both fungi and insect (Anobidi and Termites) attacks to the sapwood are apparent, where the humidity content is larger then 13%, and typical widespread ring shakes are present on all the elements (Fig. 2.14b);
- The resistographic investigations evidenced that three beams (15A, 17A, 11B) have the cross section reduced due to past insect attacks;
- The pine beam adjacent to the Court Theatre is at risk of biological attack at the end, because it has higher humidity content (23%), probably owing to the infiltration of water from the toilets of the premises above to the wall which supports it;
- The secondary transversal beams are not realized by a continuous element, but they are interrupted at the pine beam (17) location and at the middle span where they are connected to the adjacent part by means of a “flute beak” connection;

- The beam 1A adjacent to the west façade is completely dug owing to the water seepage (Fig. 2.14c);
- The nailed connections among the elements are often inefficient (Fig. 2.14d);
- The beam 5A is collapsed due to bending overstress (Fig. 2.14e);
- The longitudinal struts 8B and 10B are collapsed because of compression overstress (Fig. 2.14f).

Figure 2.14. Diplomatic Hall (II) – Failure diagnosis: a) Beam support; b) Ring shakes; c) Beam 1A damage; d) Disconnection among elements; e) Beam 5A collapse for bending overstress; f) Strut crushing for compression overstress.

The classification of the floor beam elements is summarized in Table 2.11.

Table 2.11. Diplomatic Hall (II) – Visual grading of the beam floor elements (UNI 11119, 2004).

Structural element	**Class**
Beam 3A -4A-8A-9A-10A-12A-14A-16A-17A	I
Beam 1A -7A	II
Beam 2A-6A-10A-11A-13A-15A	III
Beam 2B-7B-13B-14B-16B-17B	I
Beam 1B -4B-6B-10B-11B-12B	II
Beam 3B-5B-8B-9B-15B	III
Secondary beams	II
Longitudinal strut 4A-6A-11A-12A-13A-14A-4B-6B-9B	II
Longitudinal strut 5A-7A-8A-9A-10A-11A-5B-7B-10B-11B-12B-13B-14B	III
Transversal strut 14A2-15A2-16A1-15A2-16A2-14A2-17A2-3B1-4B'-3B2-3B3	I
Transversal strut 16A2-17A2-1B1-2 B1-2 B2-4 B2-1 B3-4 B3	II
Transversal strut 15A3-14A1-15A1-2B3	III

2.6.3 *Structural modelling*

Figure 2.15 shows the extruded models of both each structural unit and whole complex in 3D view (SAP 2000, v. 9.1.6). Due to the high level of variability and irregularity, the geometrical modelling is affected by some approximation, always on the safe side. The assumptions for the main sub-structures, such as the vault, the floor beam, the truss, are following specified (Mazzolani *et al.,* 2004).

V: Vault (Fig. 2.15a, d)

Ribs are modelled as single elements with a rectangular cross-section, 4×15 cm^2, and a broken axis. They are restrained at the extremities by means of hinges, whereas the connection between ribs and splines is modelled as a fixed joint. Considering the high variability of the rib spans a band criterion has been applied, in order to define the ribs inter-axis, by plotting the envelope of each rib, superimposing the four quadrants, where the plan can be divided by the symmetry axes, and using the axis of each band. In this way, the average position of the rib axes is defined, obtaining a symmetric scheme as respect to the symmetry axes. Splines are modelled as elements with rectangular cross-

section, 3×5 cm^2, spanning between the ribs, with almost the same inter-axis as the ribs. They are fixed at the extremities to the ribs. The horizontal central grid at the vault crown is modelled by considering elements with circular cross-section: along the X direction, 8 cm diameter, spanning 35 cm; along the Y direction 10 cm diameter, spanning 1.00 m; at the perimeter 10 cm diameter. The grid elements are restrained at the extremities to the perimeter elements by means of hinges, whereas the connection between orthogonal grid elements is modelled as a fixed joint. The vault-floor beam wooden links are modelled with square cross-section 4×4 cm^2.

F: Floor beam (Fig. 2.15b, d)

Primary beams are modelled by a single element with a circular cross-section of a constant diameter (25 cm, mean value of the actual ones), assuming that the nail connection between the two timber stocks, which compose the beams, provides a fixed joint. The single large shaped beam is modelled with the real sizes. Beams are arranged at the same spacing, 0.95 m, it corresponding to the mean value of the actual distance. The inclined struts and the secondary beams are modelled as elements with a circular cross-section. 12 cm diameter. The system of five secondary floor beams located near the façade wall has been neglected, being limited to a small area. Concerning the restrain conditions, the following assumptions are made: for each floor beam, such as primary and secondary beams and inclined struts, the restrain at the extremities is considered as a simple hinge; the connection between secondary longitudinal beams and primary ones, realized by the system of metallic stirrups, which also embrace the tie beam of the truss, is modelled by a constraint, which allows equal displacements along the X, Y, Z directions and equal rotation around the axes; the connection between secondary transversal beams and primary ones is modelled by a constraint, which allows equal displacements along the X, Y, Z directions and equal rotation around the X axis (considering that the bending stiffness of the floor beam is larger than the torsional stiffness of the transverse secondary beam).

T: Truss (Fig. 2.15c, d)

All structural elements of the truss are modelled with the actual detected cross-section dimensions (Fig. 2.13a).

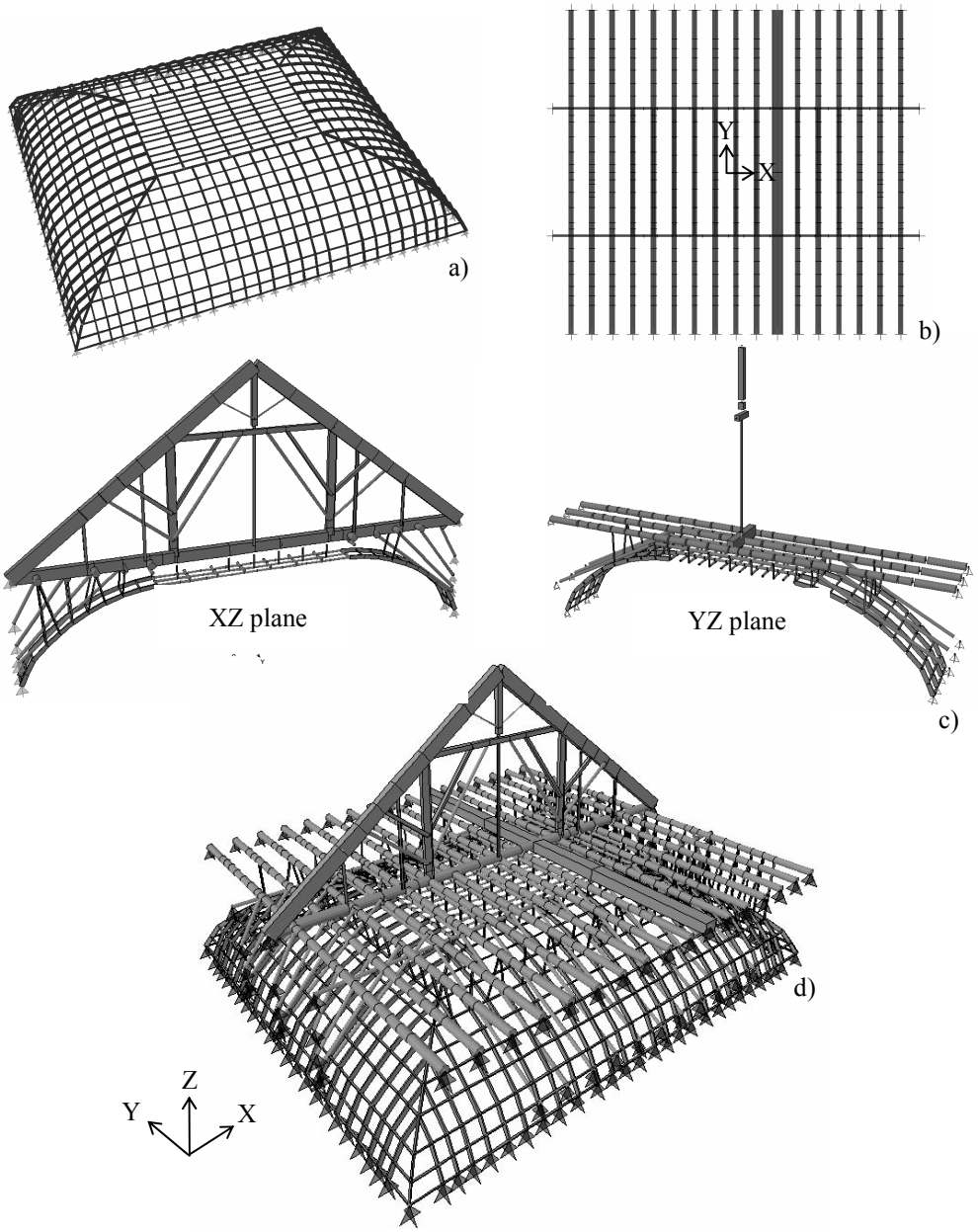

Figure 2.15. Diplomatic Hall (II) – Structural modelling: a) Vault; b) Floor beam; c) XZ and YZ planes; d) 3D model.

Aiming at analysing the behaviour of the structures during their service life, from the beginning until today, the following phases and the corresponding structural models have been identified:

Erection phases (new timber)

- Phase 1: *Erection of the beam floor structure* (Model F1)
  The structure consists of floor beam and related stiffening elements, such as primary beams, secondary longitudinal and transversal beams, longitudinal and transversal struts. Only dead load is considered ($G_{1,\ floor}$);
- Phase 2: *Erection of the truss* (Model F2)
  The structure is integrated by the truss above. Only dead load is considered ($G_{1,\ floor\ +\ truss}$);
- Phase 3: *Erection of the vault structure* (Model V1)
  The vault structure is independent by the existing floor-truss system. Only dead load are applied ($G_{1,\ vault}$);
- Phase 4: *Beam floor completion* (Model F3)
  The geometrical model is equal to Model F2. The beam floor is completed by non-structural elements. Therefore, on the floor primary beams all permanent loads are applied ($G_{1,\ floor\ +\ truss} + G_{2,\ floor}$);
- Phase 5: Vault-Floor connection and vault completion (Model VF1)
  The geometrical model consists of the beam floor, the truss and the vault. The vault is completed by lathing and stucco; therefore, all permanent load are applied on the vault grid too ($G_{1,\ vault} + G_{2,\ vault}$);
- Phase 6: *Complete structure in service conditions* (Model VF2)
  The structure is completed. Both permanent and variable actions are considered for the beam floor ($G_{1,\ floor\ +\ truss} + G_{2,\ floor} + Q_{floor}$).

Phases at the present state (ancient timber)

- Phase 7: *Complete structure* (Model VF3)
  The geometrical and loading model is equal to Model VF1, but the material is modelled as ancient timber, taking into account of the degradation effects during the time;
- Phase 8: *Complete structure in service conditions* (Model VF4)
  The geometrical and loading model is equal to Model VF2, but the material is modelled as ancient timber;

- Phase 9: *Damaged structure* (Model VF5)
  The complete geometrical model lacks of the rotten beam 1, adjacent to the main façade, and it is characterized by the truss partially supported by the floor beams for considering that the truss strut at the main façade side is completely inefficient.
- Phase 10: *Damaged structure in service conditions* (Model VF6)
  On the damaged structure, both permanent (G) and variable actions (Q) are considered.

2.6.4 *Numerical analysis*

The deformation state of the vault was evaluated for making a judgement on the direct effects on the fresco. To this purpose, the history of displacements from the erection of the vault (Model V1), through the connection to the floor beams (Model VF1), with the addition of the serviceability load (Model VF2) considering new timber properties, has been reconstructed. Then the effect of the degradation due to ancient timber, creep and moisture has been considered (Models VF3 and VF4), in order to evaluate the deformation of the vault at the present state, which determined the crack distribution requiring the restoration of the fresco.

In Figure 2.16 the deformed configurations of the vault are depicted, with reference to one of the structure quadrant at a single alignment of ribs where the wooden links, which connect the vault to the floor beams, are located. The reference points are marked with a circle on the vault model plan section. Displacements have been scaled by an amplification factor equal to 5, for evidencing the deformed shape. As it appears, the vaulted ceiling undergoes a generalized flattening, which consists of sagging at the centre with a maximum displacement equal to about 9 cm and elevation near the masonry supports, with a maximum displacement equal to about 2 cm.

In Figure 2.17, together with the crack distribution at the intrados of the vault, the bending moment distribution and the corresponding deformed configuration are drawn with reference to a central YZ structural section.

The results of the stress state analysis and the safety checks emphasize that some ribs of the vault carpentry do not accomplish the strength requirements, due to the fact that the links between vault and floor beams located near the

masonry supports are harmful, they working as struts, then exerting an additional bending action on the vault.

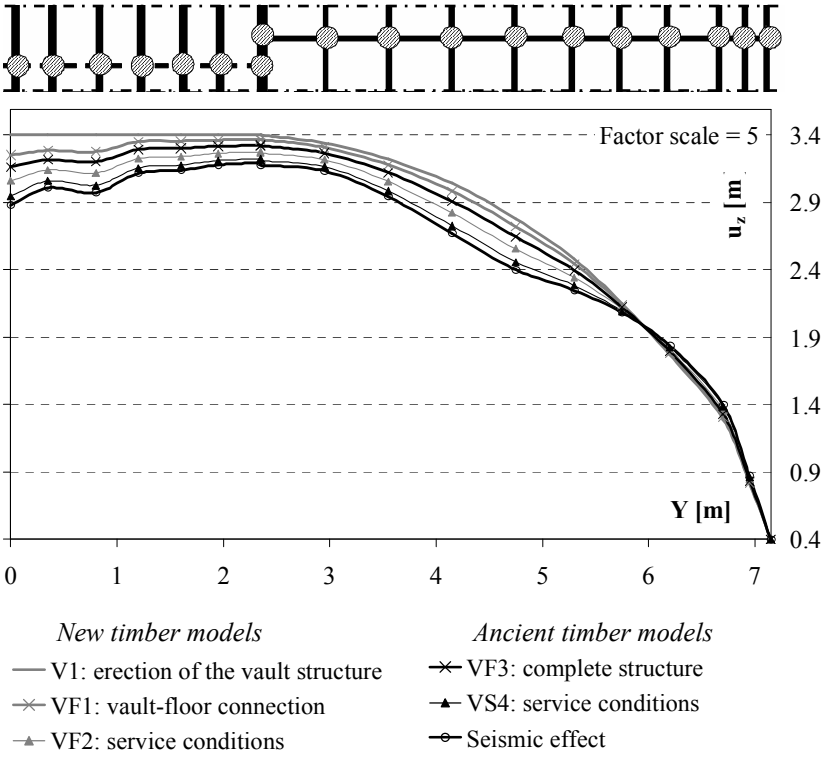

Figure 2.16. Diplomatic Hall (II) – Numerical analysis: deflection state of the vault (YZ section).

With regards to the primary beams of the floor, the results of the analysis are shown in Figure 2.18, where, at each phase of the whole structure, the vertical displacements of the middle sections are represented. It can be observed that the first four beams at each side of the floor, where the transversal struts converge, have a negligible displacement as respect to the other primary beams.

In each erection phase of the structure, when new wood is considered, the beams deflections are insignificant, below 2 cm. On the contrary, the degradation of the material and the time dependent effects of creep and moisture contents (Models VF3 and VF4) induce an important increment of

deflections, especially for the beams not connected to the tie beam of the truss. Therefore the beneficial effect of the truss induces a significant deflections reduction in the connected floor beams. While, the effect of the truss partially supported by the floor, further to the lack of stiffening is a significant increase of the displacements (Models VF5 and VF6), which for the central primary beams, apart from the large beam n. 11, is beyond the safety limit value, equal to about 4 cm (L/350; EN 1995-1-1, 2004).

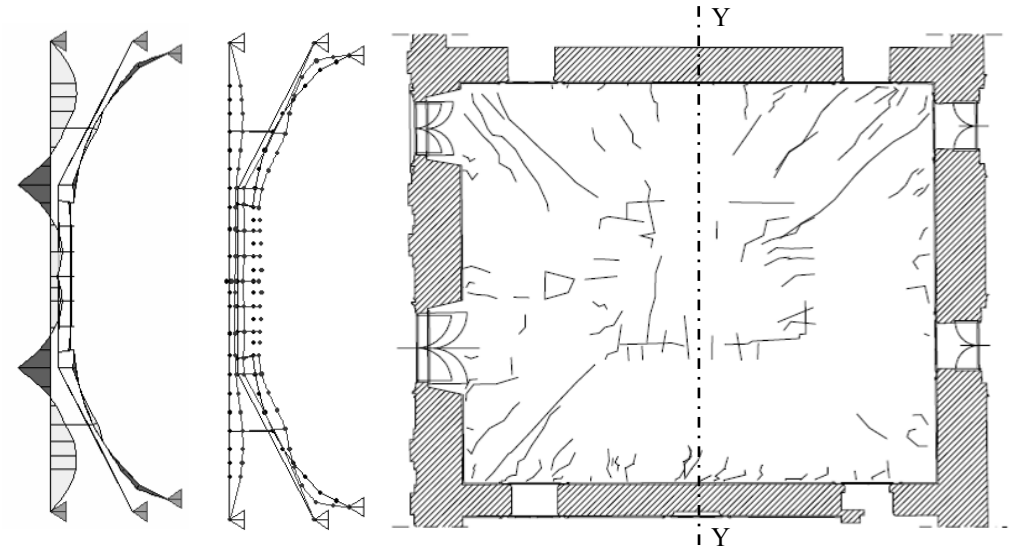

Figure 2.17. Diplomatic Hall (II) – Deflection and stress state of the vault (YZ section):
a) Bending moment distribution and the corresponding deformed configuration;
b) Crack distribution at the vault intrados.

With reference to two typical central sections of the floor-truss-vault system (Model VF3), located in the XZ and YZ planes, Figure 2.19 shows the internal forces distribution in terms of axial force (A), shear force (S) and bending moment (M). In particular, with regards to the beam floor elements, the structural analysis has evidenced that the struts of the beams stiffening systems do not satisfy the stability checks, according to EC5. Whereas, the stress state in all the other structural elements is acceptable.

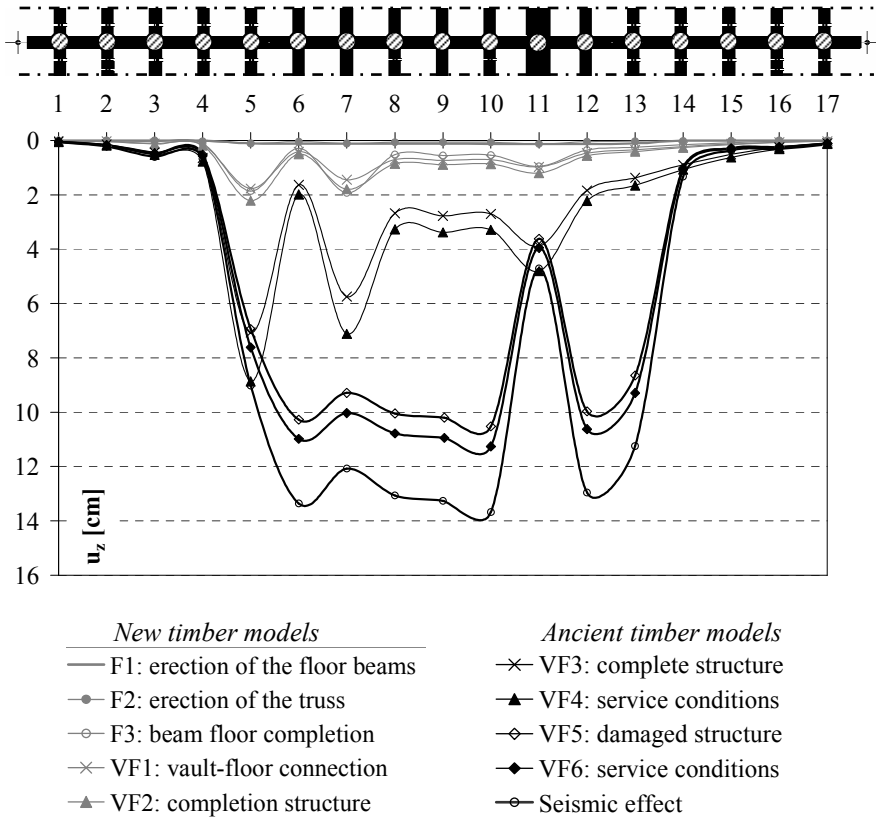

Figure 2.18. Diplomatic Hall (II) – Numerical analysis: deflection state of the floor beams middle sections (X direction).

2.6.5 *Adopted retrofitting interventions*

2.6.5.1 Design requirements

On the basis of the results of the safety checks it has been evidenced that:

- For some beam deflections are beyond the serviceability limits;
- All the floor stiffening struts do not satisfy the stability check;
- The vault undergoes a flattening, consisting of a large sagging at the centre of the vault crown, which caused cracks of the stucco layer at the intrados.

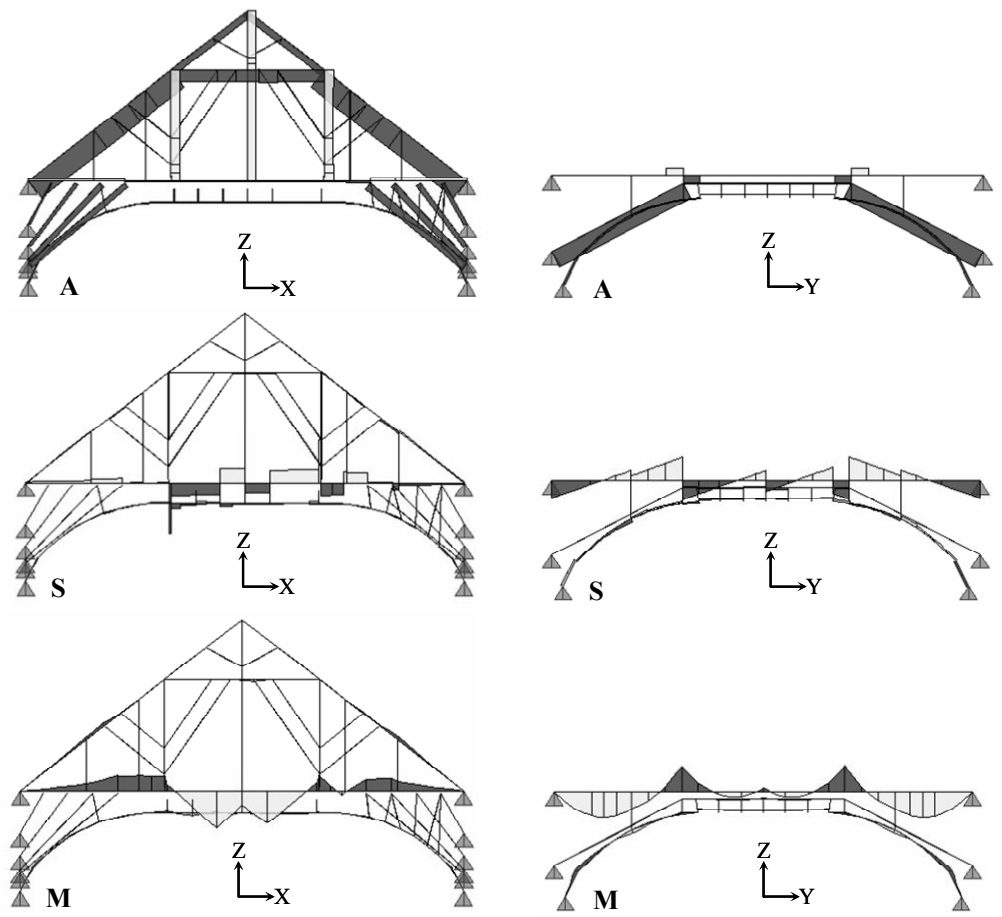

Figure 2.19. Diplomatic Hall (II) – Numerical analysis – Internal forces distribution (Model VF3): a) XZ section; b) YZ section.

As a consequence retrofitting interventions, both local and global, are required, aiming at (Mazzolani *et al.,* 2005; Mazzolani *et al.,* 2009):

- The restoration of the structural safety level relevant to the destination of use of the hall above the Diplomatic Hall;
- The stiffening of the complex vault-beam floor wooden structure for avoiding further damage of the fresco.

2.6.5.2 Vault

For the vault, the retrofitting intervention involves the vault-floor links only. In fact, from the examination of the internal action distribution within the vault structural members, it appears that links between vault and floor beams located near the masonry supports are harmful, they working as struts, then exerting an additional bending action within the ribs. The removal of all these links placed at the vault curved sides induces a strong reduction of the internal actions. As a consequence, the intervention consists in the removal of all the wooden links, replacing them only at the horizontal vault crown by means of steel connections (Fig. 2.20a). They are cables, 3 mm diameter, connected above to UPN profiles and below to the timber elements of the vault crown. The UPN profiles are supported by the timber beams of the floor (Fig. 2.20b, c).

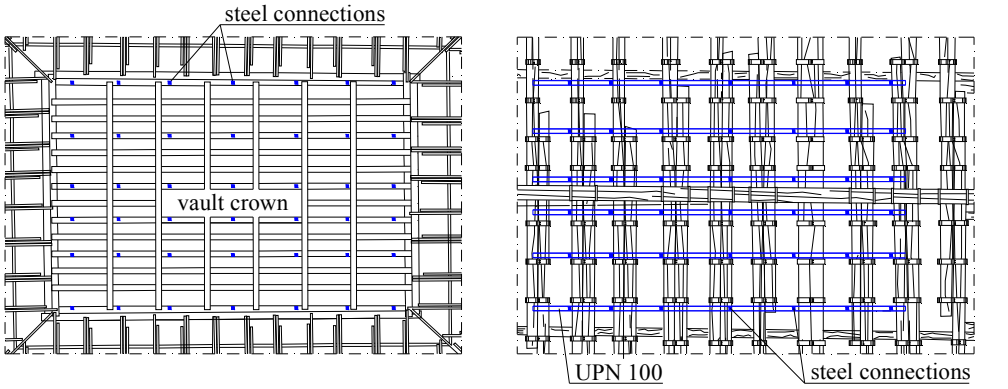

a)

b)

Figure 2.20. Diplomatic Hall (II) – Retrofitting interventions – Vault-floor connection: a) Plan layout; b) UPN profiles disposition; c) Steel cables details. (continues)

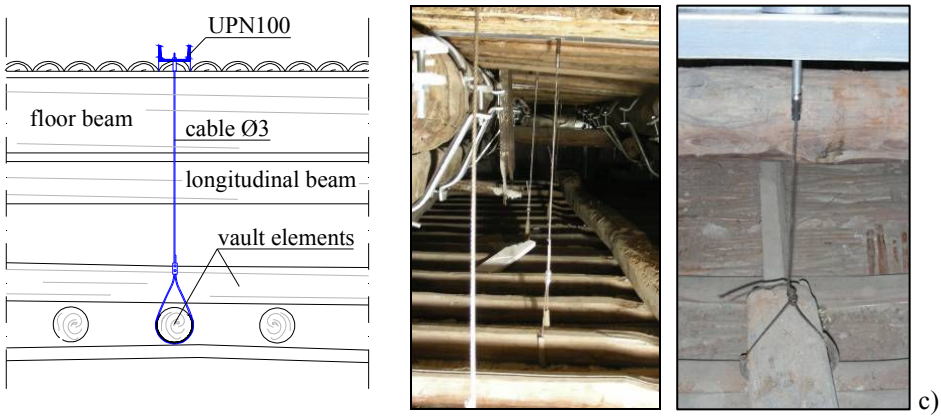

Figure 2.20. Diplomatic Hall (II) – Retrofitting interventions – Vault-floor connection: a) Plan layout; b) UPN profiles disposition; c) Steel cables details.

2.6.5.3 Beam floor

For the beam floor the retrofitting intervention consists of the following systems:

- *Casting of a reinforced lightened concrete slab*, which collaborates with the floor beams by means of a system of steel connectors purposely conceived with an "ad hoc" shape.
  The r.c. slab (1800 kg/m^3 weight; f_{lck}=20 MPa; B450C steel bars) is 20 cm thick, it is lightened by polystyrene blocks, 10 cm high. The slab is reinforced by a net of steel rebars, 6 cm diameter and 20 cm mesh, disposed at the extrados. The concrete slab is cast on fir planks, 3 cm thick, with the function of fix formworks. The wooden planks should be protected from the water of the cast by a plastic film and in any case the water content of concrete should be limited (Fig. 2.21).
  Timber beams - r.c. slab connectors are realized by sleeves, as collars, made of cold formed S275 steel, which are composed by four parts (Fig. 2.22a, b). They have perpendicular drilled wings at the ends and they are connected each other by means of bolted connections between the wings. The vertical superior wings serve as connectors and they are immersed in the concrete cast, it guaranteeing the transmission of the sliding actions (Fig. 2.22b). Therefore, steel sleeves have a twofold function: 1) they exert

a transversal ringing action on the beams; 2) they realize the beam-concrete slab connection without the need to drill the beams. In particular, such connectors do not weaken the cross section and produce a beneficial effect of confinement. Due to the variability of the beams cross-section, in order to avoid to make a number of different sleeve geometries, for the adaptation to the actual beams cross-section, the system is conceived in only three different types and for each type the adaptation is optimized by the interposition of a layer of rubber, which is vulcanized to the steel sleeve in the workshop.
The three different types of connection system have the following features

- A: sleeve for beams with a single circular cross-section (Fig. 2.23a);
- B: sleeve for beams with a single rectangular cross-section (Fig. 2.23b);
- C: sleeve for beams with multiple cross-section (Fig. 2.23c).


a)


b)


c)

Figure 2.21. Diplomatic Hall (II) – Retrofitting interventions – R.c. slab: a) Before the cast; b) During the cast; c) After the cast.

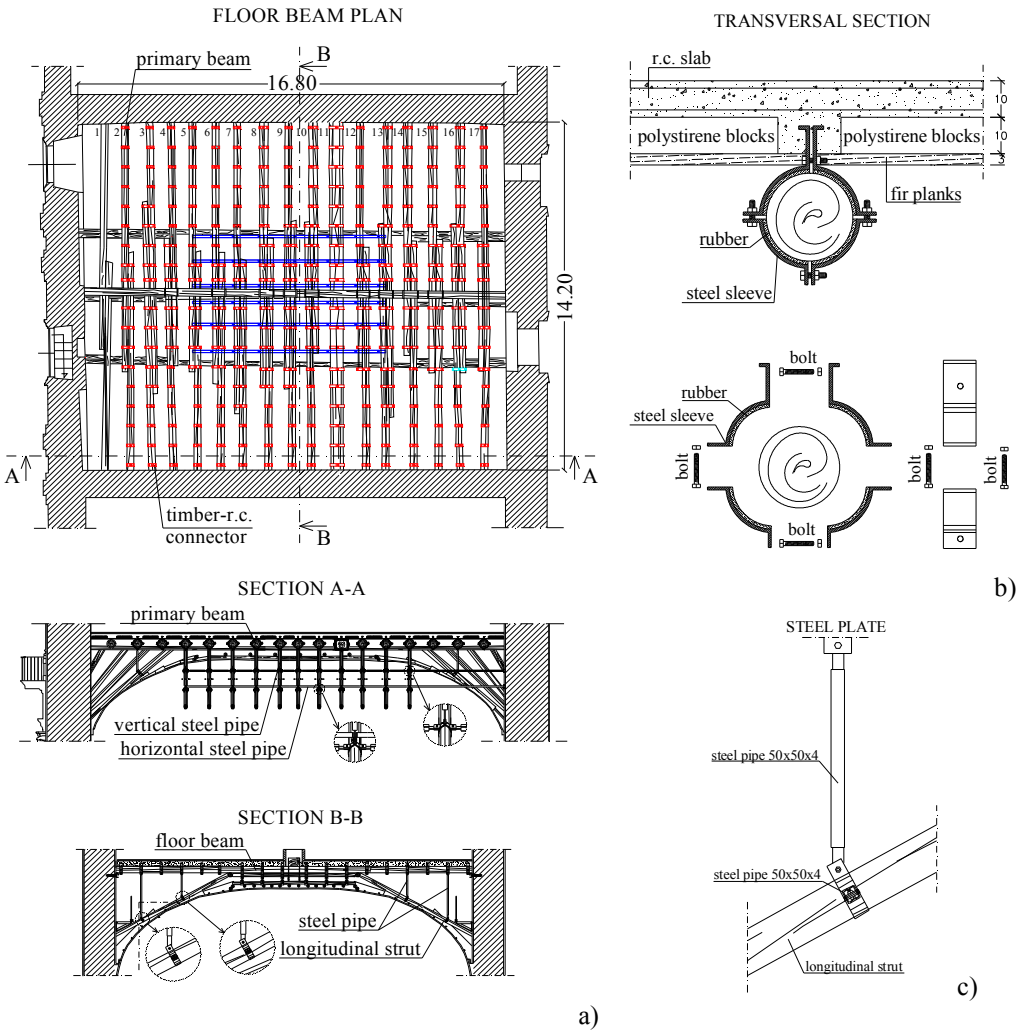

Figure 2.22. Diplomatic Hall (II) – Retrofitting interventions – Beam floor: a) Plan and sections; b) Timber beam-slab connector; c) Stiffening systems for longitudinal struts.

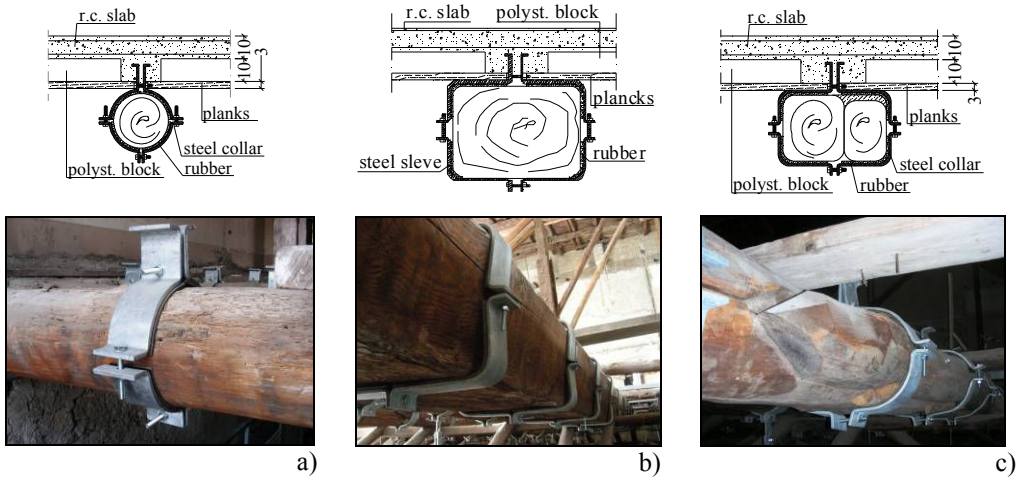

a) b) c)

Figure 2.23. Diplomatic Hall (II) – Retrofitting interventions – Beam-slab connectors:
a) Single circular cross-section; b) Single rectangular cross-section; c) Multiple cross-section.

- *Reinforcement of the unstable longitudinal and transverse radial struts,* by means of both horizontal and vertical stiffening elements (Fig. 2.24).
  At the longitudinal and transversal struts a steel vertical pipe and a steel plate, respectively, are bolted at both ends, above, to the collar connector, and below, to the steel sleeve astride the struts, in order to stiffen the struts in the vertical plane (Fig. 2.25a, b). Furthermore, tubular horizontal steel profiles connect the vertical steel pipes each other and to the perimeter masonries, in order to stiffen the struts in the horizontal plane (Fig. 2.25b).

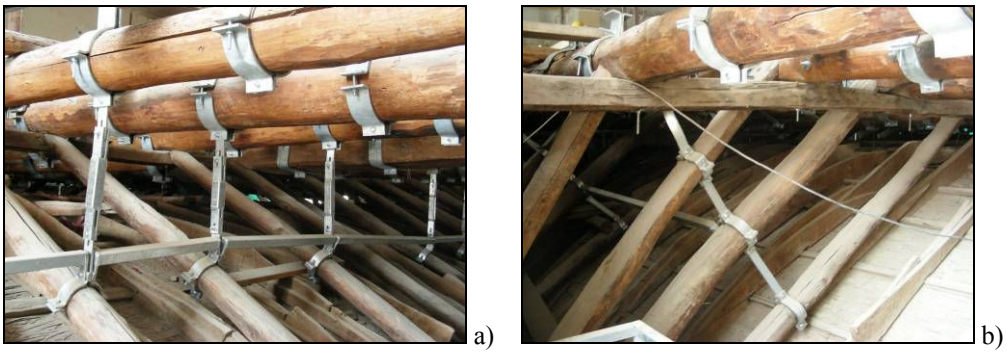

a) b)

Figure 2.24. Diplomatic Hall (II) – Retrofitting interventions – Stiffening systems for struts:
a) Longitudinal; b) Transverse radial.

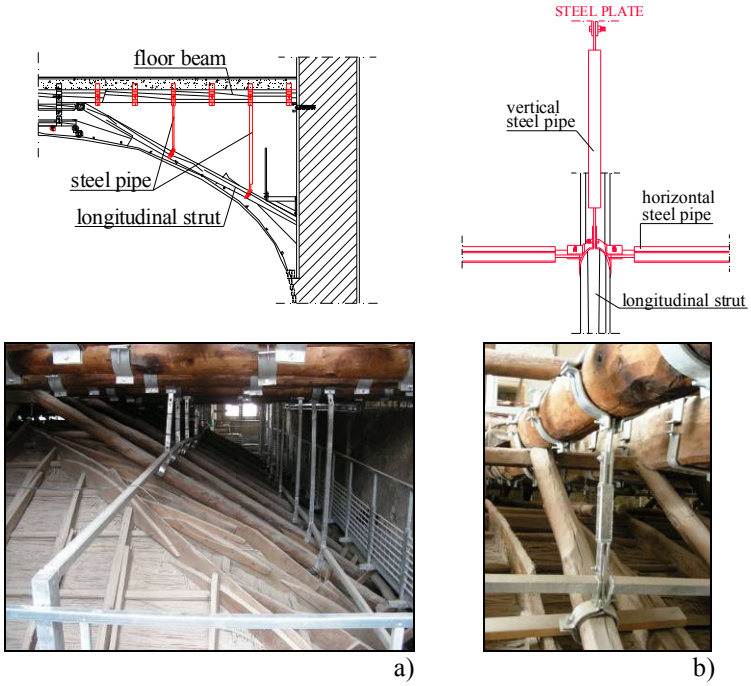

Figure 2.25. Diplomatic Hall (II) – Retrofitting interventions – Stiffening systems for longitudinal struts: a) Structural section and general view; b) Vertical and horizontal steel pipe details.

2.6.5.4 Local interventions

For the primary beams of the floor the local interventions consisted in:

- Restoration of the connections between the two timber stocks placed side by side at the mid-span of the floor, realized by means of metallic hinges (Fig. 2.26a);
- Repairs and stiffening at the beams supports on the masonry walls, obtained, respectively, by prosthesis and a cold-formed steel profile (Fig. 2.26b, c);
- Prosthesis at the beam 1, adjacent to the west façade, which was completely dug owing to the water seepage. It has been realized by new wood elements, connected each other by means of resin conglomerate cast (Fig. 2.26d).

For the truss:

- Repair of the strut, supported by the west façade wall, which was damaged by biological attacks due to water seepage (Fig. 2.26e);
- Restoration of the all connections among truss elements (Fig. 2.26f).

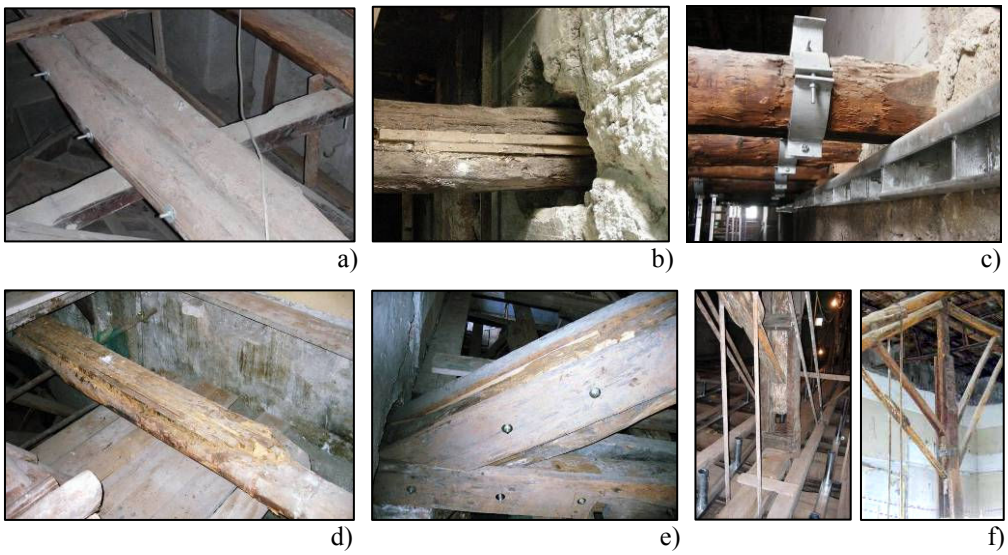

Figure 2.26. Diplomatic Hall (II) – Retrofitting interventions – Local interventions: a) Beams connections restoration; b) Repair at beams supports; c) Cold-formed steel profile support; d) Prosthesis at the beam 1; e) Repair of the truss strut; f) Restoration of truss elements connections.

2.7 THE COVERING STRUCTURE OF THE THIRD ANTEROOM (V)

2.7.1 *Geometrical survey*

The timber covering structure of the Third Anteroom (V) belongs to the third typology (see chapter 2.5.1), the vault being connected to an ad-hoc structure above, independent from the floor. Therefore, it is realized by three

main units (Fig. 2.27): 1) vaulted ceiling (V); 2) vault supporting structure (VS); 3) beam floor (F), following described.

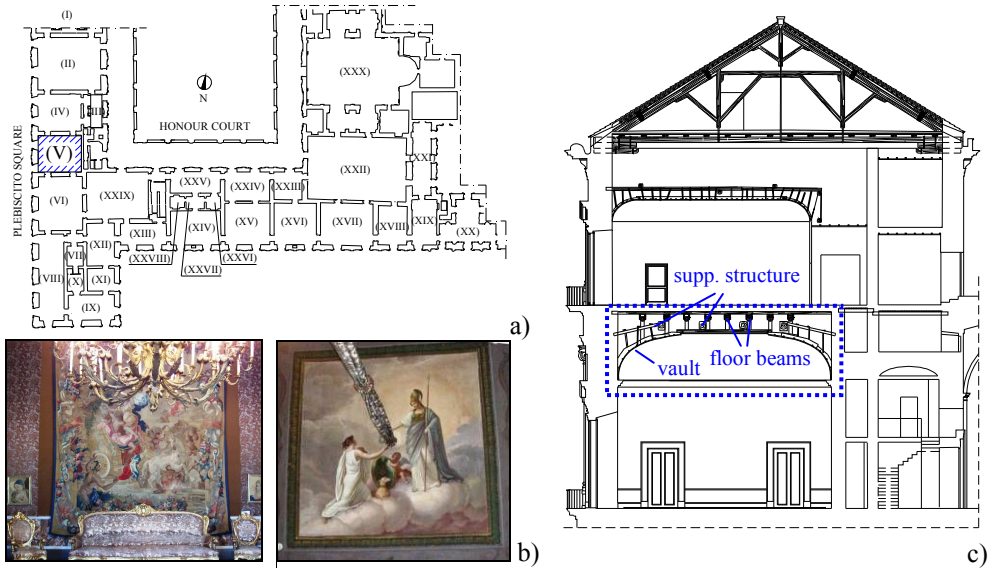

Figure 2.27. Third Anteroom (V) – Geometrical survey: a) Plan layout; b) Internal view and vault fresco; c) Structural section of the Royal Palace at the Hall V location.

V: Vaulted ceiling (Fig. 2.28)

The vault covers the Hall V, 11.50×10 m^2 sized. The bearing structure is composed by a grid of elements, such as ribs and splines. Each rib is obtained assembling some layers of planks, upright arranged, with different length and variable sizes, 4 cm thick and 10 to 15 cm high, connected each other by iron nails. The ribs are disposed at constant span, equal to about 30 cm. The splines are arranged orthogonally to ribs and fitted into them by a typical fixed joint used for timber elements of small size. They have a rectangular cross-section, about 5×6 cm^2. The vault crown has a rectangular shape, realized by a grid of elements. In particular, the vault crown perimeter is composed by four elements with circular cross-section (10 cm diameter), nailed one each other at their intersections. The vault is supported along the perimeter by the vertical masonry and it is partially suspended to the supporting structure by means of wooden links, with variable size (about 3×5 cm^2).

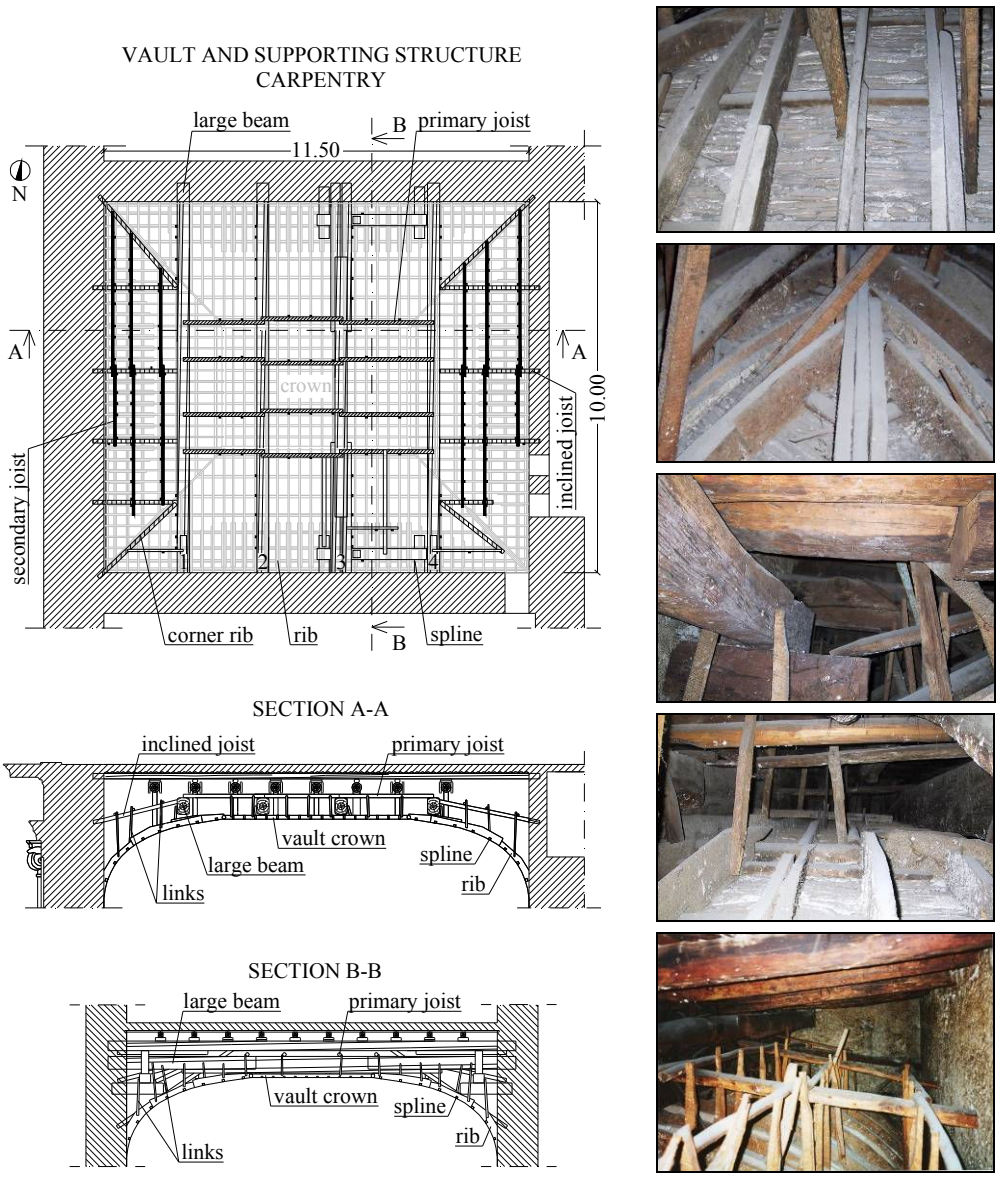

a) b)

Figure 2.28. Third Anteroom (V) – Geometrical survey – Vault and supporting structure: a) Carpentry and structural sections [m]; b) Photographic survey.

VS: Vault supporting structure (Fig. 2.28)

The supporting structure of the vault is composed by different systems, forming all together a complex grid of elements. Four large beams, with rectangular 33×45 cm^2 cross-section, are arranged along the minor span of the hall, about 40 cm below the primary beams of the floor. All beams support a system of horizontal primary joists (10 cm diameter), whereas the lateral ones support a grid of inclined (10 cm diameter) and secondary joists (6 cm diameter), orthogonal each other.

F: Floor beam (Fig. 2.29)

The floor beam is composed by two frames of timber beams. Eight primary beams, which have a circular variable cross-section (about 26 cm mean diameter) are arranged along the minor span of the floor with almost equally distance, about 1 m They are stiffened by longitudinal struts (about 15 cm diameter) and strengthened by two rectangular wooden thick planks, placed at both sides of the beam ends. Near the support abut to the masonry walls, the single beam 6 is stiffened by means of a different system, composed by a vertical saddle and a horizontal beam, which is supported by two cantilever elements. The ten secondary beams, 90 cm spacing, have a rectangular cross-section of 13×15 cm^2 sizes. Each secondary beam is supported by the primary ones with the interposition of wooden wedges.

2.7.2 *Failure diagnosis and visual grading*

For the wood species identification, all the structural elements of the beam floor, as well as of the vault supporting structure, are made of chestnut, whereas the skeleton of the vault and the links are in poplar wood, according to the constructional practice of that time.

The visual inspections (Level I) have evidenced that the timber elements of the vault are in a proper conservation state, even if at the intrados of the stucco some humidity spots and fissures of the stucco are evident, near the vault crown and at the corners, caused by water seepages (Fig. 2.30a). The large beam 2 of the vault supporting structure presents an important shake next the support to the wall, due to shrinkage (Fig. 2.30b).

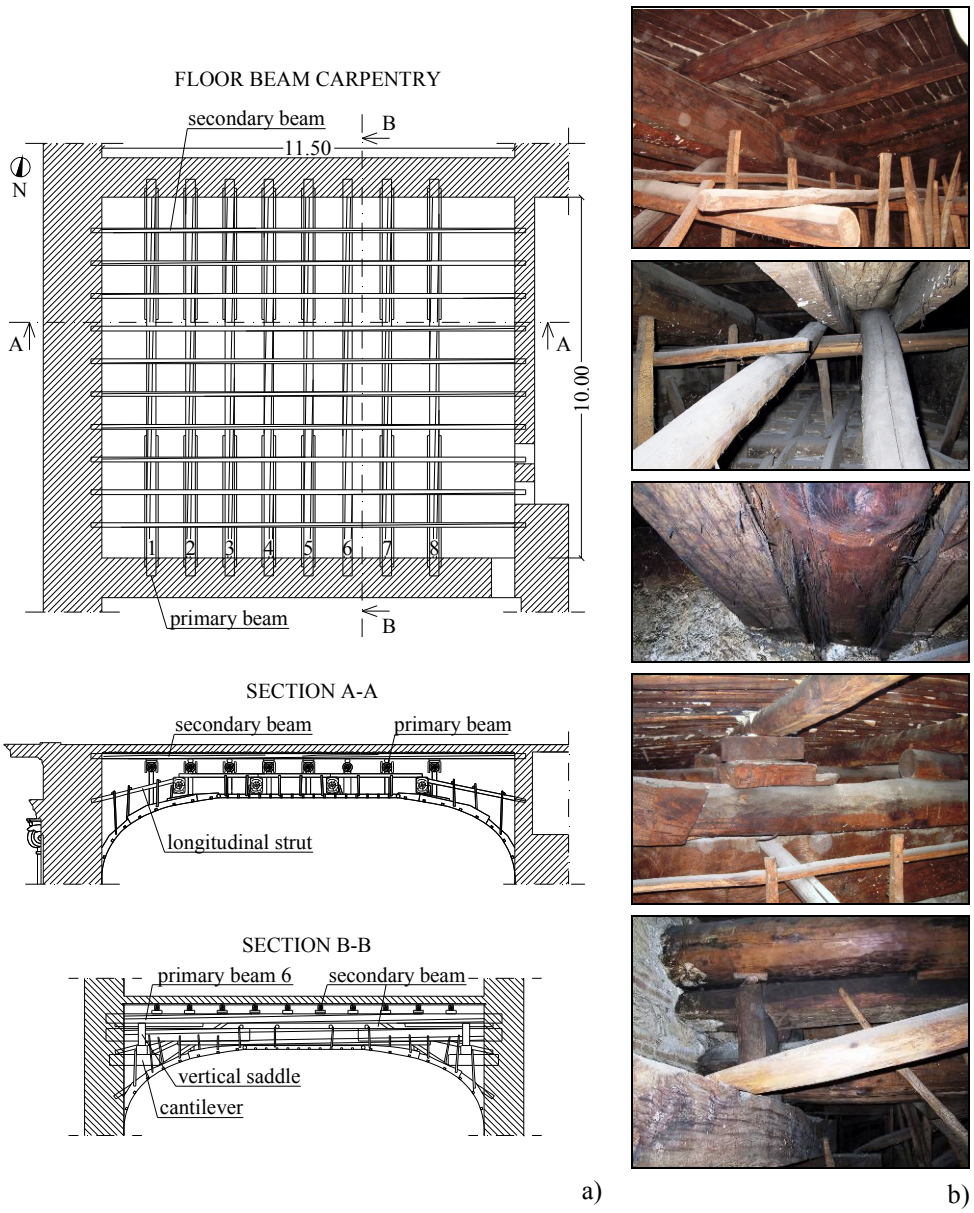

a) b)

Figure 2.29. Third Anteroom (V) – Geometrical survey – Floor beam structure: a) Carpentry and structural sections [m]; b) Photographic survey.

Concerning the floor beam structure, the primary beams 6, 7, 8 show evident mid-span deflections and diffuse fissures; in particular, the beam 7 presents an evident crack for bending overstress (Fig. 2.30c). Furthermore, the struts of the beams appear failed for compression. Finally, the planks, placed at both sides of the beam ends, are disconnected, so they cannot guarantee their strengthening function.

Superficial attacks by insect and fungi have been detected on many elements of the structures, together with natural defects, such as large knots and ring shakes, which are typical of chestnut timber. Therefore, all element are classified in third category, according to UNI 11119.

a) b) c)

Figure 2.30. Third Anteroom (V) – Failure diagnosis: a) Fissures of the fresco at the intrados of the vault; b) Large shake at vault supporting beam 2; c) Rupture for bending overstress of the floor primary beam 7.

2.7.3 *Structural modelling*

3D FEM models of each sub-structure has been set-up by mean of the program of structural calculation SAP 2000 v. 9.1.6 (Fig. 2.31).

The modelling adopted assumptions are following illustrated.

All timber elements are modelled with the least detected cross-section size. In particular, ribs and splines of the vault are modelled as single elements, 4×15 cm^2 and 5×6 cm^2, respectively. The primary beams of the floor are considered with a mean diameter, equal to 26 cm. The secondary elements, with 13×15 cm^2 size, are simply supported by the primary ones. Planks placed at the floor beam ends and the supporting wedges are neglected. The connections between ribs and splines, primary floor beams and secondary ones, are modelled as fixed joints, the link joints as internal hinges and the restraints at the perimeter masonries as simple support.

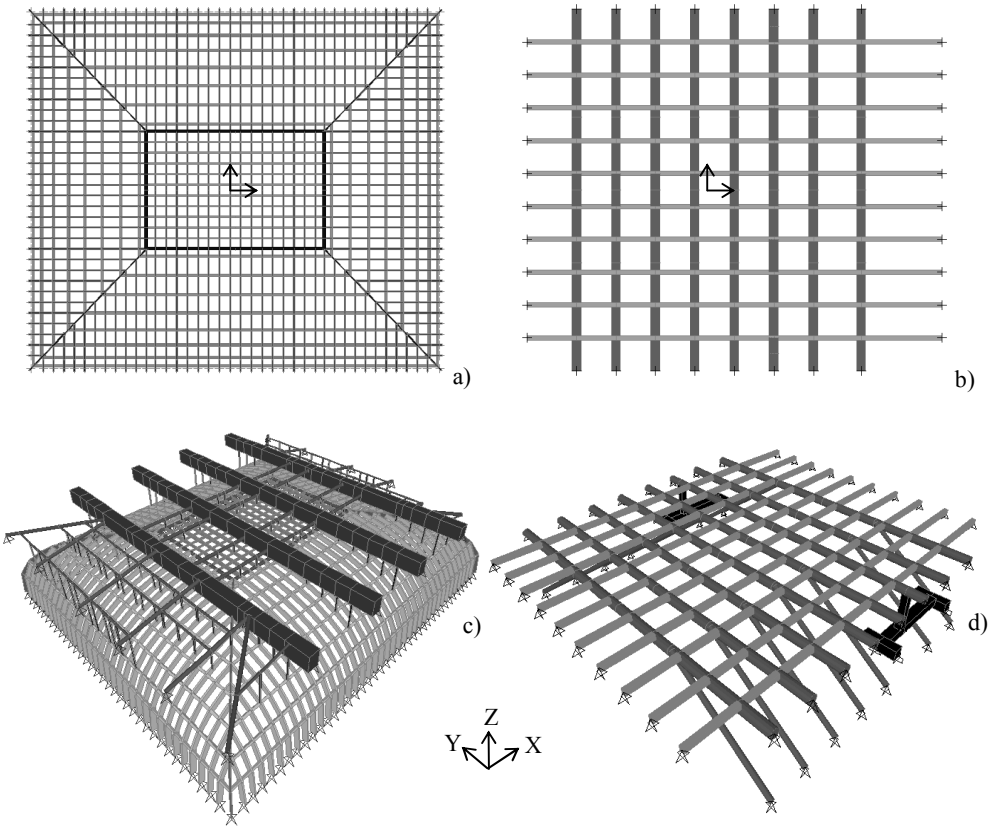

Figure 2.31. Third Anteroom (V) – Structural modelling: a) Vault plan; b) Floor beam plan; c) 3D model of the vault linked to the supporting structure; d) 3D model of the floor beam.

V: Vault

Erection phases (new timber)

- Phase 1: *Erection of the vault structure* (Model V1)
  The structure consists of vault elements, such as ribs, splines and vault crown frames. Only dead load is considered ($G_{1,\ vault}$).
- Phase 2: *Vault-Supporting structure connection and vault completion* (Model V2)
  The vault is linked to the supporting structure and completed by lathing and stucco. All permanent load are applied ($G_{1,\ vault} + G_{2,\ vault}$).

Phase at the present state (ancient timber)

- Phase 3: *Complete vault* (Model V3)
  The geometrical and loading model is equal to Model V2, but the mechanical properties are referred to the ancient timber.

F: Floor beam

Erection phases (new timber)

- Phase 1: *Erection of the floor beam structure* (Model F1)
  The structure consists of floor beam elements, such as primary and secondary beams, longitudinal struts. Only dead load is applied ($G_{1,\,floor}$).
- Phase 2: *Floor beam completion* (Model F2)
  The floor beam is completed by non-structural parts. All permanent load are considered ($G_{1,\,floor} + G_{2,\,floor}$);
- Phase 3: *Floor beam in service conditions* (Model F3)
  Both permanent and variable actions are applied ($G_{1,\,floor} + G_{2,\,floor} + Q_{floor}$).

Phases at the present state (ancient timber)

- Phase 4: *Complete floor beam* (Model F4)
  The geometrical and loading model is equal to Model F2, but the material is modelled as ancient timber.
- Phase 5: *Complete floor beam in service conditions* (Model F5)
  The geometrical and loading model F5 and F3 are identical, but for Model F5 the ancient timber is considered.

2.7.4 *Numerical analysis*

In Figure 2.32 the deformed configuration of the vaulted ceiling of the Third Anteroom (V) are shown, with reference to a vault quadrant, at the mid YZ section. The displacements of the internal joints between ribs and splines, marked with circles on the vault model plan, are assumed as deformation parameters. Displacements are scaled by an amplification factor equal to 10 for evidencing the deformed shapes.

It can be noticing that, at the present state (Model V3) the combined effect of the material degradation, creep and moisture has induced a generalized flattening at the centre of the vault, which consists of sagging with a maximum vertical displacement of about 5 cm. The seismic effect induces a

negligible displacements amplification, equal to about 1 cm. Therefore, the preservation of stucco, at the intrados of the vault, is not compromised by the actual deformation state.

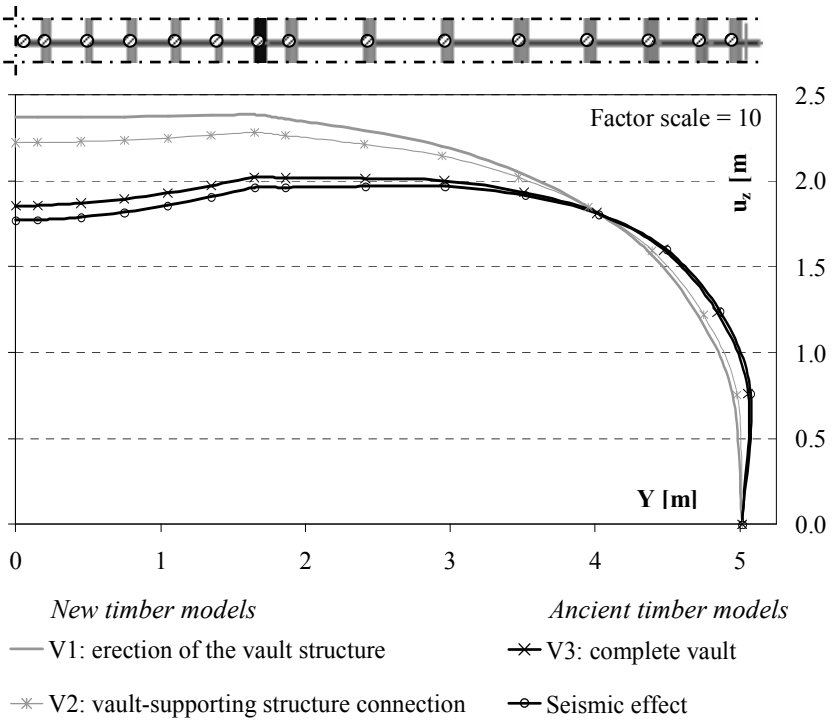

Figure 2.32. Third Anteroom (V) – Numerical analysis: deflection state of the vault (YZ section).

Aiming at assessing the effectiveness of the wooden links which connect the vault to the upper supporting structure, they have been gradually removed. Therefore the following additional models in ancient timber have been analyzed:

- Model V4: *Connection only in vault crown*
  The complete vault is connected to the supporting structure by means of wooden links only located at the vault crown;
- Model V5: *Self-bearing vault*
  All wooden links are removed so that the self-bearing vault is considered.

The beneficial effect of the vault suspension to the upper supporting structure is emphasized in Figure 2.33, where the Models V3, V4 and V5 are compared in terms of deformation state.

In particular, the comparison between the Models V3 and V4 shows that the removal of the links located at the curved sides of the vault does not significantly modify the deformed shape of the structure. At the contrary, the self-bearing vault configuration (Model V5), obtained removing all wooden links, induces a strong increment of displacements in vault crown, equal to about 6.5 cm, which could inevitably damage the stucco at the intrados.

Therefore, only links located within the vault crown appear efficient. This assumption is also confirmed by the analysis of the stress state in the vault elements. In Figure 2.34 the internal forces distribution are depicted with reference to the Model V3. The diagrams of the bending moment and shear force are amplified of ten times respect to axial force ones.

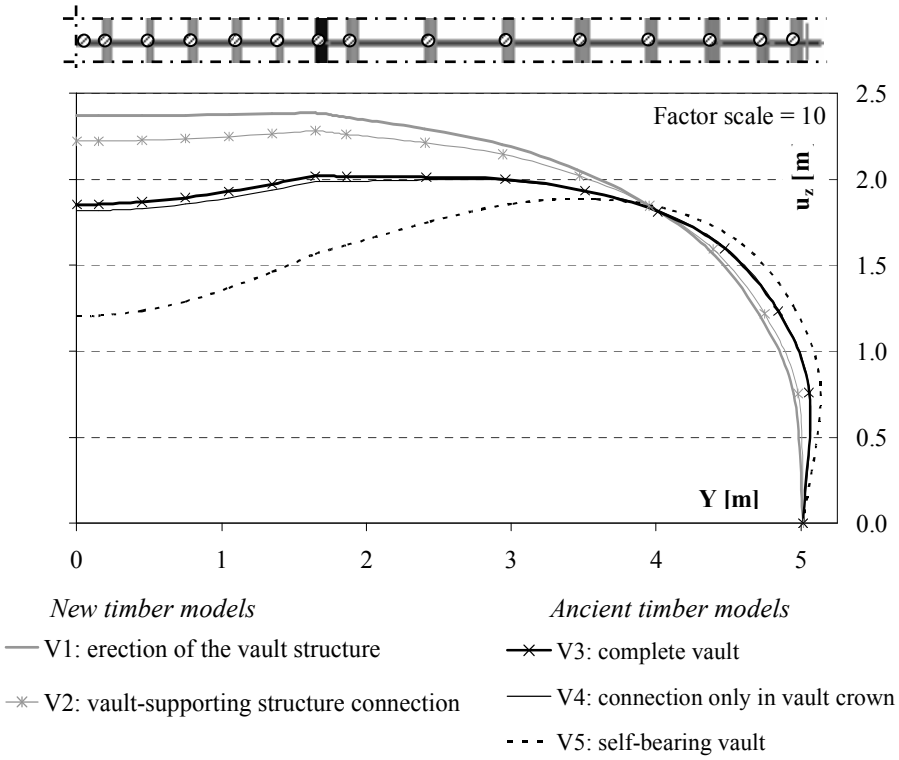

Figure 2.33. Third Anteroom (V) – Numerical analysis: deflection state of the vault (YZ section).

It is worth noticing that, some links outside the vault crown area, working as struts, induce important variations of the stresses in the sections where the structure is connected to the upper supporting system. In particular, the ribs which are directly connected to the upper large beams of the supporting structure (Fig. 2.34; section Y'-Y'), are overstressed for both bending moment (M), shear (S) and axial force (A) in the sections near to the masonry supports. This stress state could be reduced removing the links outside the vault crown, as shown in Figure 2.35, where the Models V3 and V4 are compared in terms of internal forces.

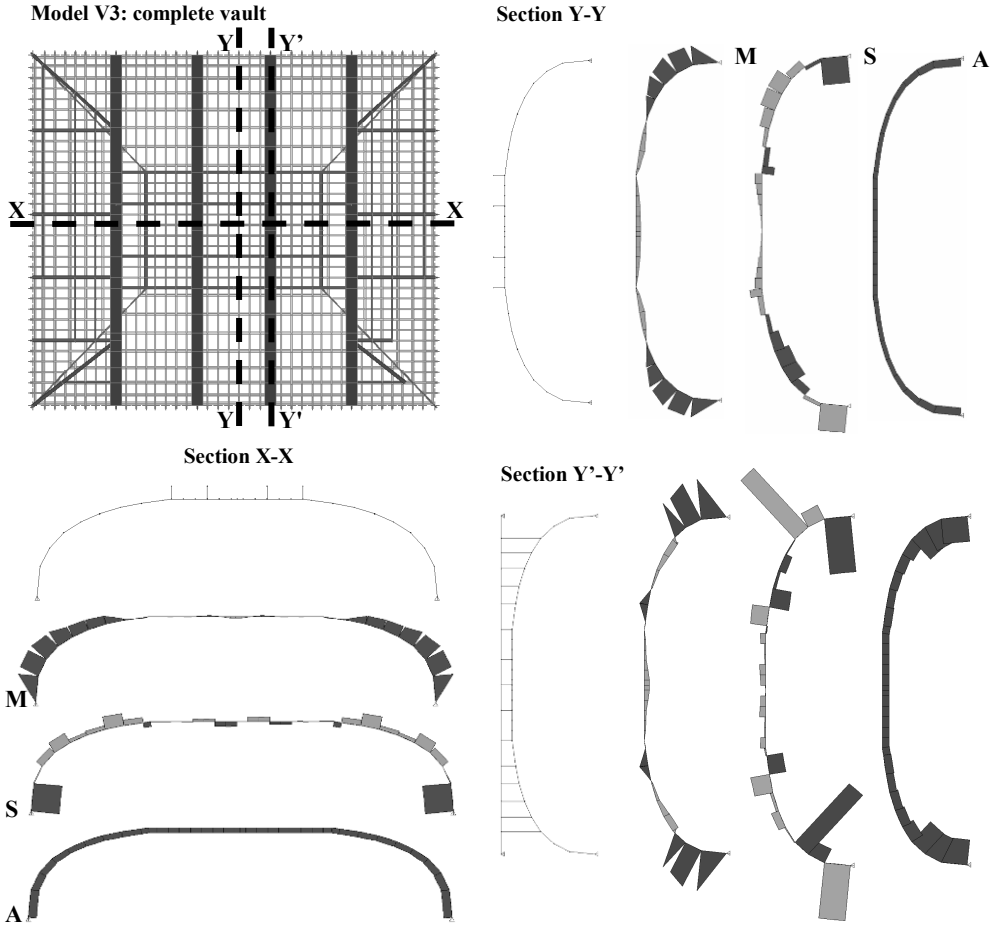

Figure 2.34. Third Anteroom (V) – Numerical analysis: internal forces distribution in the vault elements (Model V3).

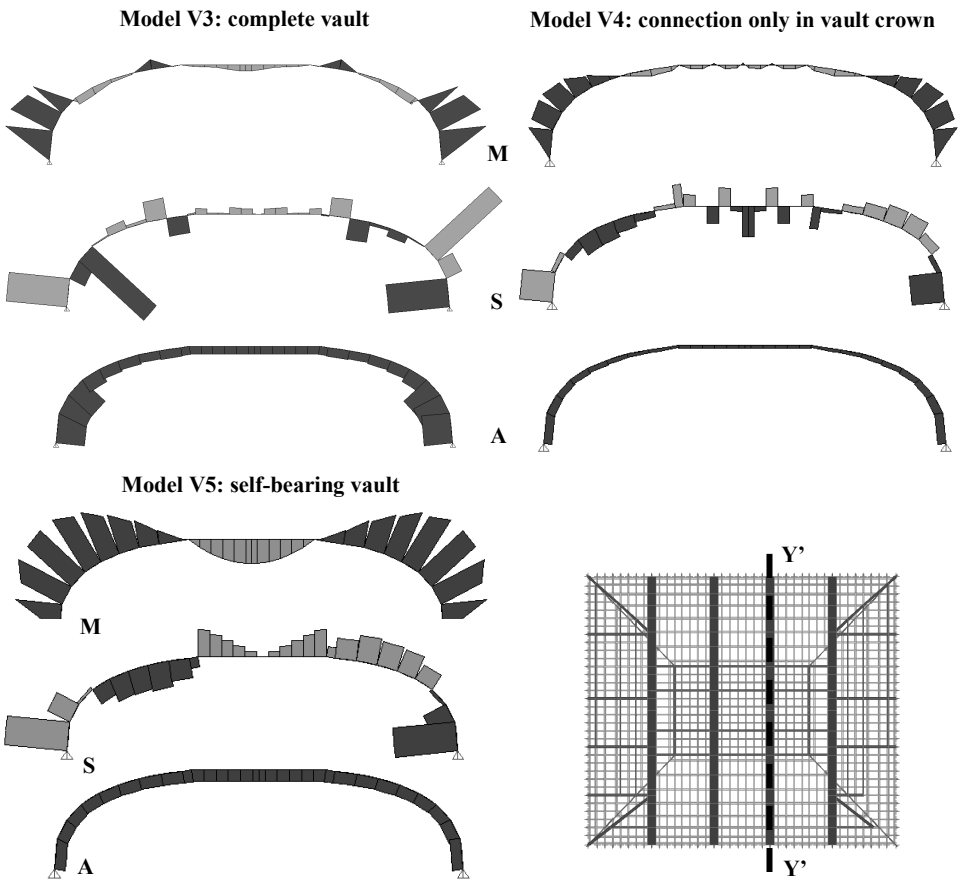

Figure 2.35. Third Anteroom (V) – Numerical analysis: comparison of internal forces distribution in the vault elements (Models V3, V4 and V5; section Y'-Y').

The vertical deformed configurations of the central secondary beam of the floor are shown in Figure 2.36. As reference parameters, the displacements of the middle sections of the eight primary beams, marked with circles, have been considered.

As it appears, the floor beam shows the greater deflections at west side of the structure, where the last primary beams 6, 7, 8 are located, predominantly caused by the lack of an suitable stiffening system of the beam 6. By comparing the Models F2 and F4, it can be observed that the effects of creep and degradation of timber amplifies the deflection of about three times. Therefore, at the present state, when ancient timber is considered and the

permanent load are applied (Model F4), the deflections of the beam 6 do not satisfy the verification at the Serviceability Limit State (SLS), according to EC5. In fact, the vertical displacement is beyond the limit value, equal to about 2.8 cm (L/350). In the serviceability conditions (Model F5), the variable actions produce an increment of deflection equal to 12%, which exceeds the limit values for the primary beams 7 and 8 too. The vertical seismic motion is negligible.

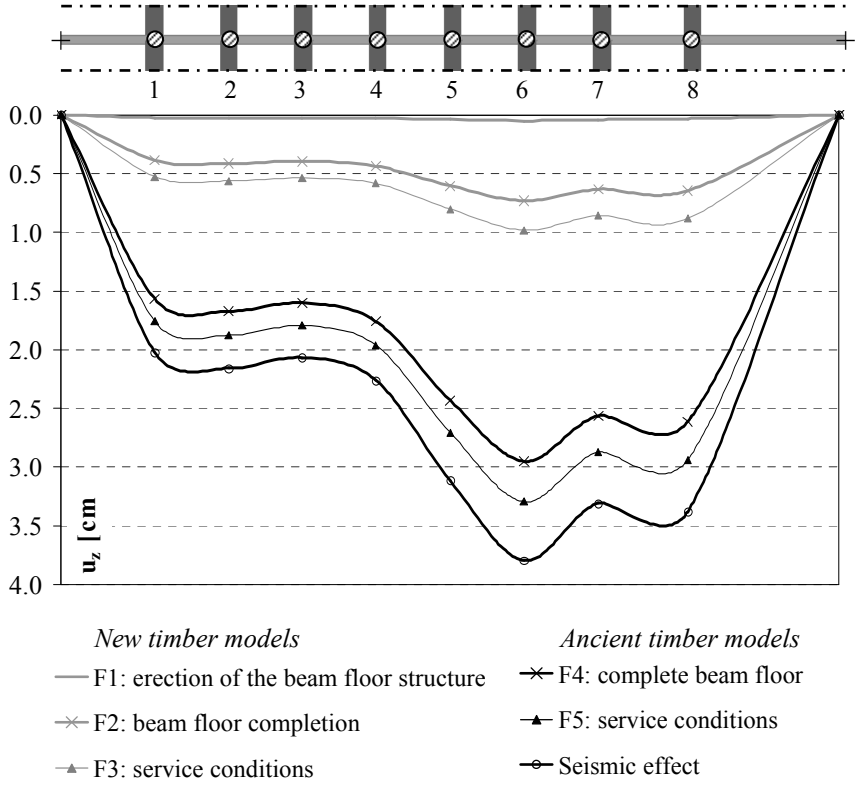

Figure 2.36. Third Anteroom (V) – Numerical analysis: deflection state of the floor beam (X direction).

In Figure 2.37 the stress state in the beam floor elements is qualitatively described in terms of Moment (M), Shear (S) and Axial Force (A) diagrams for both primary and secondary beams (Model F4). The diagrams of the bending moment and shear force are amplified of 10 times respect to axial force ones.

According to EC5 and with reference to the characteristic strength values given in the Italian Code UNI 11035-2 (2003) for the relevant stress conditions and wood species, the safety checks have evidenced that the primary floor beam 8 and the secondary beams 3 and 8 do not accomplish the strength requirements; whereas all the struts of the floor beams stiffening system do not satisfy the stability check.

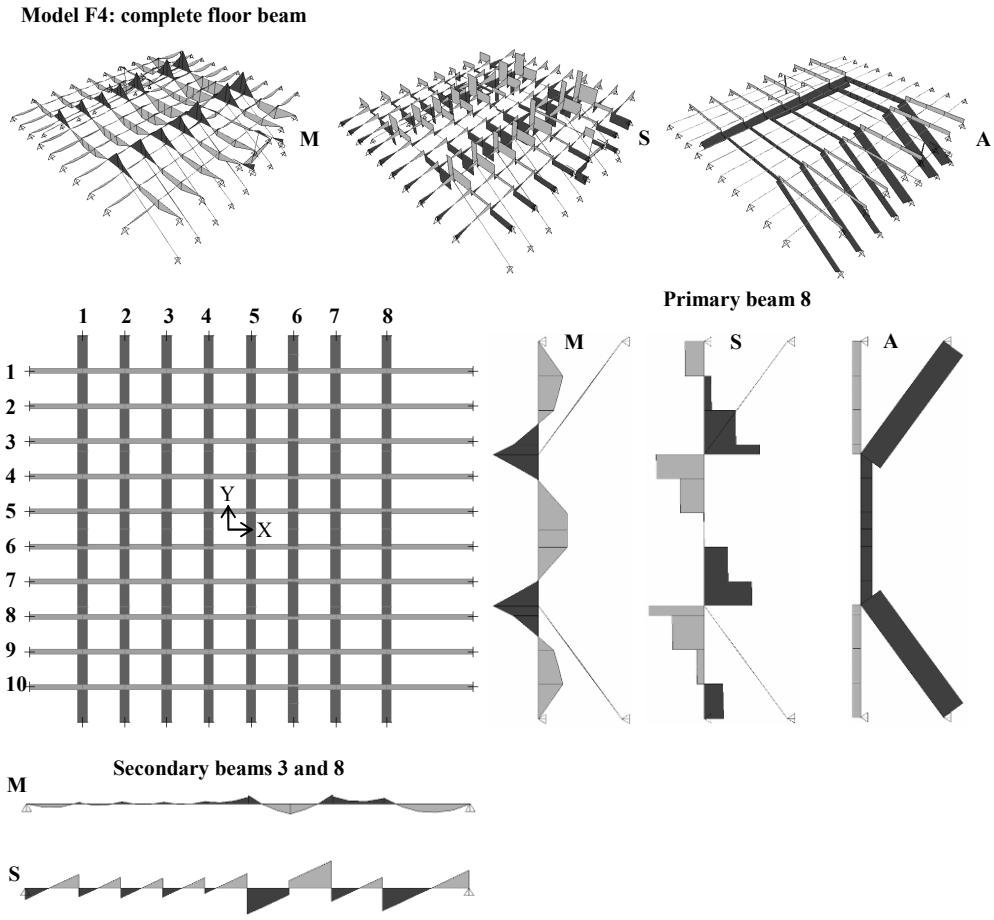

Figure 2.37. Third Anteroom (V) – Numerical analysis: internal forces distribution in the floor beam elements (Model F4).

2.7.5 *Proposed restoration interventions*

2.7.5.1 Vault

For the vault, the state of the stucco at the covering intrados is not compromised by the present deformed shape. However, it was observed that only the wooden links inside the vault crown are efficient, suspending the vault to the upper large beams and primary joists of the supporting structure. In fact, the connection to the inclined and secondary joists grid above, do not significantly increase the stiffness of the structure. In addition, the analysis of the stress state has emphasized that the links located near the masonry supports induce important additional actions in the ribs elements, working as struts.

Therefore, aiming at the preservation the vaulted ceiling fresco in the time, the following restoration interventions are proposed:

- Removal of all links placed at the vault curved sides;
- Stiffening of the large beams of the vault supporting structure by means of inclined struts, made of chestnut wood (Fig. 2.38);
- Restoration of the vault-supporting structure connection at the vault crown only, by means of new timber elements (Fig. 2.38).

In Figure 2.39 the deformed configurations of two vault central sections are depicted at the investigated phases of the intervention (after intervention models), compared to the ones corresponding to the present structure state (before intervention models). In particular, the benefits of the restoration is apparent comparing the Models V3 and V6. Furthermore, the effect of the creep at infinite time insignificantly increases the displacements of the structure, equal to below 1 cm in the vault crown (comparison between Models V6 and V7).

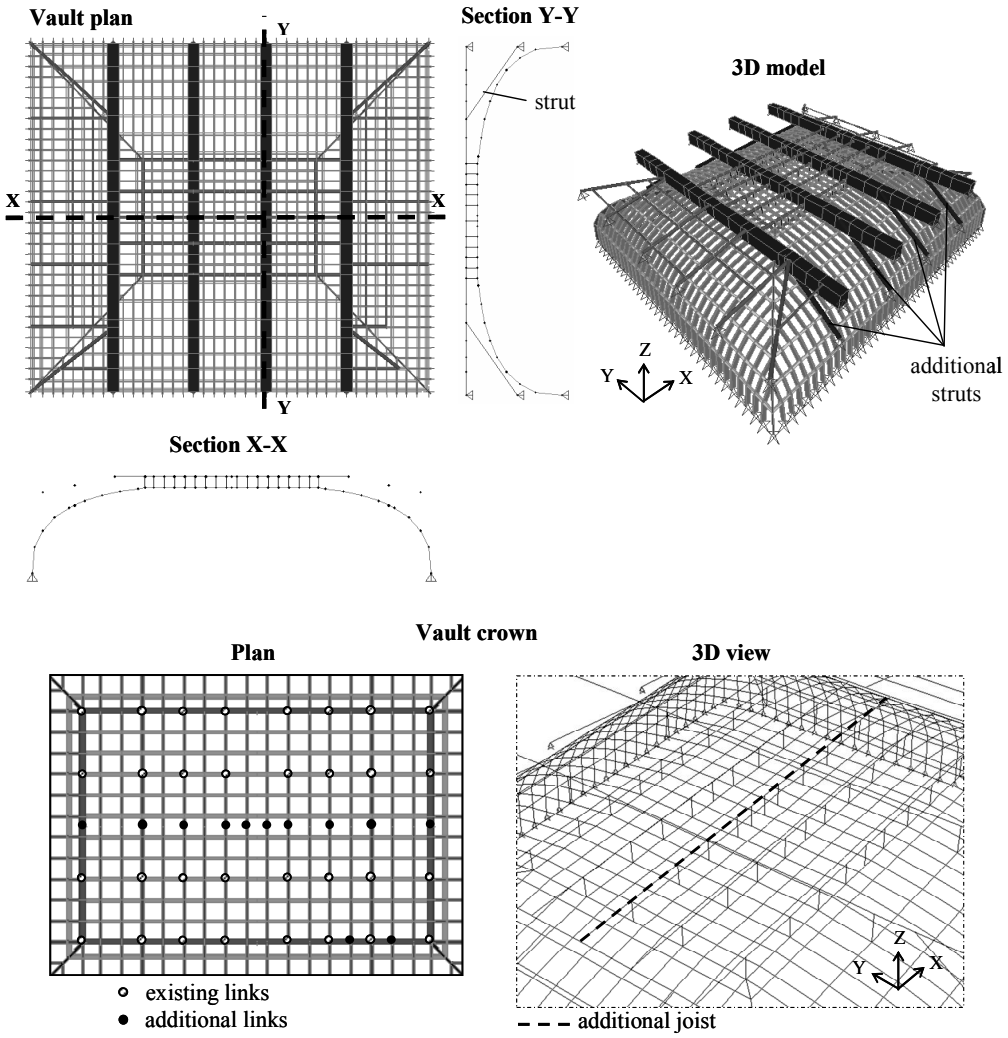

Figure 2.38. Third Anteroom (V) – Restoration interventions: model of the stiffened vault-supporting structure system.

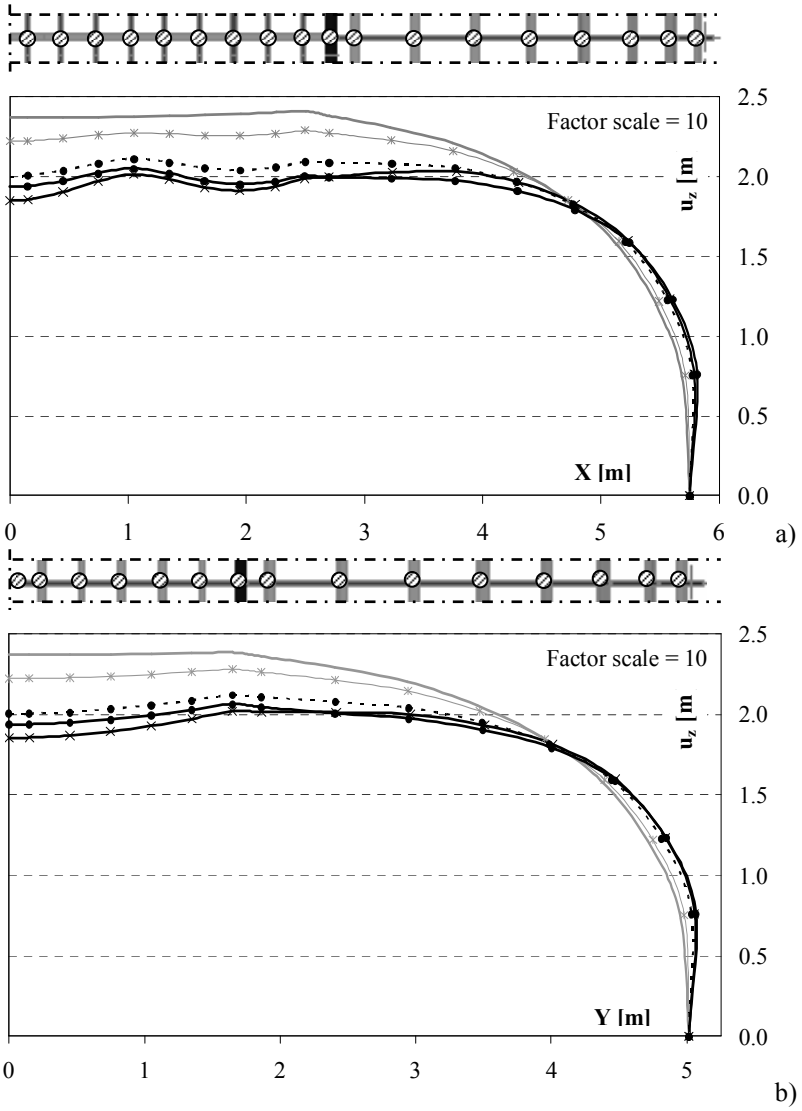

Figure 2.39. Third Anteroom (V) – Restoration interventions – Deflection state of the vault before and after intervention; a) XZ section; YZ section.

2.7.5.2 Floor beam

For the floor, the numerical analysis has evidenced that some primary and secondary beams do not satisfy the safety checks at both serviceability and ultimate limit state and the inclined stiffening struts do not accomplish the stability requirements, according to EC5. Therefore, the following retrofitting interventions are proposed:

- Installation of a new timber primary beam 9 (26 cm diameter), between the beam 8 and the parallel wall, made of chestnut wood and stiffened with two longitudinal struts (15 cm diameter) (Fig. 2.40a);
- Stiffening of the primary beam 6 with the same portal frame system of the other beams (Fig. 2.40a);
- Reinforcement of the unstable longitudinal struts, by means of both horizontal and vertical stiffening steel elements (Figs. 2.40b and 2.41);
- Restoration of the efficiency of the connections between the structural elements; in particular, the strengthening function of the two planks, placed at both sides of the beam ends, should be restored by means of bolts, to be located in the holes of the existing nails, and suitably tightened; in the case of short planks, which do not reinforce the beam at the strut connection where the shear assumes the maximum value, they should be substituted by opportunely longer elements, made of chestnut wood;
- Casting of a reinforced lightened concrete slab (5 cm thick; 1600 kg/m^3 weight; f_{lck}=20 MPa; B450C steel bars), in substitution of the floor completion layers, achieving a twofold effect, such as the decrement of permanent actions and therefore of stresses in the beams, and an improved load surface distribution. Moreover, aiming at the improvement of the transfer of horizontal forces to vertical structures in case of seism, the slab should be fixed on the perimeter masonry walls by means of ad hoc steel bars (Fig. 2.42).

The beneficial effect of the retrofitting interventions are shown in Figures 2.43a, b, where the internal forces in the floor elements at the present state (Model F4) are compared with the same ones after the intervention phase (Model F6), when all permanent loads are applied. The reduction of the stress state is evident for both bending moment (M), shear (S) and axial force (A).

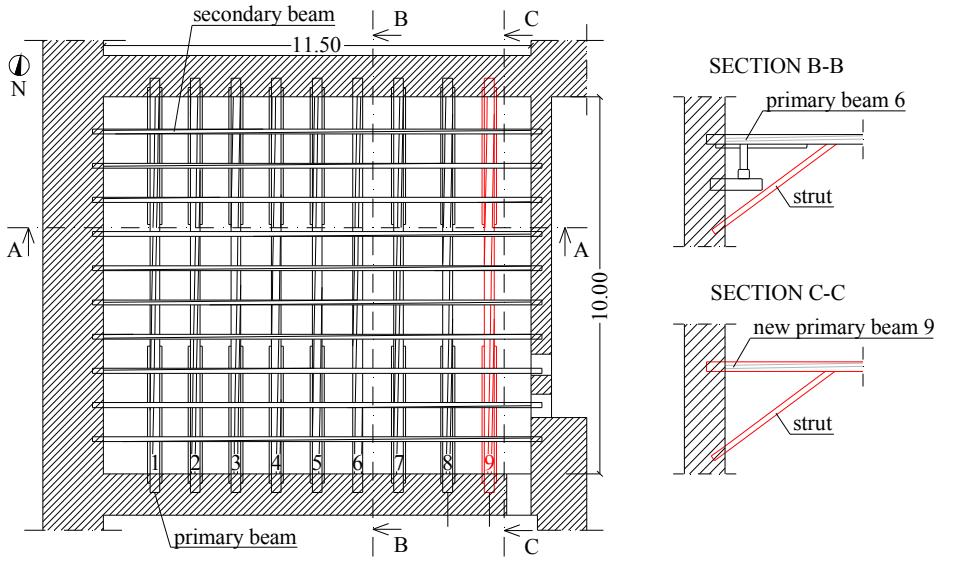

a)

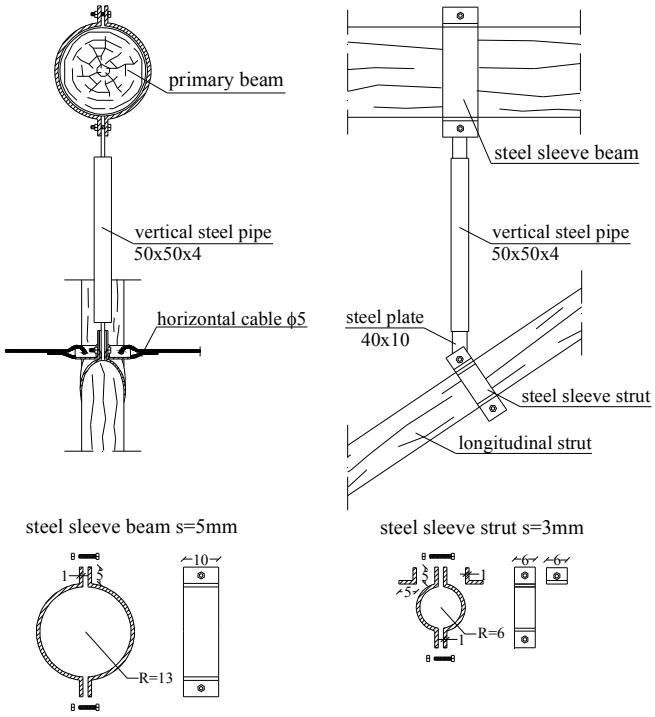

b)

Figure 2.40. Third Anteroom (V) – Restoration interventions – Floor beam: a) Plan layout; b) Stiffening systems for longitudinal struts.

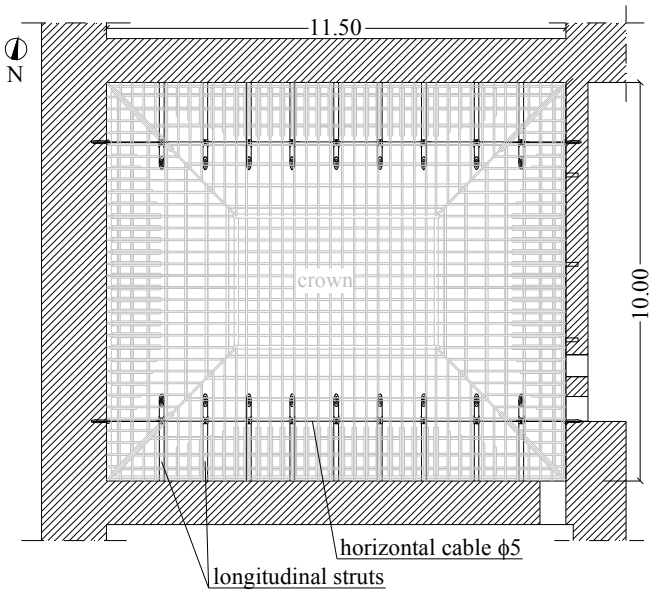

Figure 2.41. Third Anteroom (V) – Restoration interventions – Floor beam: disposition in plan of horizontal stiffening systems for longitudinal struts.

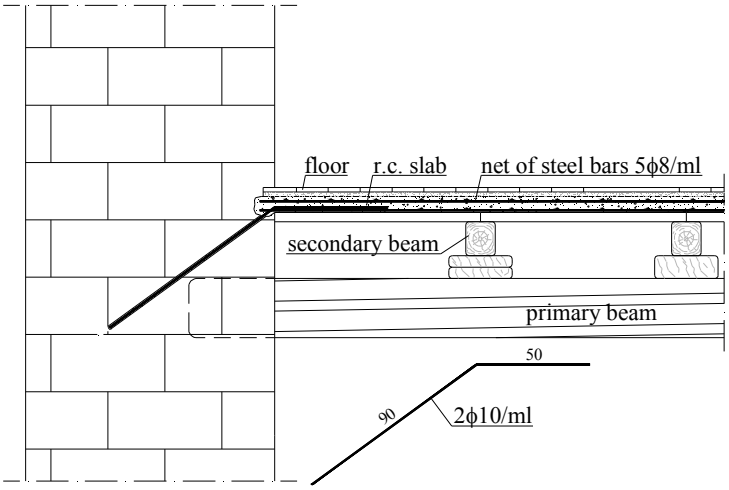

Figure 2.42. Third Anteroom (V) – Restoration interventions – Floor beam: details of r.c. slab.

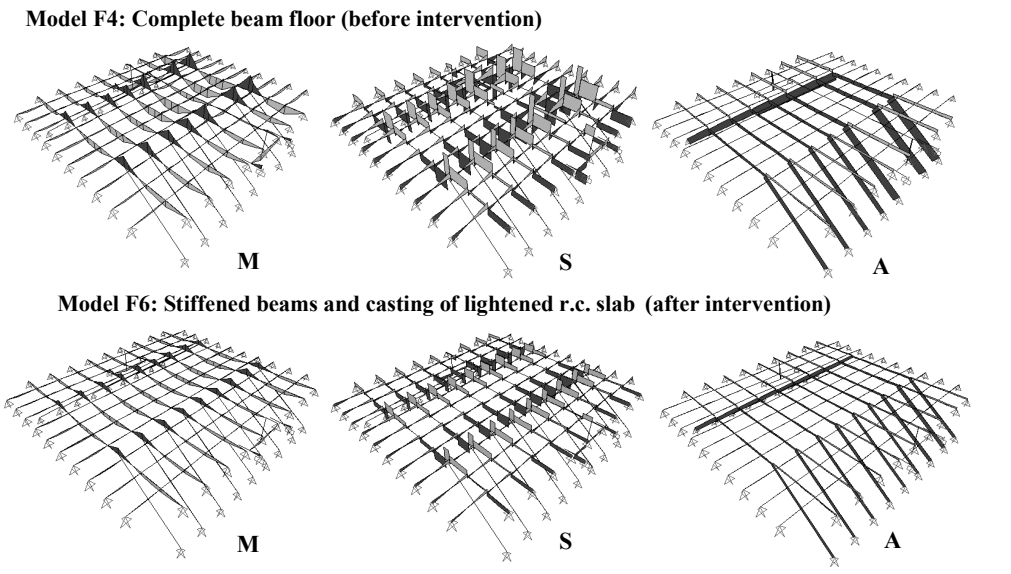

a)

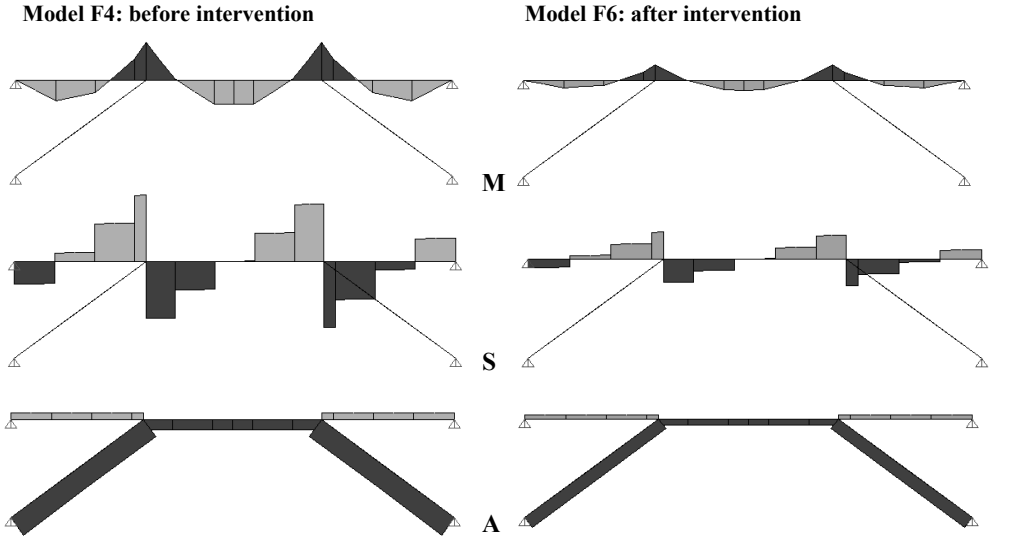

b)

Figure 2.43. Third Anteroom (V) – Restoration interventions – Internal force distribution in the floor beam elements before and after intervention: a) Model 3D; b) Primary beam 8.

2.8 THE VAULTED CEILING OF THE GUARD ROOM (XXIX)

2.8.1 *Geometrical survey*

The peculiar covering structure of the Guard Room (XXIX; Fig. 2.44a) is composed by a large vaulted ceiling with a central skylight (Fig. 2.44b), which is connected to the timber supporting structure above by means of wooden links (Fig. 2.44c) and suspended at the vault crown perimeter to the upper r.c. roof of the Palace (Fig. 2.44d) by means of metallic ties. Therefore, the two main superimposed units, connected each other, are: 1) vaulted ceiling (V); 2) vault supporting structure (VS), following illustrated.

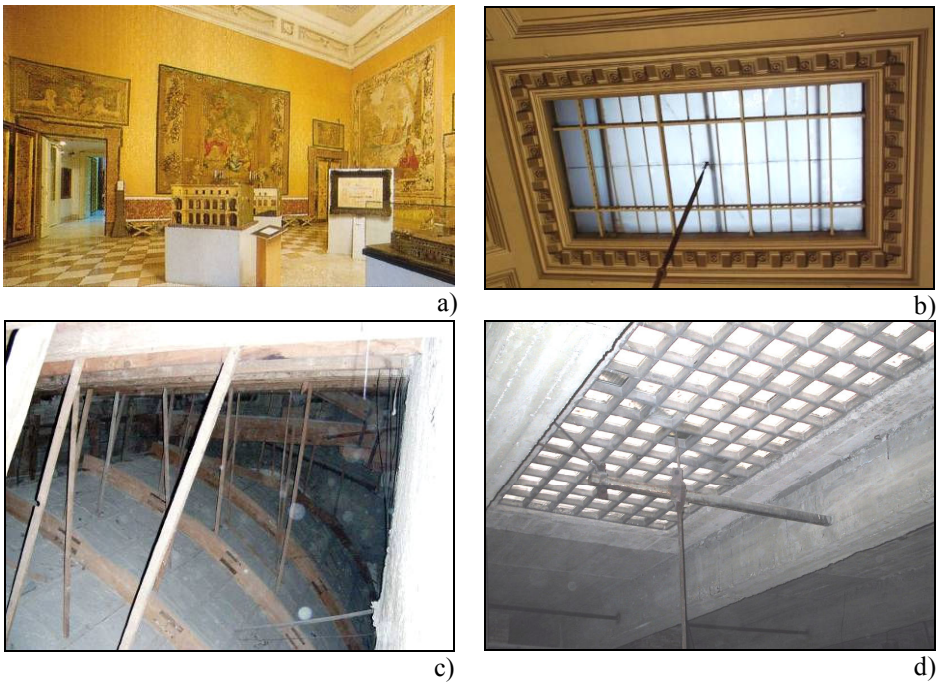

Figure 2.44. Guard Room (XXIX) – Geometrical survey: a) Internal; b) Central skylight; c) Vaulted ceiling-supporting structure connection; d) R.c. roof.

V: Vaulted ceiling (Fig. 2.45)

The light vault if the guard Room (XXIX) covers a large surface of 12.50×16.60 m^2 sized. It is shaped as a reversal boat keel with a central skylight at the vault crown. The structure timber skeleton is realized by means of ribs, splines and four main ribs, placed at the vault corners. The rib curvature is conferred by connecting aligned elements, upright arranged and having 5×20 cm^2 size, by metal plates and iron nails. The ribs are connected to the upper floor structure along the major sides, while it is connected to the purposely supporting beams along the minor sides, by means of wooden links, 3×5 cm^2.

Regular grids of splines elements are fitted between two contiguous ribs, connected to them by means of fixed joints. Splines have a rectangular cross-section, 4 cm high and 6 cm width.

At the vault crown perimeter four circular elements, 10 cm diameter, are nailed one to another at the intersection points. These border elements are linked to the upper tie trusses beams along the minor sides and to the stiffening frames, which are orthogonal to the trusses, by means of timber elements, 3×6 cm^2. They are also connected to the upper r.c. roofing structure by means of 12 metallic ties, three for each side, 30 mm diameter.

The completion of the vault is realized by metallic net, 1 mm size, within a layer of plaster cast, typical construction practice of the XX century for the vaulted ceilings realization.

The skylight is located at the vault crown and covers a rectangular surface of 7.70×3.90 m^2 size. The structure is realized by four timber beams, nailed to the adjacent vault perimeter elements, with rectangular cross section 15×20 cm^2. They are suspended to both the trusses ties and stiffening frames elements by means of wooden links. A double frame of reticular metallic beams are connected to the perimeter ones. Eight metallic plates support the transparent sheet of the skylight. The chain of the lamp is suspended to the glass-concrete skylight of the above r.c. roofing structure.

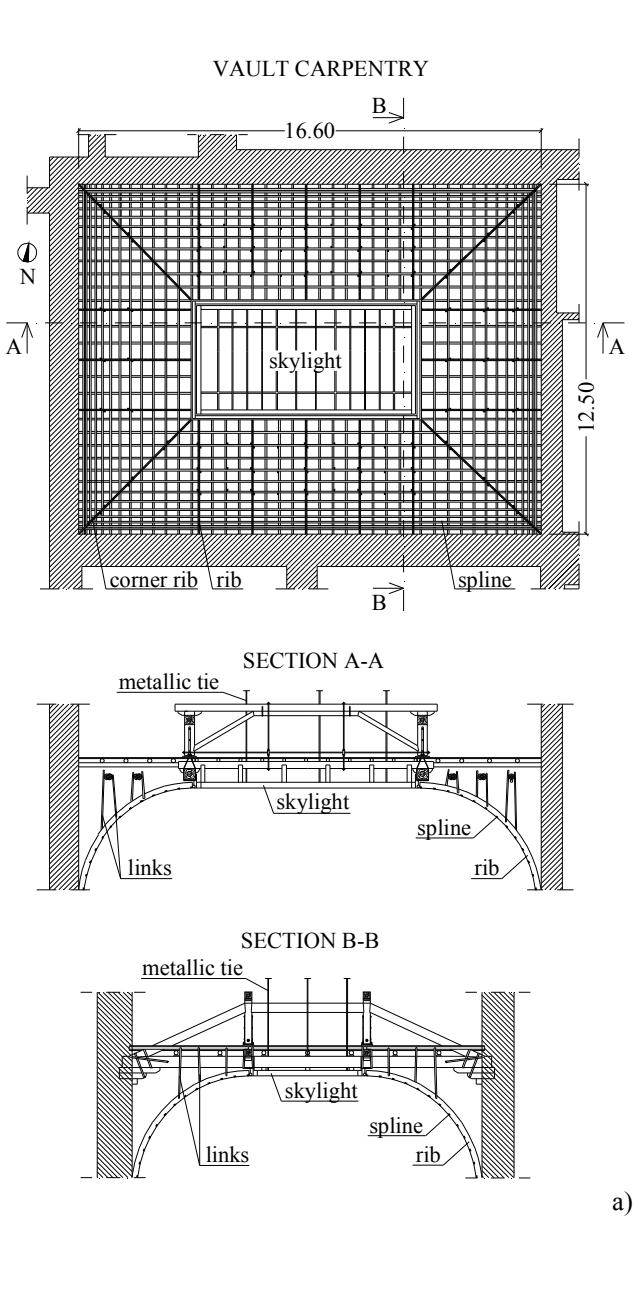

a)

b)

Figure 2.45. Guard Room (XXIX) – Geometrical survey – Vault structure: a) Carpentry and structural sections [m]; b) Photographic survey.

VS: Vault supporting structure (Fig. 2.46)

Upon the vault there is a complex timber structure at which the vault ribs and the crown perimeter elements are connected by wooden links. It is composed by a floor beams, realized by several frame systems, and five large beams, below the floor beams and arranged along the minor span of the hall.

The supported structural units of the floor beams are two trusses and two stiffening frames orthogonal to them, placed above the skylight perimeter and arranged, respectively, along the minor and major sides of the floor. The elements cross sections of these structural units are plotted in Figure 2.47.

The floor is composed by the following timber frame systems:

- System A, composed by two frames of elements orthogonal each other, with circular cross-section, 15 cm diameter. The primary ones are seven beams, located at the both sides of the floor and parallel to the major span, which are supported to the masonry wall and to the truss ties; the secondary elements are parallel to tie beams of the trusses and are the support of the wooden planks, which has 3 cm thick.
- System B, realized by squared elements, 10×10 cm^2, parallel to the minor side of the floor, propped up by the trusses stiffening frames and the masonry walls. They are the support of the wooden planks.

Each vault supporting beam is composed by two stocks placed side by side at the mid-span for about 3 m superposition length, connected one each other by large nails. Each trunk has a circular cross section, 20 cm diameter, and is strengthened by thick planks located next the supports to the masonry walls. The thick planks have a rectangular section 7×20 cm^2 and are connected to the beams by means of metallic plates. The last beam, located at the east side, is stiffened by means of longitudinal secondary beam and inclined struts with diameter of about 15 cm.

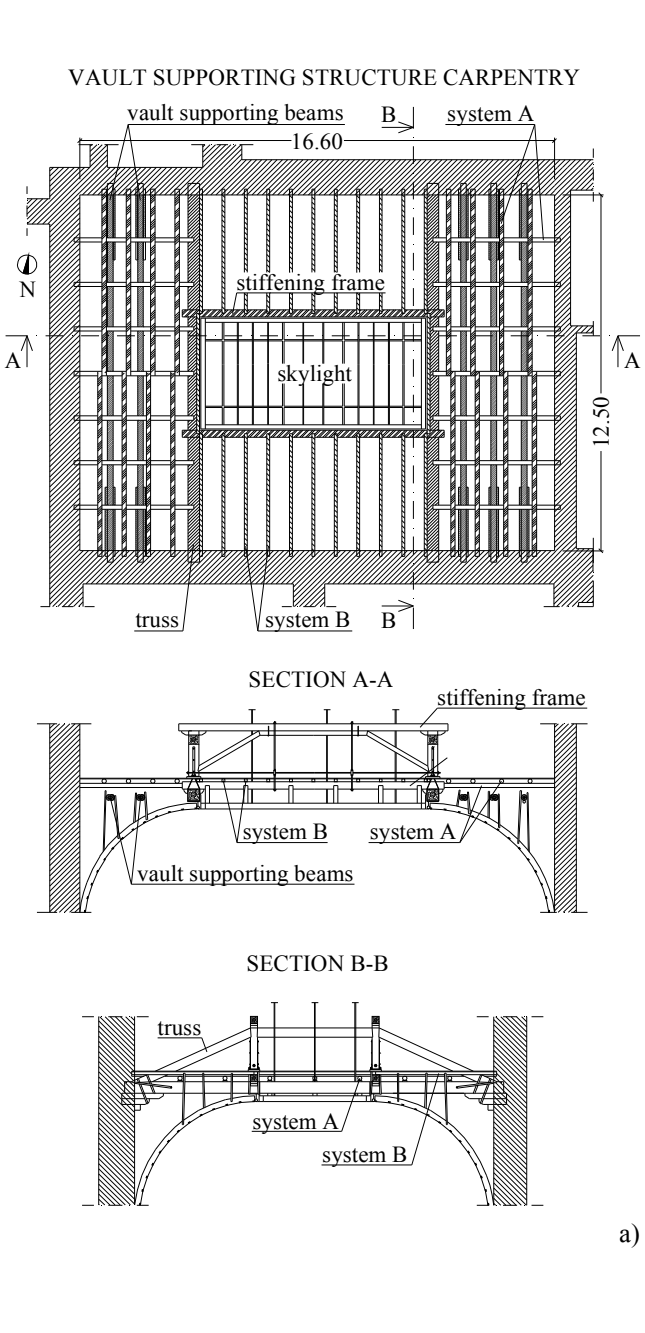

a)

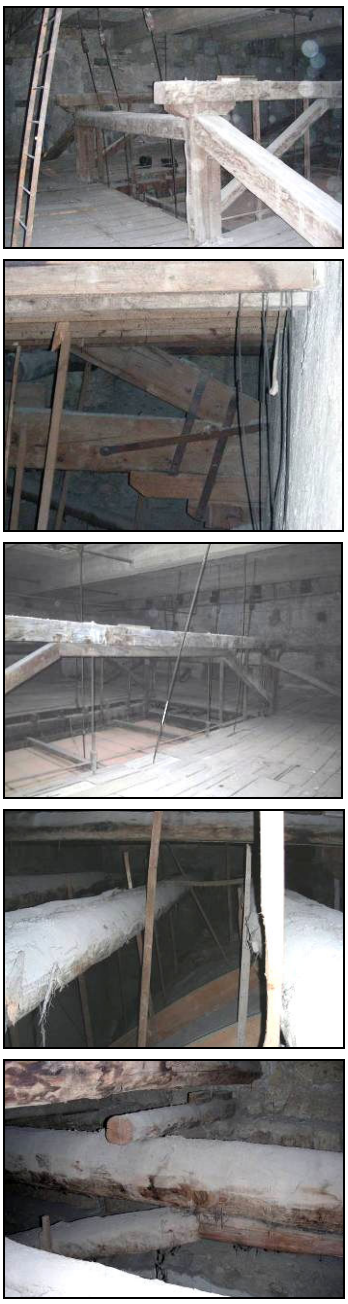

b)

Figure 2.46. Guard Room (XXIX) – Geometrical survey – Vault supporting structure:
a) Carpentry and structural sections [m]; b) Photographic survey.

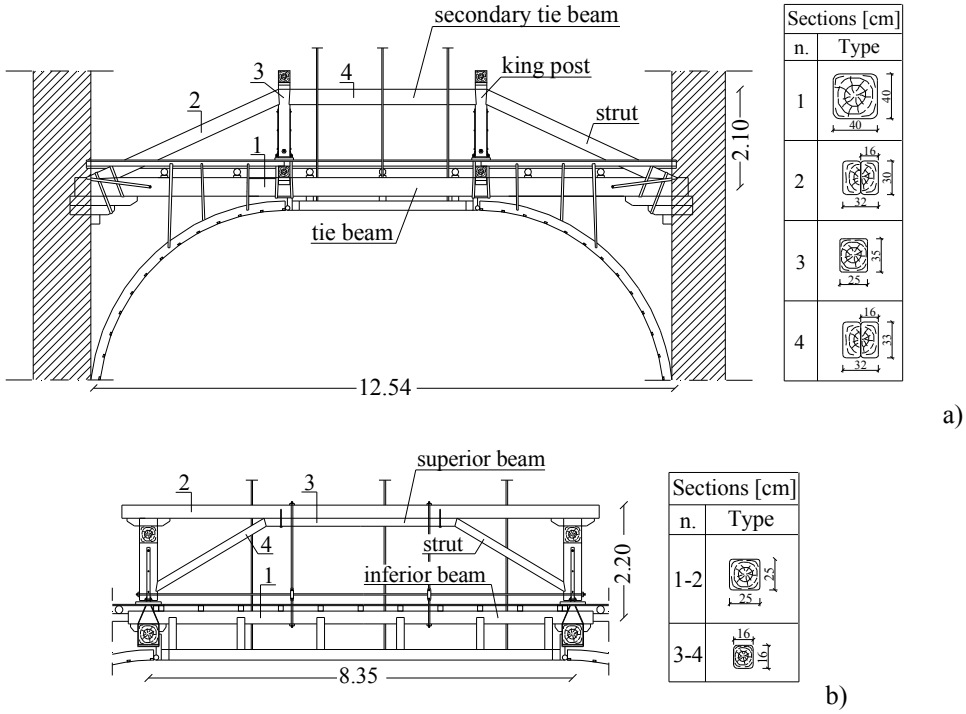

Figure 2.47. Guard Room (XXIX) – Geometrical survey – Vault supporting structure [m]: a) Truss; b) Stiffening frame.

2.8.2 *Failure diagnosis and visual grading*

Concerning the wooden species identification, ribs, splines and links are made of poplar, whereas all timber elements of the vault supporting structure are in chestnut wood.

Visual inspections have evidenced that the timber skeleton of the vault are in a proper conservation state because the vaulted ceiling has been recently realized, datable in the second half of the XX century. Whereas, wide water infiltrations were detected in several zones of the covering. In fact, at the intrados of the vault many humidity spots are highlighted, due to seepage from the above r.c. roof (Fig. 2.48a, b). In addition, diffuse cracks have been surveyed at the supports on the perimeter walls and at corners vault (Fig. 2.48a).

With regards to the vault supporting beams, the inefficiency of connection among the timber trunks have been evidenced, and the unfastened metallic stirrups, through which the thick planks should be jointed at the beam ends, do not guarantee the strengthening function (Fig. 2.49a).

On many elements of the trusses, stiffening frames and floor beams, natural defects of the material have been detected, as knots, shakes and longitudinal fissures due to the shrinkage. Furthermore, some timber elements of the trusses are locally rotten or subjected to biological attacks, as the king post located at northern-west and the strut which converges to it (Fig. 2.49b). The latter one is realized by three elements placed side by side, inefficiently connected one to another by means of nailed wooden planks. Finally, the planks of the floor are disjointed to the below structural elements and they lack in many parts.

All structural elements have been classified in third category, according to UNI 11119.

a)

b)

Figure 2.48. Guard Room (XXIX) – Failure diagnosis: a) Humidity spots and fissures of the fresco at the intrados of the vault; b) Damage of r.c. roof.

a) b)

Figure 2.49. Guard Room (XXIX) – Failure diagnosis: a) Inefficiency of connection of vault supporting beams; b) Biological attacks of truss king post.

2.8.3 *Structural modelling*

In Figure 2.50 the structural FEM models related to each sub-structure are depicted, together with the 3D model of the whole system, which has been set-up by means of the SAP 2000 v. 9.1.6 software. The structural elements are modelled with the actual cross-section size, detected during the geometrical survey.

The following different phases and corresponding material mechanical models and load conditions, which the structure to have undergone during its life, have been examined.

Erection phases (new timber)

- Phase 1: *Erection of the structure* (Model VF1)
  In this phase, the geometrical model is composed by all structural elements of the vault, skylight and vault supporting structure. The vault is connected to the upper structure by means of both wooden links and metallic ties. Only dead load is considered ($G_{1,\ structure}$).
- Phase 2: *Complete structure* (Model VF2)
  The vault, skylight and floor beams are completed, respectively, by a layer of plaster cast, transparent sheet and plank. All permanent loads are applied ($G_{1,\ structure} + G_{2,\ vault+floor}$);
- Phase 3: *Complete structure in service conditions* (Model VF3)

The structure is completed. Permanent load are applied on the vault ($G_{1,\ vault}$ + $G_{2,\ vault}$) and both permanent and variable actions are considered for the beam floor ($G_{1,\ floor}$ + $G_{2,\ floor}$ + Q_{floor}).

Phases at the present state (ancient timber)

- Phase 4: *Complete structure* (Model VS4)
  The geometrical and loading model is equal to Model VF2, but the material is modelled as ancient timber.
- Phase 5: *Complete structure in service conditions* (Model VF5)
  The geometrical and loading model VF5 and VF3 are identical, but for Model VF5 the ancient timber is considered.

Aiming at evaluating the effectiveness of the metallic ties which suspended the vault elements at the crown perimeter to the upper r.c. roof, the following additional model in ancient timber has been analyzed:

- Model VF6: *Complete structure without metallic ties*
  The geometrical and loading model is equal to Model VF4, but the metallic ties are removed; therefore the vault is only connected to the upper timber supporting structure by wooden links.

2.8.4 *Numerical analysis*

The analysis of the deformation state of the vault is presented in Figure 2.51, where all deformed configurations at each phase of its life are depicted with reference to the central YZ structural section. The displacements are scaled by an amplification factor equal to 15.

It is worth noticing that negligible deformations are due to the application on the variable action on structure above and to the vertical seismic motion. On the other hand, the creep and material degradation amplify the displacements of about two times (comparison between Models VS2 and VS4). By comparing the Models VS4 and VS6, at the perimeter elements of the vault crown, the beneficial effect of the vault suspension by metallic ties to the upper r.c. roof is apparent.

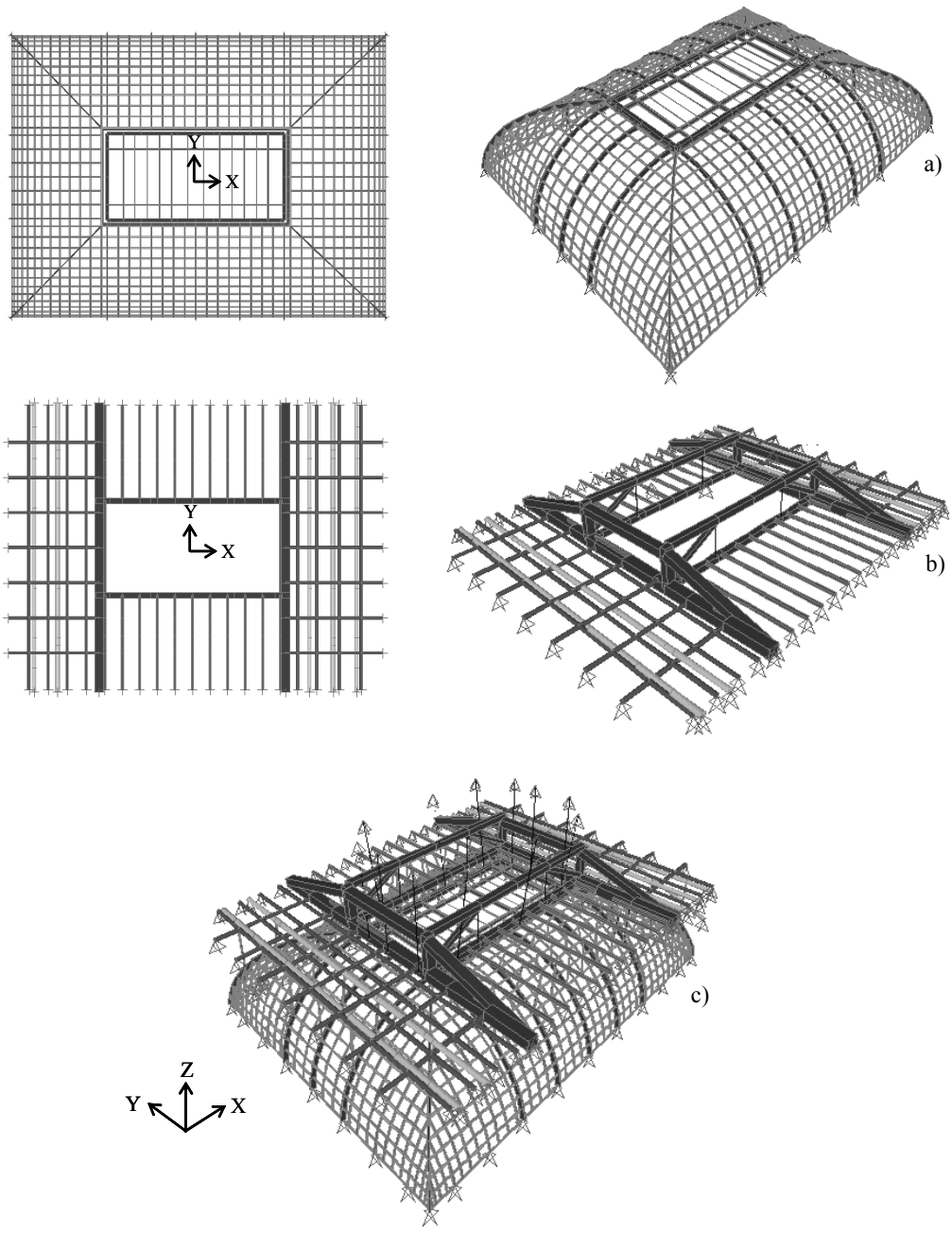

Figure 2.50. Guard Room (XXIX) – Structural modelling: a) Vault; b) Floor beam; c) 3D model.

The wooden links which connect the ribs to the upper elements of the floor, in the sections marked with black circles in the model plan, work as struts. In fact, the vault in "ancient timber" shows a flattening at the high zone and horizontal deformations in the curved side, near the masonry supports; however, the maximum vertical and horizontal displacements are negligible, under 3 cm. Therefore, the preservation of stuccos at the intrados of the vaulted ceiling is not compromise by the actual deformation state.

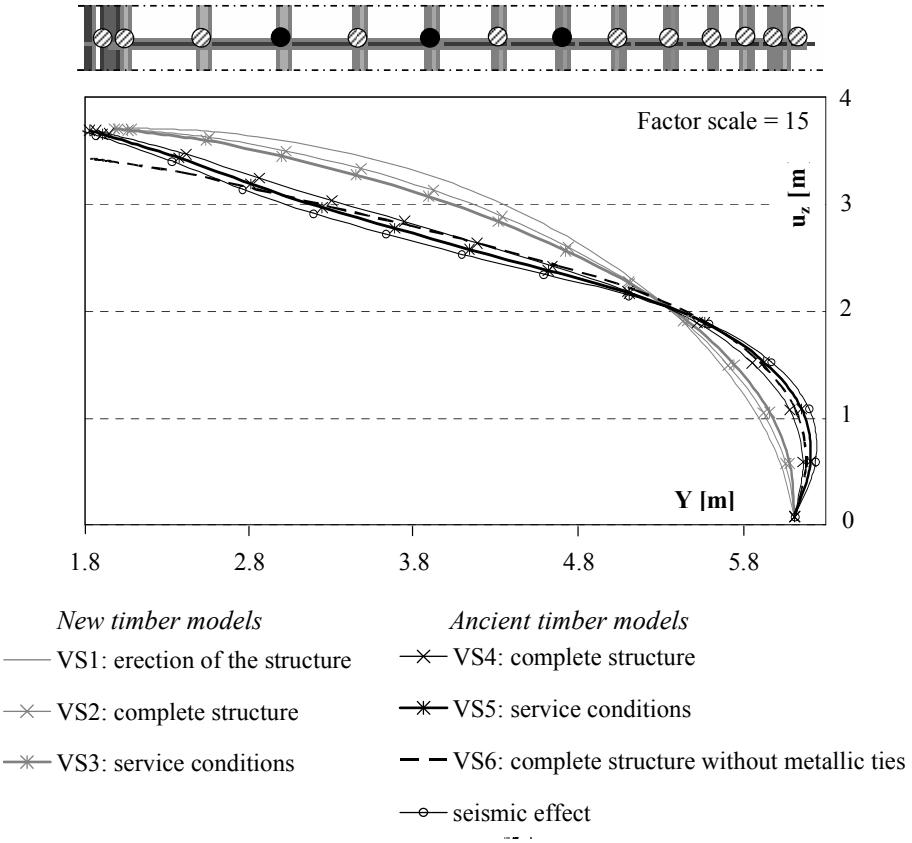

Figure 2.51. Guard Room (XXIX) – Numerical analysis: deflection state of the vault (YZ section).

In Figure 2.52 the stress state in vault structure is described in terms of Moment (M), Shear (S) and Axial force (A). The diagrams of the bending moment and shear force are amplified of ten times respect to axial force ones.

The safety checks at the ultimate limit state are satisfied for all structural elements, according to EC5.

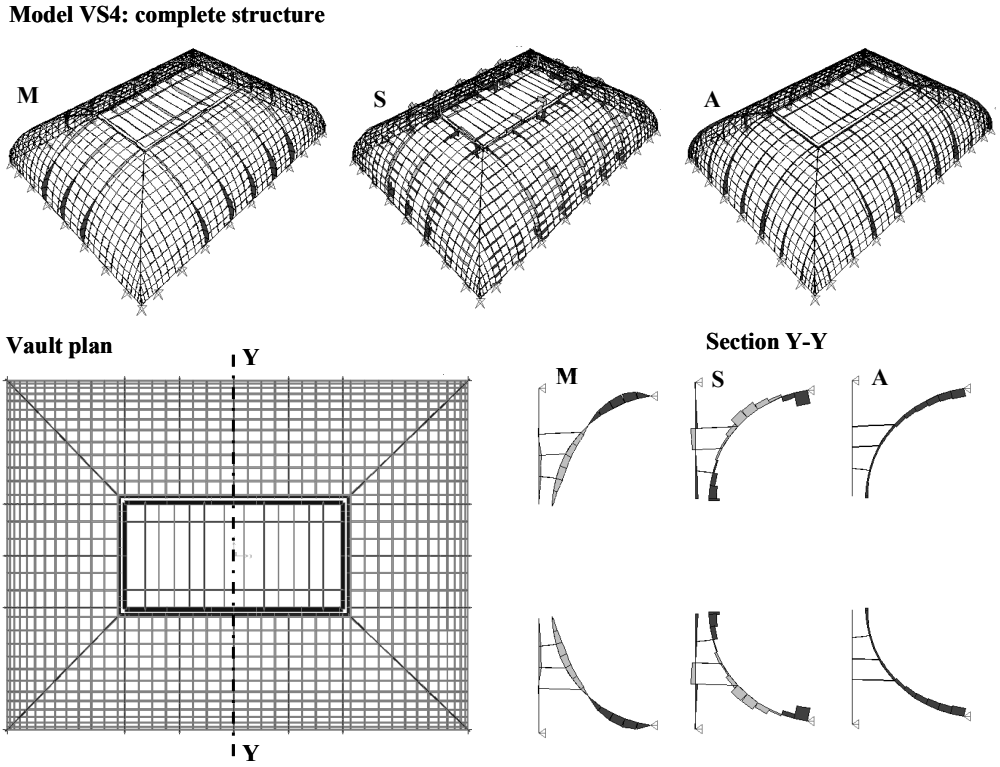

Figure 2.52. Guard Room (XXIX) – Numerical analysis: internal forces distribution in the vault elements (Model VS4).

The vertical deformed configurations of the tie beam of truss are plotted in Figure 2.53. It is possible to notice that the maximum displacement at the mi-section are unimportant, inferior to 1 cm. The removal of the metallic ties (Model VS6) produces an evident increment of deflections, due to the fact that, in this case, the vault crown perimeter is only supported by the bearing timber structure above, composed by trusses and transversal stiffening frames. In these main structural units, the benefits of the suspension of the vault by the metallic ties, are evident in terms of stress state, as shown in Figure 2.54.

All elements of the vault supporting structure accomplish the deformation and strength requirements, according to EC5.

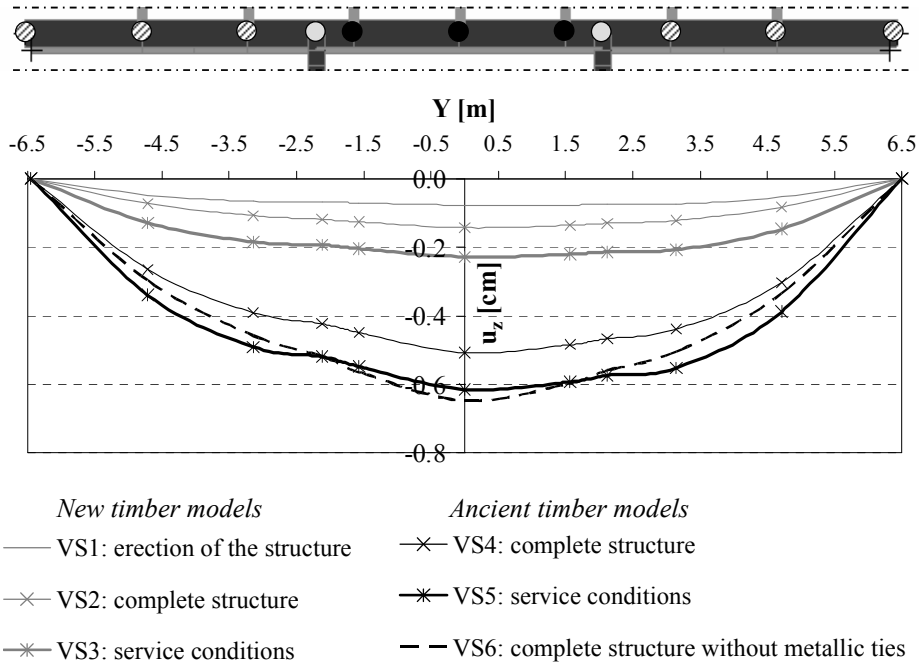

Figure 2.53. Guard Room (XXIX) – Numerical analysis: deflection state of the truss tie beam (Y direction).

2.8.5 *Proposed restoration interventions*

For the covering structure of the Guard Room, the proposed consolidation interventions mainly concern the restoring of the static function of the structural elements, required for biological degradation or connections inefficiency.

For the vault the timber members are globally in good condition and exhibit no structural damage, even if treatment against xylophagous insect is needed. Concerning the structural situation at the present state, the numerical analysis has shown that the links located at the curved sides, do not improve the stiffness of the vault; therefore only wooden links and metallic ties at the vault crown guarantee the conservation of the structure and fresco in the time.

However, the preservation of the vault implies the following local intervention for the elements of the upper supporting structure:

- Repair of the king post of the truss, located near the west main façade, which is damaged by fungi due to water seepage and substitution of the strut which converges to it;
- Restoration of all nailed connections among elements;
- Replacing the planks, which is disconnected by timber beams in some parts of the floor.

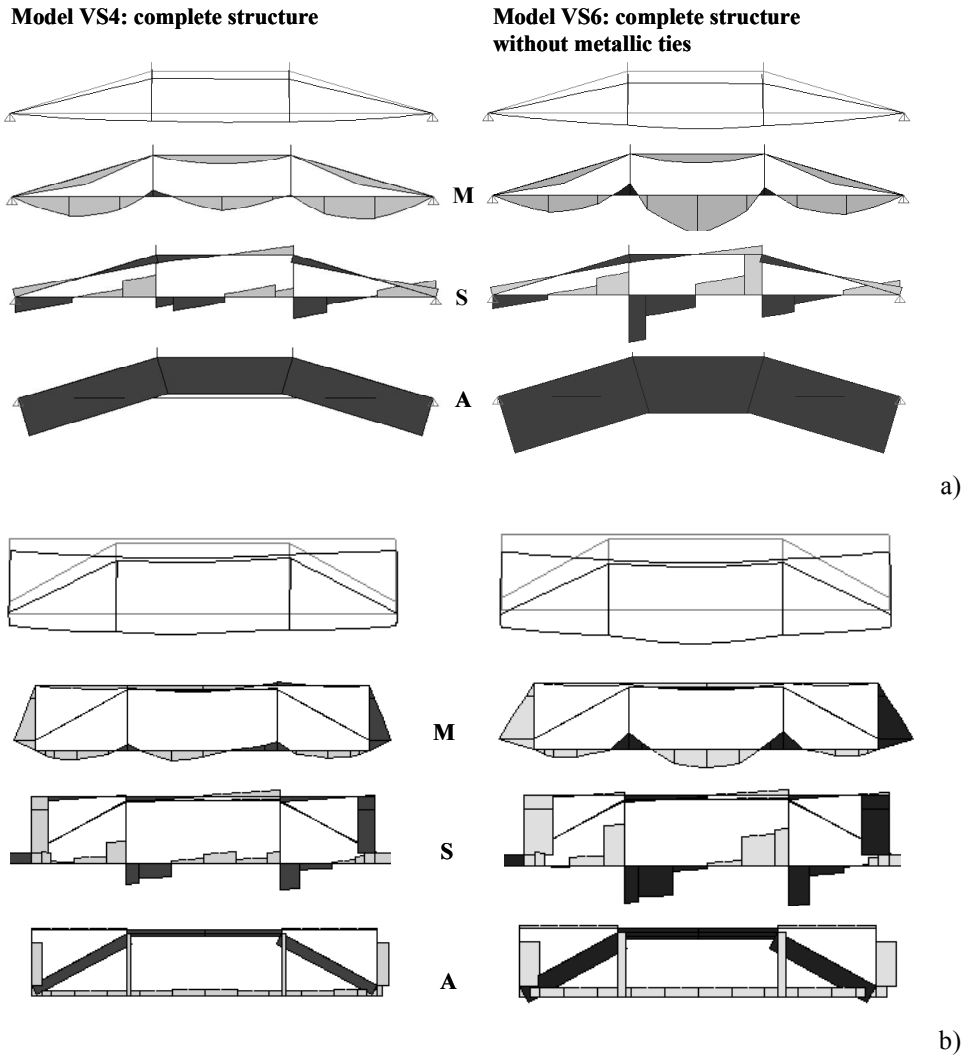

Figure 2.54. Guard Room (XXIX) – Numerical analysis: comparison of internal forces distribution in the truss and stiffening frame elements (Models VS4 and VS6).

Chapter 3

An innovative system for composite r.c.-timber floor: experimental investigations

3.1 GENERAL

Ancient masonry building are widely spread in all the European Countries. Floor structures in such constructions are typically made of timber primary beams with circular or rectangular cross-section, supporting wooden secondary elements, on which a inert mortar slab is cast. These floors are generally designed for modest live loads that do not meet the requirements of the present codes. In addition, as a consequence of long-term loads, timber floors often have excessive deformations that compromise their functionality.

In the framework of the restoration of ancient timber floor, the wood-concrete composite system represents a reliable solution for the upgrading of the existing floor slab, in case the old beams have both inadequate strength and stiffness, with consequent unacceptable deformations, or in case the beam floor does not accomplish the function of a rigid diaphragm in its plane when the building is subjected to horizontal forces.

Such an intervention generally consists of a concrete thin slab connected to the timber beams by means of connectors, like screws, nails, and studs, which require to drill the existing members. In such composite systems the beam resists the tensile forces, the concrete slab is able to withstand the compressive forces generated by bending and the connectors absorb the slip actions

developed at the interface between the concrete slab and the beam. This technology has been successfully used in many application since the 1980'. In fact it is characterized by short time of construction and it does not require the removal of old floors, what allows the preservation of the integrity of historical painted ceiling, when they are present at the floor intrados.

In order to avoid any strength reduction of the existing timber beams, which could be certainly caused by the perforation for the installation of traditional connectors, an innovative type of connections has been conceived for both circular and rectangular beams shape (Faggiano *et al.,* 2009d).

The connector between the timber beam and the concrete slab consists of a steel collar which is composed by two or more parts, bolted together at appropriate folded wings. The superior ones have the function of connectors and are immersed in the concrete cast. A layer of rubber is interposed between the sleeve and the wooden beam, in order to assure the adaptability of the system to the irregular surface of the existing ancient beams. The friction at the wood-steel surface is guaranteed by the bolt tightening force, which also provides a transversal ringing action on the beam.

In this chapter, monotonic push-out tests on several circular shaped configurations of the studied system are presented. Different types of connector, which correspond to further improvement of the system, are studied, pointing out the following aspects: the evaluation of the system failure mechanism; the optimization of the wood-rubber-steel contacts; the system improvements due to the bolts tightening increment.

Furthermore, bending test on full-scale r.c.-timber floor is presented, which has been carried out for studying the global performance of the composite system and the local behaviour of the connections. The experimental results emphasize the effectiveness of the proposed technique in terms of both flexural stiffness and strength.

The experimental investigations have been developed at the Laboratory of the Department of Structural Engineering (DIST) of the University of Naples "Federico II", within the international research project PROHITECH "Earthquake Protection of Historical Buildings by Reversible Mixed Technology", Prof. F.M. Mazzolani coordinator.

3.2 DESCRIPTION OF THE CONNECTION SYSTEM

The experimental investigations concern an innovative connection system for composite wood-steel-concrete floors, which is purposely conceived with the twofold aim to realize local strengthening of ancient beams with circular cross-section and to allow the stiffening of the existent floors by means of a collaborating concrete slab.

Several types of connectors are produced, like screws, nails and studs inserted in the beam by drilling the existing members. In such composite systems the timber beam resists the tensile forces generated by bending and the connectors absorb the relative slip between the timber beam and the concrete slab.

In order to avoid any strength reduction of the beams, which could be certainly caused by the perforation for the installation of traditional devices, an innovative connection system is proposed (Mazzolani *et al.*, 2005).

It consists of a steel collar composed by two parts, astride the timber beam, bolted together at adjacent wings (Fig. 3.1a). At the steel collar-timber beam interface a rubber layer should assure the complete adherence between elements, filling the gaps due to the surface irregularities of the timber beam. The function of connector is carried out by the couple of wings located at the superior edge of the beam and immersed in the concrete cast (Fig. 3.1a, b). The complete transmission of the slipping force through the connectors between the concrete slab and the timber beam is possible thanks to the bolt tightening that provides the necessary transversal ringing action, which guaranties the friction at the interface.

The design of the proposed connection system has been carried out by imposing the equivalence with the traditional stud connection system in terms of both strength and stiffness by assuming the perfect adherence at the timber beam-rubber layer contact surface (Gelfi *et al.,* 1998).

Definitely system fills evidently the twofold aim to act as a connector and to realize a local strengthening of the ancient timber beams. The main prerogatives of such system are the reversibility, the lightness, the ductility, the easiness of supply, transportation and erection.

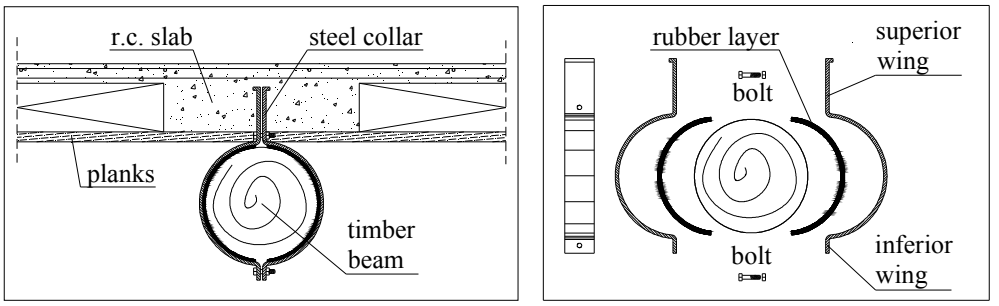

Figure 3.1. Composite timber-steel-concrete floor: a) Structural section; b) Collar system elements.

3.3 MONOTONIC PUSH-OUT TESTS

3.3.1 *Characteristics of the specimens*

Each tested specimen is composed by the following parts:

- Timber stock made of ancient chestnut with approximately circular cross section, about 15 cm diameter and 30 cm height, with surface irregularities and defects (Fig. 3.2a);
- Two cold formed steel Ω shaped elements (Fig. 3.2b), made of S275 steel grade, 60 mm width and 7 mm thickness, bolted at both superior and inferior wings. The latter are shorter as respect to the superior ones which work as a connector. Bolts are 8.8 grade and both 8 mm and 10 mm diameters are used;
- Two layers of natural rubber (SISMI60), 5 mm thickness, 235 mm length and 60 mm width.

After the connection of the steel collar wing, the macroscopic lacks of contact between the collar and the timber stock, which cannot neither be filled by the rubber layer, are due to the large surface irregularities of the stock (Fig. 3.2c).

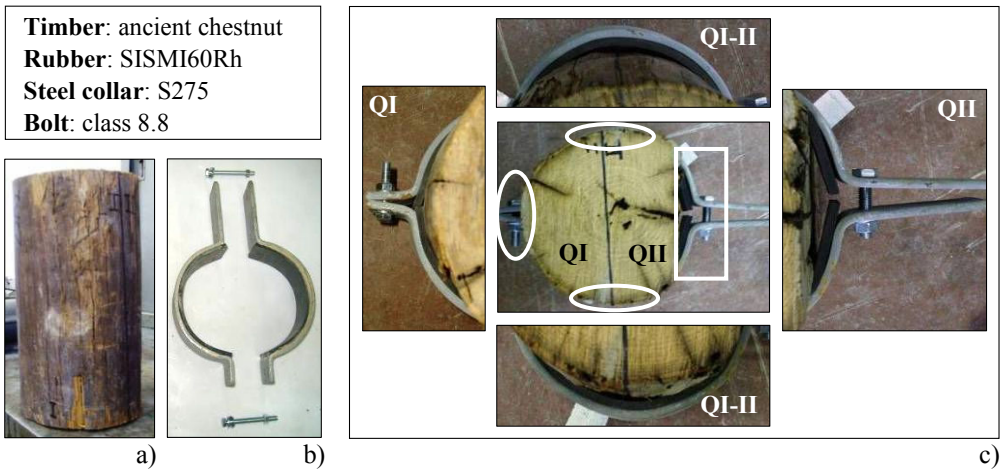

Figure 3.2. Monotonic push-out tests – Characteristics of the specimens: a) Timber stock; b) Steel collar; c) Lack of the collar-stock contact.

3.3.2 *Testing apparatus and set-up*

The testing equipment used consists of the following tools:

- Load machine Amsler, having 300 kN capacity, which applies a load with controlled velocity gradient (Fig. 3.3a);
- Purposely designed steel frame, realized as a support for the specimens (Fig. 3.3b). It is composed by three main elements: 1) a fixed base plate; 2) two movable plates, bolted to the base by means of extended holes; 3) two vertical pipes. The wings of the steel collar are inserted into appropriate slots and fixed to the steel support by means of blocking plates, so that any movement of wings is hindered during the load application. The steel frame is adaptable for different wooden specimens diameter, ranging from 10 to 30 cm;
- Load cell HBM, having 5 kN capacity (Fig. 3.3c);
- Electric displacement transducers (LVDT) HBM, having a maximum stroke of 50 mm and an accuracy of 1×10^{-3} (Fig. 3.3c).

Both transducers and actuator are connected to an electronic device and to a PC, in order to allow data acquisition and recording by means of the

program CATMAN (v. 6.2). For all tests, a quasi static loading procedure has been applied, using a constant displacement velocity equal to 0.01 mm/sec.

3.3.3 *Testing programme*

Twelve specimens, grouped in six series, are tested aiming at determining the collapse mode of the connection system, evaluating both the optimization of the friction at rubber-steel interface and the system improvement due to the bolts tightening increment (Marzo *et al.,* 2009).

Therefore, the three following system types are analyzed (Fig. 3.4):

- (R): simple rubber-steel contact, given that the rubber is simply in contact with the collar internal surface;
- (GR): glued contact by vulcanizing glue REMA SC 2000, fixing the rubber to the steel collar;
- (R-TS): grooved steel collar with a ribbed rubber. Two longitudinal rubber ribs, glued to the rubber layers by means of a vulcanizing glue, realize a mechanical blocking of the rubber layer to the steel collar, they being inserted in the steel throat surface, where purposely grooves are cut.

The bolted connection of the steel collar parts around the timber stock is improved by means of both the use of higher bolts grade, such as one M10, and the use of two bolts M8 at each couple of wings (Fig. 3.4). As a result the total tightening ($N_{s,t}$) is equal to 104 kN (26 kN at each bolt) for the first connection type and to 132 kN (16.5 kN at each bolt) for the second one.

In Table 3.1 the main features of the specimens are given, such as: series number, push-out test label, rubber-steel contact type, bolts number, total tightening force ($N_{s,t}$).

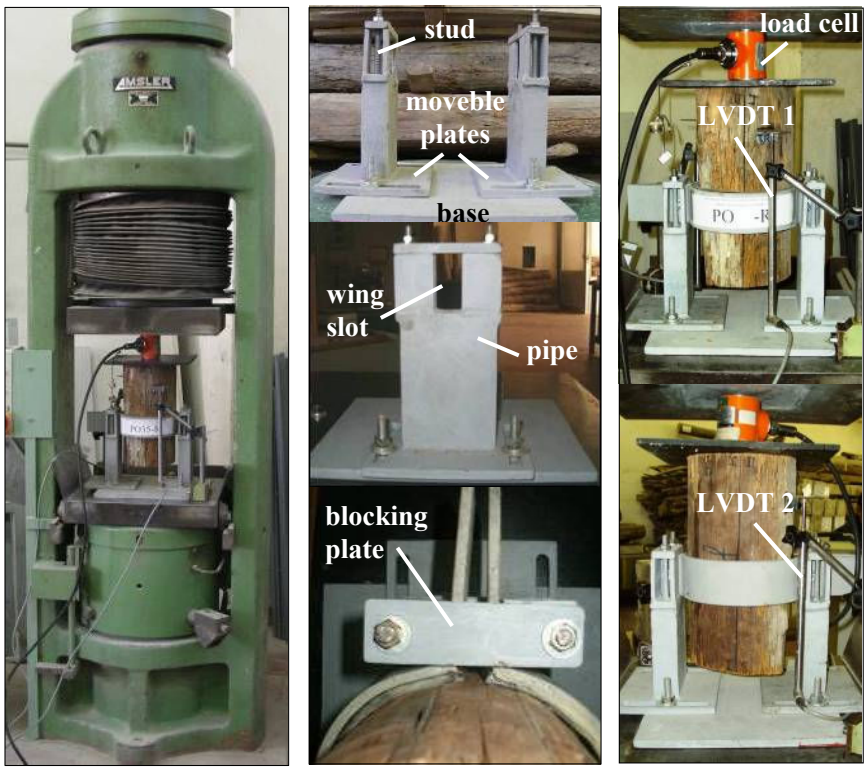

Figure 3.3. Monotonic push-out tests – Testing apparatus and set-up: a) Load machine Amsler; b) Support steel frame; c) Specimen equipped for test.

Table 3.1. Monotonic push-out tests: main features of the tested specimens.

Series	Label	Contact type	Bolts	$N_{s,t}$ [kN]
I	PO1 PO2	(R)	2M10	104
II	PO3 PO4	(R)	4M8	132
III	PO5 PO6	(GR)	2M10	104
IV	PO7 PO8	(GR)	4M8	132
V	PO9 PO10	(R-TS)	2M10	104
VI	PO11 PO12	(R-TS)	4M8	132

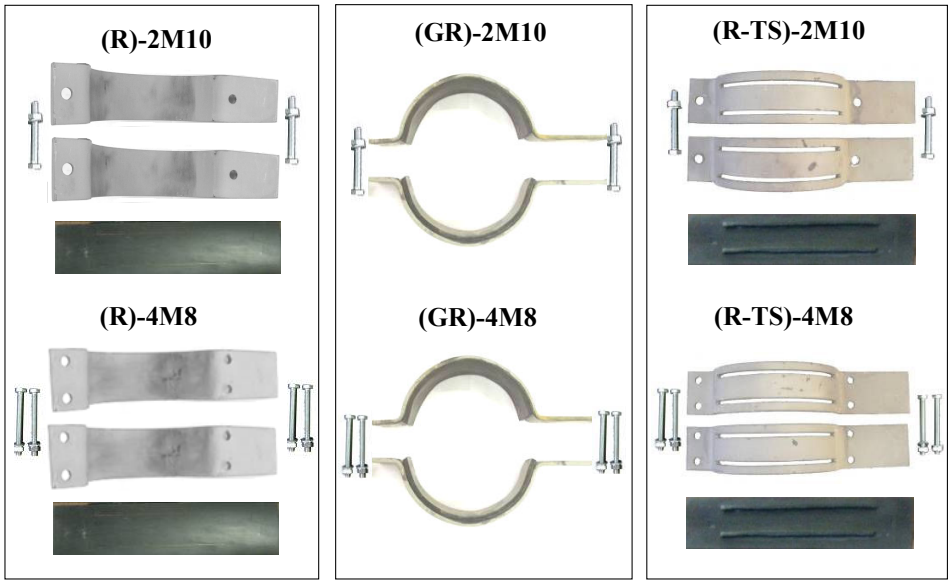

Figure 3.4. Monotonic push-out tests – Testing programme: three connection system types.

3.3.4 *Applied methodology for data processing and interpretation*

The acquired data from each push out test are the applied forces and the relative displacements among the timber stock and the steel collar. Force (F)-Slipping (S) diagrams are plotted for each single transducer (LVDT), together with the average curve. Moreover the average curve among the F-S diagrams of each series of tests is determined too.

It is generally observed that the initial linear growing branch corresponds to the shear deformation of the rubber layer; whereas the flat branch corresponds to the failure mechanism of the tested de-vices. For intermediate values of applied force, several sources of non linearity can be identified, such as some relative rotations between the collar parts and different extent of the rubber layer depending on the contact irregularities between rubber layers and wooden stock.

Aiming at analyzing the experimental responses, two parameters of the average curves are considered: the initial tangent stiffness (K_i) and the maximum friction force (F). For the sake of comparison, the elasto-plastic theoretical curves, are also given. The theoretical stiffness (K_{th}) is calculated

considering the reduction of the rubber thickness for effect of the bolts preloading force, while the slipping resistance is obtained multiplying the friction factor (μ) for the total bolts tightening ($N_{s,t}$) (Table 3.2).

Table 3.2. Monotonic push-out tests: theoretical stiffness and bolts tightening.

Bolts	K_{th} [kN/mm]	N_s [kN]	$N_{s,t}$ [kN]
2M10	6.16	26.0	104
4M8	6.21	16.5	132

3.3.5 *Results and discussion*

Experimental results of push-out tests are presented in Figures 3.5 to 3.7 in terms of F-S curves for each series of specimens. Tables 3.3 to 3.5 provide the values of both initial tangent stiffness (K_i) and maximum friction force (F_{max}) for each average F-S curve.

For the rubber-steel simple contact (R) the system collapse consists in a large slipping at the steel-rubber interface (Fig. 3.7a).

For the devices with chemical and mechanical blocking of the rubber to the steel collar (GR, R-TS), the system rupture consists in an evident damage of the rubber, jutted out of the edge, depending on the contact irregularities at the rubber-wood interface (Fig. 3.7b, c). In particular, during the tests of the R-TS systems a separation of the rubber ribs from the layer is occurred (Fig. 3.7c). The latter one should be improved as respect to the TS tested one, by using a rubber layer directly moulded as ribbed.

Furthermore, the tested connector with one M10 bolt per wing allows the occurrence of a relevant rotation between the collar parts, with consequent bending of the bolts (Fig. 3.7d). Therefore the improved connection by means of two bolts M8 at each couple of wings, avoids any rotation between the collar elements.

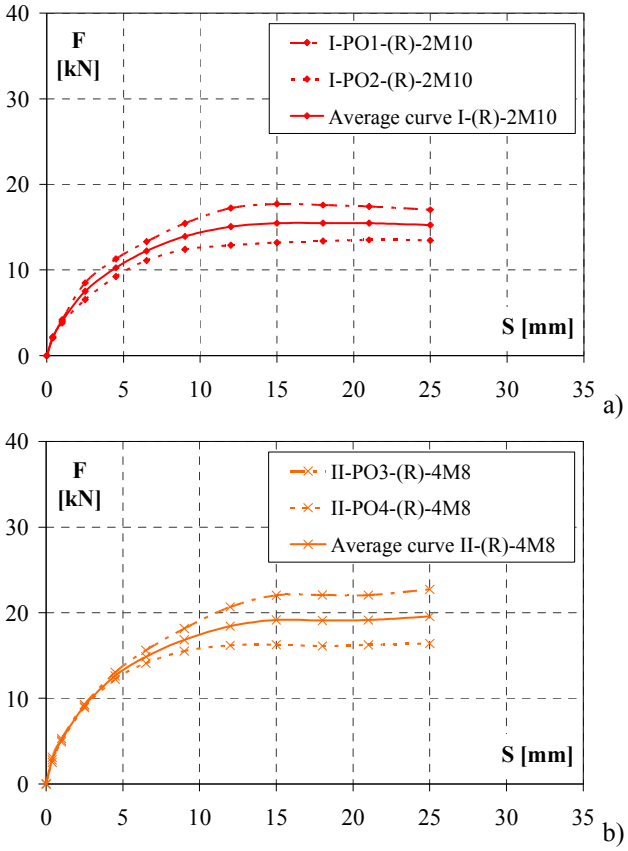

Figure 3.5. Monotonic push-out tests – Experimental results – (F-S) curves: a) Series I-(R)-2M10; b) Series II-(R)-4M8.

Table 3.3. Monotonic push-out tests – Initial tangent stiffness (K_i) and maximum friction force (F_{max}): series I-(R)-2M10 and II-(R)-4M8.

Series I, II	**K_i [kN/mm]**	**F_{max} [kN]**
Av. I-(R)-2M10	4.00	15.11
Av. II-(R)-4M8	5.10	19.04

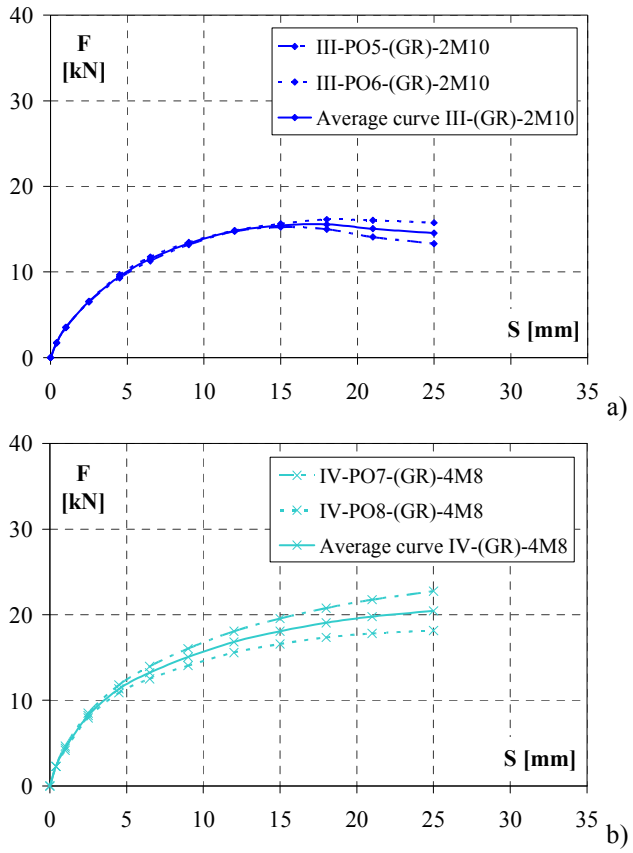

Figure 3.6. Monotonic push-out tests – Experimental results – (F-S) curves: a) Series III-(GR)-2M10; b) Series IV-(GR)-4M8.

Table 3.4. Monotonic push-out tests – Initial tangent stiffness (K_i) and maximum friction force (F_{max}): series III-(GR)-2M10 and IV-(GR)-4M8.

Series III, IV	**K_i [kN/mm]**	**F_{max} [kN]**
Av. III-(GR)-2M10	3.53	15.22
Av. IV-(GR)-4M8	4.40	19.74

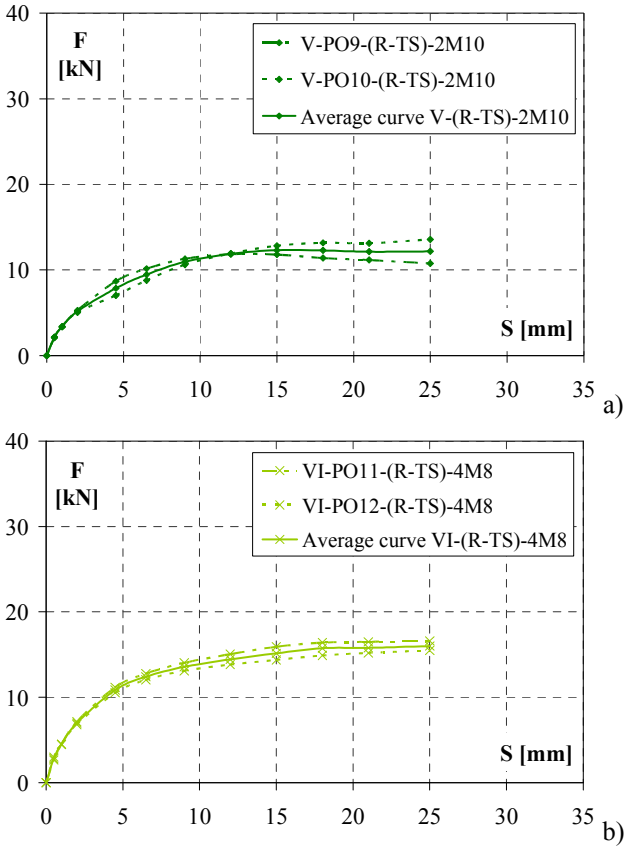

Figure 3.7. Monotonic push-out tests – Experimental results – (F-S) curves:
a) Series V-(R-TS)-2M10; b) Series VI-(R-TS)-4M8.

Table 3.5. Monotonic push-out tests – Initial tangent stiffness (K_i) and maximum friction force (F_{max}): series V-(R-TS)-2M10 and VI-(R-TS)-4M8.

Series V, VI	**K_i [kN/mm]**	**F_{max} [kN]**
Av. V-(R-TS)-2M10	3.38	12.13
Av. VI-(R-TS)-4M8	4.50	15.76

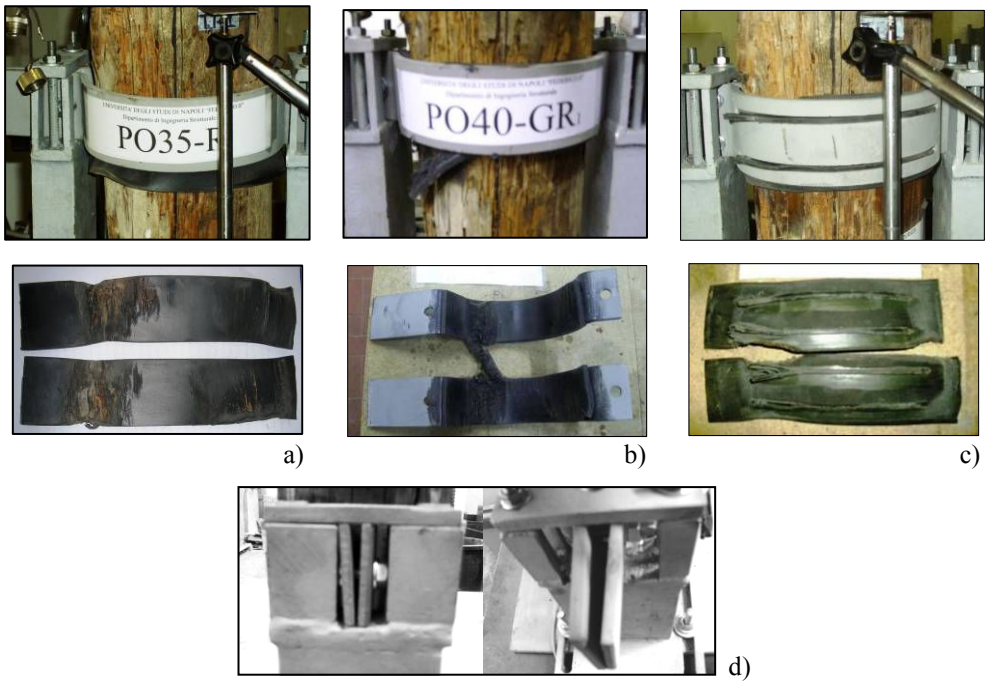

Figure 3.7. Monotonic push-out tests – Failure mechanisms: a) Simple contact (R); b) Glued contact (GR); c) Grooved steel collar (R-TS); d) Rotation between the collar parts (one bolt M10 per wing).

Aiming at the evaluation of the beneficial effect of the bolts tightening increment, the F-S average curves of two series of tests, for one and two bolts per each wing, with corresponding different total tightening force (2M10 – $N_{s,t}$=104 kN; 4M8 – $N_{s,t}$=132 kN), are compared in Figure 3.8 for each analyzed system type (R, GR, R-TS). The elasto-plastic theoretical curves and the friction factors (μ) are also indicated.

The improvement in terms of both stiffness (K_i) and maximum friction force (F_{max}), due to the presence of two bolts per wing instead of one, is quantified in Table 3.6. It is worth to noticing that the percentage increment of initial tangent stiffness (ΔK_i) and strength (ΔF) corresponds to about the same one of the total bolts tightening ($\Delta N_{s,t}$), equal to 27%.

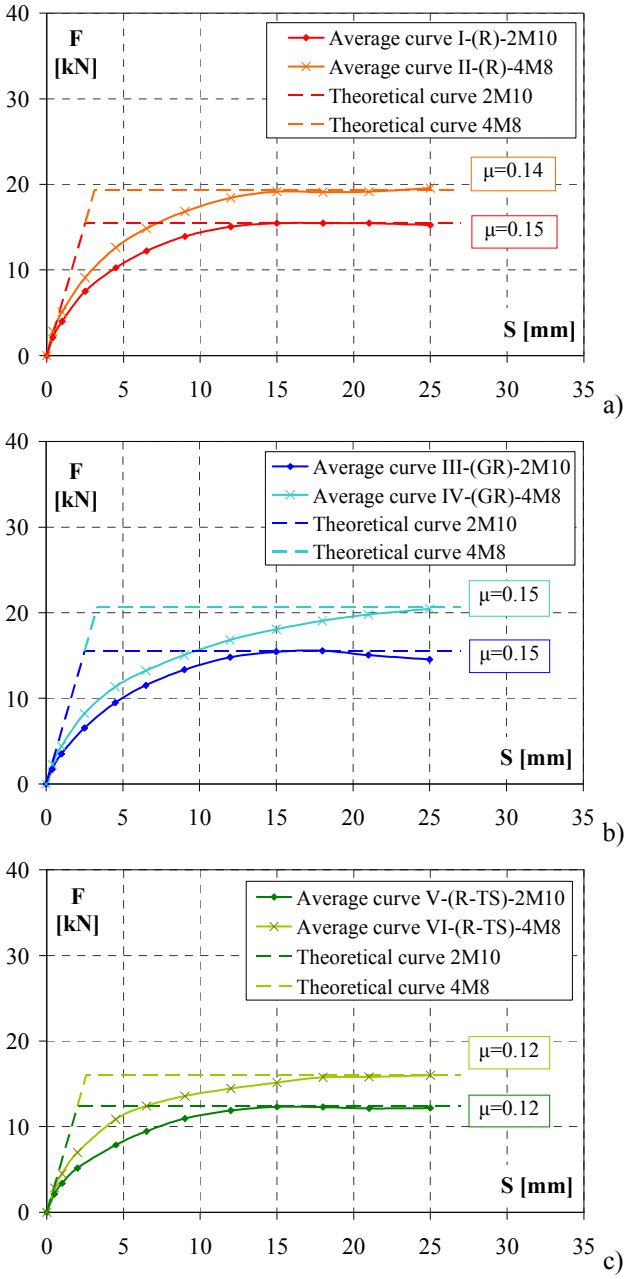

Figure 3.8. Monotonic push-out tests – Comparison among F-S average curves: a) Simple contact (R); b) Glued contact (GR); c) Grooved steel collar (R-TS).

Table 3.6. Monotonic push-out tests – The stiffness (ΔK_i) and strength (ΔF) increment [%] for systems improved by larger bolts tightening.

Rubber-steel contact type	K_i [kN/mm]	F_{max} [kN]	μ	ΔK_i [%]	ΔF [%]
(R)-2M10	4.00	15.11	0.15	27.5	26.0
(R)-4M8	5.10	19.04	0.14		
(GR)-2M10	3.53	15.22	0.15	24.6	29.7
(GR)-4M8	4.40	19.74	0.15		
(R-TS)-2M10	3.38	12.13	0.12	33.1	29.9
(R-TS)-4M8	4.50	15.76	0.12		

In Figure 3.9 the comparison among F-S average curves of the three analyzed connection devices, provided with 2M10 and 4M8 bolts respectively, is shown. It can observe that the simple (R) and glued (GR) rubber-steel contact types reveal a similar response being characterized by the same friction force (μ=0.15); whereas in the case of the mechanical blocking of rubber layers to the steel collar (R-TS) the system behaviour shows a worse performance (μ=0.12).

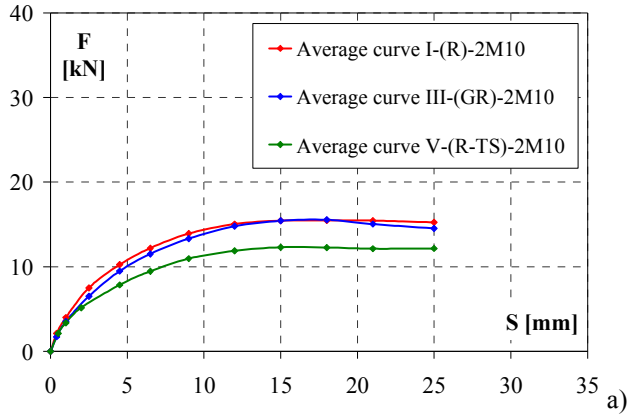

Figure 3.9. Monotonic push-out tests – Comparison among F-S average curves: a) Systems with 2M10 bolts; b) Systems with 4M8 bolts. (continues)

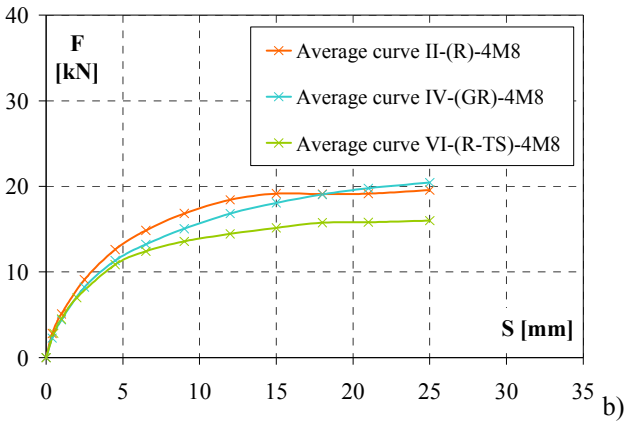

b)

Figure 3.9. Monotonic push-out tests – Comparison among F-S average curves: a) Systems with 2M10 bolts; b) Systems with 4M8 bolts.

On the basis of the experimental evidence, it is possible to conclude that the optimum collar system should compulsory require a bolted connection between the parts by means of two bolt per wing and chemical blocking of the rubber to the steel collar. The influence of the timber stock shape, irregularities and defect on the system performance is worth to be deeply investigated.

3.4 BENDING TEST ON TIMBER-STEEL-CONCRETE FLOOR

3.4.1 *Characteristics of the system*

The r.c.-timber composite floor consists of two beams made of ancient chestnut, with circular cross-section, 12 cm diameter, placed at inter-axis of 0.70 m and with 2.00 m length (Fig. 3.10). The overall floor size is 1.80×1.10 m^2. The r.c. slab is 12 cm thick, it is lightened by polystyrene blocks, 7 cm high. The concrete slab is cast on layer of wooden planks, 2 cm thick, so-called “panconcelle”. The slab is reinforced by steel rebars Φ8/25 cm and a steel net Φ6/25 (Fig. 3.10).

The used connection system consists of steel collars, surrounding the wooden stock, which are composed by two parts, bolted together at appropriate folded wings, the superior ones having the function of connectors.

The collar is composed by two cold formed steel Ω shaped elements made of S275 steel grade, 60 mm width and 7 mm thickness, bolted at both superior and inferior wings. Bolts 8.8 grade with 10 mm diameter are used. At the interface between the steel collar and the wooden beam, a rubber layer, glued to the collars by vulcanizing glue REMA SC 2000, guarantees the complete adherence between elements. Three connectors are used per each beam.

In Table 3.7 the mechanical properties of the used materials are given. In particular, the stiffness and strength properties of chestnut timber are the 5-percentile values which have been obtained by means of experimental tests on structural elements in compression parallel to the grain and in bending (see chapters 6.2.5 and 7.6).

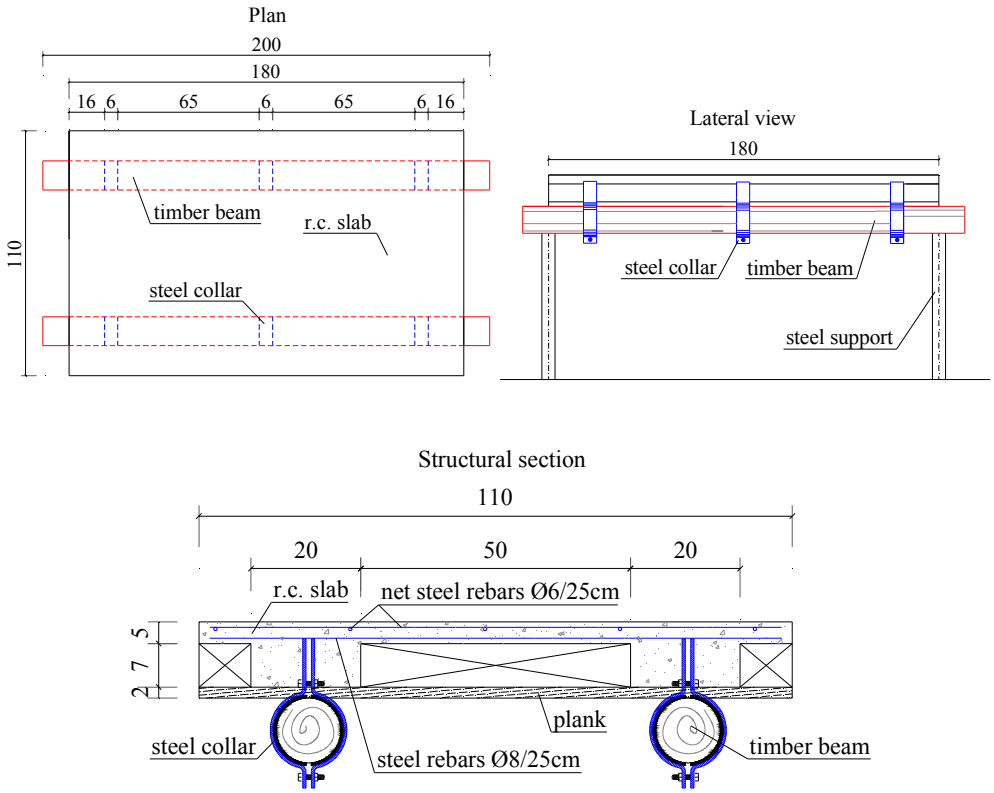

Figure 3.10. Bending test on composite floor: geometric characteristics of the system.

Table 3.7. Bending test on composite floor: material properties.

Concrete C20/25	
cubic strength (R_{ck})	25 N/mm^2
cylindrical strength (f_{ck})	20 N/mm^2
modulus of elasticity (E_c)	30500 N/mm^2
Timber (ancient chestnut)	
bending strength (f_m)	32 N/mm^2
compression strength ($// f_{c,0}$)	20 N/mm^2
flexural elasticity modulus ($E_{m,g}$)	11000 N/mm^2
Steel S275	
Yielding strength (f_y)	275 N/mm^2
Modulus of elasticity (E_s)	210000 N/mm^2

Table 3.8 summarizes the mechanical characteristics of the single composite beam, in accordance with the transformed sections, where, under the hypothesis of linear material, the concrete slab is considered as wood equivalent, being $n=E_c/E_w$ the ratio between concrete and wood elastic moduli. It has been conventionally assumed that the r.c. slab is characterized by a 20 cm width, whereas a height of 12 cm has been taken into account. The timber beam has a circular cross-section with a diameter of 12 cm.

Table 3.8. Bending test on composite floor: mechanical characteristics of composite beam.

Timber beam			**R.C. slab**			**Composite section ($n=E_c/E_b=2.77$)**			
E_b [N/mm^2]	I_b [cm^4]	W_w [cm^3]	E_c [N/mm^2]	I_s [cm^4]	W_s [cm^3]	$S_{s,id}$ [cm^3]	I_{id} [cm^4]	$W_{id,sup}$ [cm^3]	$W_{id,inf}$ [cm^3]
11000	1017	170	30500	2880	240	1330	28000	3491	1551

3.4.2 *Testing apparatus and set-up*

The testing equipment used consists of the following tools (Fig. 3.11):

- Load machine Mohr Federhaff AG, as contrast frame by the fix part;
- Jack which applies a manual controlled load;
- Loading cell HBM, having 740 kN capacity;
- Electric displacement transducers (LVDT) HBM with accuracy of 1×10^{-3} mm;

- Two steel portals realized by frames with tubular section, which perform the floor supports;
- Steel frame composed by two IPE 200 connected at the middle span with an HE 180, through which, for each timber beam, the four-points scheme is considered (Fig. 3.11); the jack is located on the beam HE 180 at the middle span of the floor.

The transducers measure the deflections of the two beams (w1 and w2) at the mid-span, the relative slip between the timber beam and the concrete slab (B1-S and B2-S) and the relative slip between both lower and middle part of the timber beam and the collar devices (B-C).

Both transducers and load cell are connected to an electronic device and to a PC, in order to allow data acquisition and recording by means of the program Catman (v. 6.2).

The test was performed in monotonic conditions aiming at evaluating the global performance of the composite r.c.-timber floor and determining its maximum load-bearing capacity. The load was increased up to the rupture of the system in two subsequent phases.

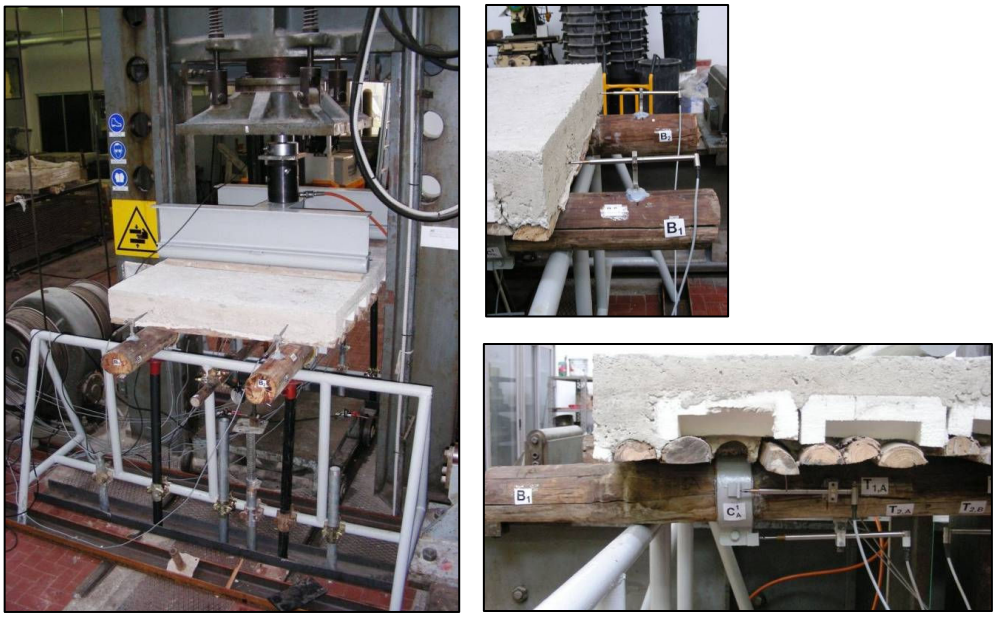

Figure 3.11. Bending test on composite floor: testing apparatus and set-up. (continues)

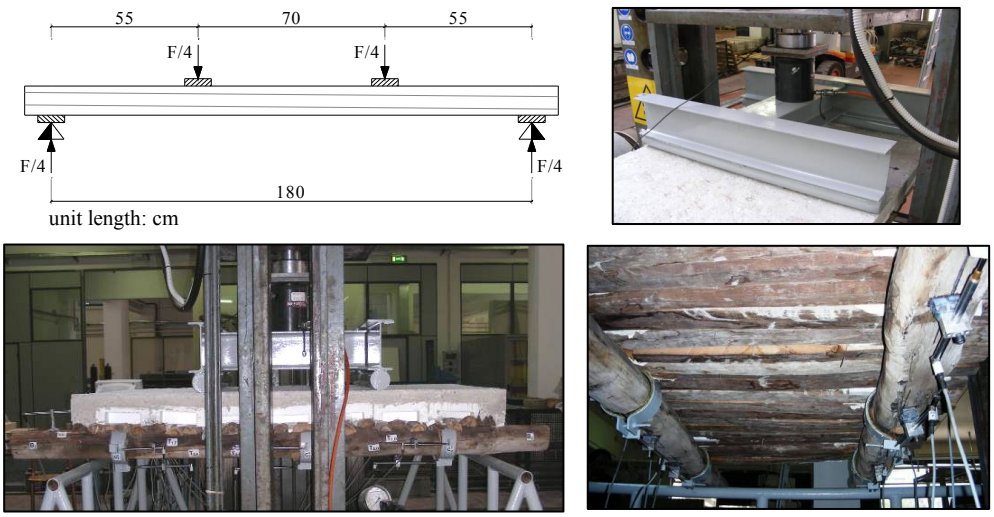

Figure 3.11. Bending test on composite floor: testing apparatus and set-up.

3.4.3 *Results and discussion*

In Figure 3.12 the experimental results are provided in terms of force (F) – vertical displacement (w) curves. The average values of the deflections at the middle section of the two beams are considered. The diagram shows an almost linear elastic behaviour up to the reached maximum force (F_{max}), equal to 175 kN, which corresponds a displacement of 30.5 mm, and significant ductility which leads to a failure of the system when displacements larger than 90 mm are attained. This is due to the rupture of the timber beams at the tension side for the presence of natural defects, such as knots and slope of grain (Fig. 3.13).

The experimental performance is compared with the idealized rigid connection behaviour, which coincides with that of the transformed section theory. Furthermore, the F-w curve of the floor beams without connection with the r.c. slab is depicted as well. It is assumed a brittle behaviour for each timber beam under bending condition, with a mean global modulus of elasticity ($E_{m,g}$) of 11000 N/mm^2 and 5-percentile ultimate flexural strength (f_m) of 32 kN/mm^2, according to the experimental evidence shown in chapter 7 for bending tests on full-scale elements in chestnut wood. Therefore, a

maximum global force of 80 kN is obtained for the floor with only timber beams .

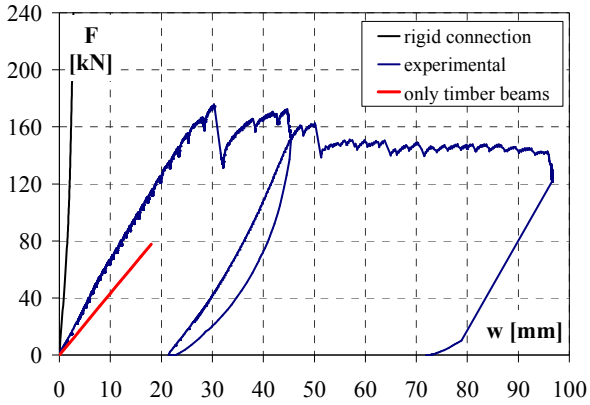

Figure 3.12. Bending test on composite floor: force (F) – vertical displacement (w) curves.

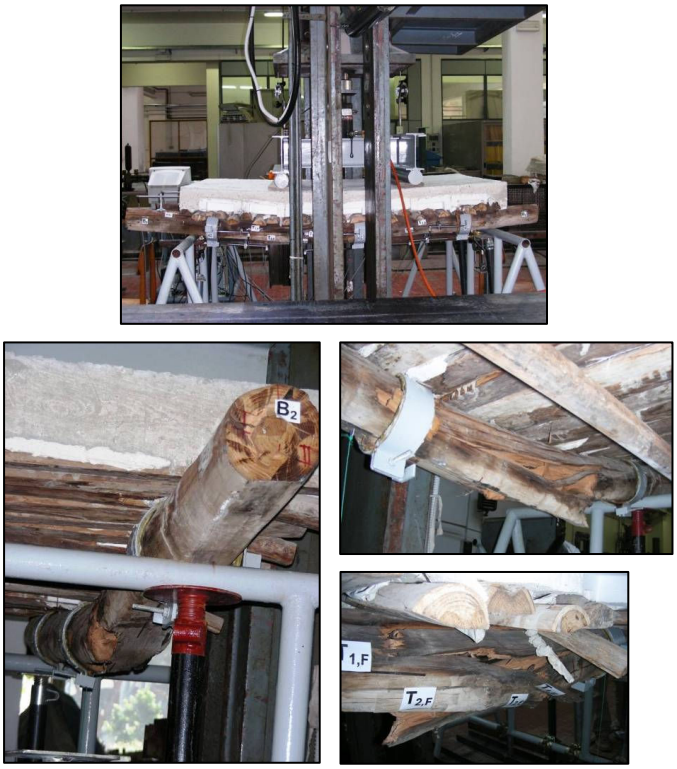

Figure 3.13. Bending test on composite floor: rupture mode.

The comparison in terms of numerical results between the experimental and the only timber beams behaviour is given in Table 3.9. It shows that the improvement percentage due to the r.c.-timber connection by means of collar device, realized with glued contact type among the steel sleeve and the rubber layers, is equal to 53 % for the initial stiffness (ΔK_i) and 119 % for the maximum resistance (ΔF_{max}).

Table 3.9. Bending test on composite floor – Comparison of results: initial stiffness (K_i) and maximum force (F_{max}).

	K_i [kN/mm]	F_{max} [kN]	ΔK_i [%]	ΔF [%]
Experimental	6.57	175	53	119
Only timber	4.30	80		

Shear vs slab-to-beam slipping curves and typical shear vs collar-to-beam slipping relationship are shown in Figures 3.14a and 3.14b respectively.

It is worth of noting that in both cases, the slipping magnitude is very small, about 6 mm for the slab-to-beam slipping and 3 mm for the collar-to-beam slipping. Both these displacements are retrieved when the corresponding maximum shear forces are attained.

Comparing these results with the ones obtained by monotonic push-out tests (see chapter 3.3.5, Fig. 3.6a), it is possible to observe that the maximum performance of the system is obtained without any failure of the connectors.

These results represent an important experimental support for further theoretical and numerical investigations on the local and global behaviour of the innovative collar system for composite r.c.-timber floor.

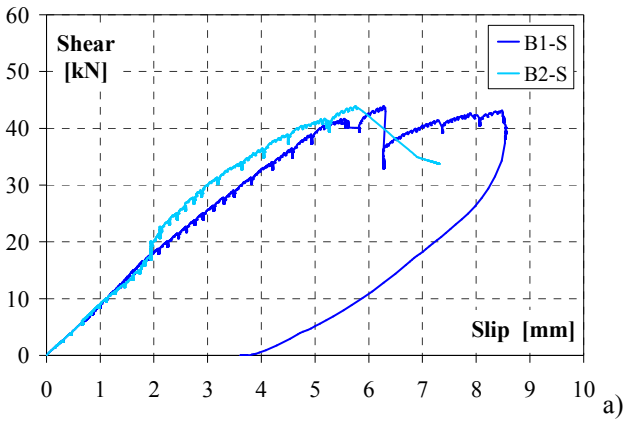

a)

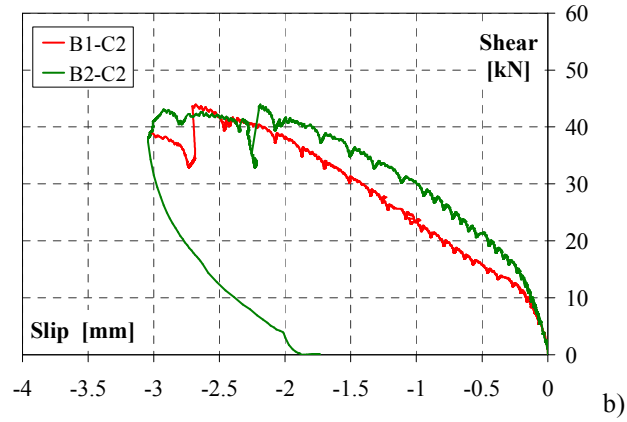

b)

Figure 3.14. Bending test on composite floor – Experimental curves: b) Shear – slip beam-to-slab; c) Shear – slip beam-to-collar.

Chapter 4

Mechanical identification of old chestnut timber: experimental activity

4.1 GENERAL

The restoration of ancient timber structures, intended as total or partial substitution of deteriorated elements or in static reinforcing interventions, is a very actual matter especially in Italy, where in many ancient buildings located in historical centres, the horizontal load bearing structures, such as roofs and floors, are made of timber. Due to its nature wood presents several defects (i.e. knots, shakes, slope of grain, etc.) and structural anomalies (i.e. cracking, deformation induced by long duration loads, connection degradation, etc.), moreover it suffers a biological deterioration, closely connected to the external environmental conditions. It is apparent as the analysis of ancient structures made of wood is very cumbersome for all the inherent difficulties to be faced at both material and structural behaviour characterization.

In order to assess the safety of old structures and preserve their original essence, *in situ* inspection and evaluation represent a first step towards diagnosis, structural analysis and the definition of possible consolidation intervention. The last decades witnessed developments in the testing techniques and equipments that allow diagnosis and inspection of historical constructions. Non-destructive techniques have an own special interest due to the fact that their application does not affect the present structural integrity

and safety of the structure. These methods can be classified in two distinct groups: Global Test Methods (GTM) and Local Test Methods (LTM). The first ones include the application of the ultrasonic and vibration methods. The LTM, with the utilization of the Resistographic and the Pilodyn as the most common NDT devices, play usually a role support in the visual grading of timber members and structures. The application concerns the evaluation of the incidence and severity of defects in the material state of conservation, with the aim of comparing the residual section with the variation of density, usually associated with the loss of mass.

The effectiveness of NDT methods aimed at the structural identification should be aided through laboratory tests by studying the variability of the mechanical properties of the timber elements. The efficiency of investigations depends upon the accuracy and adequacy in choosing complementary instruments and testing methodologies; in this respect not only non destructive testing results must be correlated with those of classical laboratory tests, but also correlations among the results of different non destructive methodologies must be determined.

In this context, an experimental campaign has been carried out at the Laboratory of the Department of Structural Engineering (DIST) of the University of Naples "Federico II", including NDT investigations and destructive tests on both full-scale and small defect-free specimens, made of old chestnut wood (*Castanea sativa* Mill.), which is usually present in noble construction of South of Italy, given not only its mechanical and durability properties, but also its aesthetic characteristics. The aim of the experimental research is to provide a methodology for *in situ* mechanical identification of timber elements by means of combined non-destructive techniques, based on statistical analysis and evaluation.

The research activity has been developed in the framework of the Italian project PRIN 2006 "*Diagnosis techniques and totally removable low invasive strengthening methods for the structural rehabilitation and the seismic improvement of historical timber structures*", prof. M. Piazza coordinator; research unit UNINA "*Experimental evaluation of the mechanical properties of wood by means of non-destructive compared techniques for the characterization of existing wooden structures"*, prof. B. Faggiano scientific responsible, M.R. Grippa and A. Marzo research team.

In this chapter the whole experimental campaign, based on non-destructive investigations (NDT), such as hygrometric, ultrasonic, sclerometric and resistographic, and destructive tests (DT) in compression and in bending, is introduced, focusing on the used material and the tested specimens features, together with the common NDT methods, used in place for non-destructive diagnosis and evaluation of the timber members and structures.

4.2 RESEARCH PROGRAM

Several phases have been involved in the research activity, such as experimental investigations, data processing, structural identification by means of combined NDT-DT relationships. The multi-phase organization is following described:

1. Supplying of the test material:
- The experimental campaign has been developed on structural members made of old chestnut wood (*Castanea sativa* Mill.). They belonged to ancient roofing trusses, from which several samples in structural dimensions and defect-free specimens were obtained for non-destructive and destructive tests.

2. Execution of non-destructive tests (NDT):
- *Hygrometric tests*, for the evaluation of the moisture content of wood, which severely affects its mechanical properties and its susceptibility to degradation by decay;
- *Ultrasonic investigations*, through which a direct relationship between the stress wave speed and the elastic properties of the material can be defined, based on the theory of acoustic wave propagation;
- *Sclerometric tests,* based on the wood test hammer system, through which the quality and hardness of superficial layers of wood are estimated by the penetration depth of a blunt pin, fired into the wood;
- *Resistographic measurements,* for the evaluation of the wood density by measuring the drilling resistance along the path of a small needle inserted into the wood with a regular advancing speed.

3. Execution of destructive tests (DT):
- *In compression,* parallel to grain on structural elements and both parallel and perpendicular to grain on small defect-free specimens, for the determination of the modulus of elasticity and strength;
- *In bending,* on full-scale members*,* for the evaluation of the local and global modulus of elasticity, together with bending strength.

The destructive investigations aim at determining the mechanical behaviour of timber elements in terms of stiffness, load bearing capacity and collapse mechanisms. The tests were carried out according to UNI EN 408 and UNI ISO standards, which specify laboratory methods for the determination of some physical and mechanical properties of wood.

4. Analysis of the experimental results, including data processing, interpretation and comparisons of results, based on statistic parameters, such as average values, standard deviations and coefficients of variation.

5. NDT-DT correlations for the mechanical characterization of timber, based on linear regression model:
- Correlations between non-destructive parameters (NDT);
- Correlations between destructive parameters (DT);
- Prediction of wood density, modulus of elasticity and strength by means of NDT-DT relationships.

4.3 MATERIAL

4.3.1 *Brief description of chestnut wood*

Chestnut is the name used for any species of the genus *Castanea*, deciduous trees of the family *Fagaceae*. They are characterized by thin-shelled, sweet, edible nuts borne in a bristly bur. Chestnut are classified in the division Magnoliophyta, class Magnoliopsida, order Fagales. The leaves are simple, ovate or lanceolate, 10-30 cm long and 4-10 cm wide sharply pointed and widely-spaced teeth, incorporating shallow rounded sinuses between. The

lowers are catkins, produced in mid summer. The fruit is a spiny cupule 5-11 cm diameter, containing 2-7 nuts.

Being largely propagated in the past for nut harvesting, chestnut tree (*Castanea sativa* Mill.), represents today one of the most diffuse hardwood species in the European Mediterranean area. The wood of chestnut is considered as moderate shrinking and not easy to dry. It shows high natural durability and it is therefore well suited for different uses. In fact, in the South of Italy, many horizontal and roofing load-bearing structures, such as beam floors and trusses located in historical buildings, are made of chestnut timber. Besides, the chestnut sawn elements are also very well suited for glue-laminated timber.

4.3.2 *Ancient timber trusses elements*

The experimental campaign was developed on structural members made of old chestnut wood (*Castanea sativa* Mill.), taken from a timber roof of an ancient masonry building, located in the historical centre of Naples, built up at the beginning of the 19th century. At the erection time, they were used as bearing elements of ten roofing trusses, assembled with typical simple palladian configuration. Recently, the trusses presented only the inclined struts and vertical king posts, having been the tie beams and knee rafters dismantled in a recent consolidation intervention (Fig. 4.1).

During the preliminary *in situ* investigation, the structural location of all timber members was defined, together with their geometric configuration. A total number of thirty elements were identified, twenty struts and ten king posts. After this first phase, the trusses were dismantled and the elements were transported in laboratory for the tests (Fig. 4.1).

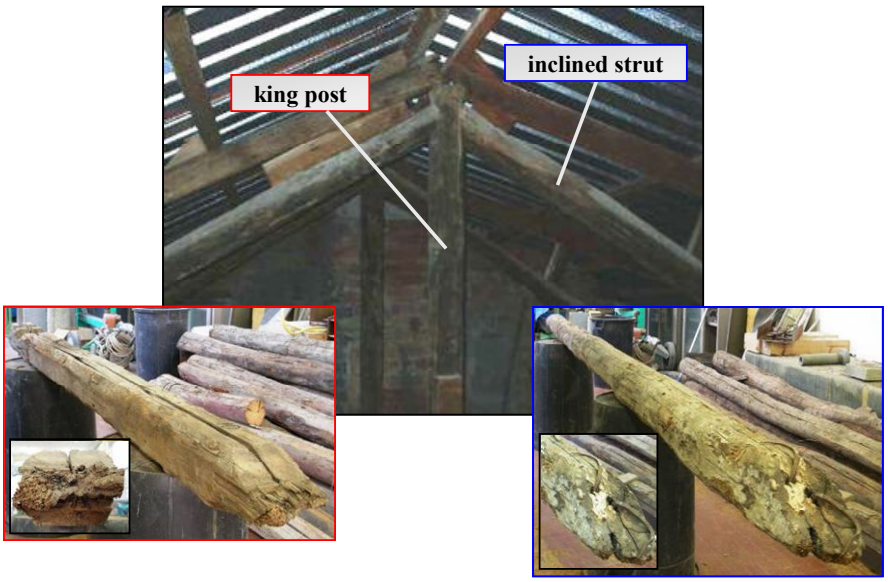

Figure 4.1. Material: timber trusses and dismantled king posts and struts elements.

After the cut of the trunks, which presented irregular and damaged end parts, a preliminary geometrical survey was carried out. As the timber members were obtained by directly disbarking the tree trunks, the cross-sections of both post and strut elements presented variable sizes through out their length. In particular, the king posts had about 1.5 m length with a square cross-section and large rounded edges, whereas the struts, with about 3.5 m length, presented a nearly circular cross-section.

4.4 TESTED SPECIMENS FEATURES

4.4.1 *Structural elements in actual dimensions*

Aiming at obtaining structural elements in actual dimensions, specimens type S_A, with standard length (UNI EN 408) for compression (C) and bending (B) tests, by measuring the perimeter at the end cross-sections (A and B) and at the middle ones (M) of the members, a nominal mean diameter (D) has been calculated for each element, ranging between 14.5 and 16 cm for king posts, and from 15 to 16.5 cm for the struts.

Therefore, two pieces were obtained from each king post element, among which fourteen specimens with standard length equal to about 6D have been selected for NDT and compression tests parallel to grain (S_A-C; Fig. 4.2a). Furthermore, ten struts with standard length equal to about 19D were selected as full-scale beams for NDT and bending tests (S_A-B; Fig. 4.2b).

Firstly, the conservation state of the selected elements has been examined by means of a visual inspection. It is the most simple and oldest non-destructive evaluation method, which consists in checking wood features and defects, signs of damage and deterioration, providing a quick means of identifying critical areas which need further investigations by means instrumental non-destructive tests.

In this way, on the lateral faces of the members several shape irregularities and extended degradation state of the base material have been detected, mainly consisting of knots, longitudinal splitting, cracks, ring shakes, slope of grain, biological damage and holes, due to nails and insect attacks. In particular, most of the specimens type S_A-C presented macroscopic longitudinal cracks due to shrinkage. Whereas, ring shakes, large isolated knots or knots groups have surveyed on the specimens type S_A-B.

The visual inspection has been aided by a detailed photographic survey. In Figure 4.3 a general geometric relief and typical defects patterns are shown. The visual inspections has been limited at the macroscopic defects which could affect the results of non-destructive analysis and the collapse modes of the element during the destructive tests.

The non-destructive (NDT) and destructive (DT) test typologies, which are carried out on the structural elements in actual dimensions are specified in Table 4.1 for each group of specimens.

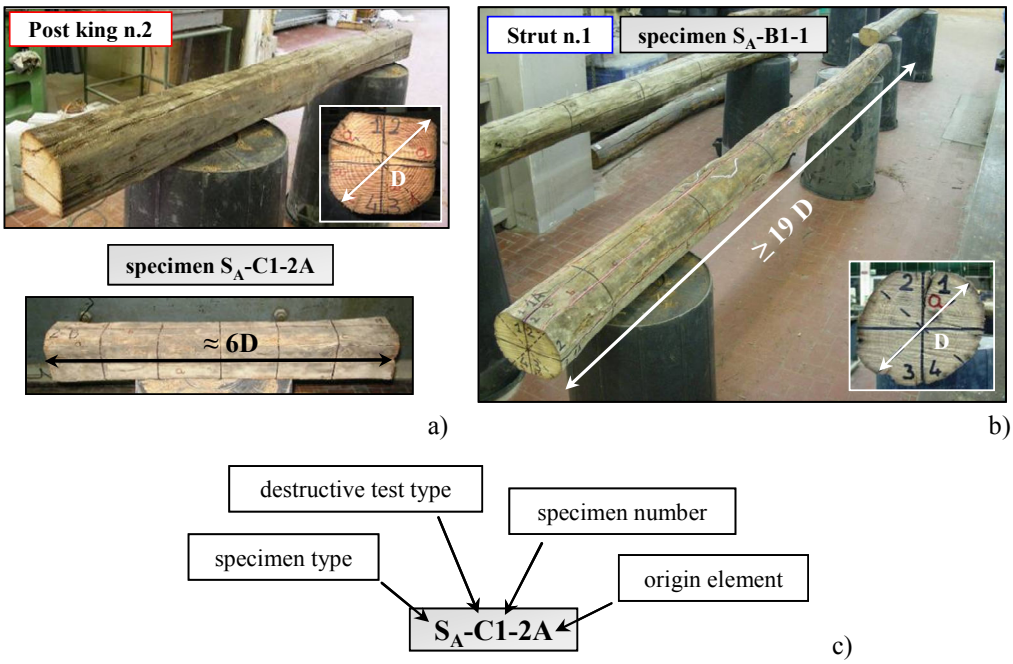

Figure 4.2. Tested specimens features – Structural elements in actual dimensions:
a) Type S_A-C; b) Type S_A-B; c) Specimen label definition.

Table 4.1. NDT and DT tests on structural elements in actual dimensions (S_A-C and S_A-B).

		Non destructive tests (NDT)				Destructive tests (DT)		
Specimen type	**n.**	H	U	S	R	C //	C ⊥	B
S_A-C	14	x	x	x	x	x		
S_A-B	10	x	x	x	x			x

(*) NDT tests: hygrometric (H); ultrasonic (U); sclerometric (S); resistographic (R).
DT tests: compression parallel (C *//*) and perpendicular (C ⊥*)* to grain; bending (B).

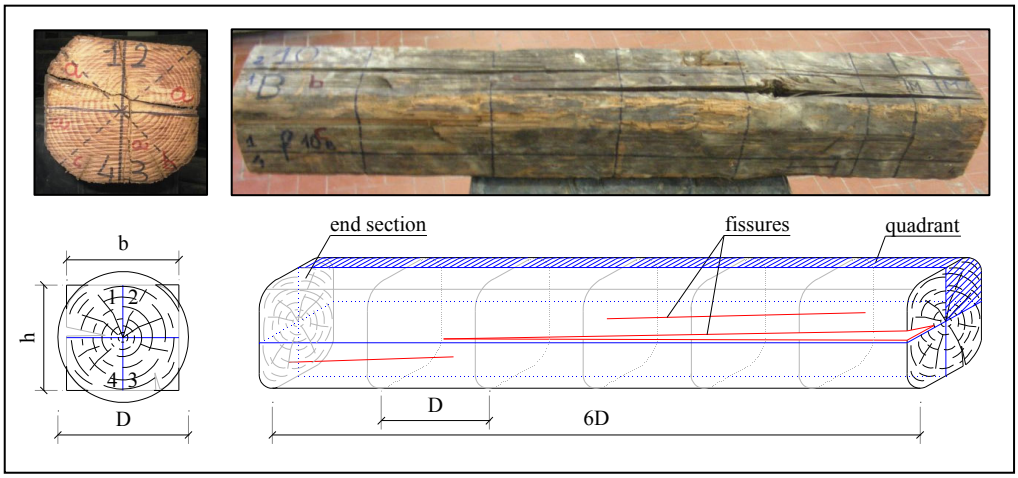

a)

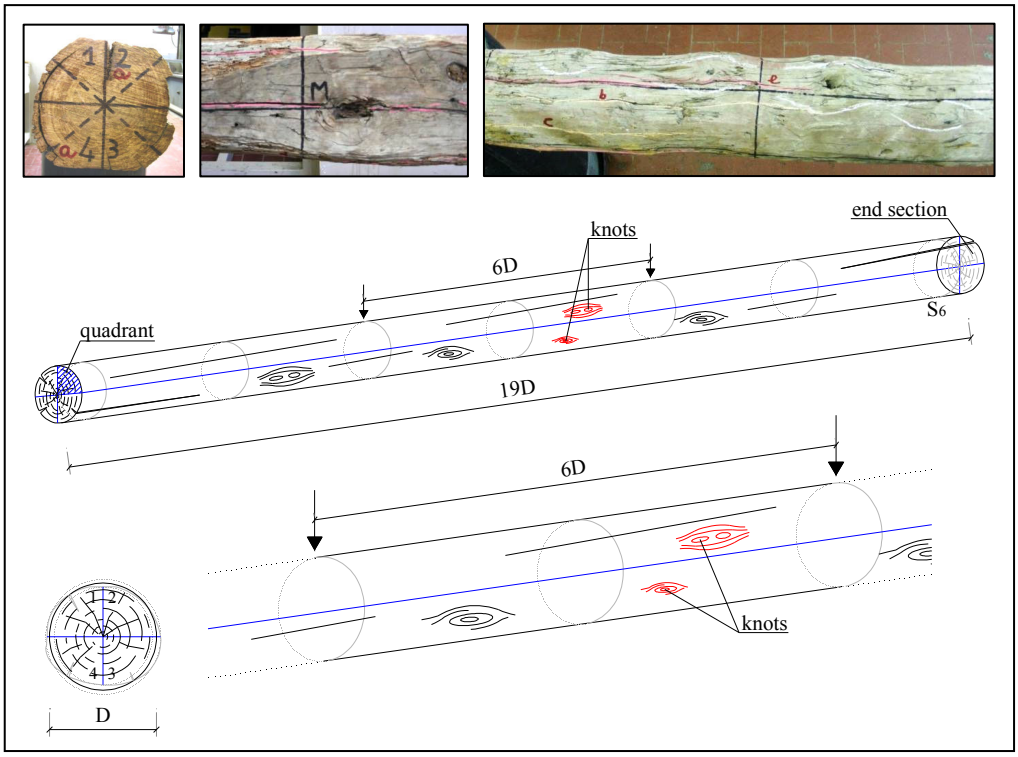

b)

Figure 4.3. Testes specimens features – General relief of the structural elements in actual dimensions and visual inspection: a) Type S_A-C; b) Type S_A-B.

4.4.2 *Structural elements in small dimensions*

After the destructive tests in compression parallel to grain, from eleven tested specimens in actual dimensions, several pieces, about two from each element, were extracted with square cross-section, 5×5 cm^2 size, and with variable length, ranging between about 40 and 55 cm (Fig. 4.4a). Then, each timber piece was cut in two samples: one for both non-destructive and destructive testing and one for only NDT investigations. Therefore, two groups of elements in small dimensions were obtained (Table 4.2):

1. Type S_S-C: twenty specimens with standard length (30 cm), equal to six times the width of the element (5 cm), for NDT investigations and DT tests in compression parallel to grain, according to UNI EN 408 (Fig. 4.4b);
2. Type S_S-NDT: sixteen samples, with 5×5 cm^2 cross-section and 9-25 cm length, for hygrometric, sclerometric and resistographic tests (Fig. 4.4c).

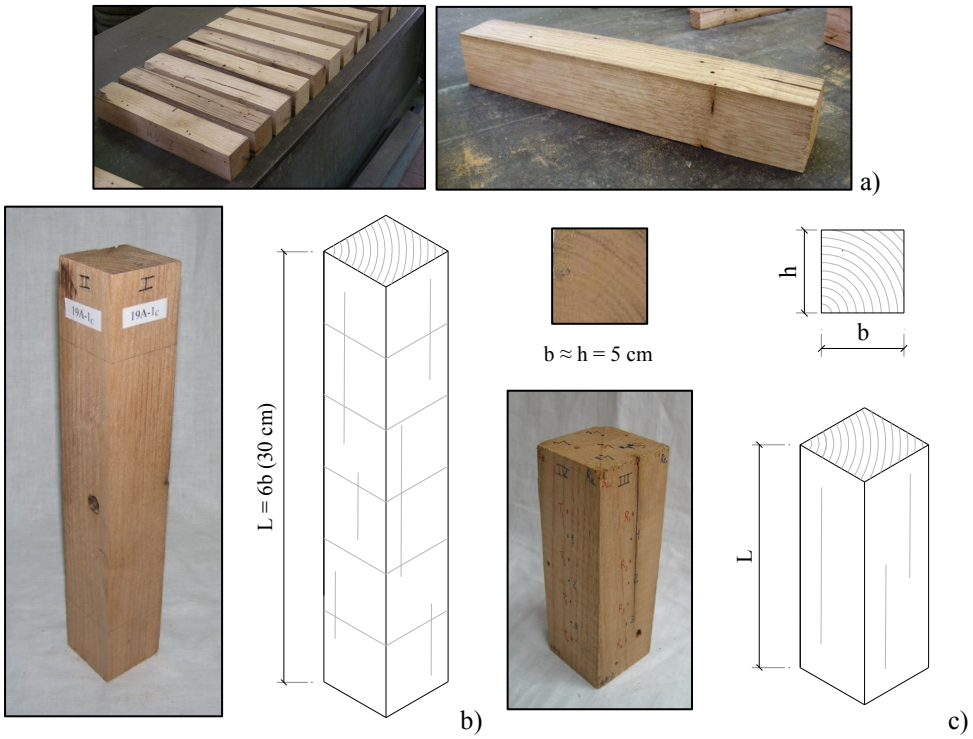

Figure 4.4. Tested specimens features – Structural elements in small dimensions: a) Extracted pieces; b) Type S_S-C; b) Type S_S-NDT.

Table 4.2. NDT and DT tests on structural elements in small dimensions (S_s-C and S_s-NDT).

		Non destructive tests (NDT)				Destructive tests (DT)		
Specimen type	**n.**	H	U	S	R	C //	C ⊥	B
S_s-C	20	x		x	x	x		
S_s-NDT	16	x		x	x			

(*) NDT tests: hygrometric (H); ultrasonic (U); sclerometric (S); resistographic (R).
DT tests: compression parallel (C //) and perpendicular (C ⊥) to grain; bending (B).

By means of visual inspection on each specimen the number and dimension of knots, ring shakes, longitudinal cracks and slope of grain were detected (Fig. 4.5), being the worst elements discarded.

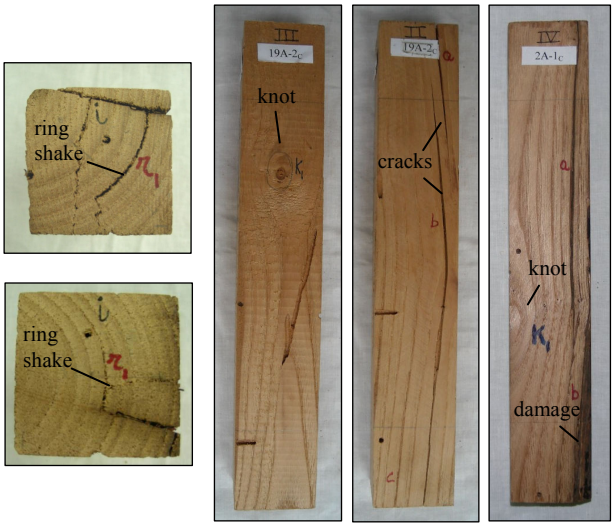

Figure 4.5. Tested specimens features – Structural elements in small dimensions: natural defects pattern.

4.4.3 *Defect-free specimens*

The samples consist of clear wood elements with no visible defect and biological damage, so-called defect-free, with non-structural dimensions. They were obtained by cutting squared boards (Fig. 4.6a) extracted from the eleven structural elements through which the specimens in small dimensions were obtained as well.

The specimens had dimensions of 2×2×4 cm^3, with the longitudinal axis being oriented along the parallel to the grain orientation according to UNI ISO Italian codes (Fig. 4.6b).

In order to analyze the behaviour in compression of the base material in both parallel and perpendicular to grain direction, the specimens were also divided in different groups, taking into account the orientation of the annual growth rings with respect to the direction of the applied load. Therefore the following three groups were considered (Table 4.3; Fig. 4.6c):

1. Type DF-C_L: thirty-tree specimens, three from each origin element, for longitudinal compression tests, according to UNI ISO 3787;
2. Type DF-C_{rad}: twenty-two samples, two from the single structural element, for perpendicular compression tests, along the radial direction, according to UNI ISO 3132;
3. Type DF-C_{tg}: twenty-two specimens, two from each origin element, for compression tests perpendicular to grain in tangential direction, according to UNI ISO 3132.

Table 4.3. NDT and DT tests on defect-free specimens (DF-C_L, DF-C_{rad} and DF-C_{tg}).

		Non destructive tests (NDT)				**Destructive tests (DT)**		
Specimen type	**n.**	H	U	S	R	C //	C ⊥	B
DF-C_0	33	x				x		
DF-$C_{90, rad}$	22	x					x	
DF-$C_{90, tg}$	22	x					x	

(*) NDT tests: hygrometric (H); ultrasonic (U); sclerometric (S); resistographic (R).
DT tests: compression parallel (C *//*) and perpendicular (C ⊥*)* to grain; bending (B).

Figure 4.6. Tested specimens features – Defect-free specimens (DF): a) Extracted boards; b) Geometric features; c) Annual growth rings orientation with respect to the load direction.
(continues)

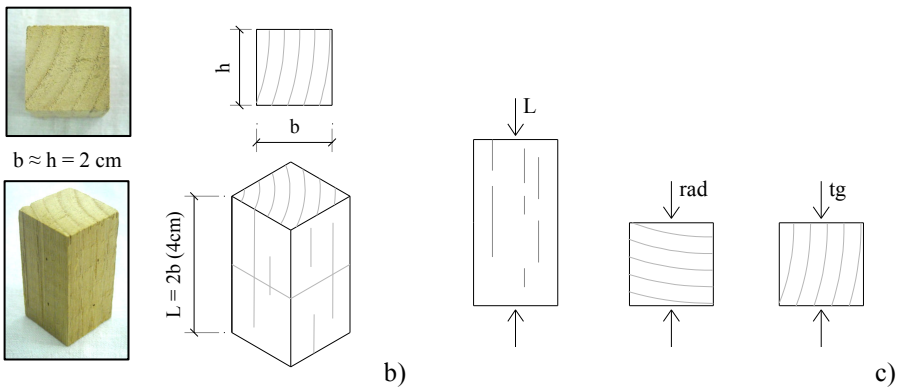

Figure 4.6. Tested specimens features – Defect-free specimens (DF): a) Extracted boards; b) Geometric features; c) Annual growth rings orientation with respect to the load direction.

4.5 NON-DESTRUCTIVE METHODS

4.5.1 *Global test methods (GTM)*

4.5.1.1 Ultrasonic stress wave method

Ultrasonic stress wave is one of the most popular NDT global method used for wood, based on the propagation of sound waves through the investigated element. It is similar to the sonic stress wave method but it uses higher frequencies (20 kHz – 100 MHz). In wood and wood composites materials this technique is less effective due to the porous and inhomogeneous nature of the material. Therefore, low frequencies (20 kHz – 500 kHz) are often used in wood because of high wave attenuation.

In the experimental campaign, the Ultrasonic System CMS was used for ultrasonic investigations, equipped by a data acquisition unit combined either with high-piezoelectric transducers (>1.6 Kv), the transmitter TSG-20, fitted with threaded conic tips, and the cylinder-shape receiver RSG-55 (Fig. 4.7).

Although stress wave and ultrasonic methods are affected by numerous factors, including moisture content, wood species and growth ring orientation, they are useful means of detecting the condition of wood in structures. In fact, this method can be used, with an extraordinary accuracy, to provide

information on the internal condition of members and their residual load-carrying capacity, allowing a good interpretation of the local properties of the timber elements *in situ*.

It is well known that stress waves velocity can be directly related to the elastic properties of timber since impedance contrasts in the material cause scattering of elastic waves. It is normally possible to measure the propagation time, so called "Time of Flight" (TF, Fig. 4.7)., of a set of elastic waves in the axial direction of the wooden elements or in the perpendicular directions to this. The propagation velocity of the stress waves depends essentially on the stiffness and the density properties.

For prismatic, homogeneous and isotropic elements and for those with a section width smaller than the stress wavelength, the relation holds:

$$E_{dyn} = V^2 \cdot \rho$$

where E_{dyn} represents the elasto-dynamic modulus of elasticity (N/mm^2); V is the propagation velocity of the longitudinal stress waves (m/s) and ρ is the density of the specimens (kg/m^3).

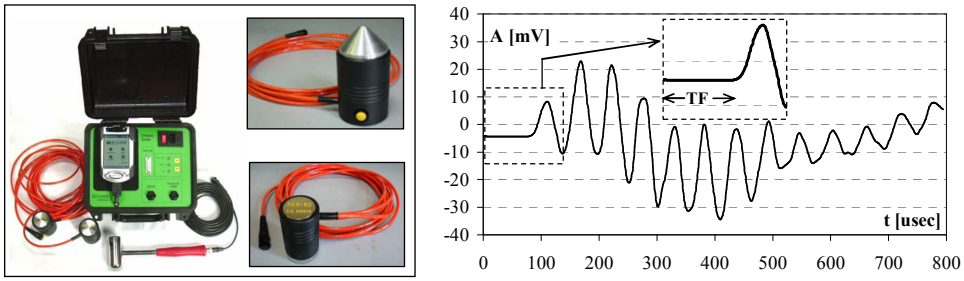

Figure 4.7. Non-destructive methods – Ultrasonic stress wave method: system CMS v. 3.1 used in the experimental campaign.

For practical purpose, the relation between the dynamic modulus of elasticity and the static value is particularly relevant, explained by the viscous-elastic behaviour of wood (Bonamini *et al.,* 2001). Generally a linear relation is adequate. Therefore, the propagation velocity of elastic waves, together with the material density, immediately show information on the stiffness

coefficients of the material. This and other fundamental efforts, suggest this method as one of the most used in timber evaluation.

In high dispersive materials as wood, while travelling inside the material the wave suffers a series of reflection events originating new waves with different polarizations and each having a characteristic velocity. Most of ultrasonic equipments available considers only the fastest wave to arrive at the receiver probe. It is expected that this wave travels through the highest quality zones of a wood element bypassing weaker zones (showing, knots, decay, slope of grain) and therefore not allowing the local characterization of that wood element. If the signals is deviated, the transmit time increases.

Despite of their inhomogeneity, anisotropy and natural patterns of variability, it is possible to correlate the efficiency of wave propagation with the physical and mechanical properties of wood; high propagation velocities are associated with greater fracture resistance and absence of material defects.

The ultrasonic wave velocity is around three times faster in longitudinal direction than in transversal one, which enables sometimes this method to efficiently detect defects that evolves changes in grain direction, such as knots and slope of grain. In addition, discontinuities in the cells anatomy or the presence of surface decay caused by insect reduce the ultrasonic wave velocity. Other open question is the influence of environmental factors and wood characteristics in the ultrasonic method. For instance, ultrasound velocity increases as the moisture content of wood decreases.

In most of the recent studies involving this method the aim was to control the wood quality as a final product or as raw material and to inspect historic structures (Ross *et al.*, 1999). Some of the studies try to focus on the distinction between clear wood and decayed wood, comparing the results and creating “evaluation maps”, with experimental results in clear wood that could be adopted in future interventions. Other authors tried to determine residual strength of structural elements that were used in ancient constructions or that were attacked by biological agents (De Groot *et al*., 1998), or tried to determine qualitative properties by modelling wood as homogeneous isotropic material, assuming that the clear and the defected wood can be modelled as a fluid, neglecting bending stiffness (Fransson and Nilsoon, 2001).

4.5.2 *Local test methods (LTM)*

4.5.2.1 Wood test hammer system

The wood test hammer system, so-called Pilodyn method, by means of Pilodyn 4JR or similar equipment, is an alternative for fast and non-destructive estimation of wood density. The used tool in the experimental campaign on elements in old chestnut wood is the Wood Pecker mechanical test hammer (Fig. 4.8). It allows to measure the penetration of a metallic pin with 2.5 mm of diameter into wood, through the release of a spring-loaded pin, which transforms the elastic potential energy into impact energy. This dynamic impact is responsible for the penetration of the pin in the surface of the specimens, allowing to register the penetrated depth. The density of the wood or the degree of decay in the wood can be assessed by the different spring energy absorbed by the specimen.

Figure 4.8. Non-destructive methods – Wood test hammer system: Wood Pecker device used in the experimental campaign.

This technique is influenced by the state of the superficial layers of wood, often affected by the presence of longitudinal shakes or biological damage.

Empirical correlations between the penetration depth and density are proposed by several authors (Graves *et al*., 1996; Watt *et al.,* 1996; Gorlacher, 1997; Bonamini *et al.*, 2001; Kasal *et al.,* 2004), with regression coefficients ranging from 0.74 to 0.92. However, this relations are affected by several factors, such as moisture content, number of measurements and species; therefore, species-based calibrations are required.

Studies were also carried out to define correlations with mechanical properties. Relations between resistance to superficial penetration and a three

points loading bending test were found but more studies are needed to validate this results, due to its empirical nature and to the local and superficial character of the results obtained (Togni, 1995)

For the determination of the modulus of elasticity, Turrini and Piazza (1983) proposed empirical relation correlating impact force and modulus of elasticity. The authors proposed also the adoption of a reduction factor of the modulus of elasticity based on a visual grading of the elements: 80% for non-defect elements and 50% for elements presenting knots, spiral grain, shakes or small decay portions.

4.5.2.2 Resistographic analysis

The drilling resistance technique uses the Resistograph device, which is based on the resistance offered by the material to advance of a small diameter drill bit. IMLRESI *F400* model was used in the experimental activity, which, through the power consumption of the drilling device, measures the resistance of a small needle, with a diameter of 1.5 to 3.0 mm (Fig. 4.9).

In the past, core sampling using conventional drills (ϕ = 10 to 40 mm) was used to determine density properties of wood products. But these methods are hardly suited for determining density variations of structural timber due to the large boreholes. Instead, the resistographic system is considered a quasi-non-destructive method because the size of the hole in the specimen after testing does not have any weakening effect. This test allows to obtain density profiles, which are the graphic representations of the values of the drill resistance versus the penetration depth (Fig. 4.9).

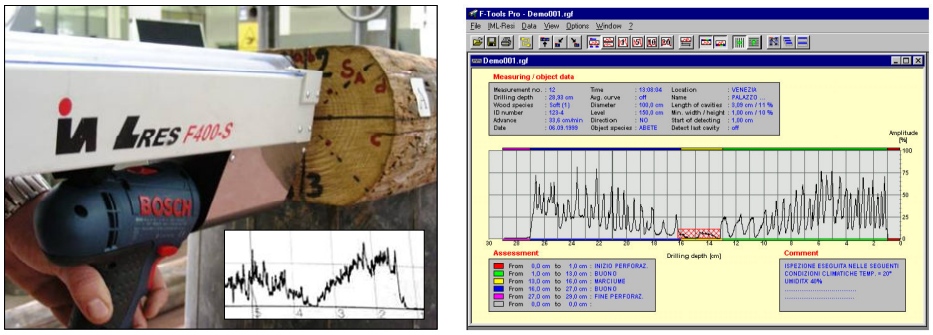

Figure 4.9. Non-destructive methods – Resistographic analysis: IMLRESI *F400* device used in the experimental campaign.

In structural inspections this technique shows great efficiency and reliability, having widespread applications: find wood decay, rot, hollow areas and cracks; analyze annual ring structures; determine growth tendency according to the width of annual rings; prevent wood damage; measure real dimensions of transversal section of structural elements, when they are not directly accessible; evaluate the residual resistant section, taking away rotten portions. Some advantages of the method are the graphical resolution, the simplicity of storing data, of transporting the equipment and performing the tests.

Some studies reveal limitations of this method, namely related to the difficulties in carrying out some inspection/test due to the location of the element (difficulty in positioning the device perpendicularly to the element), the measurements of only local characteristics of the elements and the invasive nature of the drill resistance technique (Bonamini, 1995a; Emerson *et al.*, 1998). Therefore, the resistographic method may be best employed if used in conjunction with NDE methods and techniques that provide qualitative or more global condition assessment.

Some researchers (Gorlacher and Hattich, 1990; Isik and Li, 2004) reported relatively moderate correlation between drilling resistance and wood density ($R^2 \approx 0.21\text{-}0.69$) , showing that this correlation has not yet been adequately developed for use *in situ* quantitative evaluation. It is noted that moisture content of wood has a large influence on the density values and Machado and Cruz (1997) observed that the drilling resistance decreases as moisture content increases. Works show that the resistance drilling data correlate well with the X-ray densitometry measurements (Rinn *et al.*, 1996).

Nowadays, the resistographic method is one of the most used and several campaigns were carried out using this technique.

Chapter 5
Non-destructive tests (NDT)

5.1 GENERAL

In the field of the structural analysis, diagnosis and inspection of historical timber constructions, the mechanical identification turns out particularly difficult because of the great influence of botanic species, defects, degradation and of the heterogeneous and anisotropic microstructure of the material. However it represents a fundamental action to evaluate structural efficiency and also to design restoration interventions.

Non-destructive techniques are of special interest due to the fact that their application does not affect the structural integrity and safety of the structure, being compatible with the demand of conservation. The problem of non-destructive tests is exactly the lack of standardization that implies uncertainty of the results, besides the most part of non-destructive evaluation is useful to determine physical but not mechanical characteristics, so each method has to be compared or combined to obtain reliable data. In this context, the laboratory tests have a vital role because they are a mean to explain properties and characteristics of wood and to validate NDT results.

In this chapter, the non-destructive testing phase of the whole experimental campaign is presented. The following NDT methods have been employed in the research activity: hygrometric tests to estimate wood moisture content, ultrasonic investigations as an approach to determine stress wave properties,

wood hammer tests to assess material hardness and superficial consistence, resistographic measurements to detect internal defects and density variations.

Testing equipment and experimental set-up, together with the applied methodology for data processing and interpretation, are illustrated. On the basis of a large number of experimental tests, the obtained results are statistically analyzed and compared each other, in terms of average and characteristic values, and also of coefficients of variation. In the chapter 8, the achieved non-destructive parameters will be correlated with destructive ones (provided in chapter 6 and 7) with aim to estimate the main mechanical characteristics of timber, such as density, modulus of elasticity and strength.

5.2 HYGROMETRIC TESTS

5.2.1 *Testing apparatus*

The hygrometric tests were performed by means of *Tramex Professional* device, which is a digital pin type resistance meter with built-in pins designed to take precise measurements of moisture content in wood. It incorporates the following operational features (Fig. 5.1):

1 Digital readout to 0.1% accuracy;
2 Measuring range from 7% to 40%;
3 Timed cut out after 4 minutes, saves batteries;
4 Hold facility so readings can be frozen until recorded;
5 Built-in probe pins.

The professional moisture meter works on the principle of DC resistance. When the electrode pins are pressed or driven into the wood, the electrical resistance between the electrodes is measured and indicated on the digital display. If the wood is dry, the resistance is high. If moisture is present in the wood the electrical resistance between the pins changes. The higher the moisture content the grater the reduction in resistance. The level of resistance is accurately measured by the instrument which translates it into percentage of dry weight moisture content. The professional gives moisture readings from

7% to 40%. The readings above 27% (nominal value of the fibre saturation point) are indicative only. Readings are given to the nearest 0.1%. For a correct taking moisture readings, the pins should be aligned in the parallel direction to the grain.

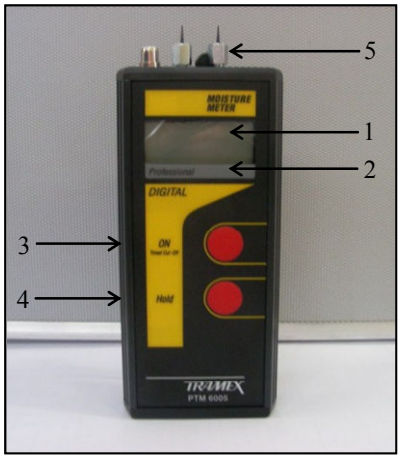

Figure 5.1. Hygrometric tests – Testing apparatus: Tramex Professional moisture meter.

Generally, the readings of all moisture meters are influenced by the characteristics of different species of wood as well as temperature and other factors listed below:

- *Species*
  Different species of wood can vary in density and conductivity which can have an effect on the electrical resistance of the wood. This can influence meter readings for the same moisture content and can also apply to similar species from different origins.
- *Temperature*
  Meter readings can be affected by wood temperature. The Professional is calibrated at 20°C (68°F). At wood temperature above or below 20°C, the meter readings are higher or lower, respectively. The temperature adjustment chart is provided in Table 5.1.

- *Chemical treatment or contamination*
  Readings may be affected by certain flame retardants, preservatives, aluminium paint and by contamination by salt water. Treat all readings on such wood as indicative readings only.

Table 5.1. Hygrometric tests – Tramex Professional moisture meter: temperature adjustment chart.

		Meter readings						
°C	°F	7%	10%	12%	15%	20%	26%	30%
		Adjustment						
5	40	+1	+2	+2	+3	+4	+5	+7
10	50	+0	+1	+1	+2	+2	+3	+4
20	68	+0	+0	+0	+0	+0	+0	+0
30	80	+0	-1	-1	-1	-1	-2	-2
40	100	-1	-2	-2	-3	-3	-3	-4
50	122	-2	-3	-4	-5	-6	-8	-10
60	140	-2	-3	-4	-5	-6	-8	-10
70	158	-3	-4	-5	-6	-8	-10	-12

5.2.2 *Test set-up*

The hygrometric measures were performed inserting the resistor pins into the lateral surface of the specimens, aligned on the parallel to grain direction in several tested sections. In particular, for the elements in actual dimensions, five primary sections were selected for the tests (labelled as S_1, S_2, S_3, S_4, S_5; Fig. 5.2a), spacing D and 3D for the samples type S_A-C and S_A-B respectively. In each section the readings were carried out in two transversal directions (x and y), orthogonal each other (Fig. 5.2).

Table 5.2 provides, for each typology and group of elements, the number of both tested sections and moisture content readings.

5.2.3 *Results and discussion*

For each tested sample, the moisture content (MC) has been defined as the average value of all readings. This value is equal to about 11% and 10-11 % for the structural elements in actual and small dimensions, respectively, and to 8-10 % for the defect-free specimens. Because the hygrometric tests have been performed at an ambient temperature of 18±5 °C, in any case the average

value has been amplified by a corrective factor, equal to +1, according to the temperature adjustment chart (Table 5.1), provided with the Tramex Professional moisture meter.

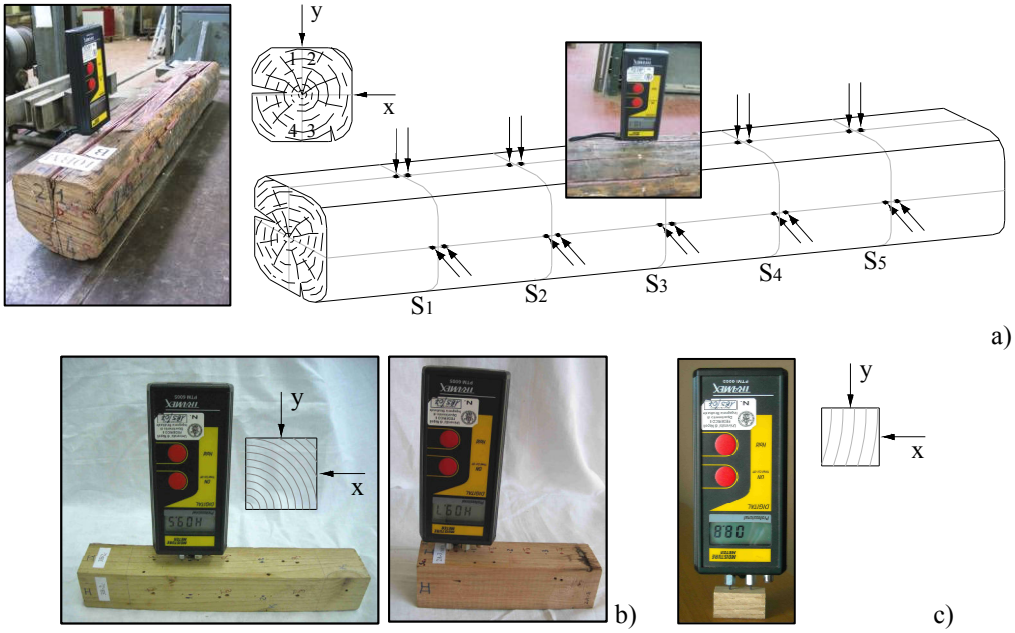

Figure 5.2. Hygrometric tests – Test set-up: a) Structural elements in actual dimensions (S_A); b) Structural elements in small dimensions (S_S); c) Defect-free specimens (DF).

Table 5.2. Hygrometric tests – Test set-up: tested sections and readings number.

Specimens type	**Group**		**Tested sections**	**Readings per specimen**	**Total readings**
	label	*n.*			
Structural elements in actual dimensions	S_A-C	14	5	10	140
	S_A-B	10	5	10	100
Structural elements in small dimensions	S_S-C	20	3	6	120
	S_S-NDT	16	3	6	96
Defect-free	DF-C_L	33	1	2	66
	DF-C_{rad}	22	1	2	44
	DF-C_{tg}	22	1	2	44

As example, for a few of elements, adjusted moisture content readings in each tested section are give in Tables 5.3 to 5.5.

It is worth to notice that, for all samples, MC is equal to about 10-12 %, which corresponds to the moisture content at "normal ambient condition" (20±2 °C of temperature and 65±5 % of humidity), according to EN 408 European standard.

Table 5.3. Hygrometric tests – Experimental results: structural elements in actual dimensions (specimens S_A-C1-2A and S_A-B5-8).

	S_A-C1-2A					**S_A-B5-8**				
Direction	**S_1**	**S_2**	**S_3**	**S_4**	**S_5**	**S_1**	**S_2**	**S_3**	**S_4**	**S_5**
x	11.2	11.4	11.6	10.8	11.2	11.4	12.4	10.8	11.6	10.9
y	11.4	11.0	11.6	11.7	11.1	11.2	10.8	11.1	10.7	9.6

Table 5.4. Hygrometric tests – Experimental results: structural elements in small dimensions (specimens S_S-C1-2A and S_S-NDT1-2A).

	S_S-C1-2A			**S_S-NDT1-2A**		
Direction	**S_1**	**S_2**	**S_3**	**S_1**	**S_2**	**S_3**
x	10.6	10.8	11.5	10.4	11.3	11.0
y	10.2	11.0	11.7	10.8	11.0	11.2

Table 5.5. Hygrometric tests – Experimental results: defect-free specimens (specimens DF-C_L1-2A, DF-C_{rad}1-2A and DF-C_{tg}1-2A).

Direction	**DF-C_L1-2A** **S_1**	**DF-C_{rad}1-2A** **S_1**	**DF-C_{tg}1-2A** **S_1**
x	11.0	11.7	11.2
y	11.4	11.5	11.0

5.3 ULTRASONIC INVESTIGATIONS

5.3.1 *Testing apparatus*

Ultrasonic System CMS (Boviar) was used for ultrasonic investigations, which is meant to evaluate elastic and dynamic features of materials. Particularly, it enables to assess the extent of homogeneity of the material under examination and the presence of any fractures or hollows (Fig. 5.3a).

The multifunction equipment is made up of a data acquisition unit combined either with a number of sensors fitted with high-power piezoelectric transducers (>1.6 Kv) or an instrumental hammer, in order to carry out measurements of the propagation time of compression waves (P) in many kinds of different materials even if they have poor propagation and velocity characteristics. The data acquisition unit enclosure contains all the electronics to generate the high-tension pulse of the transmitter and the conditioning of the signal from the receiver, as well as a 12-bit board with a frequency of 1.25 MHz which digitalizes the logged signals (full waveform).

The ultrasonic transmitter TSG-20 and the accelerometer receiver RSG-55 were used in order to induce and then capture the compression stress waves (Fig. 5.3a). Both receiver and transmitter are of active type, i.e. excitation (transmitter) and pre-amplification (receiver) electronics is contained inside the transducer. This arrangement enables to have receiving signals which are already amplified and conditioned when transmitted to main unit.

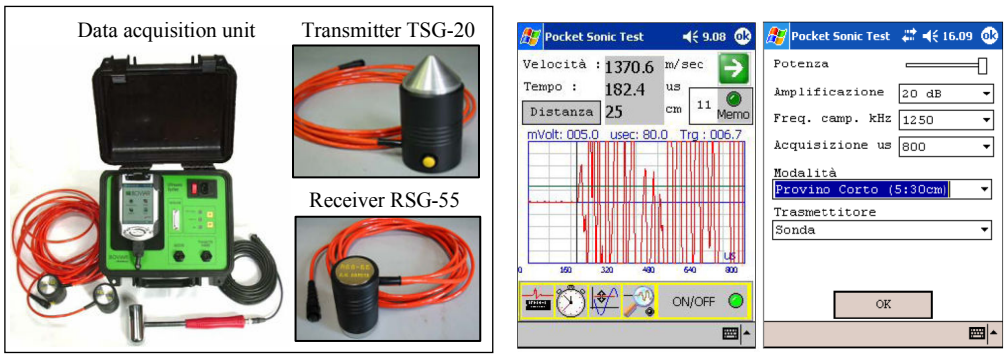

a) b)

Figure 5.3. Ultrasonic investigations – Testing apparatus: a) System CMS (Boviar); b) Signal acquisition software (Pocket Sonic).

The transducer TSG-20 is a sandwich-type transmitter with pre-charged ceramics. It can generate pulses with frequencies up to 20 kHz, suitable to flow through particularly slow materials or large size structural elements, obtaining higher receiving frequencies and hence a better resolution. The used TSG-20 is fitted with special threaded conic tips, ideal for inspections on wooden materials. The cylinder-shape piezoelectric receiver RSG-55 has been

specifically designed to have a high sensitivity in a frequency range of received signals from 50 Hz to 70 kHz.

The signals are directly stored by a Pocket computer integrated in the main unit, on which a dedicate software (Pocket Sonic) is pre-installed to run the displaying, processing and logging of the signals (Fig. 5.3b). It allows to visualize them in the same way as per an oscilloscope with time-length scale and to read the wave propagation time, so-called "Time of Flight", which represents the time requires for the stress wave to travel between the sensors. In addition, the acquisition software allows to regulate the pulse transmission power, to set the amplification (LOW POWER, 20, 40, 74 dB), frequency (from 50 KHz to 1250 KHz) and acquisition duration (from 0.8 ms to 100 ms), selecting the parameters which best fit the size and type of the material under examination.

5.3.2 *Test set-up*

The ultrasonic tests were performed on the structural elements, type S_A-C and S_A-B. Direct method was used, placing the transducers on two opposite faces of the same specimen, in longitudinal (L) and transversal (T) direction. Therefore two procedures of signal transmission were adopted: 1) direct method parallel to grain; 2) direct method perpendicular to grain.

The transmission technique of elastic waves based on the direct method parallel to the grain, allows a global evaluation of the dynamic mechanical properties of the material. In this case, the transducers were aligned along five longitudinal directions, taking measurements in selected points of the end cross-sections for each tested specimen (Fig. 5.4a).

Concerning the direct method perpendicular to the grain, local transversal measurements were performed in different points of the lateral surface. Eleven contiguous sections were investigated, spacing D/2 and 3D/2 for the specimens type S_A-C and S_A-B respectively, coupling the sensors in four directions per section, for a total number of forty-four transverse readings per specimen (Fig. 5.4b).

A thin layer of plasticine (dry elastomeric material) was used as couplant. A constant and controlled pressure was applied between the transducers and specimens under testing, allowing adequate transmission of the elastic wave

and eliminating micro-gaps at wood-receiver interface. Most of specimens shown a surface waviness or roughness which often easily caused the transducers lack of alignment. Therefore, three repetitive readings of pulse transmission have been performed for each longitudinal and transversal test, aiming at considering the measurement with faster elastic waves (minor wave transmission time), which the better alignment of the transducers corresponds.

The signals acquisition have been performed with the maximum pulse transmission power, 20 dB amplification, 1250 KHz and 0.8 ms frequency and acquisition duration.

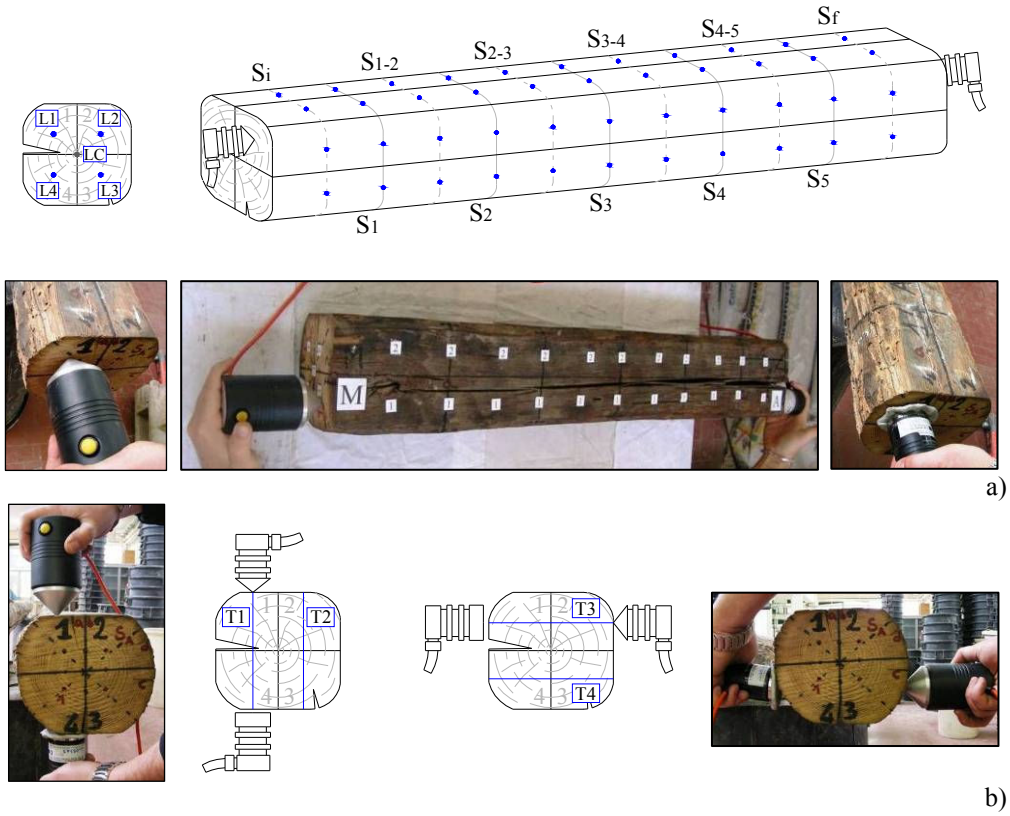

Figure 5.4. Ultrasonic investigations – Test set-up: a) Direct method parallel to grain; b) Direct method perpendicular to grain.

5.3.3 *Data processing*

The software Data Sonic was used in order to transfer the data from the equipment Pocket computer to an external PC and export the logged signals in ASCII format to get oscillograms for data processing and interpretation.

The recorder signals have been analyzed in time (t) – Amplitude (A) diagrams in order to evaluate the wave propagation time, so called "Time of Flight" (TF). It is the time lag between the externally give zero time point (t_0) and the one-set (begin) of the recorder signal. The velocity of the ultrasonic pulse, so-called Stress Wave Speed (SWS), has been easily determined dividing the distance between the probes by the stress wave transmission time.

In Figure 5.5 typical stress waveforms are depicted for longitudinal signals, which have been recorded during the tests on the specimen S_A-C14-19A, whereas Table 5.6 provides the corresponding dynamic parameters.

The transversal tests, which allowed to discover the presence of weak and critical zones of the tested crossed elements, have been performed at several points according to an appropriate distribution on the lateral faces.

In Table 5.7 the dynamic transversal parameters are given for the specimen S_A-C5-4A. It is worth noticing that, at the first five contiguous sections of the sample, the propagation wave in two directions (T3 and T4), intercepting largeness shake, generated flattened or distorted signals, preventing the evaluation of TF. The corresponding signals, recorded in two typical investigated sections, are depicted in Figure 5.6.

5.3.4 *Results and discussion*

For each tested specimen, in order to define the dynamic parameters by ultrasonic investigations, the average value of stress wave speed (SWS) are considered, for both longitudinal (L) and transversal (T) tests.

Furthermore, as the propagation of elastic waves is affected by local elastic properties of the material, on the basis of the Euler beam theory for free flexural vibrations of prismatic beams, the dynamic modulus of elasticity (E_{dyn}) is evaluated as well, according to the theoretical relationship for homogenous and isotropic elements:

$$E_{dyn} = SWS^2 \rho$$

where ρ is the wood density, determined in a simple way, weighing and measuring the dimensions of the samples.

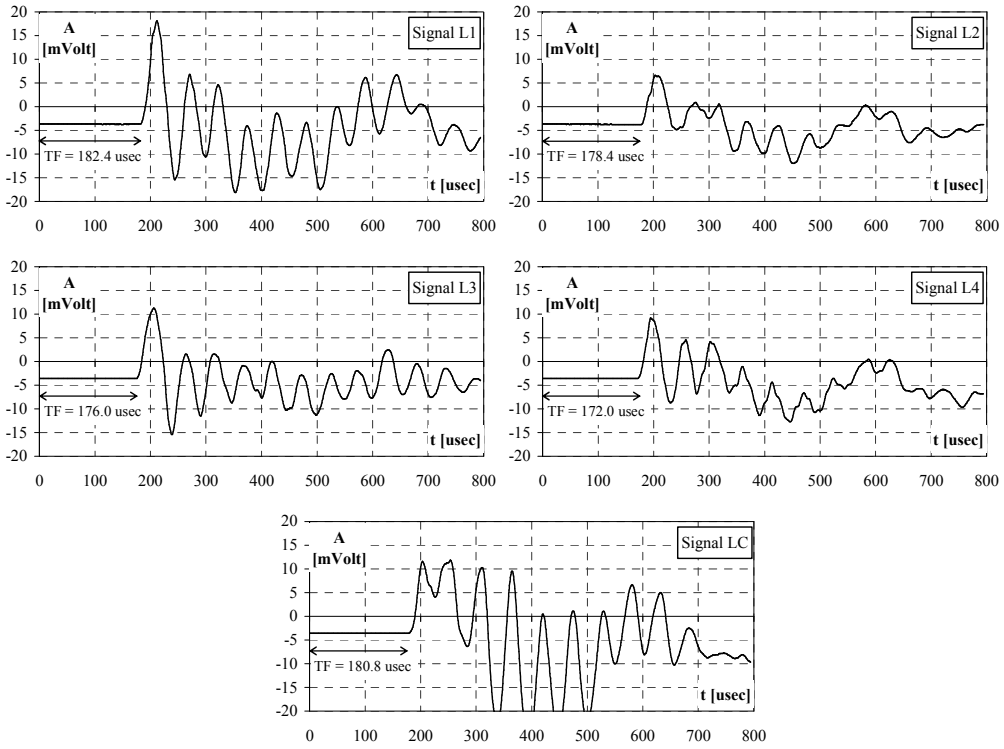

Figure 5.5. Ultrasonic investigations – Data processing: typical longitudinal waveforms (specimen S_A-C14-19A).

Table 5.6. Ultrasonic investigations – Data processing: Time of Flight (TF) and Stress Wave Speed (SWS) in longitudinal direction (specimen S_A-C14-19A).

Signals	TF [usec]	SWS_L [m/sec]
L1	181.6	5066.1
L2	178.4	5157.0
L3	176.0	5227.3
L4	172.0	5348.8
LC	180.8	5088.5

Table 5.7. Ultrasonic investigations – Data processing: Time of Flight (TF) and Stress Wave Speed (SWS) in transversal direction (specimen S_A-C5-4A).

C5-4A	**T1** d_1=13.0 cm		**T2** d_2=13.2 cm		**T3** d_3=14.4 cm		**T4** d_4=13.4 cm	
Section	**TF [usec]**	**SWS_T [m/s]**	**TF [usec]**	**SWS_T [m/s]**	**TF [usec]**	**SWS_T [m/s]**	**TF [usec]**	**SWS_T [m/s]**
S_i	81.6	1595.6	84.0	1575.0	-	-	-	-
S_1 (D)	83.2	1564.9	85.6	1545.6	-	-	-	-
$S_{1\text{-}2}$	79.2	1643.9	80.8	1637.4	-	-	-	-
S_2 (2D)	-	-	84.0	1575.0	-	-	-	-
$S_{2\text{-}3}$	79.2	1643.9	79.2	1670.5	-	-	-	-
S_3 (3D)	80.8	1611.4	78.4	1687.5	91.2	1576.8	84.0	1600.0
$S_{3\text{-}4}$	75.2	1731.4	-	-	81.6	1762.3	77.6	1732.0
S_4 (4D)	74.4	1750.0	-	-	80.8	1779.7	81.6	1647.1
$S_{4\text{-}5}$	84.8	1535.4	-	-	79.2	1815.7	80.0	1680.0
S_5 (5D)	-	-	-	-	79.2	1815.7	95.2	1411.8
S_f	74.4	1750.0	79.2	1670.5	78.4	1834.2	-	-

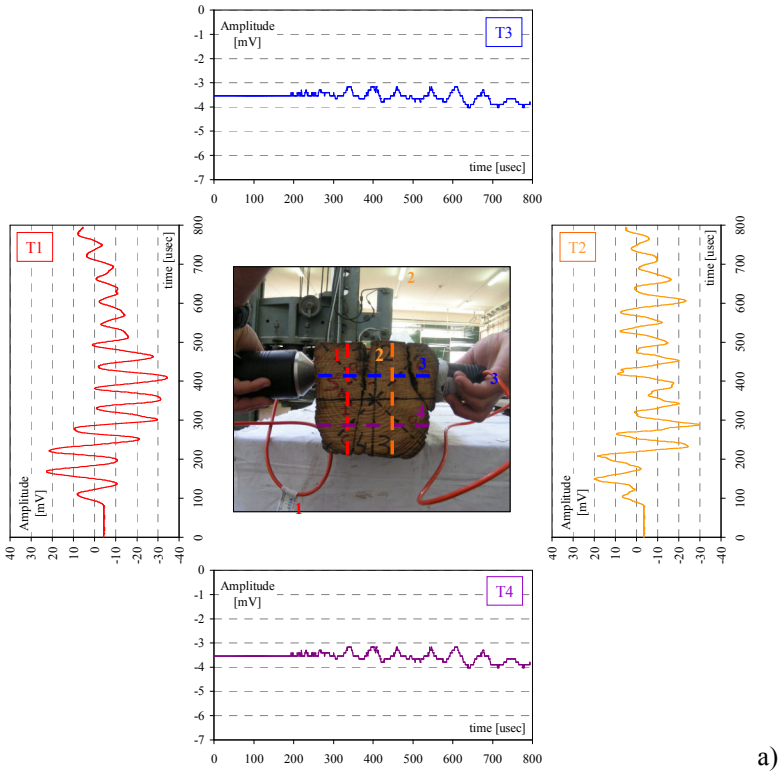

a)

Figure 5.6. Ultrasonic investigations – Data processing – Typical transversal waveforms (specimen S_A-C5-4A): a) Section S_1; b) Section $S_{2\text{-}3}$. (continues)

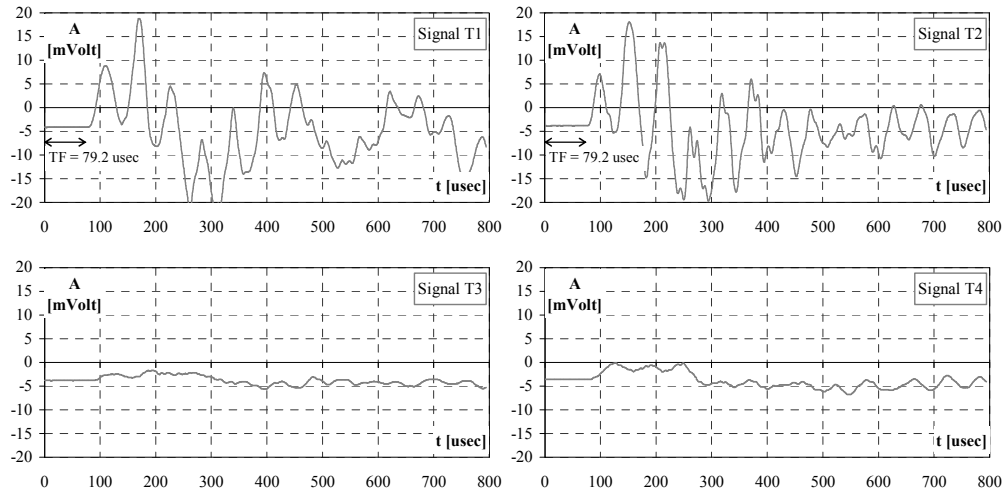

b)

Figure 5.6. Ultrasonic investigations – Data processing – Typical transversal waveforms (specimen S_A-C5-4A): a) Section S_1; b) Section $S_{2\text{-}3}$.

In Tables 5.8 and 5.9 the experimental results, in terms of SWS_L and SWS_T respectively, are provided for each specimen type S_A-C and S_A-B, including the statistical parameters, such as the standard deviation (SD) and the coefficient of variation (CV) (Fig. 5.7). In particular, for transversal tests, the ratio percentage (U) between the number of signals with read TF and the total number of measurements, equal to forty-four per specimen, are reported too. Moreover, in Table 5.10 the density and E_{dyn} values are given.

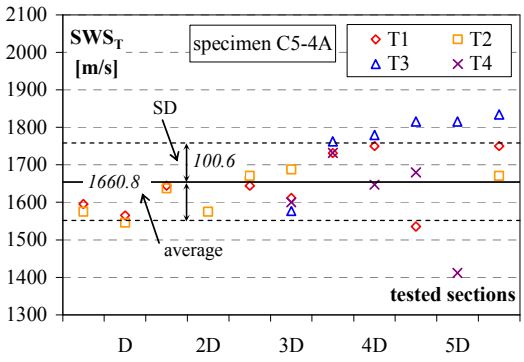

Figure 5.7. Ultrasonic investigations – Experimental results: statistical parameters definition for transversal tests (specimen S_A-C5-4A).

Table 5.8. Ultrasonic investigations – Experimental results in longitudinal direction (L): specimens type S_A-C and S_A-B.

Specimen type S_A-C	**SWS_L [m/s]**	**SD_L [m/s]**	**CV_L [%]**
C1-2A	5153.7	142.9	2.77
C2-2B	5137.4	87.7	1.71
C3-3A	5197.7	162.8	3.13
C4-3B	5127.7	109.7	2.14
C5-4A	5659.4	55.0	0.97
C6-4B	5633.4	139.9	2.48
C7-9A	4859.7	72.1	1.48
C8-10B	5644.8	92.5	1.64
C9-15A	5454.8	130.7	2.40
C10-16A	5471.0	75.9	1.39
C11-16B	5365.6	45.9	0.86
C12-17A	5113.2	96.1	1.88
C13-18A	5263.9	127.0	2.41
C14-19A	5177.5	114.7	2.21
Specimen Type S_A-B	**SWS_L [m/s]**	**SD_L [m/s]**	**CV_L [%]**
B1-1	5357.6	76.1	1.42
B2-5	5572.1	34.8	0.62
B3-7	5322.5	34.0	0.64
B4-8	5454.2	62.1	1.14
B5-12	5352.6	30.2	0.56
B6-13	4767.5	80.3	1.68
B7-21	5409.0	86.6	1.60
B8-24	5525.0	84.8	1.54
B9-25	5292.2	86.3	1.63
B10-27	5540.8	47.8	0.86

Table 5.9. Ultrasonic investigations – Experimental results in transversal direction (T): specimens type S_A-C and S_A-B.

Specimen type S_A-C	**SWS_T [m/s]**	**SD_T [m/s]**	**CV_T [%]**	**U_T [%]**
C1-2A	1848.1	147.7	7.99	34
C2-2B	1815.5	121.6	6.70	75
C3-3A	1679.1	76.6	4.56	98
C4-3B	1706.1	67.5	3.96	86
C5-4A	1660.8	100.6	6.06	61
C6-4B	1727.1	90.2	5.22	93
C7-9A	1601.8	157.7	9.84	55
C8-10B	1574.6	148.5	9.43	70
C9-15A	1668.2	68.7	4.12	82
C10-16A	1413.2	151.5	10.72	20
C11-16B	1623.1	127.6	7.86	50
C12-17A	1521.9	96.2	6.32	50
C13-18A	1604.7	103.0	6.42	66
C14-19A	1595.8	69.9	4.38	70
Specimen type S_A-B	**SWS_T [m/s]**	**SD_T [m/s]**	**CV_T [%]**	**U_T [%]**
B1-1	1746.4	105.5	6.04	91
B2-5	1643.7	152.6	9.29	52
B3-7	1682.8	114.0	6.77	77
B4-8	1669.6	112.5	6.74	75
B5-12	1584.9	135.2	8.53	64
B6-13	1658.0	117.6	7.09	84
B7-21	1609.1	132.4	8.23	57
B8-24	1559.6	108.7	6.97	64
B9-25	1640.0	111.8	6.82	70
B10-27	1551.1	110.2	7.11	77

Table 5.10. Ultrasonic investigations – Experimental results: density (ρ) and dynamic modulus of elasticity (E_{dyn}) for specimens type S_A-C and S_A-B.

Specimen type S_A-C	ρ [kg/m^3]	$E_{dyn,L}$ [N/mm^2]	$E_{dyn,T}$ [N/mm^2]	Specimen type S_A-B	ρ [kg/m^3]	$E_{dyn,L}$ [N/mm^2]	$E_{dyn,T}$ [N/mm^2]
C1-2A	617	16385	2107	B1-1	526	15085	1603
C2-2B	618	16305	2036	B2-5	638	19809	1724
C3-3A	578	15620	1630	B3-7	574	16247	1624
C4-3B	542	14247	1577	B4-8	614	18252	1710
C5-4A	565	18080	1557	B5-12	604	17303	1517
C6-4B	530	16828	1582	B6-13	622	14133	1709
C7-9A	545	12866	1398	B7-21	634	18539	1641
C8-10B	550	17537	1365	B8-24	554	16915	1348
C9-15A	595	17714	1657	B9-25	605	16936	1626
C10-16A	642	19207	1281	B10-27	627	19257	1509
C11-16B	610	17561	1607				
C12-17A	554	14496	1284				
C13-18A	577	15988	1486				
C14-19A	582	15602	1482				

For data interpretation, firstly the relation between longitudinal and transversal dynamic properties has been analyzed, as shown in Figure 5.8. For all elements, the ratio between the velocity in parallel and perpendicular to grain is equal to about three. Whereas, a great variability is provided by the same dynamic modulus ratio.

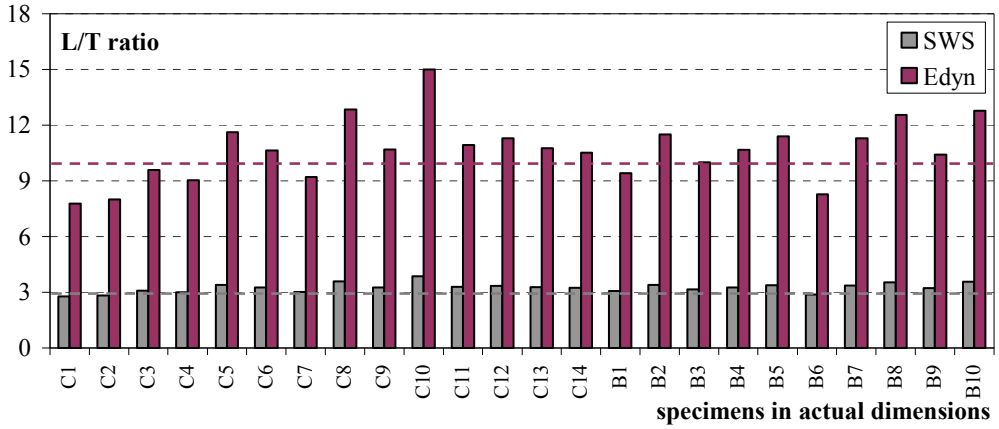

Figure 5.8. Ultrasonic investigations – Experimental results: ratio between longitudinal (L) and transversal (T) dynamic properties (specimens type S_A-C and S_A-B).

Furthermore, the transversal ultrasonic investigations are affected by the higher variability in terms of average results, as it is represented in Figure 5.9, where the coefficients of variation (CV) are reported.

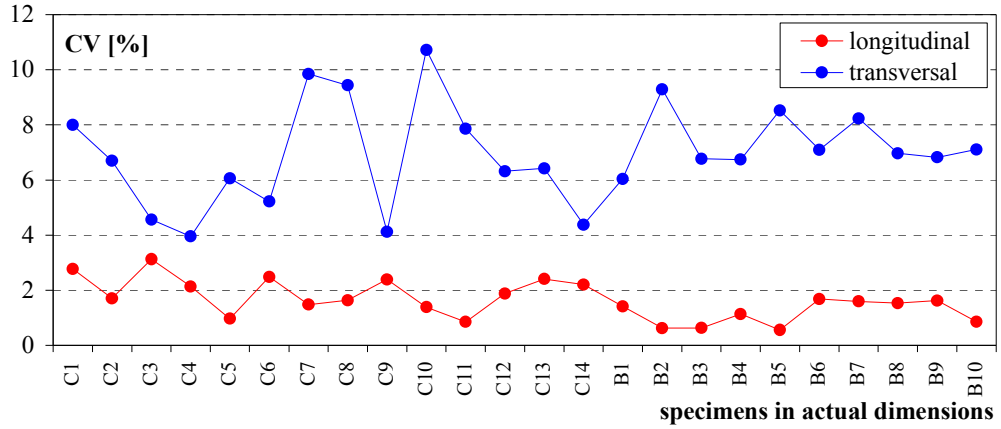

Figure 5.9. Ultrasonic investigations – Experimental results: coefficients of variation (CV) for longitudinal and transversal tests.

Correlating CV with both SWS and the U parameters, obtained in transversal ultrasonic investigations, inverse relationships have been found. As it appears, the CV decreases when the stress wave speed and the actual number of readings increase (Figs. 5.10 and 5.11).

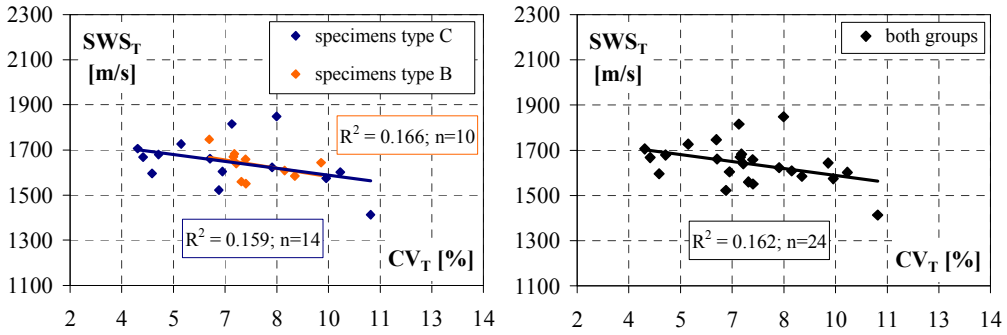

Figure 5.10. Ultrasonic investigations – Experimental results: correlations between stress wave speed (SWS) and coefficient of variation (CV) in transversal tests.

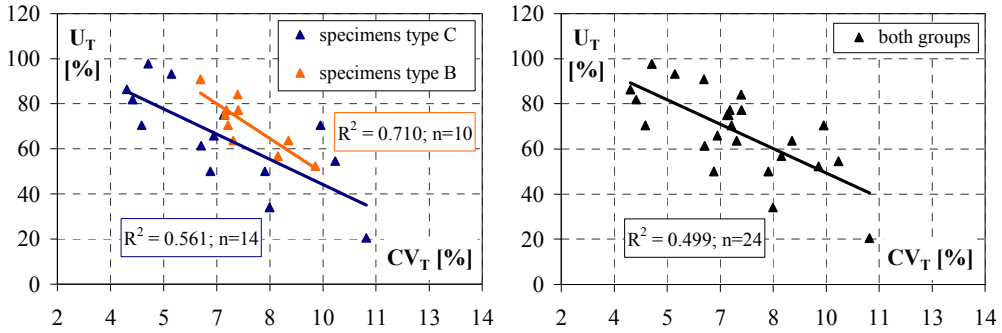

Figure 5.11. Ultrasonic investigations – Experimental results: correlations between ratio percentage (U) and coefficient of variation (CV) in transversal tests.

5.4 SCLEROMETRIC TESTS

5.4.1 *Testing apparatus*

The *Wood Pecker* mechanical test hammer for wood was used for sclerometric tests (Fig. 5.12). It is an innovative tool which provides accurate and reliable information about the quality and integrity of the tested material. It belongs to a family of proven rebound hammer, from which it has inherited the same ease of use and versatility.

The device allows, through the release of a spring that transforms the elastic potential energy into impact energy, equal to 2300 Nm, to measure the penetration of a blunt metallic needle, 2.5 mm diameter and 50 mm length, shoot into the outer millimeters of wood by means of five spring blows. The needle is protected by a plastic cap and inserted in the hole at the end of the tool percussion rod. The instrument is equipped by the penetration depth measuring system.

Figure 5.12. Sclerometric tests – Testing apparatus: Wood Pecker mechanical tests hammer.

5.4.2 *Testing set-up*

The sclerometric tests were performed on all structural elements in actual (S_A-C and S_A-B) and small dimension (S_S-C and S_S-NDT).

In order to investigate the wood superficial hardness in parallel direction to the grain, longitudinal tests were performed shooting the pins in points located on the end cross-sections of the specimens. On the other hand, the resistance to superficial penetration in the perpendicular direction to the grain was investigated by means of sclerometric shots on the lateral faces of the samples, in two directions (x and y), orthogonal each other (Fig. 5.13 and 5.14). In both methods the device was used with the direction of penetration orthogonal to the test surface.

In particular, for the specimens in actual dimensions, regular grids of nine points, 2.5 cm spacing, were used as single test areas, according to UNI EN 12504-2 (Fig. 5.13). In some cases, it was necessary to select shot locations so to avoid local defects, as deep shakes or superficial decay, and then slightly altering the results. Therefore, a mean number of seven sclerometric shots have been performed per area. Moreover, the transversal tests on the small specimens have been performed in radial and tangential direction (Fig. 5.14).

Test set-up scheme are given in Tables 5.11 and 5.12, for the specimens type S_A and S_S, respectively, where the tested sections and the number of shot points per specimen are reported.

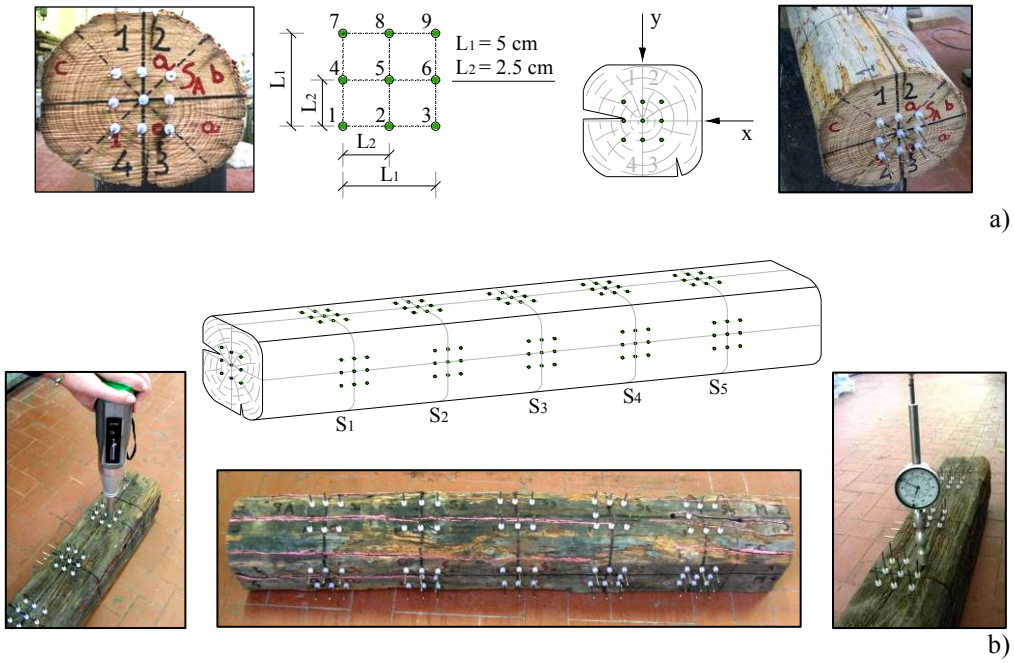

Figure 5.13. Sclerometric tests – Test set-up – Specimens type S_A-C and S_A-B: a) Longitudinal shots; b) Transversal shots.

Table 5.11. Sclerometric tests – Test set-up – Specimens type S_A-C and S_A-B: tested sections and shot points number.

Specimens group *label*	*n.*	**Direction**	**Tested sections**	**Shot points per specimen**	**Total shot points**
S_A-C	14	L	2	18	252
		T	5 (x); 5 (y)	90	1260
S_A-B	10	L	2	18	180
		T	5 (y)	45	450

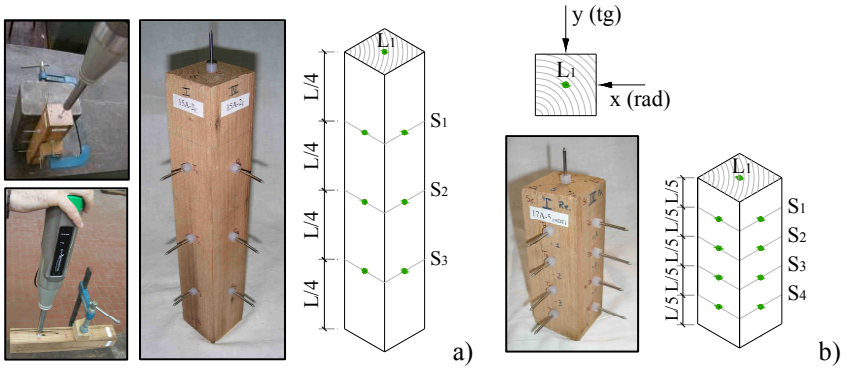

Figure 5.14. Sclerometric tests – Test set-up – Longitudinal and transversal shots on structural elements in small dimensions: a) Type S_S-C; b) Type S_S-NDT.

Table 5.12. Sclerometric tests – Test set-up – Specimens type S_S-C and S_S-NDT: tested sections and shot points number.

Specimens group *label*	*n.*	**Direction**	**Tested sections**	**Shot points per specimen**	**Total shot points**
S_S-C	20	L	2	2	40
		T	3 (x); 3 (y)	6	120
S_S-NDT	16	L	2	2	32
		T	4 (x); 4 (y)	8	128

5.4.3 *Data processing*

For data analysis, the pin penetration depth (PD) in each point has been calculated as follow:

$$PD = L_n - (L_c + D_c)$$

where L_n is the pin length (50 mm); L_c is the measuring system reading (mm); D_c is the depth of the protective plastic cap (6 mm). Readings are given with 0.01% accuracy.

As example, in Table 5.13 the penetration depth values are given in each tested area (A) for the element in actual dimension S_A-C3-3A, while Figure 5.15 shows the pictures of the specimen during the tests.

Table 5.14 gives the experimental results of two typical small specimens.

Table 5.13. Sclerometric tests – Data processing – Specimens type S_A-C: penetration depth values PD [mm] (specimen S_A-C3-3A).

Direction	Area	PD_1	PD_2	PD_3	PD_4	PD_5	PD_6	PD_7	PD_8	PD_9
L	A_A	15.92	18.98	21.45	15.67	15.21	20.24	20.25	21.74	20.09
	A_M	17.33	14.24	14.58	20.30	14.30	14.00	18.88	17.40	13.07
T_x	A_1	16.79	16.81	18.91	17.98	17.25	17.82	18.95	16.42	18.88
	A_2	18.45	19.11	19.02	18.95	18.88	18.18	18.94	19.39	19.30
	A_3	-	18.45	18.95	19.93	16.78	18.45	19.92	-	19.58
	A_4	19.08	18.47	19.14	18.24	19.36	18.96	16.54	19.87	16.60
	A_5	15.89	15.42	15.27	14.78	17.04	16.72	17.62	17.28	15.35
T_y	A_1	15.44	16.53	15.53	-	-	-	15.83	16.73	17.02
	A_2	15.87	17.17	18.12	-	-	-	15.37	16.34	16.92
	A_3	16.82	15.45	18.56	-	-	-	16.99	17.41	15.80
	A_4	15.28	16.66	15.11	-	-	-	16.33	18.14	14.82
	A_5	16.65	15.68	18.01	-	-	-	15.08	16.16	17.30


a)


b)

Figure 5.15. Sclerometric tests – Specimen S_A-C3-3A: a) Longitudinal shots; b) Transversal shots.

Table 5.14. Sclerometric tests – Data processing – Specimens type S_S-C and S_S-NDT: penetration depth values PD [mm] (specimens S_S-C13-16A and S_S-NDT11-16A).

	S_S-C13-16A			S_S-NDT11-16A			
Direction	PD_1	PD_2	PD_3	PD_1	PD_2	PD_3	PD_4
L	17.29	15.50		15.77	-		
T_x (rad)	13.18	13.48	13.31	12.48	12.79	12.61	16.11
T_y (tg)	14.46	15.79	12.30	14.43	11.35	12.08	15.19

5.4.4 *Results and discussion*

5.4.4.1 Structural elements in actual dimensions

In order to evaluate the resistance to superficial penetration by the wood test hammer system, as sclerometric parameters the average values of the penetration depth (PD) are considered for each tested element, for both longitudinal (L) and transversal (T) tests.

In Tables 5.15 and 5.16 the experimental results are presented for the structural elements in actual dimensions (S_A-C and S_A-B) in terms of non-destructive and statistical parameters, such as standard deviation (SD), coefficient of variation (CV) and value percentage (S), obtained by the ratio between the number of the performed shots and the total number of the grids points, equal to eighteen for longitudinal tests and ninety for the transversal ones (Table 5.11).

A first comparison between the sclerometric results is presented in Figure 5.16. It is possible to observe that, in terms of both mean penetration depth (PD) and variation coefficient (CV), the longitudinal parameters are generally higher than the transversal ones.

In Figure 5.17 the penetration depth parameter (PD) of each single specimen is correlated with the corresponding coefficient of variation (CV). The general trend is that CV increases when the PD decrease, for both longitudinal (Fig. 5.17a) and transversal (Fig. 5.17b) shots. This means that less variability in the results is provided by the samples with lower superficial hardness and consistence. Besides, with regards to the sclerometric tests in perpendicular to grain direction, the experimental results emphasize that the coefficient of variation is lower when a considerable number of shots were carried out on the lateral faces of the specimens, as the correlation S vs CV shows in Figure 5.18.

Table 5.15. Sclerometric tests – Experimental results in longitudinal direction (L): specimens type S_A-C and S_A-B.

Specimen type S_A-C	**PD_L [m/s]**	**SD_L [m/s]**	**CV_L [%]**	**S_L [%]**
C1-2A	16.44	2.35	14.27	89
C2-2B	18.52	2.63	14.22	94
C3-3A	17.43	2.87	16.44	100
C4-3B	18.30	3.08	16.85	100
C5-4A	20.28	2.43	12.01	94
C6-4B	19.87	1.86	9.36	100
C7-9A	18.36	1.77	9.63	94
C8-10B	19.50	2.21	11.32	89
C9-15A	20.10	1.77	8.83	83
C10-16A	18.26	2.21	12.12	89
C11-16B	17.17	1.40	8.14	94
C12-17A	20.08	1.28	6.36	94
C13-18A	18.64	2.23	11.98	78
C14-19A	20.08	1.70	8.49	78
Specimen type S_A-B	**PD_L [m/s]**	**SD_L [m/s]**	**CV_L [%]**	**S_L [%]**
B1-1	15.90	2.40	15.12	83
B2-5	14.47	2.16	14.96	72
B3-7	15.52	1.66	10.69	94
B4-8	12.72	1.76	13.85	100
B5-12	17.47	1.49	8.55	94
B6-13	12.90	1.76	13.61	100
B7-21	14.78	2.21	14.97	94
B8-24	16.62	2.27	13.68	67
B9-25	15.17	1.71	11.28	78
B10-27	15.73	2.27	14.43	89

Table 5.16. Sclerometric tests – Experimental results in transversal direction (T): specimens type S_A-C and S_A-B.

Specimen type S_A-C	**PD_T [m/s]**	**SD_T [m/s]**	**CV_T [%]**	**S_T [%]**
C1-2A	15.97	1.47	9.22	59
C2-2B	16.56	1.35	8.15	59
C3-3A	17.35	1.46	8.44	81
C4-3B	18.20	1.41	7.77	71
C5-4A	18.84	1.70	9.00	70
C6-4B	17.67	1.39	7.85	73
C7-9A	18.32	1.79	9.77	68
C8-10B	16.90	1.30	7.66	68
C9-15A	18.71	1.34	7.16	72
C10-16A	16.52	1.24	7.49	77
C11-16B	16.71	1.31	7.81	71
C12-17A	18.40	1.29	7.01	72
C13-18A	16.34	1.26	7.68	86
C14-19A	18.54	1.01	5.47	87
Specimen type S_A-B	**PD_T [m/s]**	**SD_T [m/s]**	**CV_T [%]**	**S_T [%]**
B1-1	17.33	2.04	11.75	33
B2-5	14.27	1.42	9.94	38
B3-7	15.06	1.67	11.11	42
B4-8	12.99	1.36	10.47	48
B5-12	17.85	1.51	8.48	50
B6-13	13.62	1.47	10.78	36
B7-21	15.68	1.68	10.69	40
B8-24	17.82	1.86	10.46	30
B9-25	13.52	1.51	11.14	36
B10-27	17.25	1.80	10.42	39

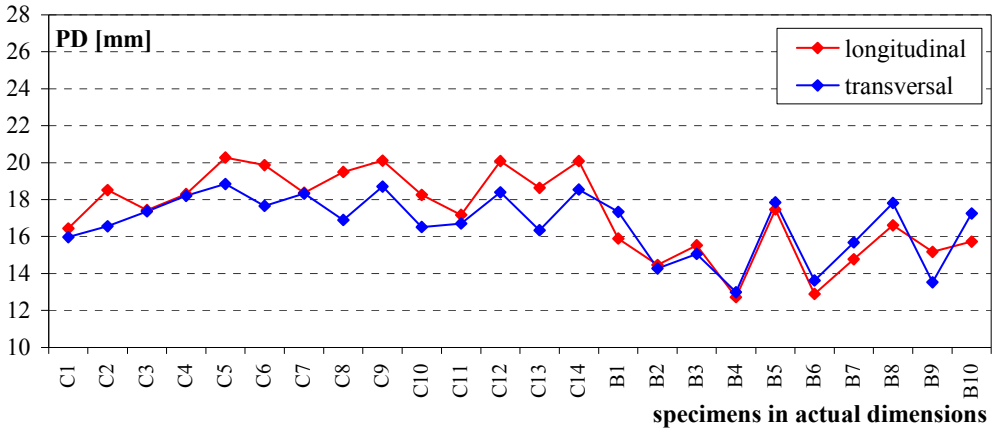

a)

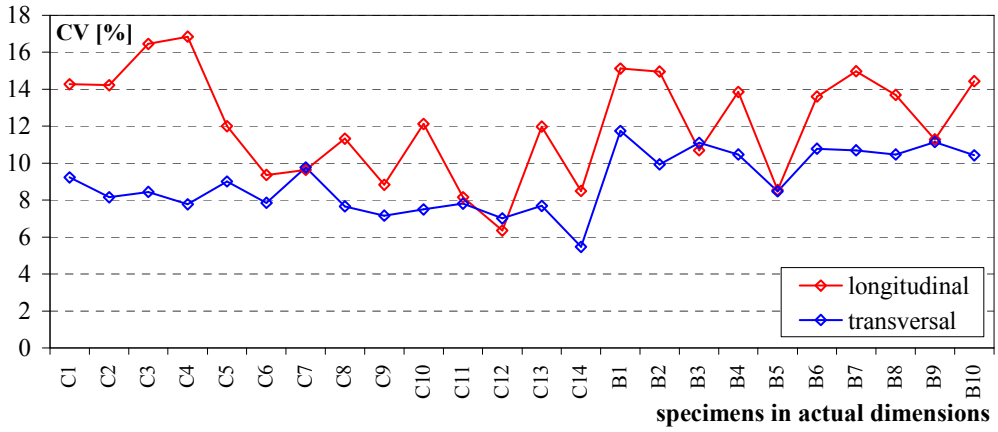

b)

Figure 5.16. Sclerometric tests – Experimental results of specimens type S_A-C and S_A-B – Comparison between longitudinal and transversal parameters: a) Penetration depth (PD); b) Coefficient of variation (CV).

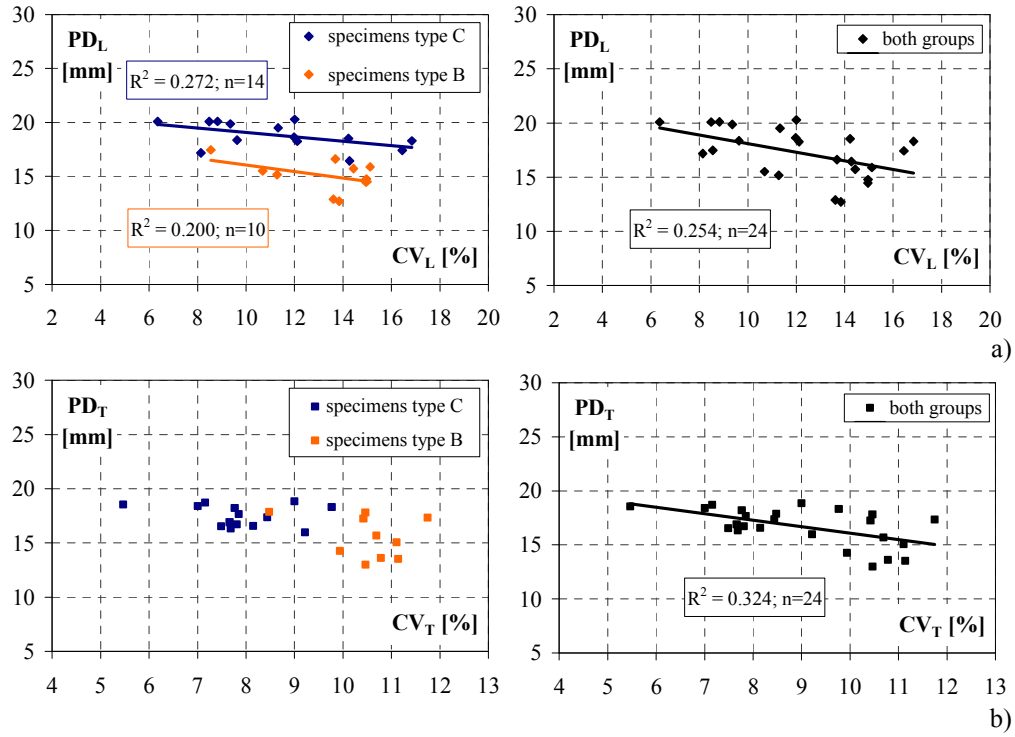

Figure 5.17. Sclerometric tests – Experimental results of specimens type S_A-C and S_A-B – Correlations between penetration depth (PD) and coefficient of variation (CV): a) Longitudinal tests; b) Transversal tests.

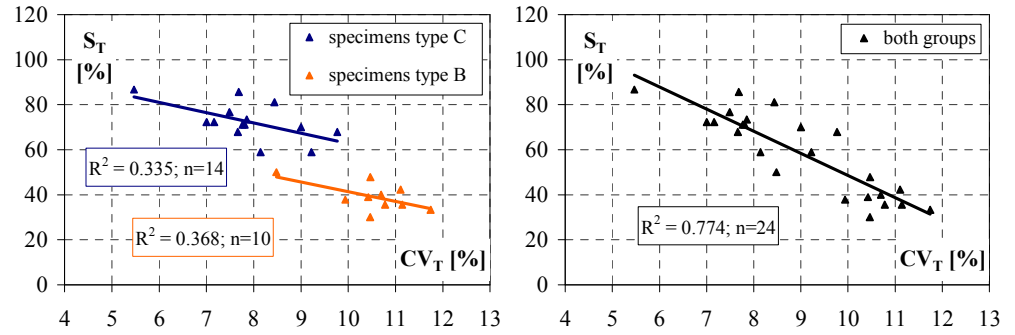

Figure 5.18. Sclerometric tests – Experimental results of specimens type S_A-C and S_A-B: correlations between ratio percentage (S) and coefficient of variation (CV) in transversal tests.

5.4.4.2 Structural elements in small dimensions

The sclerometric tests results of the elements in small dimensions (S_S-C and S_S-NDT), are provided in Table 5.17. In Table 5.18 the results are grouped for each origin element, from which the samples were extracted. For the transversal tests, the average values of the penetration depth in radial ($PD_{T\ rad}$) and tangential ($PD_{T\ tg}$) directions are given too.

The first results analysis is represented in Figure 5.19. As for the specimens in actual dimensions, the tests have provided higher longitudinal penetration depth than the transversal one. Instead, a similar response has been obtained through radial and tangential transversal tests.

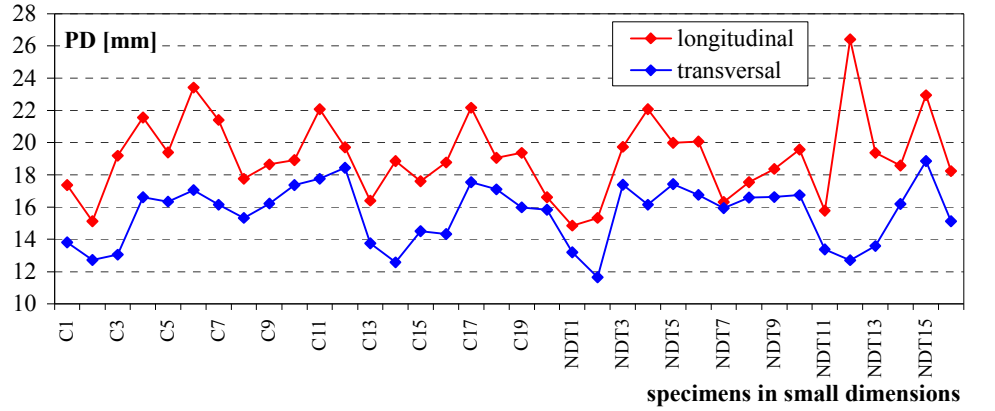

a)

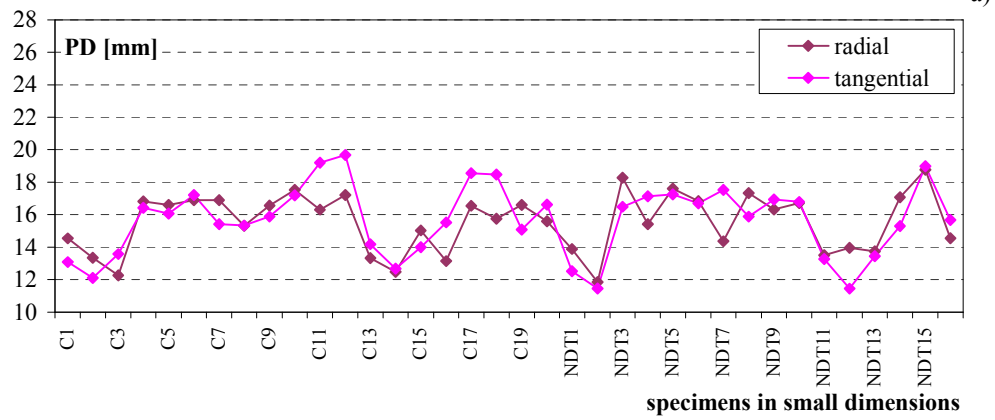

b)

Figure 5.19. Sclerometric tests – Experimental results of specimens type S_S-C and S_S-NDT– Comparison between penetration depth values (PD): a) Longitudinal and transversal; b) Radial and tangential.

Table 5.17. Sclerometric tests – Experimental results in both longitudinal (L) and transversal direction (T): specimens type S_S-C and S_S-NDT.

Specimen type S_S-C	**PD_L [mm]**	**$PD_{T\ rad}$ [mm]**	**$PD_{T\ tg}$ [mm]**	**PD_T [mm]**	**SD_T [mm]**	**CV_T [%]**
C1-2A	17.38	14.54	13.08	13.81	1.28	9.25
C2-2A	15.13	13.35	12.10	12.73	1.61	12.66
C3-2B	19.19	12.26	13.57	13.05	1.08	7.90
C4-3A	21.56	16.82	16.41	16.62	1.00	6.01
C5-3A	19.39	16.60	16.07	16.34	2.79	17.10
C6-3B	23.42	16.90	17.20	17.05	1.19	6.95
C7-3B	21.41	16.89	15.42	16.15	1.74	10.74
C8-4A	17.76	15.31	15.34	15.32	1.43	9.31
C9-4A	18.65	16.57	15.88	16.23	1.67	10.31
C10-4B	18.93	17.54	17.19	17.36	2.04	11.72
C11-15A	22.08	16.32	19.21	17.76	2.03	11.43
C12-15A	19.70	17.21	19.68	18.45	1.74	9.43
C13-16A	16.40	13.32	14.18	13.75	1.21	8.82
C14-16A	18.87	12.47	12.67	12.57	1.53	12.14
C15-16B	17.61	15.04	13.99	14.51	1.32	9.08
C16-16B	18.78	13.14	15.52	14.33	1.63	11.40
C17-17A	22.16	16.55	18.56	17.56	1.85	10.51
C18-17A	19.05	15.74	18.47	17.10	1.72	10.07
C19-19A	19.37	16.60	15.07	15.99	0.90	5.37
C20-19A	16.62	15.60	16.63	15.84	0.93	5.86
Specimen type S_S-NDT	**PD_L [mm]**	**$PD_{T\ rad}$ [mm]**	**$PD_{T\ tg}$ [mm]**	**PD_T [mm]**	**SD_T [mm]**	**CV_T [%]**
NDT1-2A	14.85	13.89	12.51	13.20	0.97	7.35
NDT2-2A	15.33	11.85	11.45	11.65	0.75	6.40
NDT3-3A	19.74	18.28	16.49	17.38	2.35	13.50
NDT4-3B	22.08	15.42	17.13	16.15	1.24	7.67
NDT5-3B	19.99	17.60	17.26	17.43	1.22	7.02
NDT6-4A	20.06	16.83	16.70	16.77	1.44	8.61
NDT7-4A	16.31	14.36	17.53	15.94	1.86	11.64
NDT8-4B	17.55	17.33	15.88	16.60	1.23	7.44
NDT9-15A	18.36	16.33	16.93	16.63	1.18	7.12
NDT10-15A	19.58	16.72	16.79	16.75	0.62	3.68
NDT11-16A	15.77	13.50	13.26	13.38	1.66	12.44
NDT12-16B	26.41	13.96	11.45	12.70	1.47	11.55
NDT13-16B	19.37	13.73	13.45	13.59	0.43	3.16
NDT14-17A	18.57	17.08	15.30	16.19	1.15	7.09
NDT15-17A	22.94	18.76	18.99	18.86	2.54	13.45
NDT16-19A	18.23	14.56	15.68	15.12	1.36	8.97

Table 5.18. Sclerometric tests – Experimental results of the specimens in small dimensions (S_S) grouped for each origin element.

Origin element	PD_L [mm]	$PD_{T\ rad}$ [mm]	$PD_{T\ tg}$ [mm]	PD_T [mm]
2A	15.17	13.44	12.30	12.85
2B	19.19	12.26	13.57	13.05
3A	20.23	17.34	16.34	16.78
3B	21.72	16.68	16.79	16.70
4A	18.19	15.74	16.47	16.06
4B	18.24	17.42	16.44	16.98
15A	19.93	15.63	16.55	15.99
16A	17.01	13.14	13.36	13.24
16B	20.54	13.95	13.44	13.78
17A	20.68	16.95	17.12	13.78
19A	18.07	15.48	15.68	15.65

5.5 RESISTOGRAPHIC MEASUREMENTS

5.5.1 *Testing apparatus*

IMLRESI F400 device was used for resistographic measurements. It is a drilling resistance measuring system based on the energy used to introduce a needle through the wood. A drilling needle with a diameter of 1.5 mm to 3.0 mm penetrates into the wooden element with a regular advancing speed. The wood is only insignificantly injured and the drilling hole closes itself, due to a special drilling angle that was customized for the drill bit. The spent energy of the drilling device is measured electronically every 0.1 mm, as a value of the drilling resistance.

The data are recorded on a wax paper strip in a scale of 1:1, instantly stored on a special electronic unit as graphic profiles, which can then be downloaded on a PC for successive elaborations (Fig. 5.20).

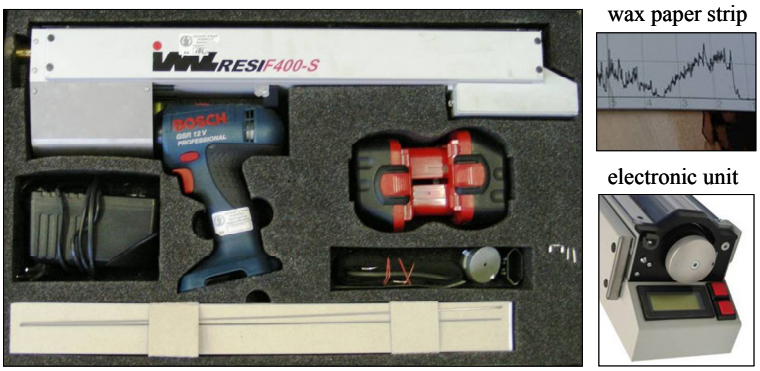

Figure 5.20. Resistographic tests – Testing apparatus: IMLRESI F400 device.

5.5.2 *Test set-up*

The resistographic tests were performed on all structural elements in actual (S_A-C and S_A-B) and small dimension (S_S-C and S_S-NDT).

The experimental tests consisted of penetrations in parallel and perpendicular direction to the grain, with an advancing speed of about 20 cm/minute.

On the elements in actual dimensions, the longitudinal measurements were carried out on the ends of the samples with a drilling depth of about 350 mm for the specimens type S_A-C and about 200 mm for the specimens type S_A-B. Two transversal perforations were carried out in eleven sections, previously selected for ultrasonic investigations. The set-up procedure, the tested sections and measures number are illustrated in Figure 5.21 and summarized in Table 5.19.

With regards to the small elements type S_S-C (Fig. 5.22a), on each end-section the parallel to grain perforations were undertaken on two test points, with a drill length of about 5 cm; while the specimens type S_A-NDT (Fig. 5.22b) were analyzed in longitudinal direction on the total their length, in four point of each element. The Table 5.20 provides the test set-up scheme for both longitudinal and transversal measures.

A workbench and a level were used to execute the drills reducing the possibility of error, by accurately controlling the specimen position and execution time.

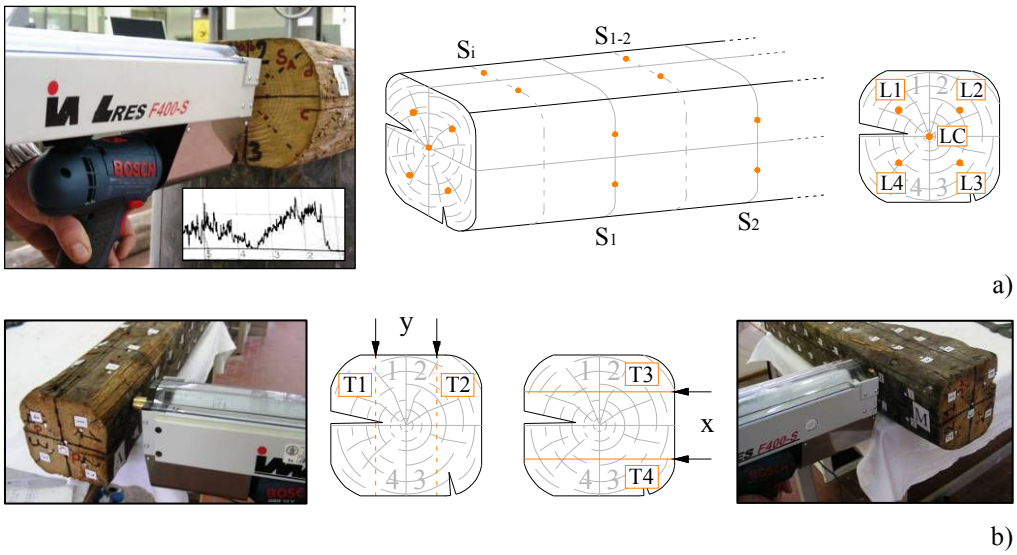

Figure 5.21. Resistographic tests – Test set-up – Specimens type S_A-C and S_A-B: a) Longitudinal measures; b) Transversal measures.

Table 5.19. Resistographic tests – Test set-up – Specimens type S_A-C and S_A-B: tested sections and measures number.

Specimens group *label*	*n.*	**Direction**	**Tested sections**	**Measures per specimen**	**Total measures**
S_A-C	14	L	2	10	140
		T	6 (x); 5 (y)	22	308
S_A-B	10	L	2	10	100
		T	6 (x); 5 (y)	22	220

5.5.3 *Data processing*

The resistographic data have been downloaded on a PC and exported in ASCII format by means of F-Tools Pro software. Therefore, the experimental results have been analyzed by means of graphic profiles relating the Drilling Depth (DD) and the drilling resistance, measured as Amplitude percentage (A).

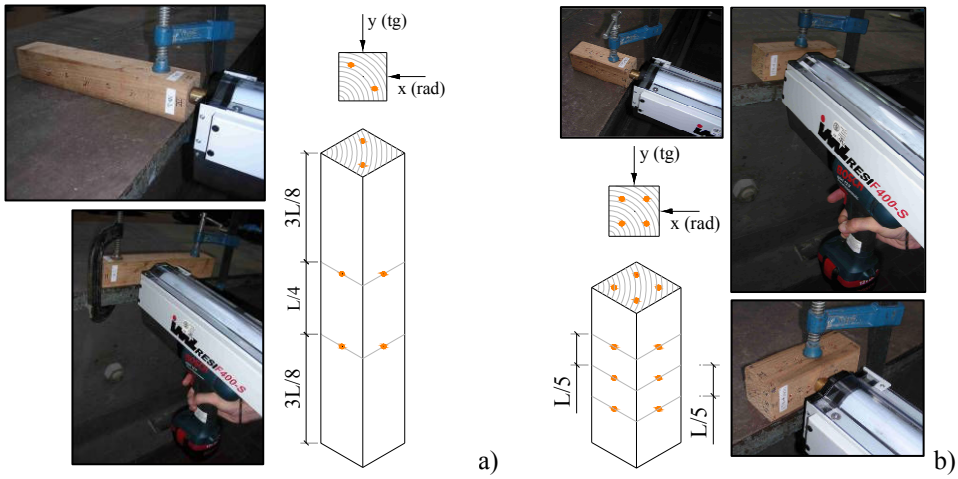

Figure 5.22. Resistographic tests – Test set-up – Longitudinal and transversal measures on structural elements in small dimensions: a) Type S_S-C; b) Type S_S-NDT.

Table 5.20. Resistographic tests – Test set-up – Specimens type S_S-C and S_S-NDT: tested sections and measures number.

Specimens group *label*	*n.*	**Direction**	**Tested sections**	**Measures per specimen**	**Total measures**
S_S-C	20	L	2	4	80
		T	2 (x); 2 (y)	4	80
S_S-NDT	16	L	1	4	64
		T	3 (x); 3 (y)	6	96

In Figures 5.23 and 5.24 typical profiles are depicted for measurements in longitudinal and transversal direction, respectively. By examining the resistographic charts, it was possible to evaluate the density variations of the wood and to detect the presence of internal defects, as damaged zones, hollow areas, cracks and other decay patterns, which return by very low values of drilling resistance. Within the good wood, the longitudinal graphs show very similar values of amplitude, which, on the contrary, is characterized by a strong variation in the transversal measurements, due to the crossing of the growth rings during the drilling path.

Different level of wood quality have been observed: level 1) wood of high quality, characterized by a strong values of amplitude for the presence of

knots on the lateral surface or internal more resistant parts (Figs. 5.23a and 5.24a); level 2) wood of good quality (Figs. 5.23b and 5.24b); level 3) wood of poor quality, with low or null values of drilling resistance where internal anomalies, as hollow areas and damaged zones, occur (Figs. 5.23c and 5.24c); level 4) wood pith with low value of amplitude due to the poor consistence of the wood core located at the centre of the cross-sections (Fig. 5.23d).

Aiming at correlating the resistographic results to the physical and mechanical properties obtained by destructive tests, as unique parameter of wood drilling resistance, the mean value of amplitude (A_m) has been calculated (Fig. 5.25). It represents the ratio between the integral of the diagram area and the depth of the needle path, given by:

$$A_m = \frac{\int_0^L \text{Area}}{L} [\%]$$

where L is the drilling path length.

It is worth noticing that, in presence of defects, the A_m parameter has been evaluated with and without considering low or null resistance measures. Obviously, the mean drilling resistance of homogeneous parts is larger than the same one calculated including internal damaged zones and hollow areas (Fig. 5.25).

As example in Figure 5.26 all longitudinal profiles of specimen S_A-B1-1 are depicted and in Table 5.21 the drilling path lengths and the mean values of amplitude are provided “with defects” and “without defects”. Concerning the transversal measurements, for the same specimen in actual dimensions, Figure 5.27 shows typical profiles, achieved in two sections of the sample, whereas in Table 5.22 all resistographic parameters are reported.

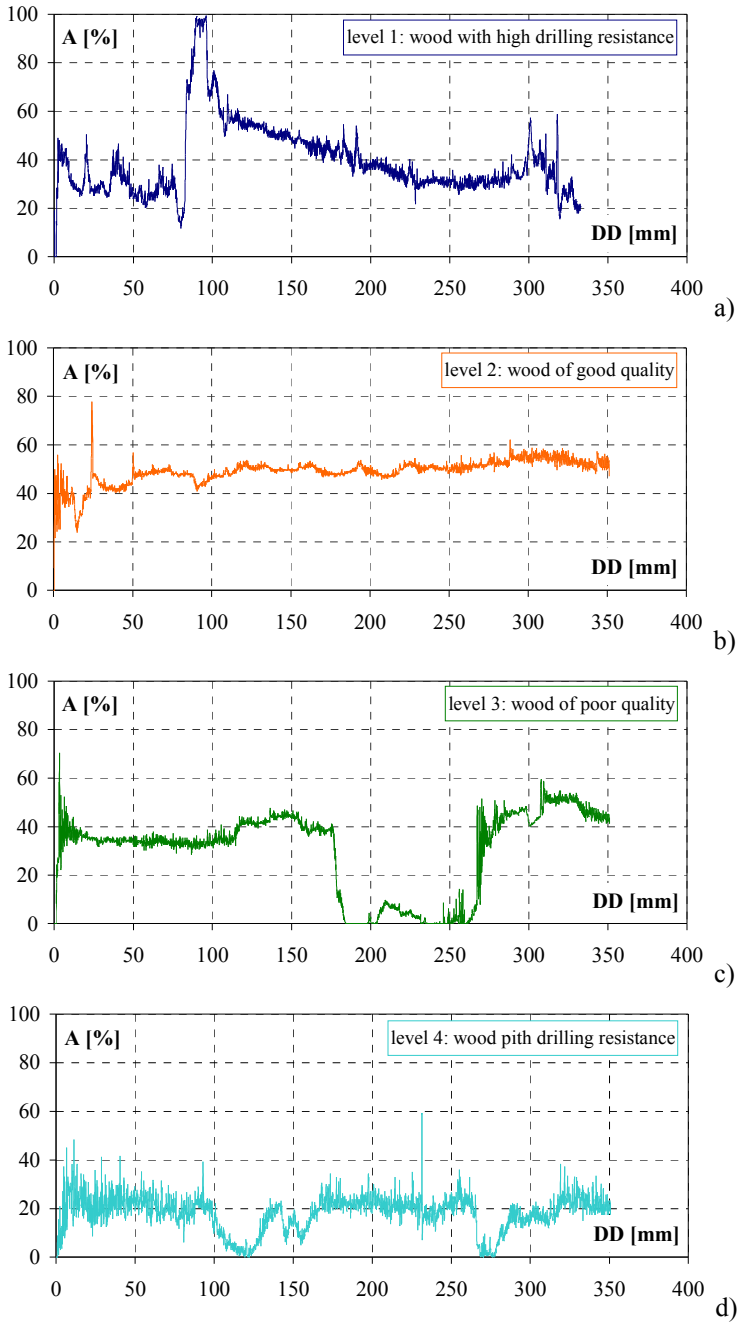

Figure 5.23. Resistographic tests – Data processing – Typical longitudinal graphic profiles: a) Level 1; b) Level 2; c) Level 3; d) Level 4.

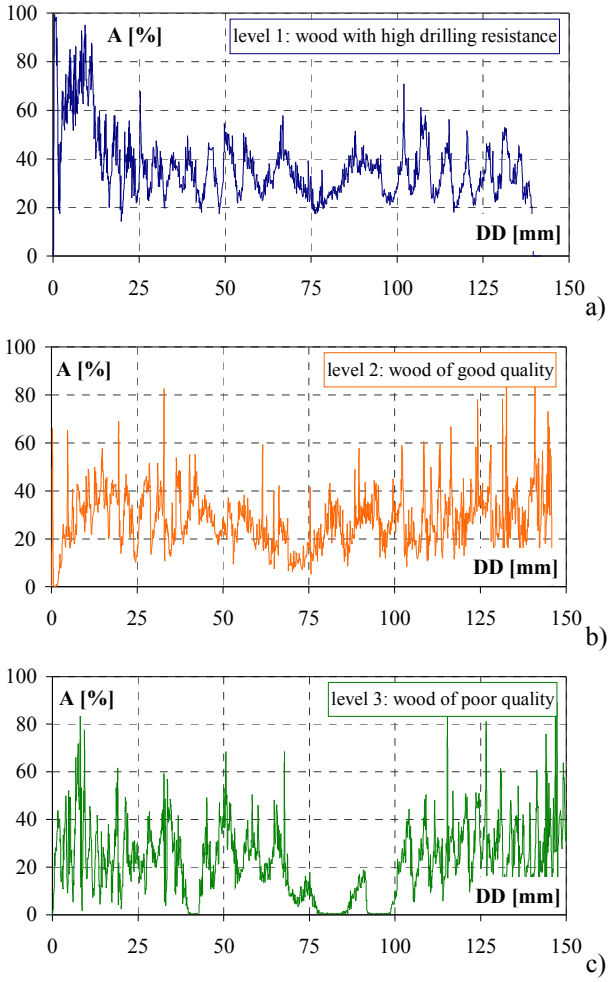

Figure 5.24. Resistographic tests – Data processing – Typical transversal graphic profiles: a) Level 1; b) Level 2; c) Level 3.

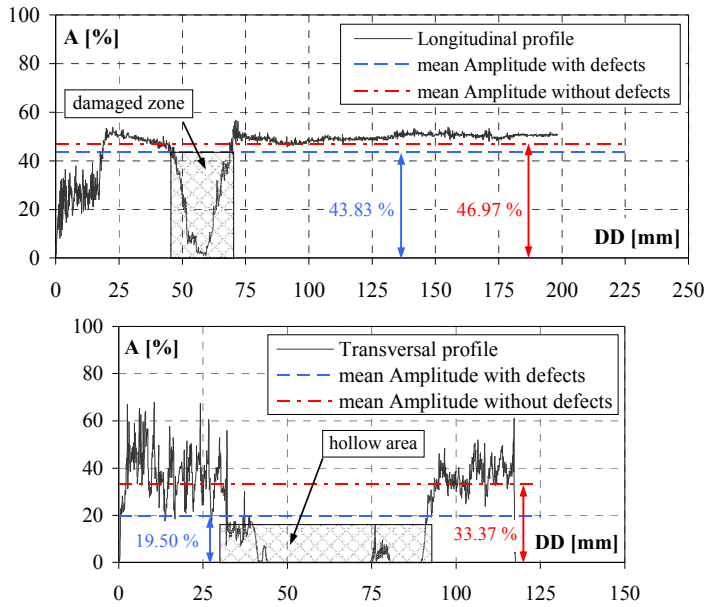

Figure 5.25. Resistographic tests – Data processing: definition of the mean amplitude.

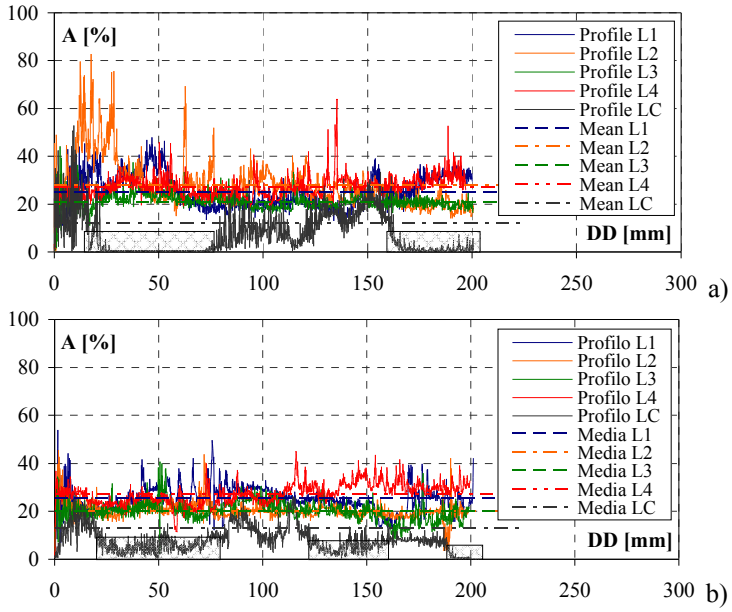

Figure 5.26. Resistographic tests – Data processing – Typical longitudinal graphic profiles (specimen S_A-B1-1): a) Section S_A; b) Section S_B.

Table 5.21. Resistographic tests – Data processing: drilling path length (L) and mean amplitude (A_m) in longitudinal measures (specimen S_A-B1-1).

B1-1A	**with defects**		**without defects**	
Profile	**L^* [cm]**	**$A^*_{m,L}$ [%]**	**L [cm]**	**$A_{m,L}$ [%]**
L1	20.01 – 20.12	25.12 – 25.35	20.01 – 20.12	25.12 – 25.35
L2	20.07 – 19.86	28.16 – 20.25	20.07 – 19.86	28.16 – 20.25
L3	20.05 – 19.91	21.07 – 20.14	20.05 – 19.91	21.07 – 20.14
L4	19.70 – 19.96	27.21 – 27.38	19.70 – 19.96	27.21 – 27.38
LC	20.05 – 19.99	7.00 – 7.92	11.15 – 5.84	11.98 – 13.15

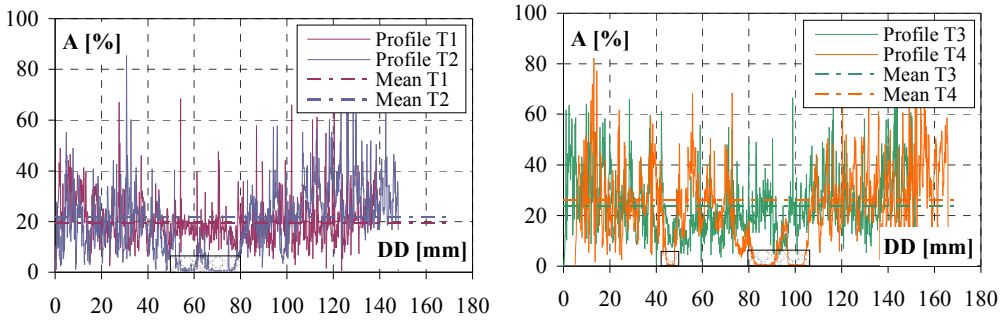

a) b)

Figure 5.27. Resistographic tests – Data processing – Typical transversal graphic profiles (specimen S_A-B1-1): a) Section S_i (3D/2); b) Section S_1 (3D).

Table 5.22. Resistographic tests – Data processing: drilling path length (L) and mean amplitude (A_m) in transversal measures (specimen S_A-B1-1).

B1-1A	**with defects**		**without defects**	
Section	**L^* [cm]**	**$A^*_{m,T}$ [%]**	**L [cm]**	**$A_{m,T}$ [%]**
S_i	13.98 – 14.81	19.64 – 19.36	13.98 – 13.21	19.64 – 21.62
S_1 (3D)	15.41 – 16.62	23.80 – 23.27	15.41 – 14.33	23.80 – 26.12
S_{1-2}	11.87 – 16.28	23.53 – 18.98	11.87 – 16.28	23.53 – 18.98
S_2 (6D)	16.28 – 16.16	22.37 – 21.72	16.28 – 14.26	22.37 – 24.31
S_{2-3}	13.33 – 13.18	25.33 – 16.34	13.33 – 12.97	25.33 – 16.59
S_3 (9D)	15.30 – 15.01	18.02 – 22.07	14.34 – 15.01	19.12 – 22.07
S_{3-4}	13.46 – 12.64	20.38 – 19.32	13.46 – 12.46	20.38 – 19.58
S_4 (12D)	15.13 – 15.20	15.39 – 24.15	13.23 – 14.63	17.51 – 25.07
S_{4-5}	12.03 – 13.18	21.89 – 16.64	12.03 – 11.60	21.89 – 18.82
S_5 (15D)	14.83 – 11.95	20.58 – 17.32	14.83 – 11.95	20.58 – 17.32
S_f	12.23 – 14.03	24.96 – 13.51	11.49 – 11.19	26.54 – 16.78

5.5.4 *Results and discussion*

5.5.4.1 Structural elements in actual dimensions

For each structural element in actual dimensions (S_A-C and S_A-B), a total number of ten longitudinal (L) measurements and twenty-two transversal (T) ones are considered for the analysis and interpretation of resistographic results. In Tables 5.23 and 5.24 the following parameters are presented: the total length of the drilling path and the average of the mean amplitude values, calculated "with defects (L^*_{tot} and A^*_m)" and "without defects (L_{tot} and A_m)". Therefore, considering the total number (n^*) of profiles where internal defects were detected, the decrement percentage of the total drilling path length (ΔL), together with the increment percentage of the drilling resistance (ΔA), due to the presence of internal decay and cavities, are also given.

Table 5.23. Resistographic tests – Experimental results in longitudinal direction (L): specimens type S_A-C and S_A-B. (continues)

	with defects			without defects				
Specimen type S_A-C	**L^*_{tot} [cm]**	**$A^*_{m,L}$ [%]**	**n***	**L_{tot} [cm]**	**$A_{m,L}$ [%]**	**CV_L [%]**	**ΔL_L [%]**	**$\Delta A_{m,L}$ [%]**
C1-2A	234.2	51.09	2	230.6	51.49	24.37	1.54	0.78
C2-2B	185.5	43.45	4	167.5	45.97	32.52	9.71	5.80
C3-3A	189.8	45.26	5	178.0	46.65	24.09	6.25	3.07
C4-3B	324.0	28.96	8	302.4	29.84	27.92	6.66	3.04
C5-4A	348.8	36.20	1	339.7	36.78	16.88	2.62	1.60
C6-4B	348.5	28.73	4	339.6	29.40	15.31	2.58	2.33
C7-9A	296.3	22.59	2	242.4	25.21	16.66	18.20	11.60
C8-10B	336.1	35.38	3	314.5	37.13	27.98	6.42	4.95
C9-15A	327.0	36.90	5	304.8	38.37	34.43	6.80	3.98
C10-16A	349.2	56.79	3	347.8	56.96	17.19	0.39	0.31
C11-16B	302.7	44.70	4	280.0	47.73	27.57	7.50	6.78
C12-17A	349.0	41.14	1	348.6	41.17	14.56	0.09	0.07
C13-18A	337.7	30.99	5	311.6	32.71	36.96	7.73	5.55
C14-19A	290.2	41.59	3	285.8	42.13	24.45	1.51	1.30

Table 5.23. Resistographic tests – Experimental results in longitudinal direction (L): specimens type S_A-C and S_A-B.

Specimen type S_A-B	with defects L^*_{tot} [cm]	with defects $A^*_{m,L}$ [%]	with defects n^*	without defects L_{tot} [cm]	without defects $A_{m,L}$ [%]	without defects CV_L [%]	ΔL_L [%]	$\Delta A_{m,L}$ [%]
B1-1	199.7	20.96	2	176.7	21.98	26.30	11.54	4.87
B2-5	206.7	55.47	1	205.8	55.63	25.98	0.46	0.29
B3-7	158.4	42.99	1	158.0	43.09	17.82	0.23	0.23
B4-8	195.0	49.14	2	191.4	49.85	17.95	1.84	1.44
B5-12	194.3	37.27	1	192.2	37.69	30.14	1.07	1.13
B6-13	196.3	44.64	0	196.3	44.64	25.65	0.00	0.00
B7-21	174.6	42.45	2	158.2	45.20	25.33	9.35	6.48
B8-24	199.6	31.06	3	169.5	34.82	24.01	15.09	12.11
B9-25	178.6	40.52	0	178.6	40.52	32.45	0.00	0.00
B10-27	200.4	36.70	2	195.1	37.62	24.61	2.66	2.51

Table 5.24. Resistographic tests – Experimental results in transversal direction (T): specimens type S_A-C and S_A-B. (continues)

Specimen type S_A-C	with defects L^*_{tot} [cm]	with defects $A^*_{m,T}$ [%]	with defects n^*	without defects L_{tot} [cm]	without defects $A_{m,T}$ [%]	without defects CV_T [%]	ΔL_T [%]	$\Delta A_{m,T}$ [%]
C1-2A	296.0	57.32	4	294.6	57.58	11.13	0.48	0.46
C2-2B	278.0	49.45	2	276.9	49.64	16.60	0.40	0.38
C3-3A	285.8	49.54	0	285.8	49.54	13.38	0.00	0.00
C4-3B	290.3	37.91	1	290.1	37.94	16.05	0.07	0.07
C5-4A	297.9	31.78	7	293.8	32.06	20.65	1.36	0.86
C6-4B	286.0	27.27	5	284.7	27.40	12.23	0.45	0.46
C7-9A	305.7	34.80	10	298.3	35.63	13.89	2.41	2.34
C8-10B	303.7	25.32	12	286.2	26.63	10.36	5.77	4.91
C9-15A	307.7	26.49	6	302.7	26.81	25.14	1.62	1.19
C10-16A	292.7	42.66	6	291.3	42.84	18.95	0.48	0.41
C11-16B	297.7	53.43	0	297.7	53.43	16.19	0.00	0.00
C12-17A	309.5	31.29	8	306.2	31.58	31.00	1.06	0.91
C13-18A	297.2	39.31	9	284.8	40.56	14.67	4.18	3.08
C14-19A	301.3	41.61	4	299.5	41.83	21.73	0.62	0.53

Table 5.24. Resistographic tests – Experimental results in transversal direction (T): specimens type S_A-C and S_A-B.

Specimen type S_A-B	with defects L^*_{tot} [cm]	with defects $A^*_{m,T}$ [%]	with defects n^*	without defects L_{tot} [cm]	without defects $A_{m,T}$ [%]	without defects CV_T [%]	ΔL_T [%]	$\Delta A_{m,T}$ [%]
B1-1	312.9	20.39	11	298.1	21.27	14.50	4.72	4.14
B2-5	358.8	53.61	5	357.1	54.18	14.59	0.48	1.04
B3-7	316.6	34.46	2	314.8	34.54	19.69	0.57	0.24
B4-8	290.2	42.23	6	288.4	42.46	17.47	0.65	0.56
B5-12	323.5	34.27	7	319.2	34.66	16.28	1.34	1.13
B6-13	301.1	38.68	1	300.4	38.74	18.36	0.22	0.14
B7-21	323.9	39.28	4	318.3	39.85	14.44	1.72	1.43
B8-24	294.9	30.62	5	290.5	31.07	18.87	1.51	1.44
B9-25	308.8	34.69	5	306.9	34.90	15.79	0.64	0.59
B10-27	281.1	37.97	2	274.5	38.73	14.48	2.34	1.97

The comparison between longitudinal and transversal results is presented in Figure 5.28. In particular, for most of the specimens, the measurements in axial direction provide high coefficient of variation (CV) of drilling resistance.

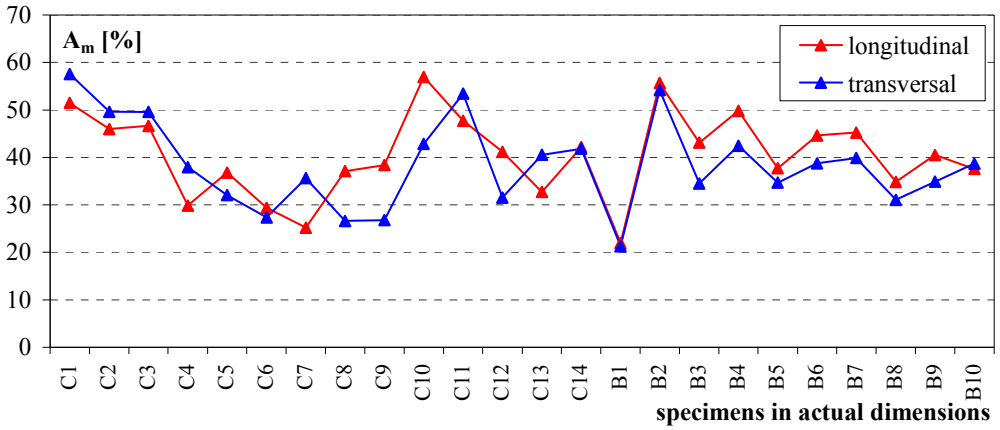

a)

Figure 5.28. Resistographic tests – Experimental results of specimens type S_A-C and S_A-B – Comparison between longitudinal and transversal parameters: a) Mean amplitude (A_m); b) Coefficient of variation (CV). (continues)

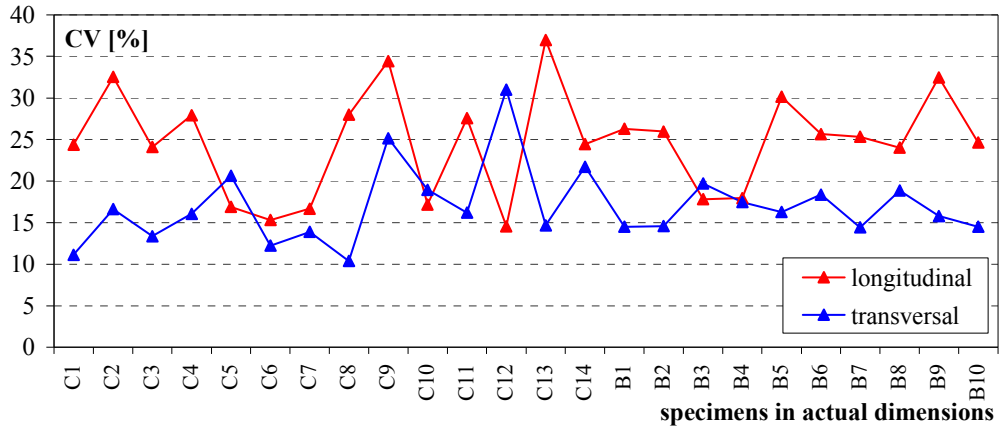

b)

Figure 5.28. Resistographic tests – Experimental results of specimens type S_A-C and S_A-B – Comparison between longitudinal and transversal parameters: a) Mean amplitude (A_m); b) Coefficient of variation (CV).

In Figure 5.29, the increment percentage of mean amplitude (ΔA) is related to the corresponding decrement of the total drilling path length (ΔL). The obtained good correlations allow to estimate the drilling resistance on homogeneous parts, being known the size of the internal damaged parts by means of the analysis of the graphic profiles.

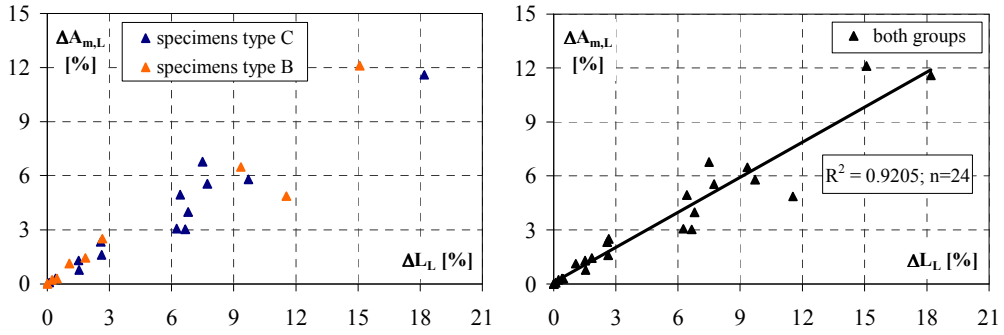

a)

Figure 5.29. Resistographc tests – Experimental results of specimens type S_A-C and S_A-B – Correlations between drilling resistance increment percentage (ΔA_m) and drilling path length decrement percentage (ΔL): a) Longitudinal tests; b) Transversal tests. (continues)

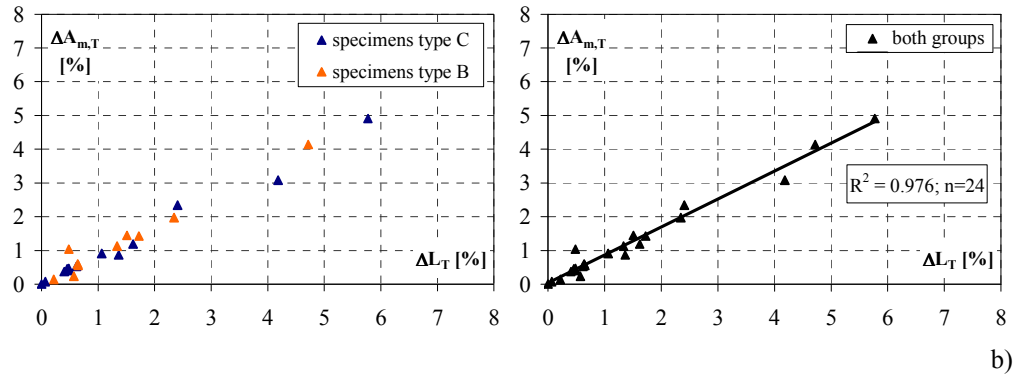

b)

Figure 5.29. Resistographic tests – Experimental results of specimens type S_A-C and S_A-B – Correlations between drilling resistance increment percentage (ΔA_m) and drilling path length decrement percentage (ΔL): a) Longitudinal tests; b) Transversal tests.

5.5.4.2 Structural elements in small dimensions

For each structural elements in small dimensions (S_S-C and S_S-NDT), the average values of mean amplitude (A_m) and the corresponding coefficients of variation (CV) are provided in Table 5.25, for both longitudinal (L) and transversal (T) measurements. The latter ones includes the perforations carried out in radial (rad) and tangential (tg) direction.

In addition, in Table 5.26 the results are grouped for each origin element, from which the small specimens were obtained. It is worth to notice that, since a few of resistographic profiles revealed the presence of internal defects and alterations, the Tables above-mentioned give only the so-called parameters "without defects".

The results are also represented in Figures 5.30 and 5.31, which emphasize the relation between the longitudinal and transversal parameters and the radial and tangential ones. As it is shown, independently from the tests direction, all specimens exhibit a similar response, in terms of both A_m and CV.

Table 5.25. Resistographic tests – Experimental results in both longitudinal (L) and transversal direction (T): specimens type S_S-C and S_S-NDT.

Specimen type S_S-C	**$A_{m,L}$ [%]**	**CV_L [%]**	**$A_{m,T\ rad}$ [%]**	**$A_{m,T\ tg}$ [%]**	**$A_{m,T}$ [%]**	**CV_T [%]**
C1-2A	38.51	11.79	39.25	45.32	42.29	8.51
C2-2A	40.76	3.43	39.15	49.05	44.10	17.11
C3-2B	34.41	17.27	44.06	42.69	43.37	5.07
C4-3A	29.71	11.19	29.07	28.71	28.89	13.46
C5-3A	37.02	10.09	26.09	24.93	25.51	7.58
C6-3B	27.31	13.70	31.99	27.14	29.56	15.11
C7-3B	22.00	25.97	28.96	29.14	29.05	2.07
C8-4A	42.43	8.70	33.07	33.56	33.32	7.41
C9-4A	44.86	9.69	34.47	38.62	36.55	15.25
C10-4B	37.10	17.55	39.69	45.04	42.36	19.33
C11-15A	38.44	4.97	19.93	24.13	22.03	12.52
C12-15A	27.47	10.34	23.17	22.86	23.02	4.00
C13-16A	35.91	11.07	33.02	38.73	35.87	11.12
C14-16A	65.28	13.87	46.11	52.77	49.44	12.56
C15-16B	31.68	4.25	35.67	37.32	36.50	8.16
C16-16B	60.43	28.43	51.29	55.14	53.21	8.13
C17-17A	27.10	13.08	25.29	28.29	26.79	8.27
C18-17A	26.73	19.27	26.18	28.03	27.10	5.54
C19-19A	30.82	1.84	33.05	33.62	33.34	13.52
C20-19A	51.39	9.75	38.52	48.17	43.34	18.26
Specimen type S_S-NDT	**$A_{m,L}$ [%]**	**CV_L [%]**	**$A_{m,T\ rad}$ [%]**	**$A_{m,T\ tg}$ [%]**	**$A_{m,T}$ [%]**	**CV_T [%]**
NDT1-2A	28.69	6.70	42.24	42.66	42.45	1.98
NDT2-2A	41.87	7.37	42.74	49.22	45.98	8.79
NDT3-3A	28.50	15.58	21.99	19.47	20.73	14.02
NDT4-3B	11.60	0.91	20.81	21.79	21.30	9.42
NDT5-3B	14.44	18.19	23.29	26.94	25.11	8.23
NDT6-4A	32.54	14.45	27.40	30.54	28.97	8.78
NDT7-4A	32.00	27.75	25.03	32.25	28.64	18.39
NDT8-4B	28.56	11.83	24.38	31.68	28.03	15.95
NDT9-15A	16.44	6.55	22.78	23.85	23.32	4.72
NDT10-15A	21.32	14.94	18.89	19.96	19.43	4.97
NDT11-16A	36.37	15.87	32.65	37.30	34.98	10.24
NDT12-16B	26.52	1.53	34.02	35.98	35.00	7.34
NDT13-16B	37.86	20.95	33.52	41.65	37.59	16.88
NDT14-17A	18.60	9.86	23.46	25.02	24.24	5.13
NDT15-17A	16.77	15.69	19.62	21.99	20.81	8.27
NDT16-19A	28.38	6.11	31.77	30.52	31.14	5.50

Table 5.26. Resistographic tests – Experimental results of the specimens in small dimensions (S_S) grouped for each origin element.

Origin element	$A_{m, L}$ [%]	$A_{m, T\ rad}$ [%]	$A_{m, T\ tg}$ [%]	$A_{m, T}$ [%]
2A	37.46	42.78	46.13	44.70
2B	34.41	44.06	42.69	43.37
3A	29.07	25.19	23.67	25.04
3B	18.83	25.42	25.87	26.26
4A	28.94	29.24	33.27	31.87
4B	30.35	30.5	37.02	35.20
15A	25.92	21.12	22.54	21.95
16A	37.45	36.6	42.13	40.10
16B	31.45	37.65	41.78	40.57
17A	22.30	23.22	25.36	24.73
19A	27.97	34.06	36.45	35.94

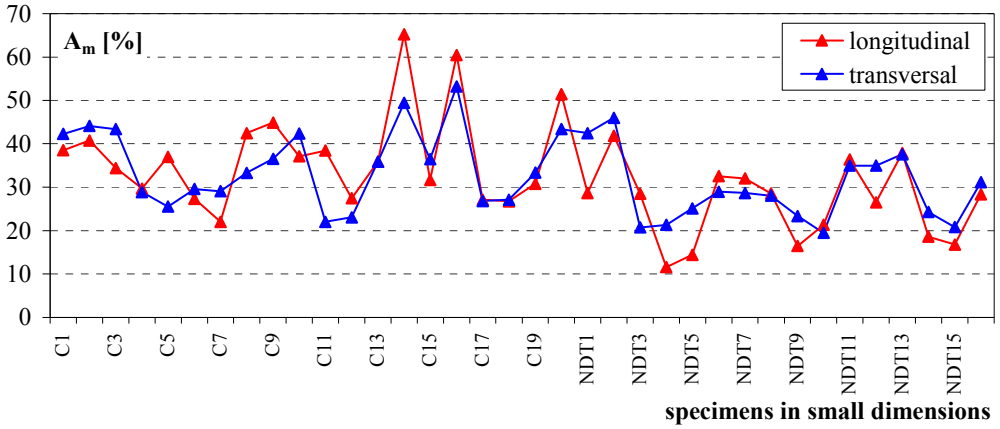

a)

Figure 5.30. Resistographic tests – Experimental results of specimens type S_S-C and S_S-NDT – Comparison between longitudinal and transversal parameters: a) Mean amplitude (A_m); b) Coefficient of variation (CV). (continues)

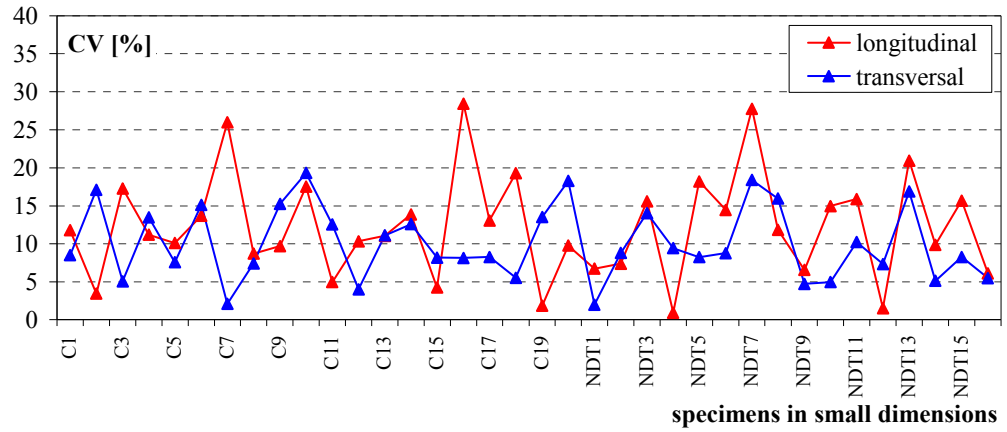

b)

Figure 5.30. Resistographic tests – Experimental results of specimens type S_S-C and S_S-NDT – Comparison between longitudinal and transversal parameters: a) Mean amplitude (A_m); b) Coefficient of variation (CV).

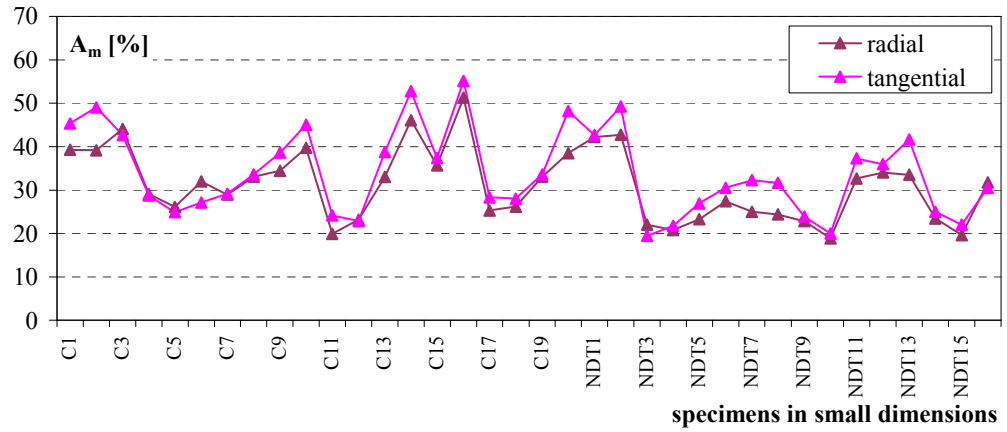

Figure 5.31. Resistographic tests – Experimental results of specimens type S_S-C and S_S-NDT: comparison between radial and tangential mean amplitude (A_m).

5.6 COMPARISON OF NDT RESULTS

5.6.1 *Sclerometric tests*

The comparison between the specimens in actual (S_A) and small (S_S) sizes in terms of the superficial hardness is shown in Figure 5.32, where the penetration depth values, given in Tables 5.15, 5.16 and 5.18, are reported for both longitudinal (Fig. 5.32a) and transversal (Fig. 5.32b) results. In particular, the transversal sclerometric shots on S_A elements are higher than those on S_S specimens. This fact is due to the presence of superficial layers with low consistence and affected by large longitudinal cracks and alterations, which were surveyed by visual inspection, and then detected by NDT tests on the specimens in actual dimensions. Therefore, it is assumed that the mean decrement percentage of penetration depth, due to the presence of natural defects, is equal to about 18 %.

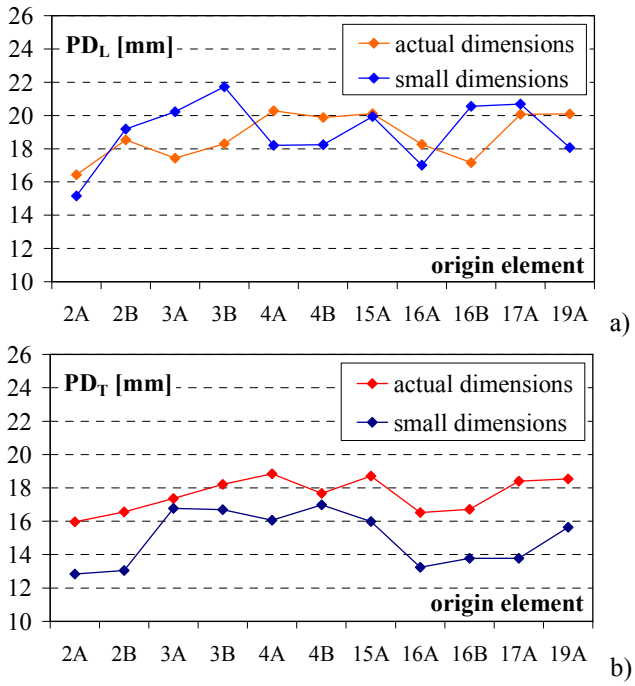

Figure 5.32. Comparison of NDT results – Penetration depth (PD) of elements in actual and small dimensions: a) Longitudinal tests; b) Transversal tests.

5.6.2 *Resistographic measurements*

In Figure 5.33 the resistographic results obtained on the specimens in actual (S_A) and small (S_S) dimensions, given in the Tables 5.23, 5.24 and 5.26, are compared. As it appears, for both longitudinal (Fig. 5.33a) and transversal tests (Fig. 5.33b), the mean amplitude (A_m) evaluated on the specimens type S_A is higher than that obtained on the specimens type S_S. This increment, equal to about 30-40 %, is due to the presence on the elements in actual sizes of large knots and extend more resistant internal parts, which were detected by resistographic profiles.

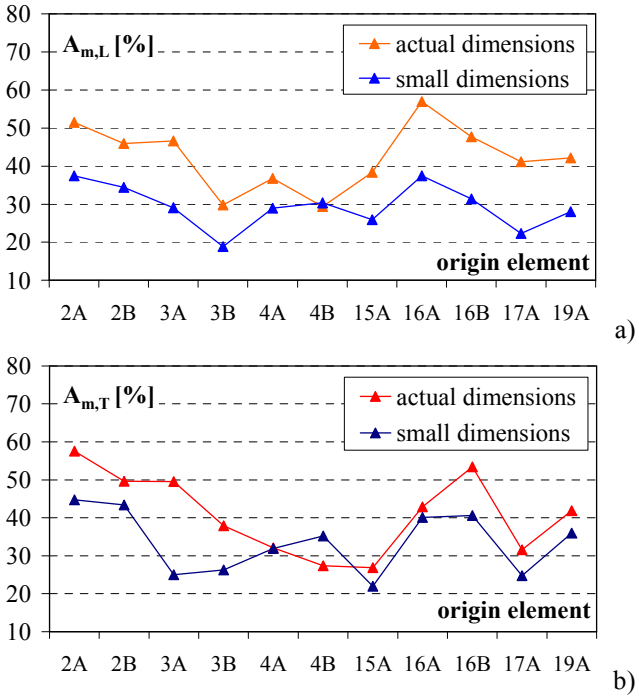

Figure 5.33. Comparison of NDT results – Mean drilling resistance (A_m) of elements in actual and small dimensions: a) Longitudinal tests; b) Transversal tests.

5.6.3 *Coefficients of variation*

The non-destructive experimental results on the specimens in actual dimension (S_A-C + S_A-B) in terms of coefficients of variation (CV) (Fig. 5.34) show that the resistographic tests, in both parallel and perpendicular to grain direction, are characterized by greater variability due to the presence of internal defects which influence the local measures of the drilling-resistance.

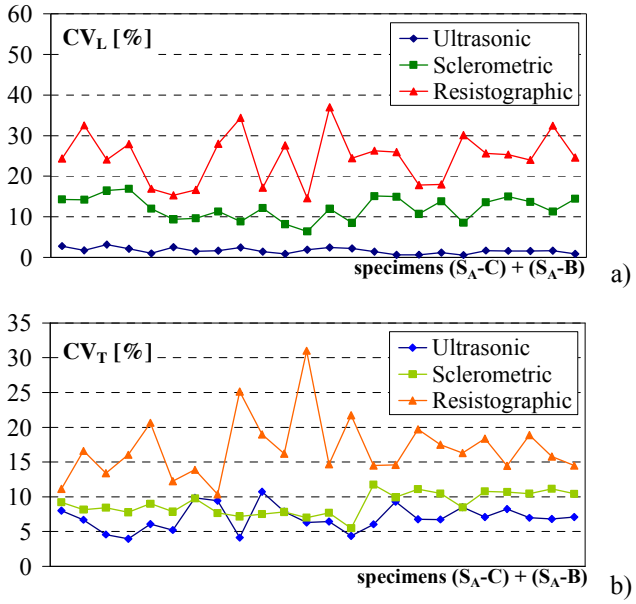

Figure 5.34. Comparison of NDT results – Coefficients of variation (CV) of structural elements in actual dimensions: a) Longitudinal tests; b) Transversal tests.

Instead, the variation coefficients of resistographic and sclerometric tests are similar for the small specimens (Fig. 5.35), which were affected by superficial defects, not extended to the whole size of the samples.

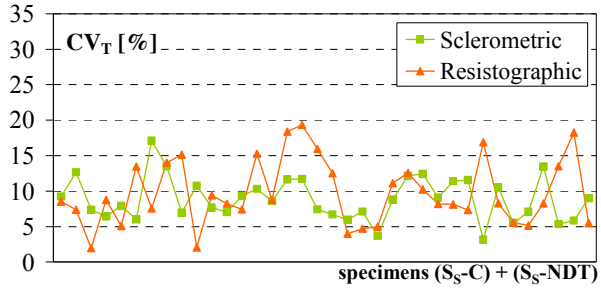

Figure 5.35. Comparison of NDT results: coefficients of variation (CV) of structural elements in small dimensions in transversal tests.

5.6.4 *Mean and characteristic NDT parameters*

For each NDT test typology, all measures have been analyzed by means of statistical analysis. With reference to the specimens in actual dimensions, typical normal curves of frequency distribution are depicted in Figure 5.36, whereas all statistical parameters are given in Tables 5.27, 5.28 and 5.29, for ultrasonic, sclerometric and resistographic tests, respectively.

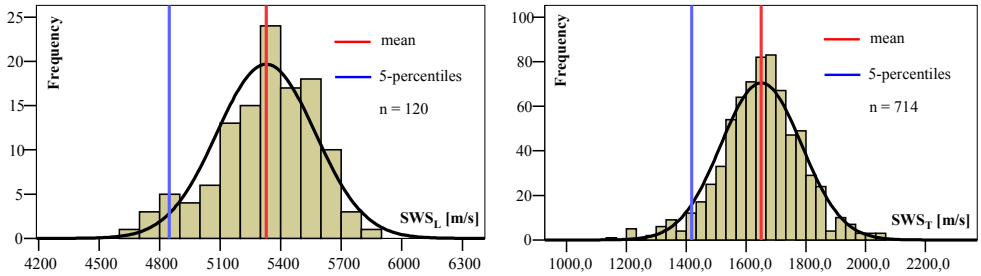

a)

Figure 5.36. Comparison of NDT results – Structural elements in actual dimensions –Normal curves: a) Stress wave speed (SWS) by ultrasonic investigations; b) Penetration depth (PD) by sclerometric tests; c) Mean amplitude (A_m) by resistographic measurements. (continues)

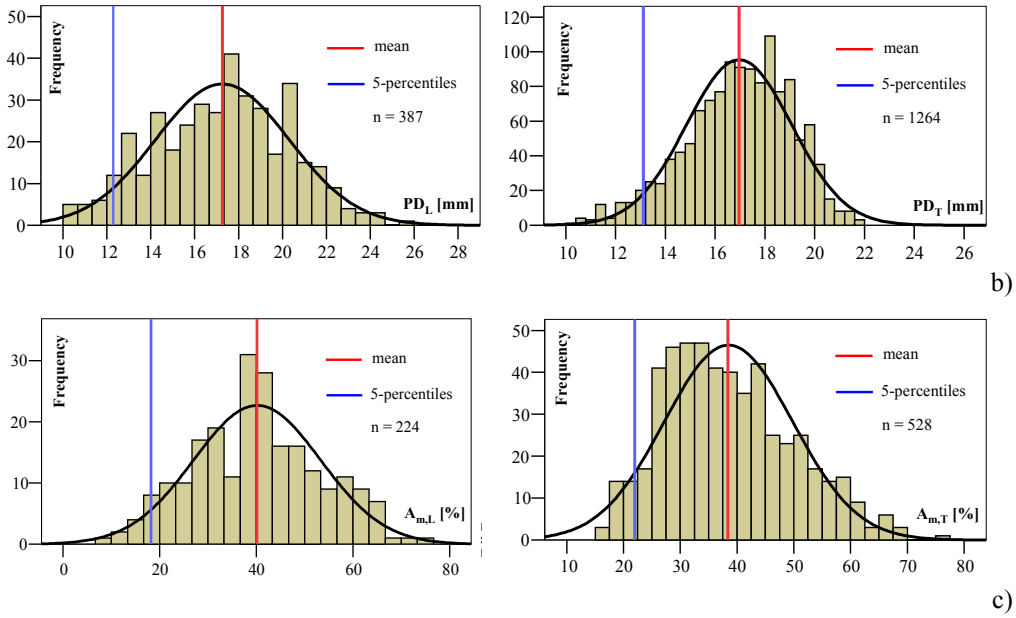

Figure 5.36. Comparison of NDT results – Structural elements in actual dimensions –Normal curves: a) Stress wave speed (SWS) by ultrasonic investigations; b) Penetration depth (PD) by sclerometric tests; c) Mean amplitude (A_m) by resistographic measurements.

Table 5.27. Comparison of NDT results – Structural elements in actual dimensions: statistical parameters of stress wave speed (SWS) by ultrasonic investigations.

	Structural elements in actual dimensions (S_A-C + S_A-B)						
	n_{tot}	**min**	**mean**	**max**	**5-percentiles**	**SD**	**CV [%]**
SWS_L [m/s]	120	4666.3	5327.2	5829.0	4847.9	243.3	4.57
SWS_T [m/s]	714	1159.4	1650.9	2057.3	1418.9	134.8	8.16

Table 5.28. Comparison of NDT results – Structural elements in actual and small dimensions: statistical parameters of penetration depth (PD) by sclerometric tests.

	Structural elements in actual dimensions (S_A-C + S_A-B)						
	n_{tot}	**min**	**mean**	**max**	**5-percentiles**	**SD**	**CV [%]**
PD_L [mm]	387	10.41	17.26	25.62	12.29	3.04	17.61
PD_T [mm]	1264	10.20	16.96	21.82	13.12	2.12	12.50
	Structural elements in small dimensions (S_S-C + S_S-NDT)						
	n_{tot}	**min**	**mean**	**max**	**5-percentiles**	**SD**	**CV [%]**
PD_L [mm]	56	13.00	19.07	26.41	14.47	2.96	15.52
PD_T [mm]	242	10.80	15.42	22.24	11.60	2.18	14.14

Table 5.29. Comparison of NDT results – Structural elements in actual and small dimensions: statistical parameters of mean amplitude (A_m) by resistographic measurements.

	Structural elements in actual dimensions (S_A-C + S_A-B)						
	n_{tot}	**min**	**mean**	**max**	**5-percentiles**	**SD**	**CV [%]**
$A_{m,L}$ [%]	224	7.48	40.16	75.03	18.21	13.41	33.39
$A_{m,T}$ [%]	528	16.59	38.49	75.34	21.97	11.33	29.44
	Structural elements in small dimensions (S_S-C + S_S-NDT)						
	n_{tot}	**min**	**mean**	**max**	**5-percentiles**	**SD**	**CV [%]**
$A_{m,L}$ [%]	136	10.27	28.69	45.43	14.08	7.86	27.40
$A_{m,T}$ [%]	174	17.70	31.91	57.60	18.83	9.43	29.55

Chapter 6
Destructive tests in compression (DT)

6.1 GENERAL

The need of restoration of ancient timber structures implies a careful characterization of the material by means of mechanical standardized laboratory tests in order to reach an accurate modelling of the material for the evaluation of the conservation condition, the stress state and the residual performance capacity of existing structures.

In this context, aiming at the structural identification of timber elements, made of old chestnut wood (*Castanea sativa* Mill.), a wide experimental campaign, including non destructive (NDT) and destructive tests (DT), was performed on both full-scale, small and defects-free specimens.

In this chapter a part of the extensive laboratory activity, based on destructive tests, is presented, pointing out on the mechanical characterization of chestnut timber in compression. Destructive tests were performed taking into account the methods specified in UNI and ISO specific codes, in order to identify stiffness and strength properties of the material and evaluate the influence of defects and deteriorations in timber structural behaviour.

It is recognize that the mechanical characterization of wood by means of tests on specimens in small dimension can be inadequate to have reliable and complete information on timber behaviour of elements in actual sizes. However, a knowledge of clear material properties is essential for a basic understanding of the key problems in timber engineering.

Therefore, three different kind of specimens, with standard dimensions, were tested during the experimental campaign:

1) *Structural elements in actual dimensions*, which were king post members, recently dismantled by timber roofing trusses of an ancient masonry building of Naples. They were characterized by macroscopic defects on the lateral surface, such as knots, slope of grain and longitudinal cracks, with irregular cross-section shape;
2) *Structural elements in small dimensions*, with superficial defects and prismatic configuration;
3) *Defect-free specimens*, free from faults and irregularities, with square cross-section.

The global influence of the typical defect pattern on the mechanical performance in compression parallel to grain has been evaluated by comparing the overall behaviour of the structural elements with the same one of small and clear specimens, in terms of both mechanical properties, like modulus of elasticity and strength, and failure modes. Furthermore, the orthotropic nature of the chestnut wood has been investigated by means of compression tests on defect-free specimens in both parallel and perpendicular direction to the grain, taking into account the orientation of the annual rings with respect to the direction of the applied load. Therefore three groups of samples were tested, respectively, in longitudinal, radial and tangential direction.

In this chapter, for each test typology, the characteristics of the specimens are given, testing apparatus and set-up are illustrated and destructive tests are discussed on the basis of the observed collapse mechanisms and taking into account the effect of wood anatomy on the stress – strain relationships. Finally the experimental results are examined by means of tests statistics and compared with the mechanical properties assumed by European and Italian codes.

6.2 COMPRESSION TESTS PARALLEL TO GRAIN ON STRUCTURAL ELEMENTS IN ACTUAL DIMENSIONS

6.2.1 *Characteristics of the specimens*

Compression tests parallel to the grain were performed on fourteen structural elements in actual dimensions, so-called specimens type S_A-C, made of old chestnut wood, aiming at evaluating the modulus of elasticity, the compression strength and collapse modes, according to UNI EN 408 standard.

The following specimens features are given in Table 6.1: mean diameter (D_{mean}), mean cross-sectional area (A_{mean}), total length ($L \approx 6D_{mean}$), central gauge length ($L_1 \approx 4D_{mean}$) and wood density (ρ).

Table 6.1. Compression tests parallel to grain on specimens type S_A-C: geometric characteristics (D_{mean}, A_{mean}, L, L_1) and wood density (ρ).

Specimen type S_A-C	**D_{mean} [cm]**	**A_{mean} [cm^2]**	**L ($\approx 6D_{mean}$) [cm]**	**L_1 ($\approx 4D_{mean}$) [cm]**	**ρ [kg/m^3]**
C1-2A	15.0	167.9	89	59.3	617
C2-2B	15.0	156.8	89	59.3	618
C3-3A	14.7	154.2	88	58.7	578
C4-3B	14.5	164.8	88	58.7	542
C5-4A	15.2	170.5	90	60.0	565
C6-4B	15.3	174.2	90	60.0	530
C7-9A	15.6	173.9	95	63.3	545
C8-10B	15.4	174.0	94	62.7	550
C9-15A	15.8	173.3	95	63.3	595
C10-16A	15.6	164.8	94	62.7	642
C11-16B	15.4	165.3	94	62.7	610
C12-17A	16.2	185.7	97	64.7	554
C13-18A	15.4	167.8	95	63.3	577
C14-19A	15.0	155.2	92	61.3	582

6.2.2 *Testing equipment and set-up*

The compression tests parallel to the grain were carried out under force control using the Mohr & Federhaff AG testing machine (Fig. 6.1a). The hydraulic press is constituted by a top fixed head and a moveable loading-base plate, under which an hydraulic actuator was placed with a loading capacity of 5000 kN (Fig. 6.1a, b).

A loading cell HBM of 740 kN and displacement transducers (LVDTs) with accuracy of 1×10^{-3} were used during the tests (Fig. 6.1b). An electronic device (HBM-Spider 8), capable of measuring the load with an accuracy of 1% and the deformation with an accuracy of 0.001 mm, and a Personal Computer were setting up in order to allow data acquisition and recording by means of the software Catman (v. 6.2).

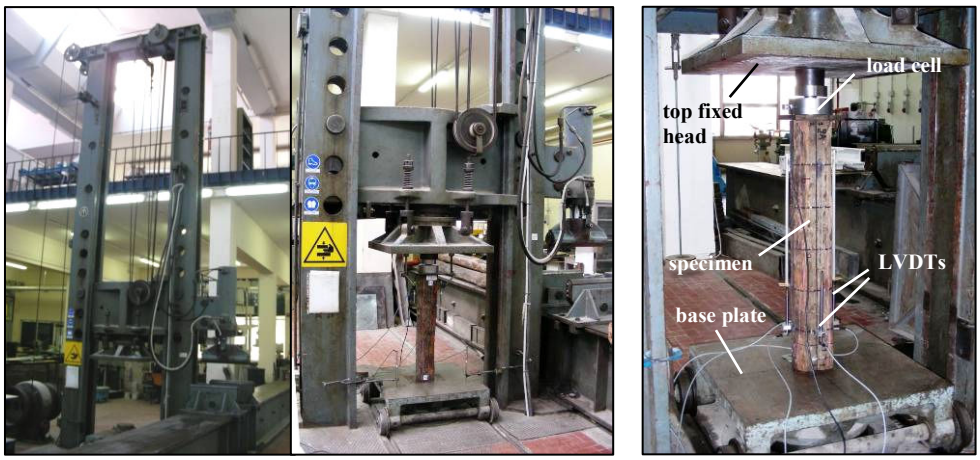

Figure 6.1. Compression tests parallel to grain on specimens type S_A-C – Testing equipment: a) Mohr & Federhaff AG machine of 5000 kN capacity; b) Specimen arrangement.

The tests were performed in two phases:

1) Elastic cycles, for the determination of the elasticity modulus;
2) Failure cycles, for the determination of the compression strength, post-elastic behaviour and collapse modes of the tested samples.

For the evaluation of the modulus of elasticity, in order to measure the relative displacements over the central gauge length (L_1), 4 LVDTs (1, 2, 3, 4) were located on the opposite faces of the specimen to avoid bending effects. Furthermore, during the failure cycles, 2 LVDTs (5, 6) were placed on the loading-base plate of the testing machine, measuring thereby the base displacements of the samples (Fig. 6.2).

6.2.3 *Elastic cycles*

For the determination of the modulus of elasticity in compression parallel to the grain, a quasi-static loading procedure was applied in three elastic cycles with load ranges (ΔF) equal to 50, 100, 150 kN for the first, second and third cycle respectively. The maximum applied force was limited within the conventional elastic value, assumed equal to 0.4 F_{max}.

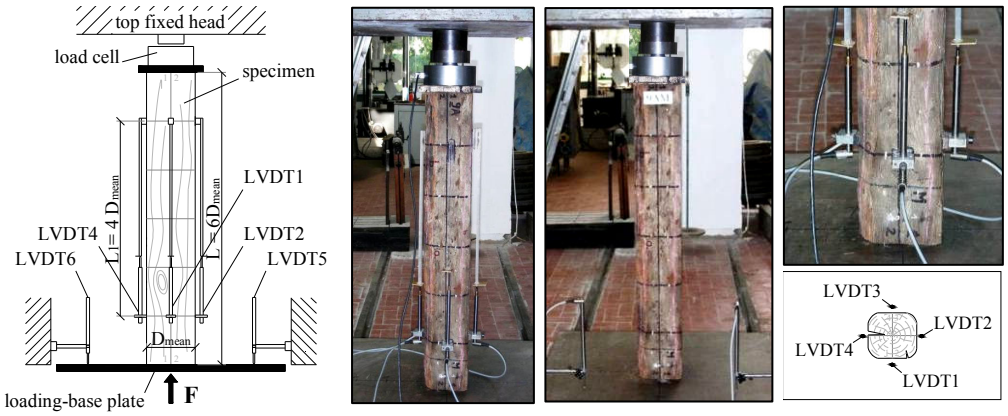

Figure 6.2. Compression tests parallel to grain on specimens type S_A-C – Test set-up: transducers (LVDTs) location.

The expected collapse load (F_{max}) has been preliminarily calculated with reference to the characteristic strength in compression ($f_{c,0,k}$), according to UNI 11035-2 standard, and considering the average value of the specimens cross-section area (A_{mean}) (Fig. 6.3).

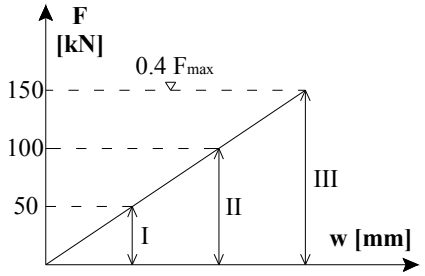

$f_{c,0,k}$ = 22 N/mm^2 (UNI 11035-2)

A_{mean} = 170 cm^2

F_{max} = 22×17000 = 374000 N = 374 kN

0.4 F_{max} = 0.4×374 = 150 kN

Figure 6.3. Compression tests parallel to grain on specimens type S_A-C – Elastic cycles: load ranges.

Considering the relative displacements (w) over the central gauge length of the specimens (average LVDT 1, 2, 3, 4) and the corresponding reaction force (F), measured by means of the load cell, the experimental results were provided in F-w curves.

In each elastic range, the modulus of elasticity ($E_{c,0}$) is calculated as follow:

$$E_{c,0} = \frac{L_1 \Delta F}{A \Delta w}$$

where ΔF is the load increment on the straight-line portion and Δw is the increment of displacement corresponding; L_1 is the specimen central gauge length; A is the cross-section area.

Given that a similar response in terms of stiffness is shown in all elastic cycles, the average value of the elasticity modulus was considered for each specimen. As example, typical F-w curves are shown in Figure 6.4, with reference to the specimen S_A-C13-18A.

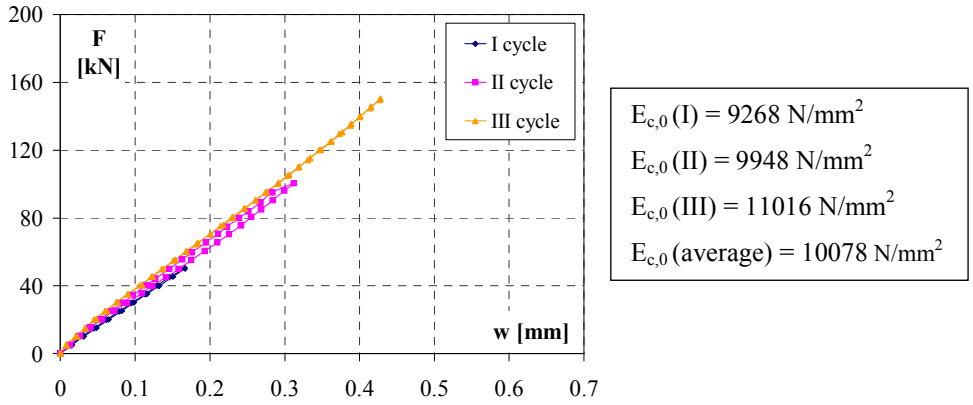

Figure 6.4. Compression tests parallel to grain on specimens type S_A-C – Elastic cycles: typical F-w curves (specimen S_A-C13-18A).

6.2.4 *Failure cycles*

Destructive tests were performed in following loading-reloading failure cycles, aiming at evaluating the maximum compression strength, the residual

bearing capacity and the collapse mechanisms of the tested structural elements. In each step, the load was increased up to the failure and applied at a constant loading-base plate speed, in such a way that the maximum force (F_{max}) is reached within 300±120 sec according to UNI EN 408.

The base displacements (w) of the sample, measured as average values of LVDT 5,6 placed on the base plate of the testing machine, and the applied forces (F) have been fitted in F-w curves for each failure cycle. Furthermore, in order to analyze the structural behaviour in post-peak field, envelope curves have been depicted too (Fig. 6.5).

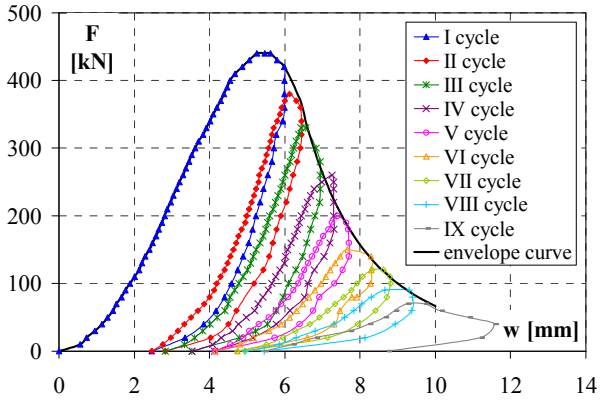

Figure 6.5. Compression tests parallel to grain on specimens type S_A-C – Failure cycles: typical F-w curves (specimen S_A-C8-10B).

With reference to the loading-line portion of the first three failure cycles, the modulus of elasticity ($E_{c,0}$) was calculated as the slope of the linear part on the F-w curves, defined by two points corresponding respectively to 10% and 40% of the maximum force, given as:

$$E_{c,0} = \frac{L(F_{40\%} - F_{10\%})}{A(w_{40\%} - w_{10\%})}$$

where L is the length of the specimen; A is the cross-section area.

The parallel compression strength ($f_{c,0}$) is taken by the maximum load (F_{max}) applied to the specimen, according to UNI EN 408, as the result of the follow equation:

$$f_{c,0} = \frac{F_{max}}{A}$$

In the following Figures 6.6 to 6.10, stress – strain relationships and envelope curve are depicted for each specimen in actual dimensions. The longitudinal compressive stress ($\sigma_{c,0}$) has been calculated with reference to the applied force and to the actual cross-section area, while the corresponding longitudinal strain ($\varepsilon_{c,0}$) has been evaluated on the total length of the sample.

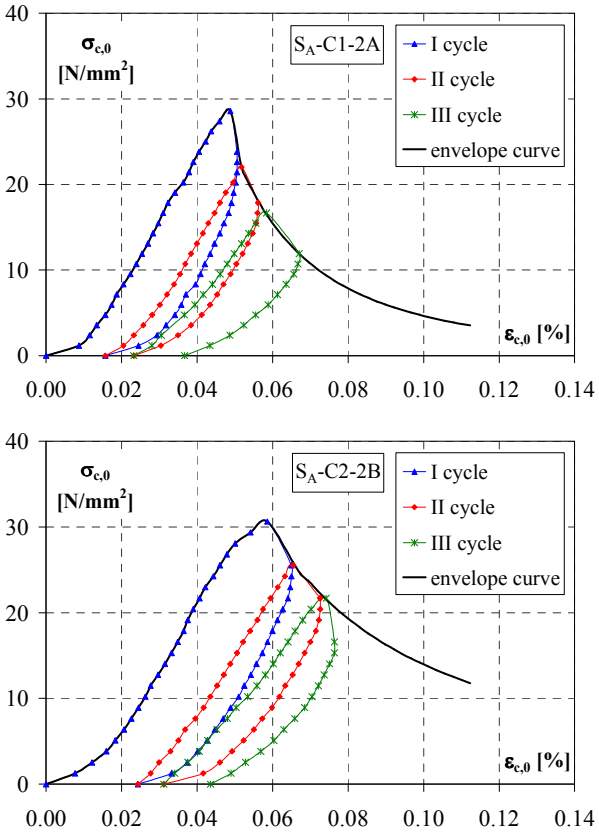

Figure 6.6. Compression tests parallel to grain on specimens type S_A-C – Failure cycles: $\sigma_{c,0}$-$\varepsilon_{c,0}$ curves (specimens S_A-C1-2A and S_A-C2-2B).

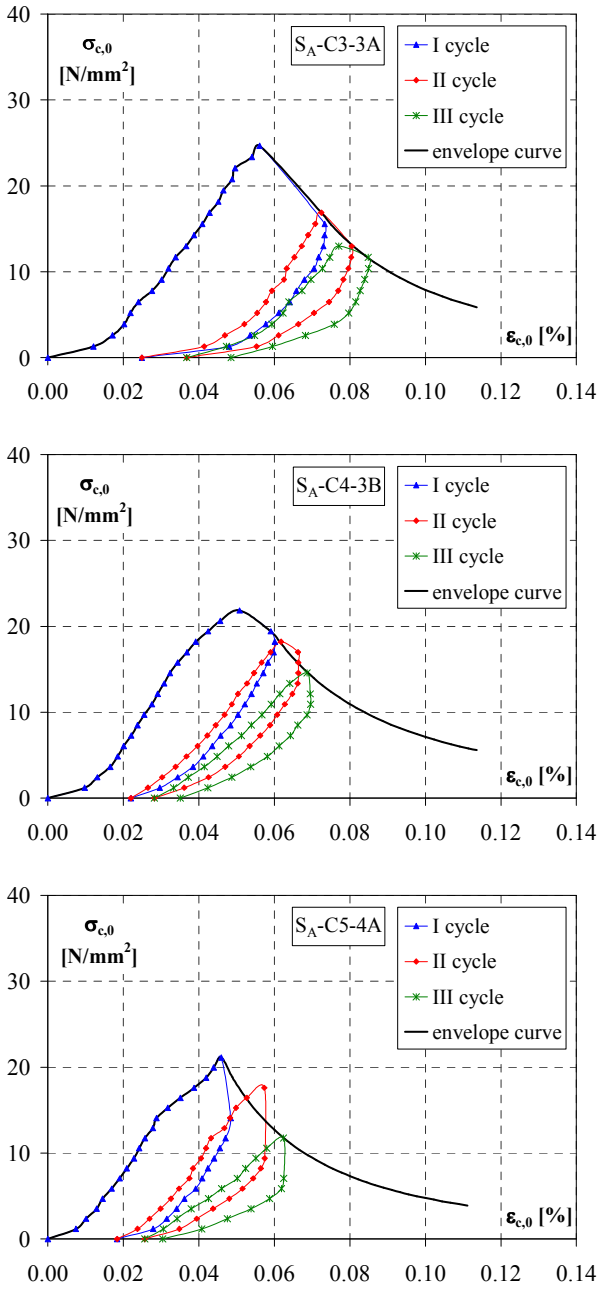

Figure 6.7. Compression tests parallel to grain on specimens type S_A-C – Failure cycles: $\sigma_{c,0}$-$\varepsilon_{c,0}$ curves (specimens S_A-C3-3A, S_A-C4-3B and S_A-C5-4A).

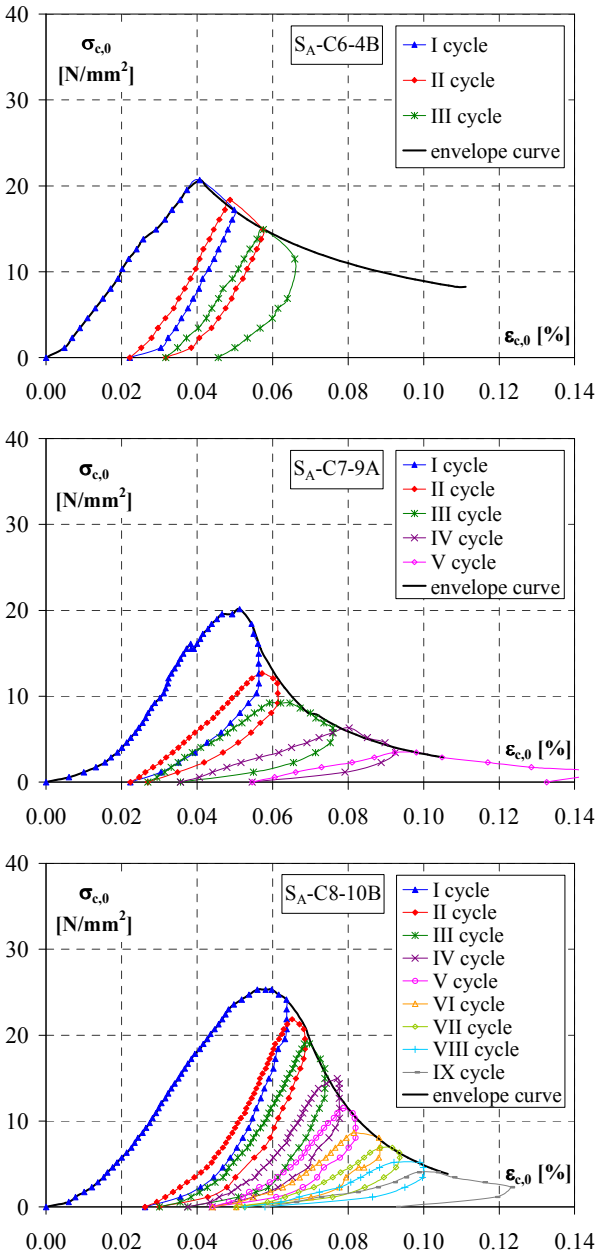

Figure 6.8. Compression tests parallel to grain on specimens type S_A-C – Failure cycles: $\sigma_{c,0}$-$\varepsilon_{c,0}$ curves (specimens S_A-C6-4B, S_A-C7-9A and S_A-C8-10B).

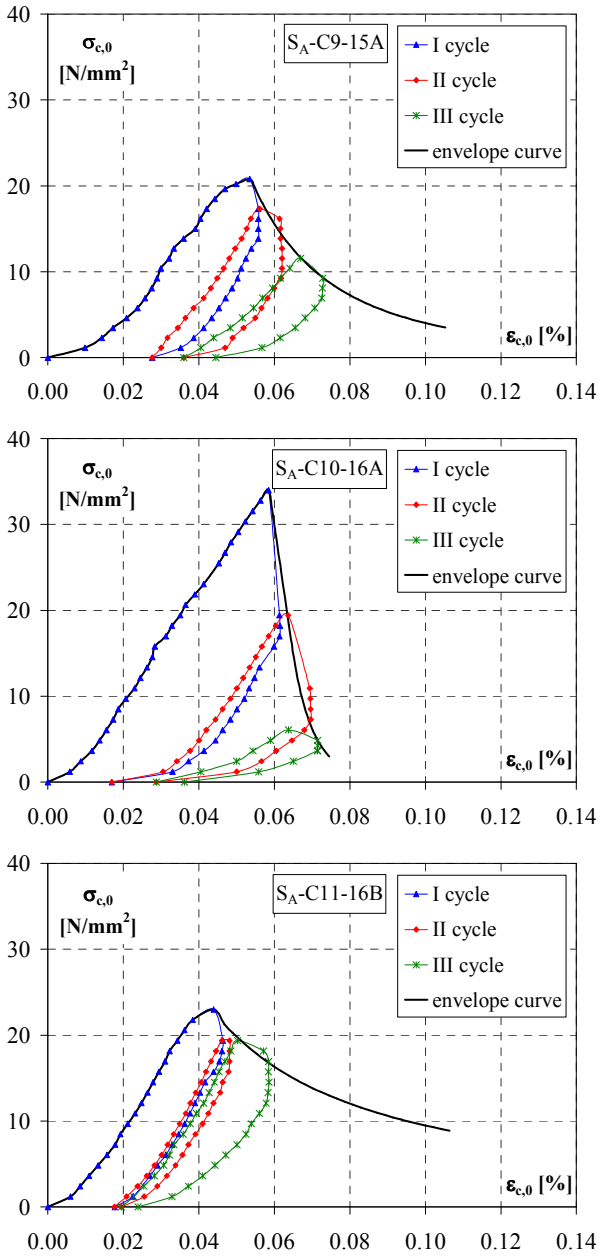

Figure 6.9. Compression tests parallel to grain on specimens type S_A-C – Failure cycles: $\sigma_{c,0}$-$\varepsilon_{c,0}$ curves (specimens S_A-C9-15A, S_A-C10-16A and S_A-C11-16B).

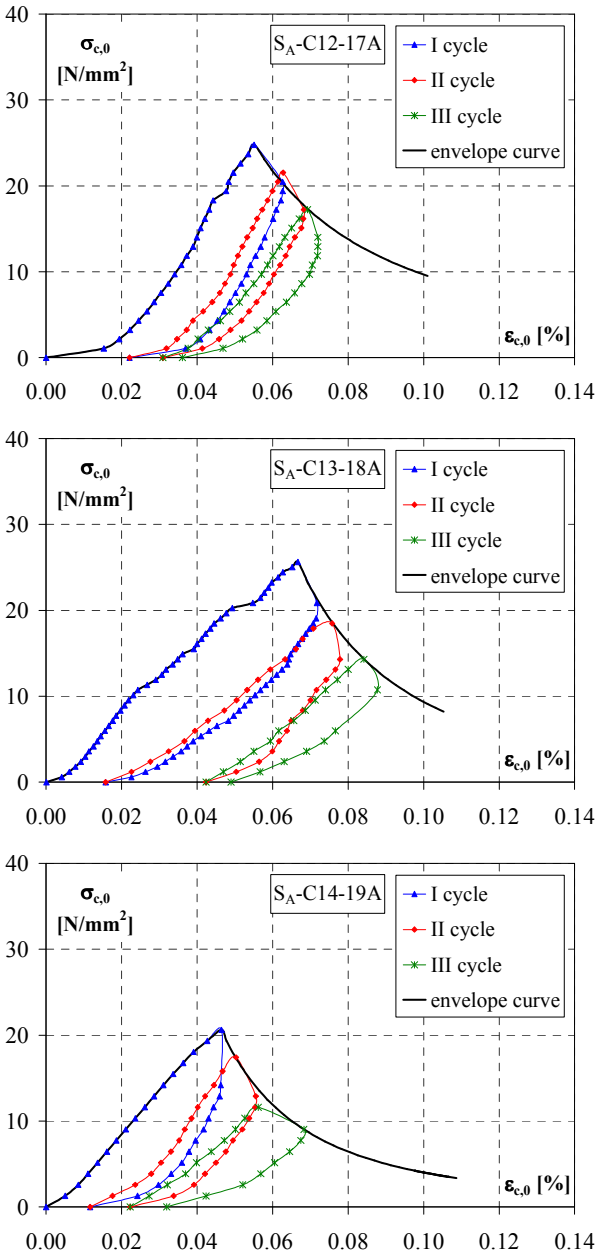

Figure 6.10. Compression tests parallel to grain on specimens type S_A-C – Failure cycles: $\sigma_{c,0}$-$\varepsilon_{c,0}$ curves (specimens S_A-C12-17A, S_A-C13-18A and S_A-C14-19A).

In Figure 6.11a all envelope curves are depicted in terms of stress-strain relationship together with the average curve. It can be observed that the global response appears more or less similar for all specimens. In fact, after an initial phase with a very low stiffness, the curves show a linear elastic branch up to the peak load reached during the test, after that they exhibit distinct non linearity, with post-peak softening branches characterized by a abrupt reduction of the stress carrying capacity. In addition, Figure 6.11b shows the comparison between the maximum, mean and minimum curves, which are assumed to characterize the compression behaviour of the tested old chestnut structural timber in compression parallel to the grain.

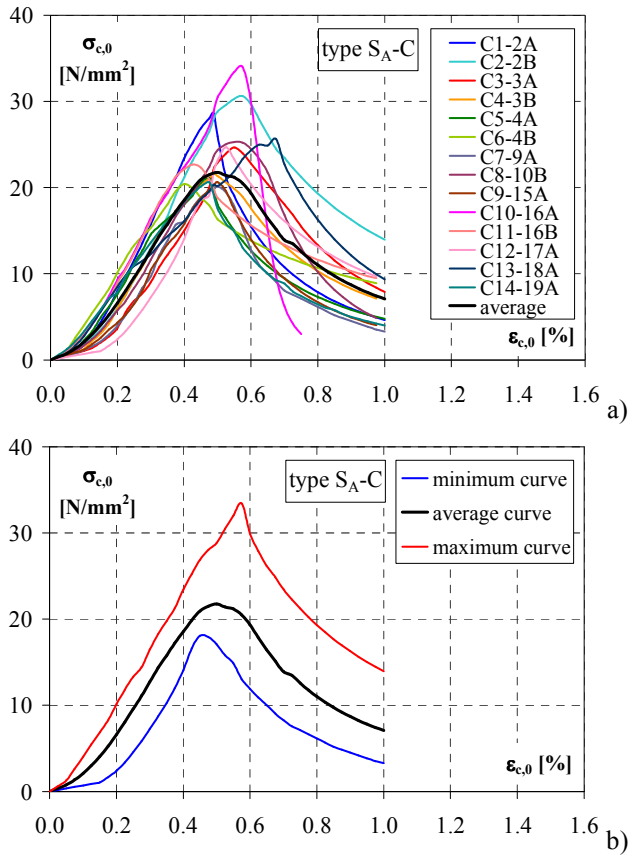

Figure 6.11. Compression tests parallel to grain on specimens type S_A-C – Failure cycles: a) $\sigma_{c,0}$-$\varepsilon_{c,0}$ envelope curves; b) Minimum, average and maximum $\sigma_{c,0}$-$\varepsilon_{c,0}$ curves.

After the destructive tests, the failure modes and the cracks location have been analyzed by a further visual inspection of the tested samples. Similar collapse mechanisms have been observed for all elements, due to the attainment of the splitting almost parallel to the grain with consequent buckling of the fibres (Fig. 6.12a), which were developed with fractures in the radial direction (Fig. 6.12b), cleavages along the annual growth rings (Fig. 6.12c) or in multi-directions (Fig. 6.12d).

The propagation of this typical failure patterns were caused by the longitudinal cracks and ring shakes previous to the tests. In some cases, local growth at the section fracture was occurred for the presence of natural defects, as knots and slope of grain (Fig. 6.12e).

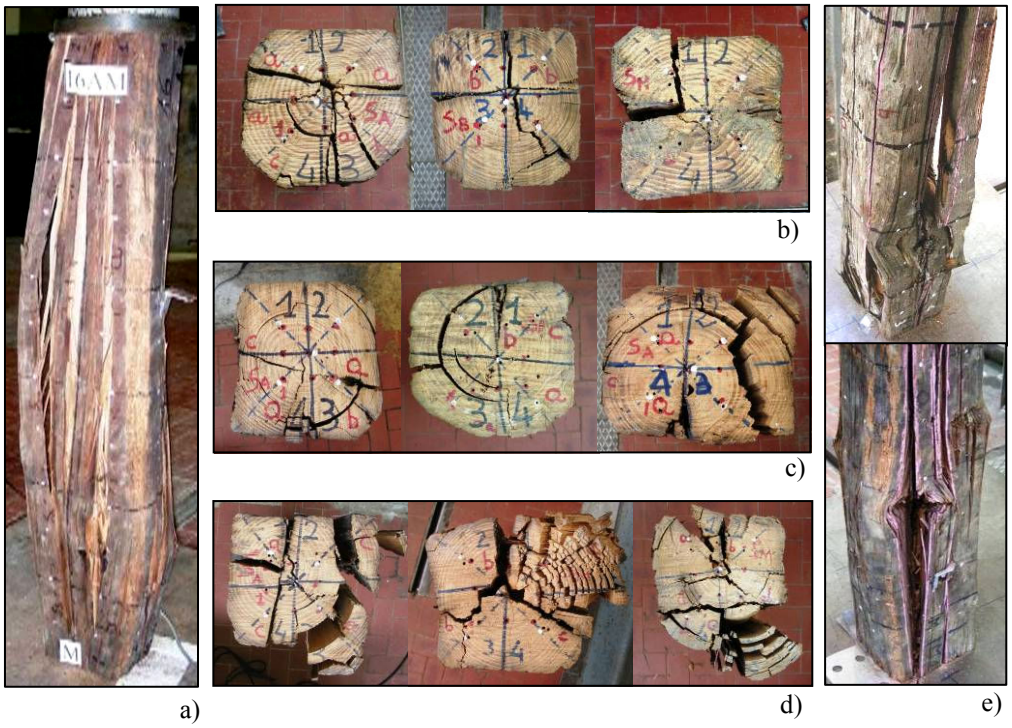

Figure 6.12. Compression tests parallel to grain on specimens type S_A-C – Typical collapse mechanisms: a) Longitudinal splitting; b) Fractures in radial direction; c) Growth rings cleavage; d) Multi-directional rupture; e) Section fracture due to the presence of knots and slope of grain.

6.2.5 *Results and discussion*

For each specimen in actual dimensions, type S_A-C, Table 6.2 provides the experimental results in terms of modulus of elasticity ($E_{c,0}$) and compression strength ($f_{c,0}$), calculated for the first three failure cycles. In addition, statistical parameters are reported for the obtained mechanical properties, including the minimum (min), average, maximum (max) and 5-percentile values, standard deviation (SD) and coefficient of variation (CV).

Table 6.2. Compression tests parallel to grain on specimens type S_A-C: experimental results [N/mm^2].

Specimen type S_A-C	**Elastic cycles**	**Failure cycles**					
		I cycle		**II cycle**		**III cycle**	
	$E_{c,0}$	$E_{c,0}$	$f_{c,0}$	$E_{c,0}$	$f_{c,0}$	$E_{c,0}$	$f_{c,0}$
C1-2A	9552	6739	28.58	5570	22.03	4163	16.67
C2-2B	8887	5830	30.62	5625	25.51	4936	21.69
C3-3A	7464	5263	24.65	3165	16.86	2581	12.97
C4-3B	7742	5694	21.84	3853	18.20	3328	14.56
C5-4A	10600	5432	21.12	4269	17.60	2930	11.73
C6-4B	10049	5637	20.66	6358	18.37	5070	14.92
C7-9A	8103	4828	20.13	3390	12.65	3046	9.20
C8-10B	11030	5335	25.29	4437	21.84	4127	18.97
C9-15A	7961	5205	20.78	5122	17.31	3132	11.54
C10-16A	9491	6646	33.97	4739	19.41	1136	6.07
C11-16B	8341	5772	22.98	6046	19.35	6045	19.35
C12-17A	6544	5122	24.77	5076	21.54	3915	17.23
C13-18A	10078	5542	25.62	3112	18.47	3243	14.30
C14-19A	9003	5099	20.62	3330	17.40	3074	11.60
min	6544	4828	20.13	3112	12.65	1136	6.07
average	8917	5582	24.40	4578	19.04	3623	14.34
max	11030	6739	33.97	6358	25.51	6045	21.69
5-percentile	6544	4828	20.13	3112	12.65	1136	6.07
SD	1292	549	4.20	1100	3.04	1214	4.24
CV [%]	14.49	9.84	17.21	24.03	15.96	33.52	29.55

It is clearly shown by the results that the values of elasticity modulus in elastic ranges, evaluated on the central gauge length of the specimens, according to standard test method (UNI EN 408), are always higher than the same ones achieved by the first failure cycle, calculated with the total length of the samples (Fig. 6.13a).

A significant variability of the mechanical properties is generally revealed by failure cycles results, as it shown in Figure 6.13b, where the CV values are reported for both modulus of elasticity and compression strength. This conclusion is in agreement with the observation of the experimental stress-strain curves, presented in Figure 6.14 for each failure cycle.

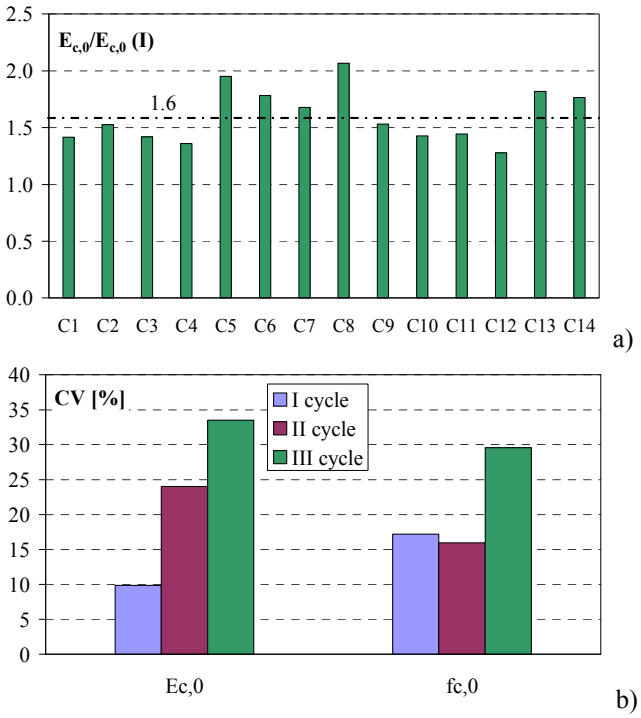

Figure 6.13. Compression tests parallel to grain on specimens type S_A-C – Experimental results: a) Ratio between elasticity moduli ($E_{c,0}$) in elastic cycles and in first failure cycle ($E_{c,0}$ I); b) Variation coefficients (CV) of the mechanical properties by failure cycles.

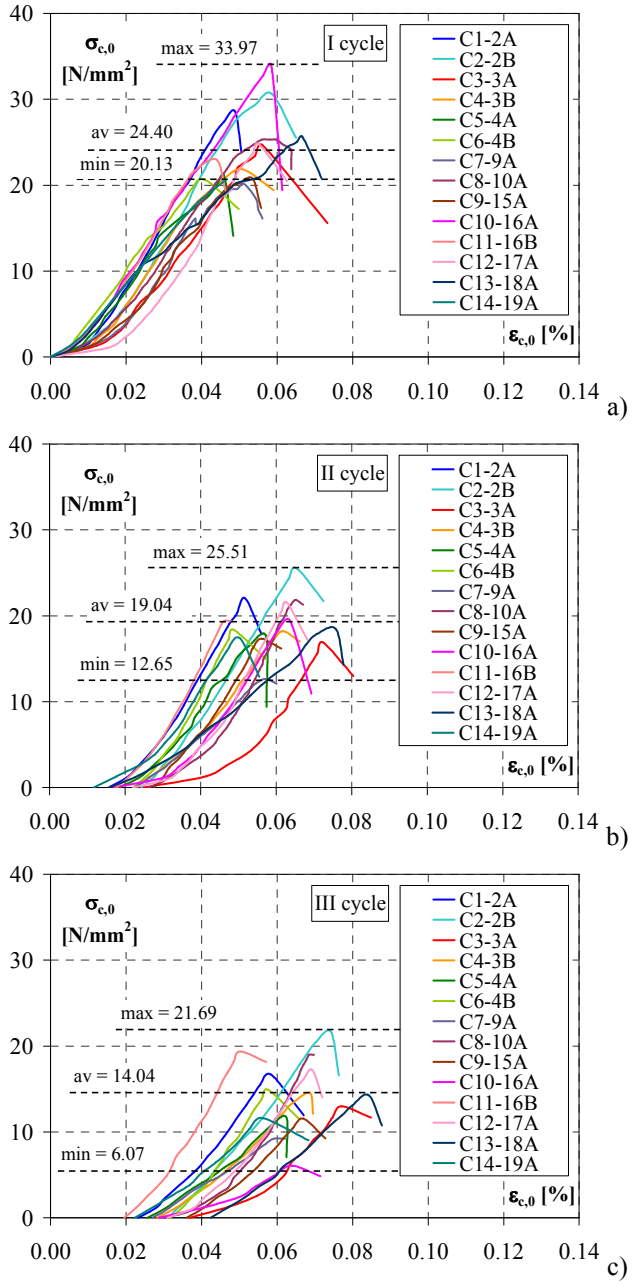

Figure 6.14. Compression tests parallel to grain on specimens type S_A-C – Experimental results – $\sigma_{c,0}$-$\varepsilon_{c,0}$ curves of failure cycles: a) I cycle; b) II cycle; c) III cycle.

With regard to the structural grading of chestnut timber, by comparing the experimental results with the values reported in Italian UNI 11035-2 (2003), it is possible to observe that:

- Good agreement is provided between the experimental 5-percentile value of compressive strength (20.13 N/mm^2) and the characteristic value assumed by the standard (22 N/mm^2);
- The main value of the modulus of elasticity ($E_{c,0}$), obtained by elastic compression cycles (≈9000 N/mm^2), is 22.2% smaller that the same one suggest by UNI 11035-2 (11000 N/mm^2).

6.3 COMPRESSION TESTS PARALLEL TO GRAIN ON STRUCTURAL ELEMENTS IN SMALL DIMENSIONS

6.3.1 *Characteristics of the specimens*

Compression tests parallel to grain were performed on twenty structural elements in small dimensions, made of old chestnut wood, so-called specimens type S_S-C. They were obtained by cutting of undivided parts of eleven specimens in actual dimensions, type S_A-C, which were previously tested in compression.

The small samples had about 5×5×30 cm^3 size (Fig. 6.15c), in accordance with the dimensional ratio between the length and the width of the specimens suggested by UNI EN 408 standard.

For each element, the main geometrical features, such as the cross-section dimensions (b×h), the length parallel to grain (L≈6b) and the density value are given in Table 6.3.

6.3.2 *Testing equipment and set-up*

The compression tests were carried out under force control by means of Mohr & Federhaff AG testing machine with 400 kN loading capacity (Fig. 6.15a). The testing apparatus was constituted of an incorporated displacement transducer and a load cell which measures the reaction force.

The small structural specimens were placed between a movable base support and an upper fixed plate, which is equipped by a spherical hinge to

guarantee an uniform distribution of the applied load on the top-end of the samples. The data acquisition and recording were carried out by means of Zwick/roell software. The test set-up arrangement is shown in Figure 6.15b.

The imposed load was applied with a constant velocity gradient, equal to about 0.50 kN/sec, so that the sample collapse was attained within 300±120 sec, according to the recommendations presented by UNI EN 408.

Table 6.3. Compression tests parallel to grain on specimens type S_S-C: geometric characteristics (b, h, L, A) and wood density (ρ).

Specimen type S_S-C	**b [mm]**	**h [mm]**	**L (6b) [mm]**	**A (b×h) [mm^2]**	**ρ [kg/m^3]**
C1-2A	50.0	50.0	300	2500	636
C2-2A	50.0	50.3	300	2515	641
C3-2B	50.5	50.0	301	2525	629
C4-3A	50.8	51.0	300	2591	534
C5-3A	50.9	50.9	300	2591	531
C6-3B	50.5	50.0	300	2525	525
C7-3B	50.0	50.0	300	2500	531
C8-4A	31.5	31.3	181	986	540
C9-4A	31.3	31.5	181	986	513
C10-4B	50.8	50.8	301	2581	536
C11-15A	51.0	50.6	301	2581	530
C12-15A	50.5	50.5	300	2550	523
C13-16A	49.2	50.0	300	2460	626
C14-16A	50.2	50.2	300	2520	622
C15-16B	50.5	50.5	301	2550	608
C16-16B	51.2	51.2	300	2621	571
C17-17A	50.5	50.5	301	2550	483
C18-17A	50.2	50.2	301	2520	502
C19-19A	50.0	49.5	300	2475	554
C20-19A	50.2	50.2	300	2520	525

a) b) c)

Figure 6.15. Compression tests parallel to grain on specimens type S_S-C – Testing equipment and set-up: a) Mohr & Federhaff AG machine of 400 kN capacity; b) Specimen arrangement; c) Specimen standard dimensions (UNI EN 408).

6.3.3 *Destructive tests*

The acquired data have been provided in terms of the applied force (F) and the corresponding displacements (w), measured by using LVDT placed in the arms of the tests machine. Therefore, the longitudinal compressive stress ($\sigma_{c,0}$), which has been determined by the applied load and the whole cross-section area of the specimen, and the longitudinal strain ($\varepsilon_{c,0}$), calculated with reference to the total length of the sample, have been fitted in $\sigma_{c,0}$-$\varepsilon_{c,0}$ relationships.

The obtained stress-strain diagrams are plotted in the following Figures 6.16 to 6.19. In each chart the average curve of the samples extracted from the same original element are also given.

It is worth noticing that, each group of specimens exhibit a similar response in terms of both stiffness and strength and behaviour before and after yielding point.

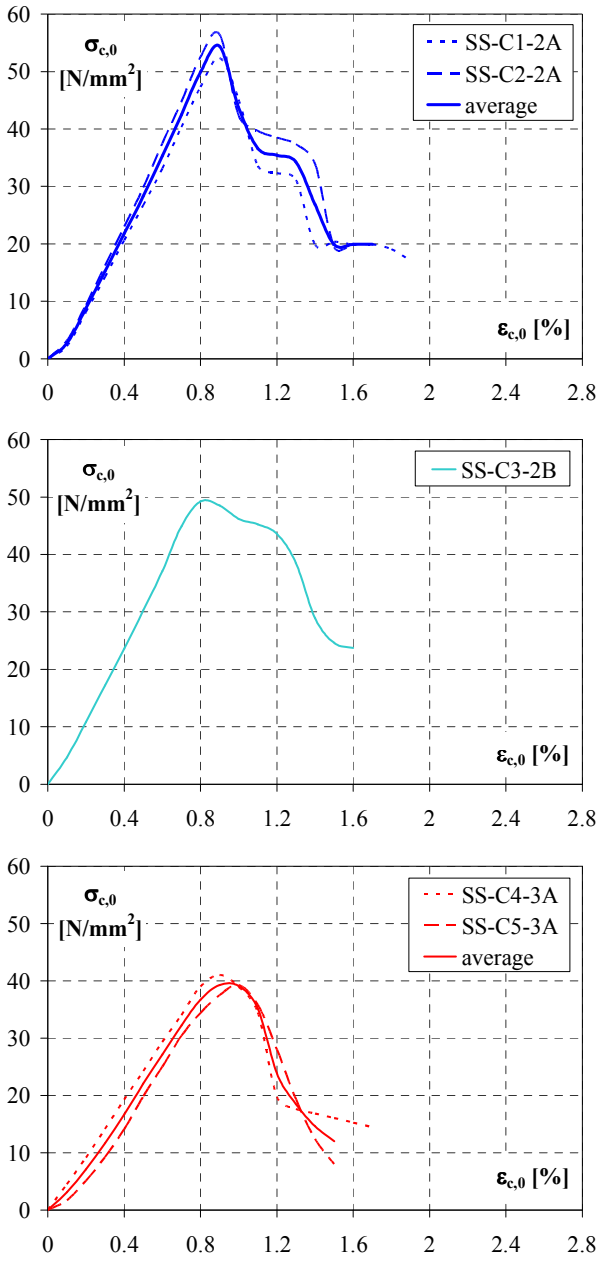

Figure 6.16. Compression tests parallel to grain on specimens type S_S-C – Destructive tests: $\sigma_{c,0}$-$\varepsilon_{c,0}$ curves (specimens extracted from 2A, 2B and 3A origin elements).

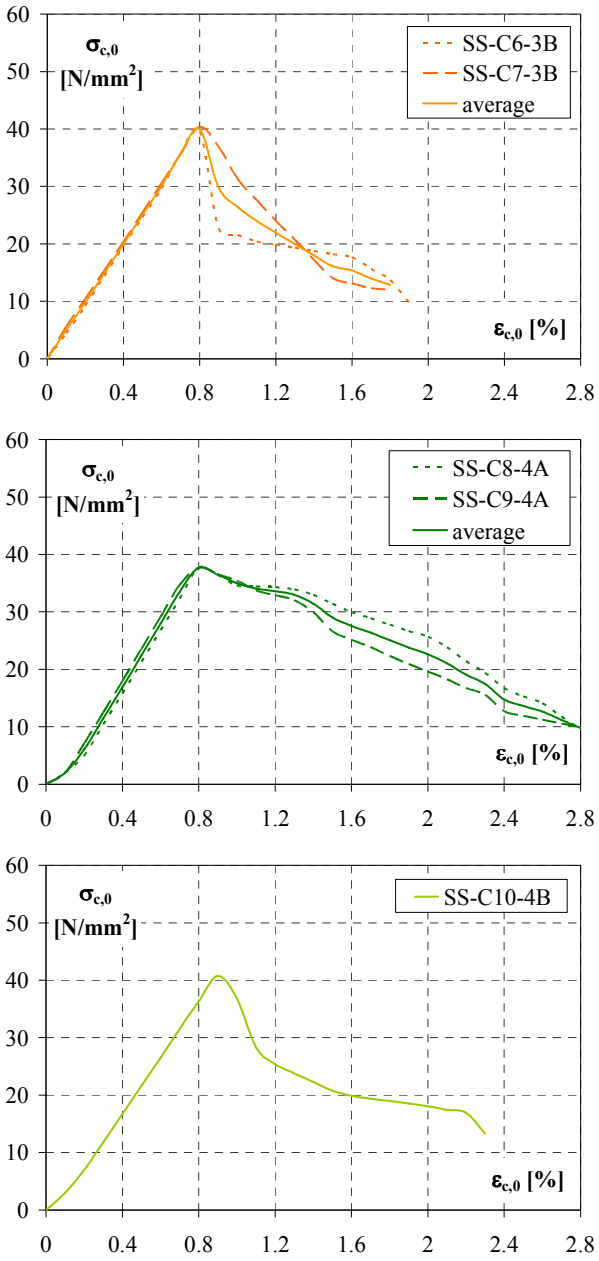

Figure 6.17. Compression tests parallel to grain on specimens type S_S-C – Destructive tests: $\sigma_{c,0}$-$\varepsilon_{c,0}$ curves (specimens extracted from 3B, 4A and 4B origin elements).

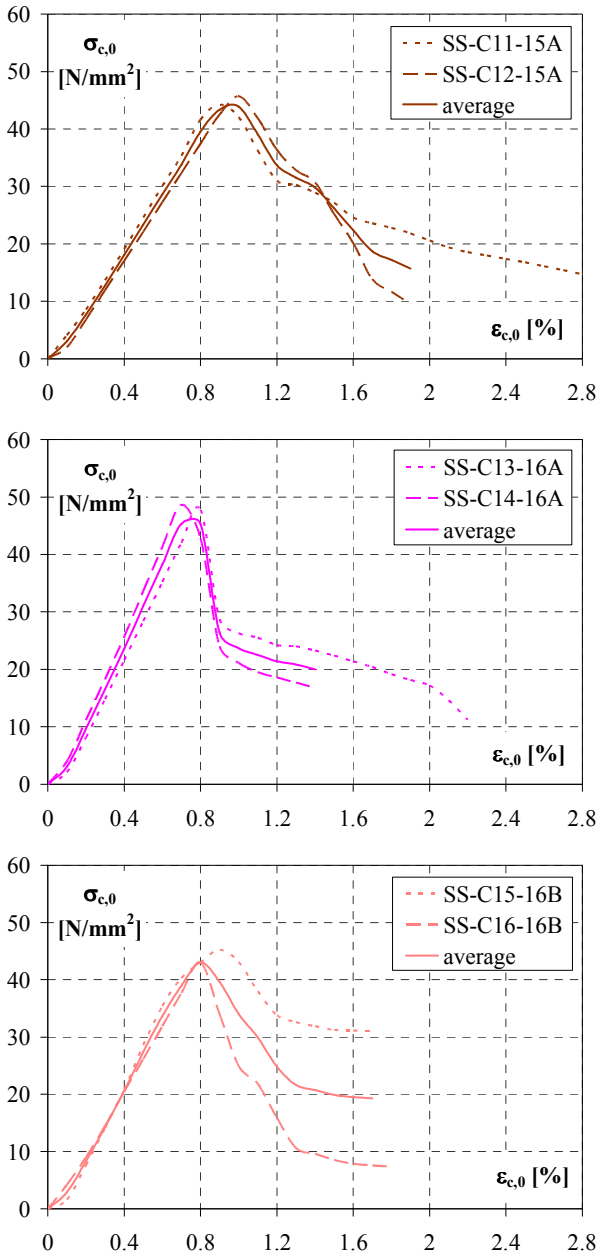

Figure 6.18. Compression tests parallel to grain on specimens type S_S-C – Destructive tests: $\sigma_{c,0}$-$\varepsilon_{c,0}$ curves (specimens extracted from 15A, 16A and 16B origin elements).

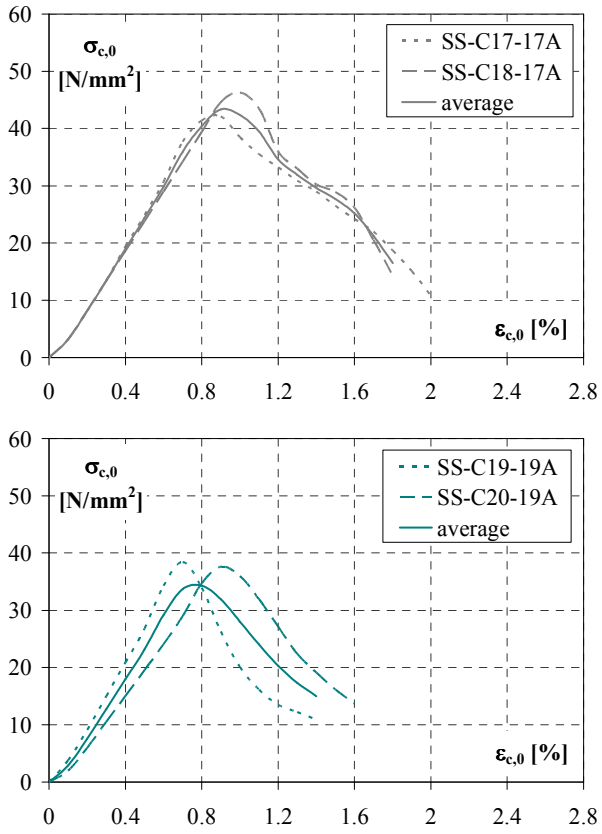

Figure 6.19. Compression tests parallel to grain on specimens type S_S-C – Destructive tests: $\sigma_{c,0}$-$\varepsilon_{c,0}$ curves (specimens extracted from 17A and 19A origin elements).

Figure 6.20a illustrates the stress-strain average curves of each group of structural specimens in small dimensions, whereas in Figure 6.20b the obtained minimum, average and maximum diagrams are depicted too. As it appears, the material shows a linear elastic branch until ultimate load, after which a drastic strength reduction is manifested beyond a strain level of about 0.8-0.9 %.

The failure was often caused by longitudinal splitting phenomena, consisting in the separation of the fibres once the limit tensile tension perpendicular to grain has been reached. These fractures usually occurred in specimens having macroscopic fissures prior to test (Fig. 6.21a).

The so-called “wedge split” mechanism was developed in some element, when the direction of the split, whether radial or tangential, has been observed (Fig. 6.21b). In any case, the slipping phenomena has been anticipated by microbuckling of the fibres, which appeared on the specimen surfaces by means of local plasticization shear bands, characterized by plan rupture making an angle of about 45° with the top of the sample (Fig. 6.21c).

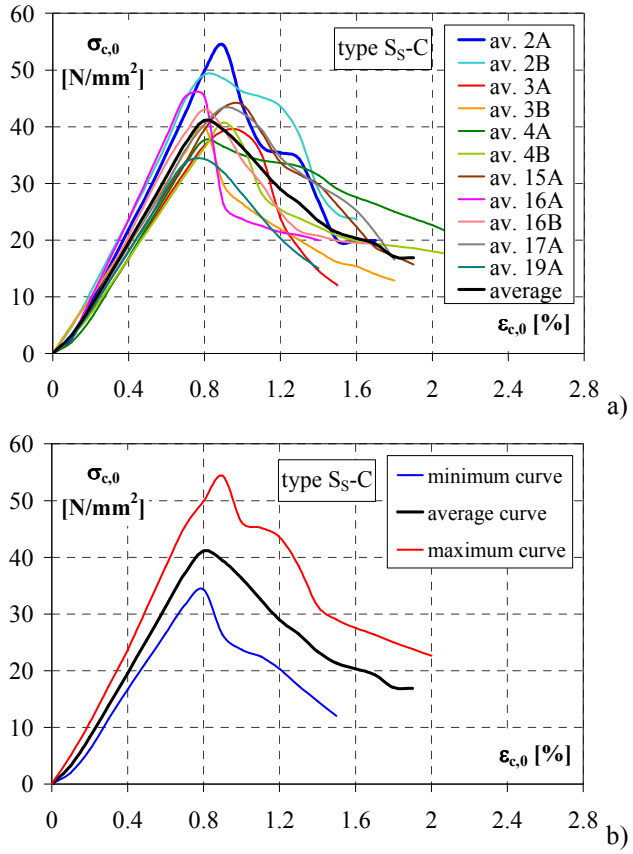

Figure 6.20. Compression tests parallel to grain on specimens type S_S-C –Destructive tests: a) $\sigma_{c,0}$-$\varepsilon_{c,0}$ average curves; b) Minimum, average and maximum $\sigma_{c,0}$-$\varepsilon_{c,0}$ curves.


a)

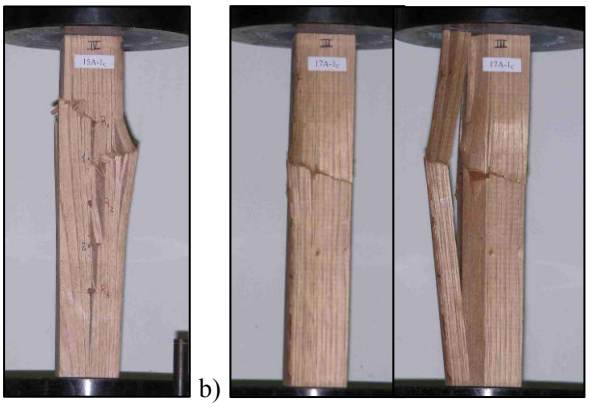
b) c)

Figure 6.21. Compression tests parallel to grain on specimens type S_S-C – Typical collapse mechanisms: a) Propagation of longitudinal splitting; b) Wedge split; c) Shearing and splitting.

6.3.4 *Results and discussion*

The experimental results of the destructive tests on structural elements in small dimensions (specimens type S_S-C) are presented in Table 6.4 in terms of both modulus of elasticity ($E_{c,0}$) and compression strength parallel to grain ($f_{c,0}$), summarizing the test statistics too.

The modulus of elasticity has been evaluated as the slope of the linear portion on the stress-strain relationship, defined by the points ($\sigma_{10\%}$; $\varepsilon_{10\%}$) and ($\sigma_{40\%}$; $\varepsilon_{40\%}$) corresponding respectively to 10% and 40% of the conventional stress, as follow:

$$E_{c,0} = \frac{\sigma_{40\%} - \sigma_{10\%}}{\varepsilon_{40\%} - \varepsilon_{10\%}}$$

The conventional stress ($f_{c,0}$) is obtained by the ratio between the maximum reached force during the test (F_{max}) and the whole cross-sectional area (A) of the specimen, according to UNI EN 408 standard.

The results are also presented for each group of samples belonging to the same original element.

Table 6.4. Compression tests parallel to grain on specimens type S_S-C: experimental results.

Specimen type S_S-C	**$E_{c,0}$ [N/mm^2]**	**$f_{c,0}$ [N/mm^2]**	**Origin element**	**$E_{c,0}$ [N/mm^2]**	**$f_{c,0}$ [N/mm^2]**
C1-2A	6258	52.58	2A	6511	54.52
C2-2A	6765	56.46			
C3-2B	6466	50.11	2B	6466	50.11
C4-3A	4926	41.07	3A	4811	40.15
C5-3A	4696	39.24			
C6-3B	5029	40.09	3B	5083	41.13
C7-3B	5137	42.18			
C8-4A	5536	37.94	4A	5553	37.80
C9-4A	5570	37.66			
C10-4B	4989	40.74	4B	4989	40.74
C11-15A	5431	44.32	15A	5265	45.19
C12-15A	5100	46.07			
C13-16A	6769	49.40	16A	7063	49.22
C14-16A	7358	49.04			
C15-16B	6774	45.22	16B	6328	44.15
C16-16B	5883	43.08			
C17-17A	5726	42.10	17A	5511	44.17
C18-17A	5296	46.25			
C19-19A	5929	38.41	19A	5272	38.73
C20-19A	4615	39.04			
min	4615	37.66			
average	5713	44.05			
max	7358	56.46			
5-percentile	4619	37.67			
SD	790	5.28			
CV [%]	13.83	11.98			

It is clearly show that the compression behaviour of chestnut timber in small sizes is quite homogeneous, as the pleasant coefficients of variation (CV) confirm, equal to 13.83 % for the modulus of elasticity and 11.98 % for the strength. Furthermore, it is important to observe that the experimental 5-percentile value of $f_{c,0}$, equal to about 38 N/mm^2, is 73% higher than the characteristic value assumed by UNI 11035-2 Italian standard, equal to 22 N/mm^2.

6.4 COMPRESSION TESTS ON DEFECT-FREE SPECIMENS

6.4.1 *Characteristics of the specimens*

Clear specimens in old chestnut wood, free from faults, with dimension of b×h×L equal to 20×20×40 mm^3 were used for compression tests, with the longitudinal axis being oriented along the grain direction (Fig. 6.22b).

The orthotropic behaviour has been analyzed taking into account the orientation of the annual growth rings with respect to the direction of the applied force (Fig. 6.22c). Therefore seventy-seven elements have been divided in three groups: 1) thirty-three for compression tests parallel to the grain, type DF-C_L; 2) twenty-two for perpendicular tests in radial direction, type DF-C_{rad}; 3) twenty-two for perpendicular tests in tangential direction, type DF-C_{tg}.

Tables 6.5, 6.6 and 6.7 provide the geometrical and physical features of the specimens, belonging to the first, second and third group, respectively.

Table 6.5. Compression tests parallel to grain on specimens type DF-C_L: geometric characteristics (b, h, L, A) and wood density (ρ).

Specimen type DF-C_L	**b [mm]**	**h [mm]**	**L [mm]**	**A (b×h) [mm^2]**	**ρ [kg/m^3]**
DF-C_L1-2A	20.3	20.7	41.0	420.2	604
DF-C_L2-2A	20.5	20.5	40.9	420.3	617
DF-C_L3-2A	20.5	20.8	41.0	426.4	612
DF-C_L4-2B	21.0	20.8	40.8	436.8	623
DF-C_L5-2B	21.0	20.7	40.8	434.7	648
DF-C_L6-2B	20.9	21.0	40.9	438.9	663
DF-C_L7-3A	20.0	21.0	41.0	420.0	546
DF-C_L8-3A	20.3	21.3	40.9	432.4	548
DF-C_L9-3A	20.9	21.2	40.9	443.1	563
DF-C_L10-3B	20.7	20.5	40.8	424.4	514
DF-C_L11-3B	20.3	20.5	40.8	416.2	501
DF-C_L12-3B	20.8	20.1	40.8	418.1	528
DF-C_L13-4A	20.5	20.8	40.0	426.4	528
DF-C_L14-4A	20.8	20.8	40.2	432.6	540
DF-C_L15-4A	20.6	20.6	40.3	424.4	526
DF-C_L16-4B	20.8	20.8	40.9	432.6	526
DF-C_L17-4B	20.7	20.8	40.8	430.6	535
DF-C_L18-4B	20.5	21.2	40.8	434.6	491
DF-C_L19-15A	21.2	21.2	40.9	449.4	539
DF-C_L20-15A	21.2	21.2	40.8	449.4	551
DF-C_L21-15A	21.2	21.0	40.8	445.2	545
DF-C_L22-16A	20.6	20.8	40.2	428.5	656
DF-C_L23-16A	20.7	21.0	40.2	434.7	664
DF-C_L24-16A	20.6	20.8	40.2	428.5	673
DF-C_L25-16B	20.7	21.2	40.8	438.8	614
DF-C_L26-16B	21.2	20.9	40.8	443.1	653
DF-C_L27-16B	21.0	20.8	41.0	436.8	720
DF-C_L28-17A	21.2	20.8	40.8	441.0	434
DF-C_L29-17A	20.8	20.8	40.8	432.6	448
DF-C_L30-17A	20.6	21.2	40.8	436.7	421
DF-C_L31-19A	20.0	21.5	40.8	430.0	479
DF-C_L32-19A	21.0	21.0	40.8	441.0	545
DF-C_L33-19A	20.4	21.3	40.8	434.5	536

Table 6.6. Compression tests perpendicular to grain on specimens type DF-C_{rad}: geometric characteristics (b, h, L, A), and wood density (ρ).

Specimen type DF-C_{rad}	**b [mm]**	**h [mm]**	**L [mm]**	**A (L×h) [mm^2]**	**ρ [kg/m^3]**
DF-C_{rad}1-2A	20.5	20.3	41.0	832	627
DF-C_{rad}2-2A	20.4	20.2	40.8	824	619
DF-C_{rad}3-2B	21.0	21.0	40.9	859	626
DF-C_{rad}4-2B	21.0	20.9	40.9	855	624
DF-C_{rad}5-3A	21.5	21.4	40.9	875	526
DF-C_{rad}6-3A	21.5	21.1	40.8	861	556
DF-C_{rad}7-3B	20.5	20.6	40.8	840	482
DF-C_{rad}8-3B	20.3	20.5	40.8	836	489
DF-C_{rad}9-4A	20.4	20.5	40.7	834	511
DF-C_{rad}10-4A	20.2	20.2	40.7	822	530
DF-C_{rad}11-4B	20.5	20.9	40.8	853	498
DF-C_{rad}12-4B	20.5	20.7	40.8	845	485
DF-C_{rad}13-15A	21.2	21.0	40.8	857	540
DF-C_{rad}14-15A	21.2	21.2	40.8	865	545
DF-C_{rad}15-16A	20.0	20.6	40.2	828	525
DF-C_{rad}16-16A	20.5	20.5	40.4	828	545
DF-C_{rad}17-16B	20.9	21.0	40.8	857	637
DF-C_{rad}18-16B	20.8	21.3	40.7	867	638
DF-C_{rad}19-17A	20.6	21.2	40.8	865	432
DF-C_{rad}20-17A	20.8	21.0	40.8	857	432
DF-C_{rad}21-19A	20.9	21.2	40.8	865	526
DF-C_{rad}22-19A	21.5	21.0	40.8	857	548

Table 6.7. Compression tests perpendicular to grain on specimens type DF-C_{tg}: geometric characteristics (b, h, L, A) and wood density (ρ).

Specimen type DF-C_{tg}	b [mm]	h [mm]	L [mm]	A (L×b) [mm^2]	ρ [kg/m^3]
DF-C_{tg}1-2A	20.2	20.2	40.8	824	655
DF-C_{tg}2-2A	20.2	20.2	40.5	818	629
DF-C_{tg}3-2B	20.5	20.9	40.9	838	662
DF-C_{tg}4-2B	20.4	21.0	40.9	834	656
DF-C_{tg}5-3A	20.8	29.8	40.7	847	396
DF-C_{tg}6-3A	20.9	20.5	40.3	842	553
DF-C_{tg}7-3B	20.5	20.8	40.8	836	489
DF-C_{tg}8-3B	20.3	19.8	40.7	826	520
DF-C_{tg}9-4A	20.3	20.8	40.7	826	512
DF-C_{tg}10-4A	20.3	20.8	40.7	826	518
DF-C_{tg}11-4B	20.6	20.7	40.8	840	506
DF-C_{tg}12-4B	20.6	21.2	40.9	843	493
DF-C_{tg}13-15A	21.3	21.0	40.8	869	548
DF-C_{tg}14-15A	21.3	21.2	40.8	869	548
DF-C_{tg}15-16A	20.8	20.3	40.8	849	668
DF-C_{tg}16-16A	20.8	20.3	40.8	849	662
DF-C_{tg}17-16B	20.7	21.2	40.8	845	614
DF-C_{tg}18-16B	21.0	21.0	40.9	859	615
DF-C_{tg}19-17A	20.8	21.0	40.8	849	415
DF-C_{tg}20-17A	20.8	21.0	40.8	849	415
DF-C_{tg}21-19A	19.4	21.2	40.8	792	507
DF-C_{tg}22-19A	20.2	21.2	40.8	824	498

6.4.2 *Testing equipment and set-up*

The tests were conducted with a mechanical tests universal machine Mohr & Federhaff AG of 400 kN capacity, under force control (Fig. 6.22a), taking into account the methods specified in UNI ISO Italian codes, 3787 and 3132 for compression tests parallel and perpendicular to grain respectively (Fig. 6.22 c). The machine is equipped by a upper spherical bearing platen to improve the alignment of the specimens and promote uniform stress distribution on cross-section surfaces. The measurements of the deformations were done by a displacement transducer placed in the arms of the tests machine and the data were acquired by means of software Zwick/roell. Specimens have been took until collapse in order to evaluate stiffness and

strength properties of the clear material, together with post-elastic behaviour and failure modes.

The load was applied at a constant loading-head movement so adjusted that in longitudinal compression the maximum force was reached between 90 and 120 sec. (about 0.4 kN/sec), while, in compression perpendicular to the grain, the proportional limit was obtained within 90±30 sec (about 0.25 kN/sec).

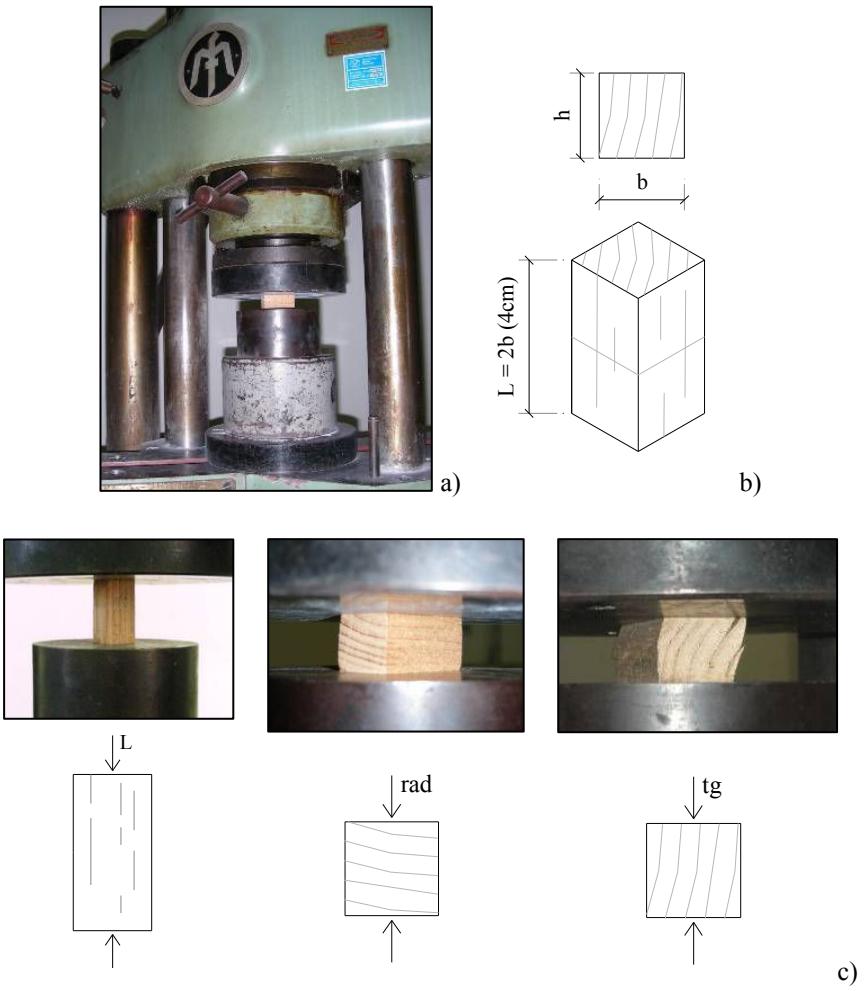

Figure 6.22. Compression tests parallel to grain on specimens type DF-C – Testing equipment and set-up: a) Mohr & Federhaff AG machine of 400 kN capacity; b) Specimen standard dimensions (UNI ISO 3787 and 3132); c) Test arrangement taking into account the orientation of the annual growth rings with respect to the direction of the applied load.

6.4.3 *Destructive tests parallel to grain*

For the thirty-three clear specimens type DF-C_L, tested in compression along the grain, in the following Figures 6.23 to 6.26 the obtained stress–strain curves are depicted. For each group of three samples, which were extracted by the same structural element, the average curve is plotted as well.

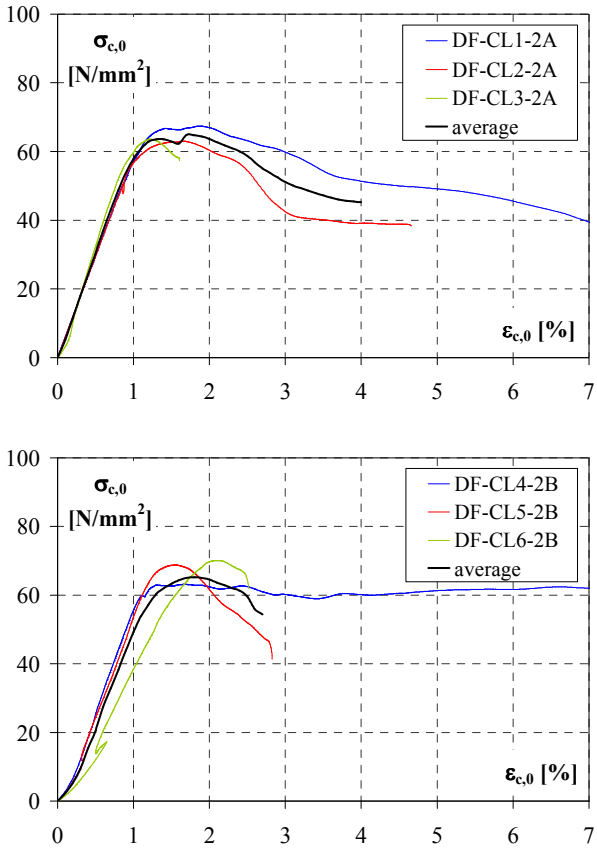

Figure 6.23. Compression tests parallel to grain on specimens type DF-C_L – Destructive tests: $\sigma_{c,0}$-$\varepsilon_{c,0}$ curves (specimens extracted from 2A and 2B origin elements).

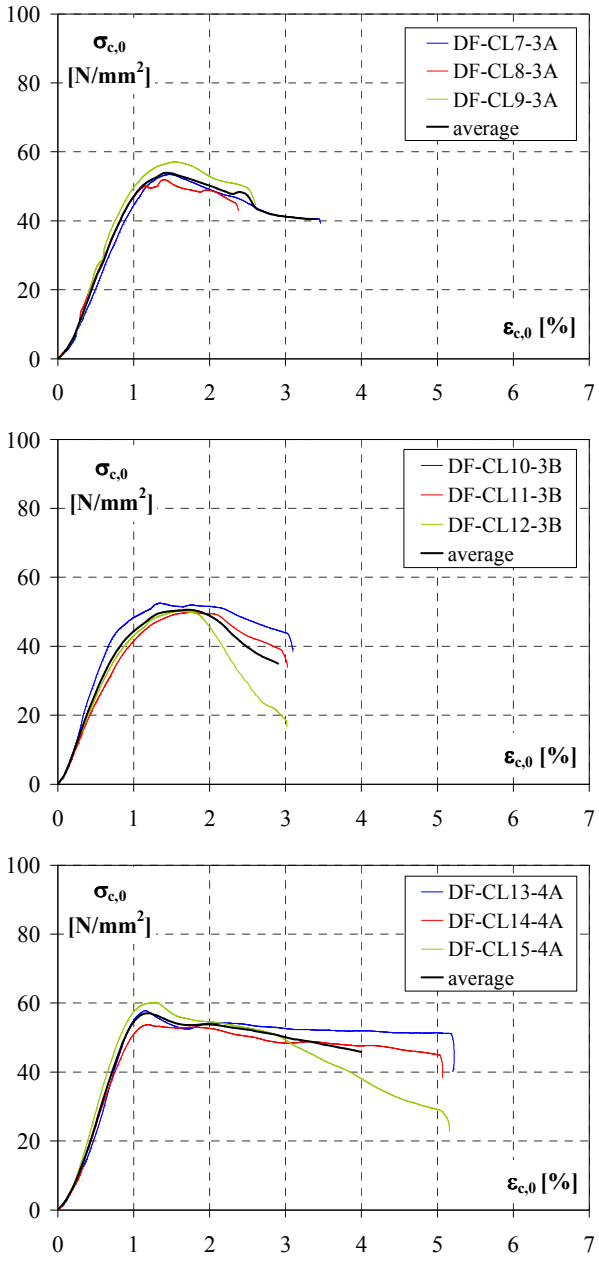

Figure 6.24. Compression tests parallel to grain on specimens type DF-C_L – Destructive tests: $\sigma_{c,0}$-$\varepsilon_{c,0}$ curves (specimens extracted from 3A, 3B and 4A origin elements).

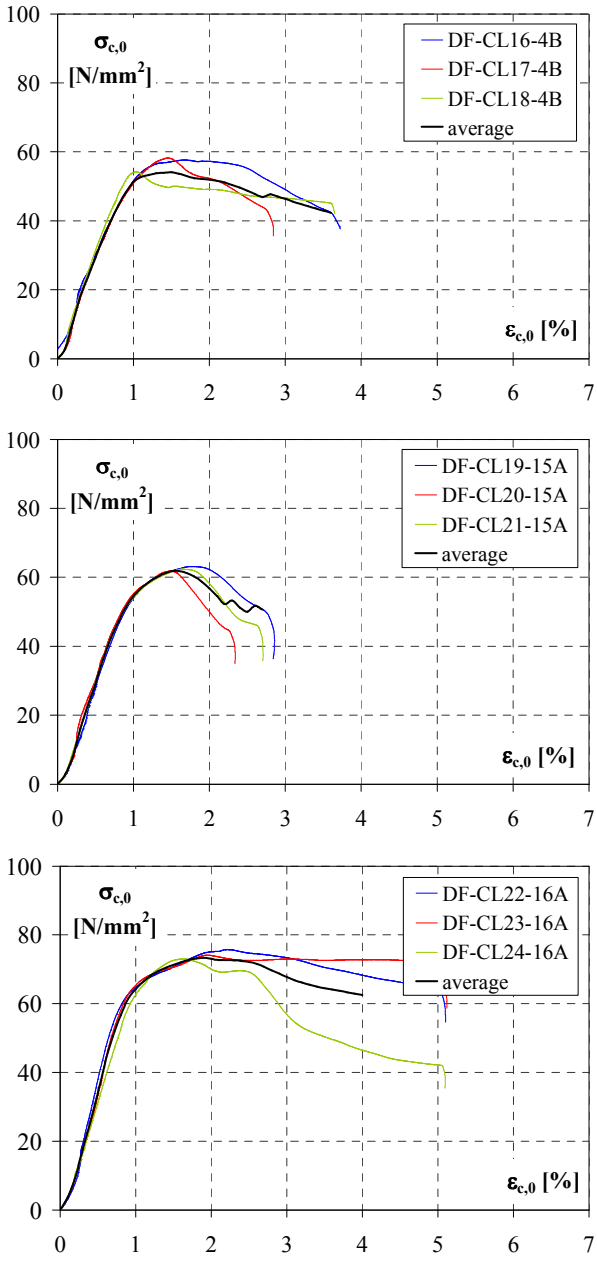

Figure 6.25. Compression tests parallel to grain on specimens type DF-C_L – Destructive tests: $\sigma_{c,0}$-$\varepsilon_{c,0}$ curves (specimens extracted from 4B, 15A and 16A origin elements).

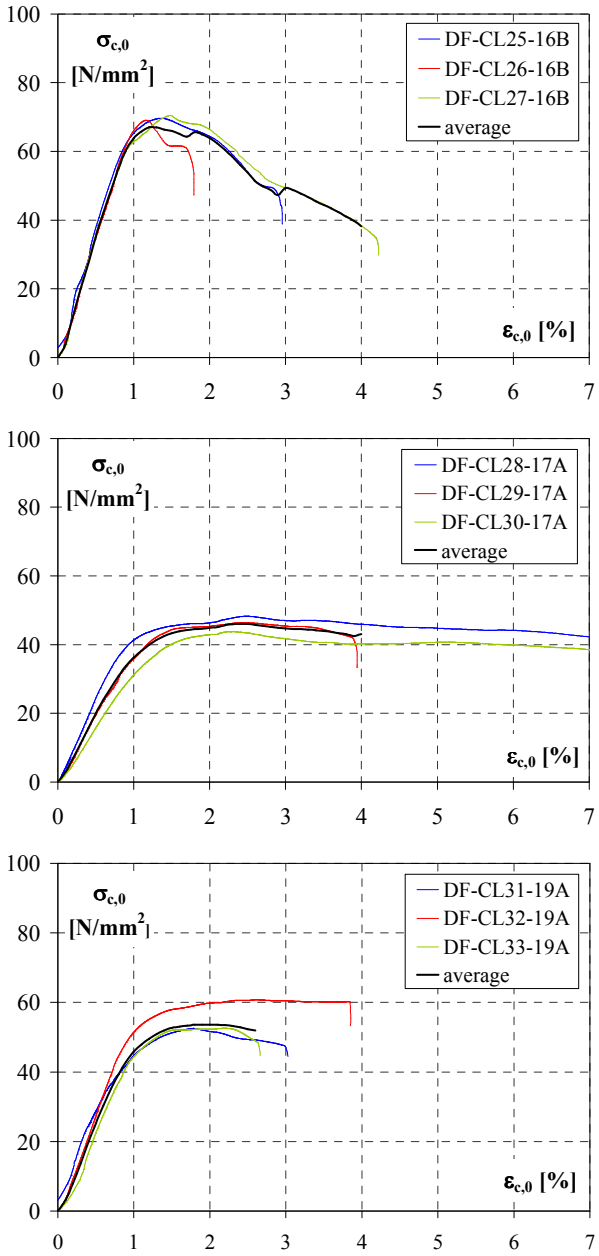

Figure 6.26. Compression tests parallel to grain on specimens type DF-C_L – Destructive tests: $\sigma_{c,0}$-$\varepsilon_{c,0}$ curves (specimens extracted from 16B, 17A and 19A origin elements).

In Figure 6.27a all average $\sigma_{c,0}$-$\varepsilon_{c,0}$ diagrams are reported, whereas in Figure 6.27b both minimum, average and maximum curves are plotted, which are assumed to characterize the mechanical behaviour in compression parallel to the grain of the base material made of old chestnut wood.

As can be seen, the limit of proportionality generally occurred at a considerable higher stress level (≅ 75%) to which a longitudinal strain of about 0.9 % corresponds. Beyond the linear range, the stress-strain diagrams exhibit non-linear response characterized by a moderate ductility behaviour. Moreover, at high level of deformations, beyond 2.0 %, a stress capacity reduction is manifested.

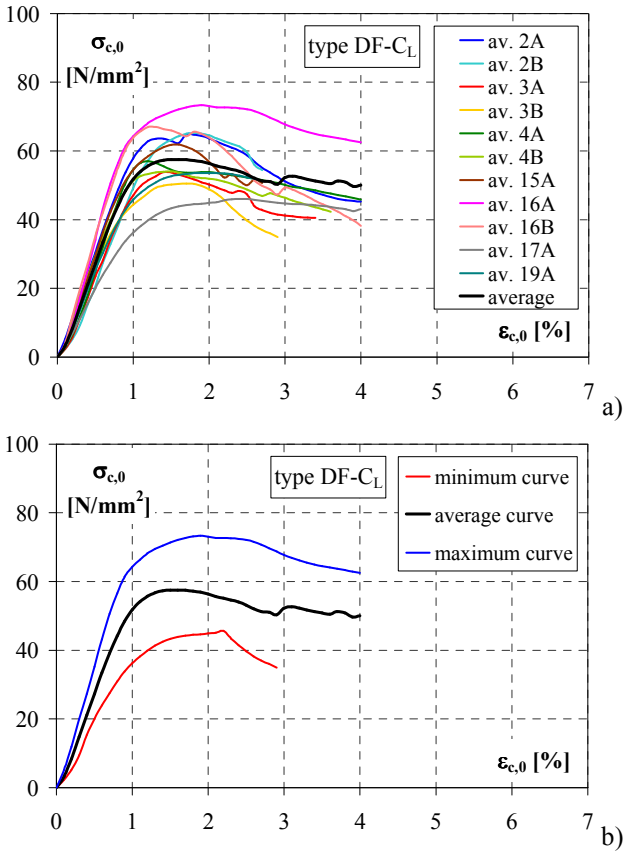

Figure 6.27. Compression tests parallel to grain on specimens type DF-C_L –Destructive tests: a) $\sigma_{c,0}$-$\varepsilon_{c,0}$ average curves; b) Minimum, average and maximum $\sigma_{c,0}$-$\varepsilon_{c,0}$ curves.

During the tests it was observed that the compression failure along the grain direction was a progressive process, usually deemed to be a result of shear stresses, so-called shearing mode. In fact, for most of the specimens, beyond the maximum stress ($f_{c,0}$) and at longitudinal strain of about 2%, structural changes began with the formation of one or two principal gross shear bands, which consisted in fracture cleavage approximately perpendicular to the longitudinal axis on the radial plane and obliquely on the tangential plane with an angle between 45° and 70° with respect to the grain orientation (Fig. 6.28).

This is in agreement with that observed by Gong and Smith (2000). What determines the angle of inclination of a single gross shear band has not been clearly elucidated. It is known that for brittle materials the fractured surface, produced by normal stresses, is normal to the longitudinal axis. For ductile materials the fractured surface has an angle of ≈ 45° to the longitudinal axis (Bodig and Jayne, 1993). Because clear wood is a natural fibre reinforced composite exhibiting moderate ductility under parallel to the grain compressive stress, and taking into account that for unidirectional fibrous glass-epoxy composite, the angle of a shear failure band is determined by the minimum combination of shear and compressive strength, gross shear bands orientation in wood specimens could be explained based on this.

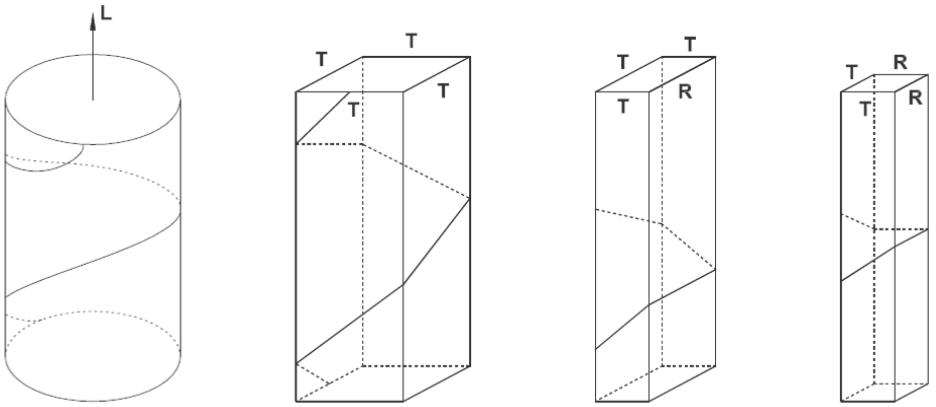

Figure 6.28. Compression tests parallel to grain on specimens type DF-C_L – Destructive tests: cleavage theory.

Principally, this kind of collapse mechanism is due to a microbuckling phenomena, macroscopically characterized by wrinkling of the fibres (Fig. 6.29).

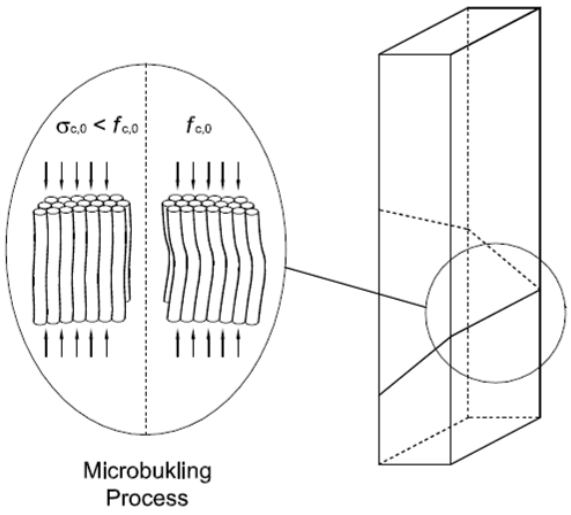

Figure 6.29. Compression tests parallel to grain on specimens type DF-C_L – Destructive tests: microbuckling modes.

For same specimen, other failure modes were observed, such as crushing, when the plane of rupture was approximately horizontal, splitting with the propagation of longitudinal cracks. In Figure 6.30 the typical failure pattern of the tested defect-free elements are shown, with reference to shearing (Fig. 6.30a), crushing (Fig. 6.30b), splitting (Fig. 6.30c) and both crushing and splitting (Fig. 6.30 d) mechanisms.

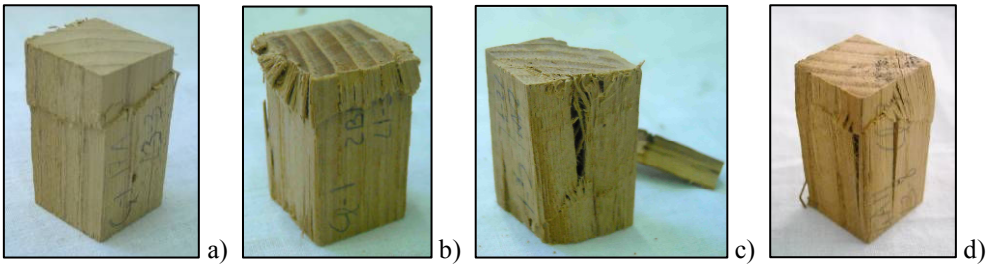

Figure 6.30. Compression tests parallel to grain on specimens type DF-C_L – Typical collapse mechanisms: a) Shearing; b) Crushing; c) Splitting; d) Crushing and splitting.

6.4.4 *Destructive tests perpendicular to grain*

6.4.4.1 Radial orientation

Compression tests in the direction perpendicular to the annual growth rings were carried out on twenty-two radial defect-free specimens, type DF-C_{rad}. In Figures 6.31 and 6.32 selected experimental stress ($\sigma_{c,90\ rad}$) – strain ($\varepsilon_{c,90\ rad}$) curves are shown, up to about 30 % total deformation.

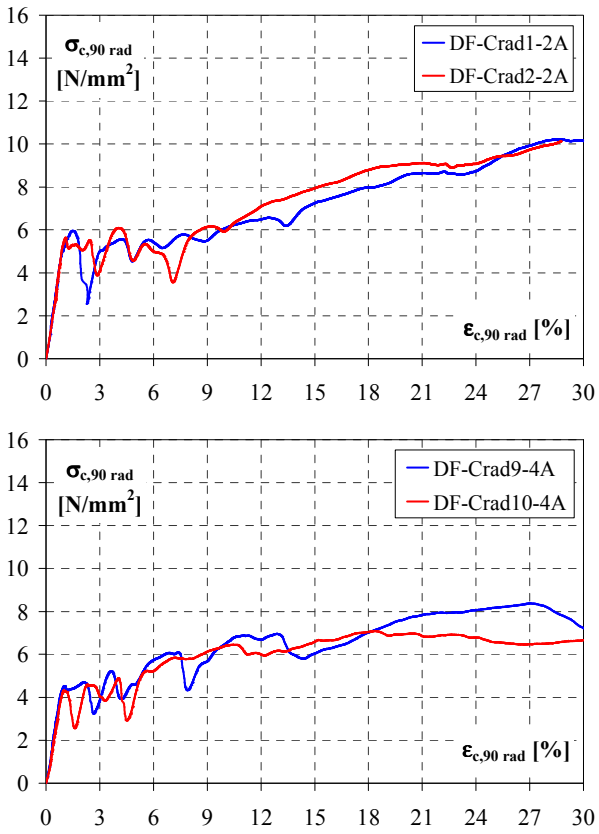

Figure 6.31. Compression tests perpendicular to grain on specimens type DF-C_{rad} – Destructive tests: $\sigma_{c,90\ rad}$-$\varepsilon_{c,90\ rad}$ curves (specimens extracted from 2A and 4A origin elements).

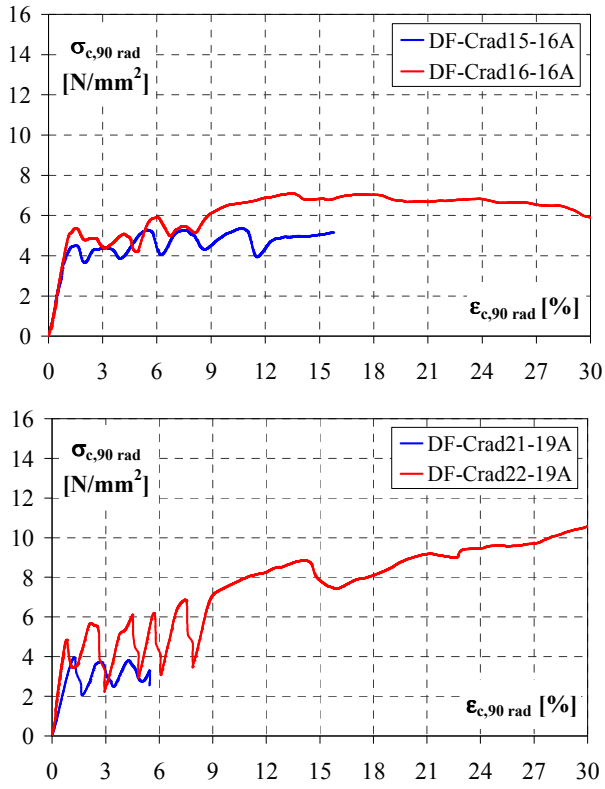

Figure 6.32. Compression tests perpendicular to grain on specimens type DF-C_{rad} – Destructive tests: $\sigma_{c,90\ rad}$-$\varepsilon_{c,90\ rad}$ curves (specimens extracted from 16A and 19A origin elements).

It is important to notice that, understanding the influence of annual ring patterns on the mechanical properties of wood, three deformation levels may occur and be easily identified when radial specimens are loaded: 1) initial elastic deformation; 2) plastic level for buckling and failure of cellular walls; 3) densification. Wood microstructure in the radial direction can be regarded usually as a sandwich construction consisting of alternating layers with completely different mechanical properties, earlywood and latewood. In fact, dense latewood layers are arranged in series between weak earlywood bands.

In radial compression the obtained stress-strain diagrams show some particularities that may be analyzed:

- First phase: the diagrams always start with a straight line. Then, the change from initial linear elastic deformation, occurs with a sudden load drop. According to several authors (Bodig, 1963; Kunesh, 1968; Tabarsa and Chui, 2000) and corroborated by this work, the initial maximum stress value is determined by the weakest earlywood layer, created naturally by various anatomical elements, for buckling of a portion of rays arranged in a growth ring, and the strength of the latewood and other earlywood layers add very little to this value. Rays act as spaced columns and fail simultaneously as a single unit.
- Second phase: a plateau is obtained, graphically represented by irregular saw-tooth shapes, reported by Bodig (1965) as "micro-stress-strain diagrams", corresponding to the fracture of individual cell walls (initial average plateau stress lies below the initial failure stress) follow by a densification zone where the additional failures occur in the same or in several other earlywood layers as the compression progresses. This densification zone is responsible for the redistribution of stress and strain to growth rings that have not failed, corresponding graphically to a stress increase;
- Third phase: the strain increase rapidly, due to the compaction of the material.

In conclusion, radial compression initial failure is caused by this earlywood "weak-layer" and follows by others with increasing load, decreasing the cross section height. As result of the large compaction of the earlywood layers, the final aspect of the specimens can be compared with a "thin" global layer. These structural changes are highlighted in Figure 6.33, where some pictures of the collapsed radial specimens are shown.

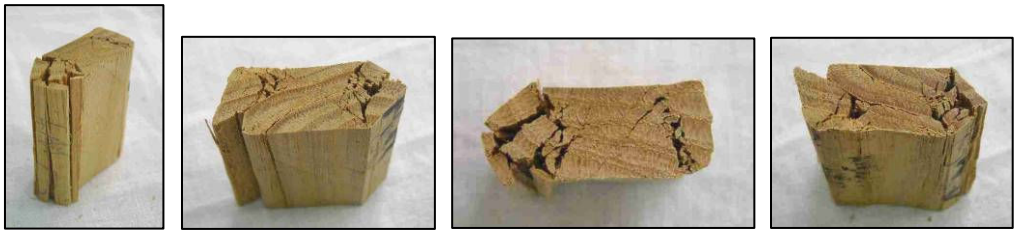

Figure 6.33. Compression tests perpendicular to grain on specimens type DF-C_{rad} – Typical radial collapse mechanisms consisting in large transversal deformations.

6.4.4.2 Tangential orientation

Transverse compression tests with tangential orientation of the annual growth rings were carried out on twenty-two specimens free from faults, type DF-C_{tg}. Figures 6.34 to 6.37 show the achieved stress ($\sigma_{c,90\ tg}$) - ($\varepsilon_{c,90\ tg}$) curves. Because a similar mechanical response was observed for each group of elements extracted by cutting of the same structural element, the average curve were also obtained, depicted in the following charts.

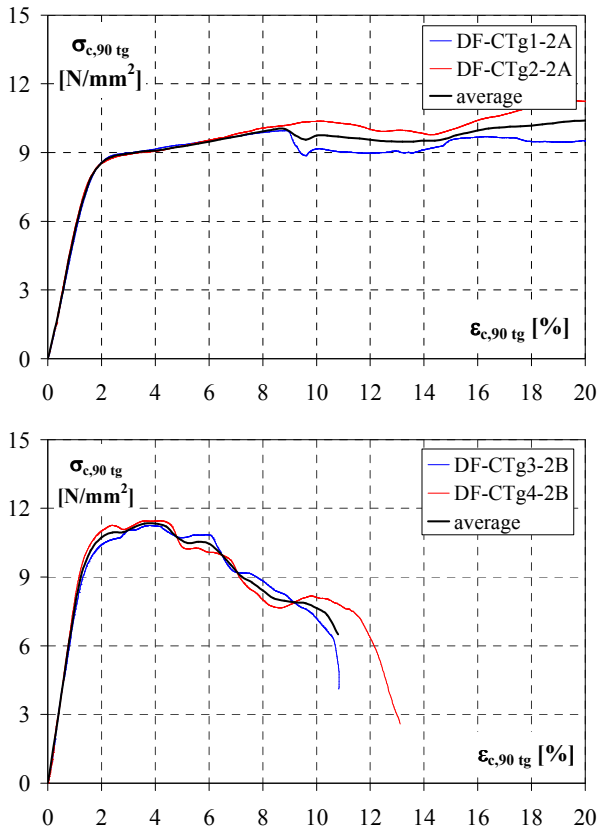

Figure 6.34. Compression tests perpendicular to grain on specimens type DF-C_{tg} –Destructive tests: $\sigma_{c,90\ tg}$-$\varepsilon_{c,90\ tg}$ curves (specimens extracted from 2A and 2B origin elements).

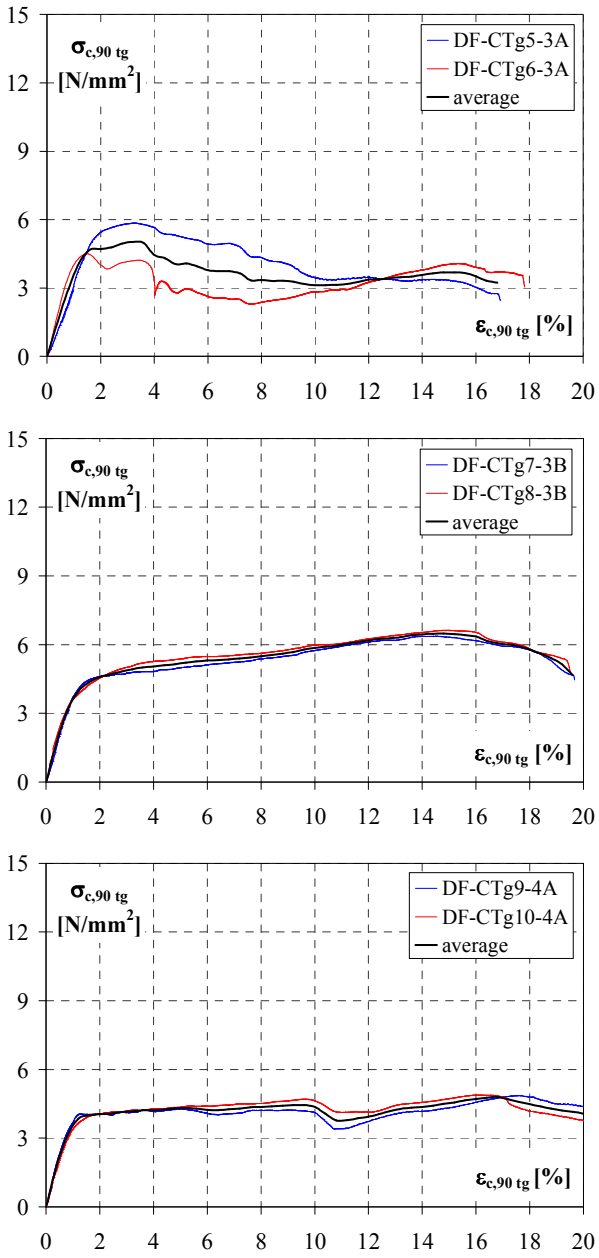

Figure 6.35. Compression tests perpendicular to grain on specimens type DF-C_{tg} –Destructive tests: $\sigma_{c,90\,tg}$-$\varepsilon_{c,90\,tg}$ curves (specimens extracted from 3A, 3B and 4A origin elements).

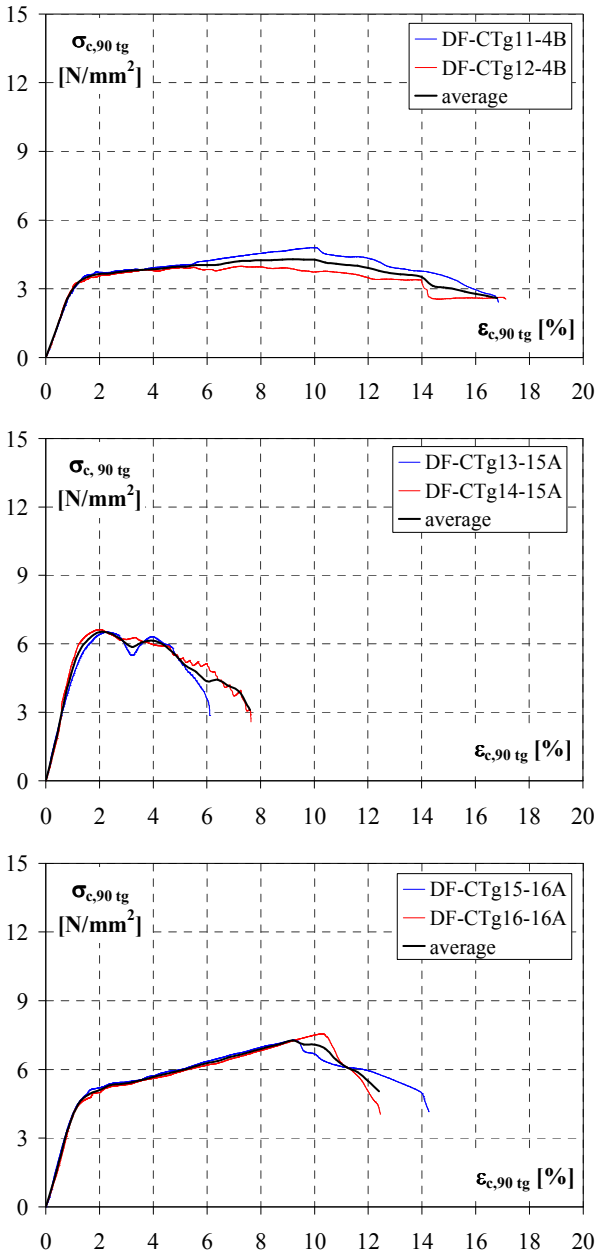

Figure 6.36. Compression tests perpendicular to grain on specimens type DF-C_{tg} –Destructive tests: $\sigma_{c,90\ tg}$-$\varepsilon_{c,90\ tg}$ curves (specimens extracted from 4B, 15A and 16A origin elements).

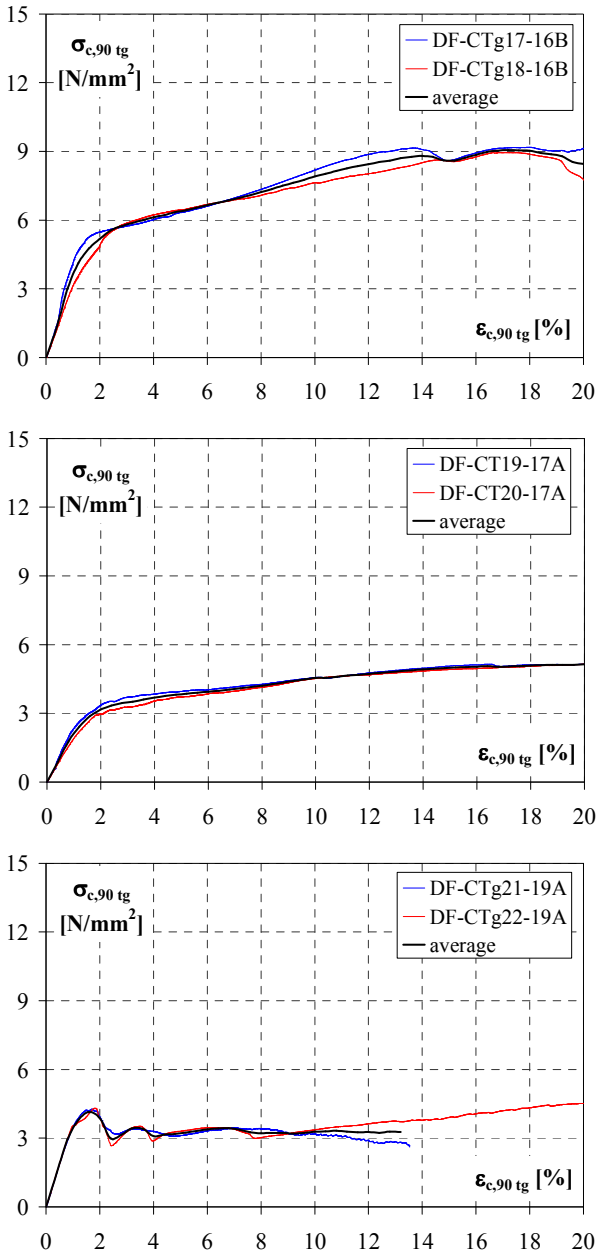

Figure 6.37. Compression tests perpendicular to grain on specimens type DF-C_{tg} –Destructive tests: $\sigma_{c,90\,tg}$-$\varepsilon_{c,90\,tg}$ curves (specimens extracted from 16B, 17A and 19A origin elements).

In Figure 6.38 the average stress-strain curves of all specimens groups are presented (Fig. 6.38a), together with the global minimum, average and maximum curves (Fig. 6.38b), which summarize the mechanical behaviour of the tested old chestnut wood under perpendicular to grain compression, with tangential orientation of the annual growth rings.

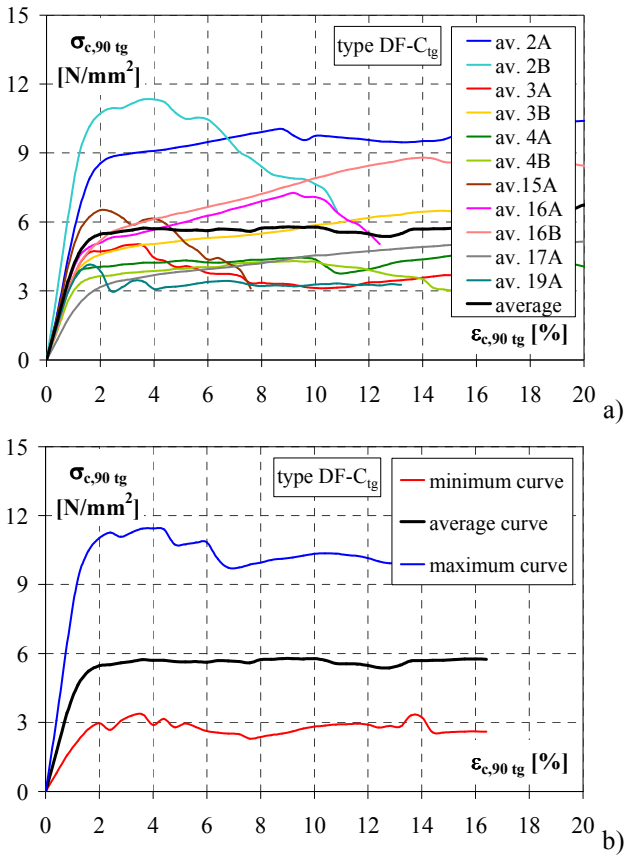

Figure 6.38. Compression tests perpendicular to grain on specimens type DF-C_{tg} –Destructive tests: a) $\sigma_{c,90\ tg}$-$\varepsilon_{c,90\ tg}$ average curves; b) Minimum, average and maximum $\sigma_{c,90\ tg}$-$\varepsilon_{c,90\ tg}$ curves.

As it appears, in tangential compression the stress-strain diagrams do not show a marked maximum stress value as in radial compression. In fact, the elastic phase gradually merges into a plateau zone until a region where the strain increases rapidly to the same load value. The tangential behaviour can

be explained by the early bond failure between earlywood and latewood layers. With increasing load a separation between these layers was observed, often with buckling failure as a result of the low slenderness of individual earlywood and latewood layers along their axes. In Figure 6.39 some collapsed tested tangential specimens are shown

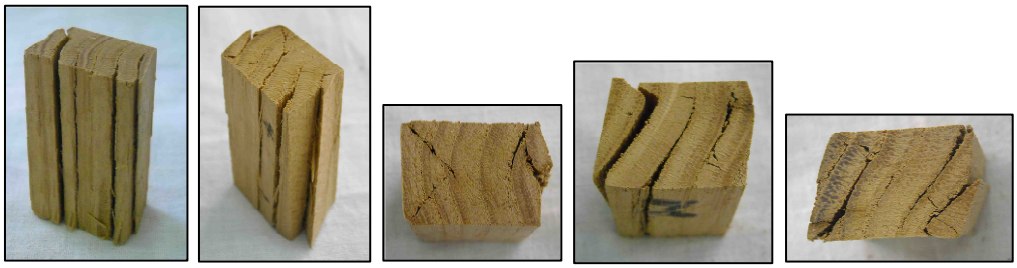

Figure 6.39. Compression tests perpendicular to grain on specimens type DF-C_{tg} – Typical tangential collapse mechanisms consisting in separation between earlywood and latewood layers.

6.4.5 *Results and discussion*

In Tables 6.8, 6.9 and 6.10 the experimental results of compression tests on defect-free elements are given, respectively for the specimens type DF-C_L, DF-C_{rad} and DF-C_{tg}, in terms of both modulus of elasticity (E_c) and compression strength (f_c). The main statistical parameters are also provided. Furthermore, the average values of these mechanical properties obtained by each group of sample extracted from the same original element are also reported.

For the compression tests parallel to grain (specimens type DF-C_L; Table 6.8), the modulus of elasticity ($E_{c,0}$) is calculated on the initial linear branch on the stress-strain curve, defined by the points ($\sigma_{10\%}$, $\varepsilon_{10\%}$) and ($\sigma_{40\%}$; $\varepsilon_{40\%}$) corresponding respectively to 10% and 40% of the ultimate stress ($f_{c,0}$), which is the conventional value determined by the maximum load applied to the specimens.

With regard to the transverse compression tests, as the stress-strain relationship is influenced by the anatomy of wood, a peak compressive stress is not identified and it is difficult to define a characteristic strength that can only be expressed in function of a global deformation value. The definition of

an appropriate strength model that defines the real resistance capacity based on material properties, involved actions and geometric conditions must be developed. In practical situations this criterion may be obtained based on (Fig. 6.40): a) value based in evident plastic behaviour; b) a random value based on the slope that the stress-strain diagram presents on the elastic domain; c) excessive deformation criterion, e.g., 10% of total deformation.

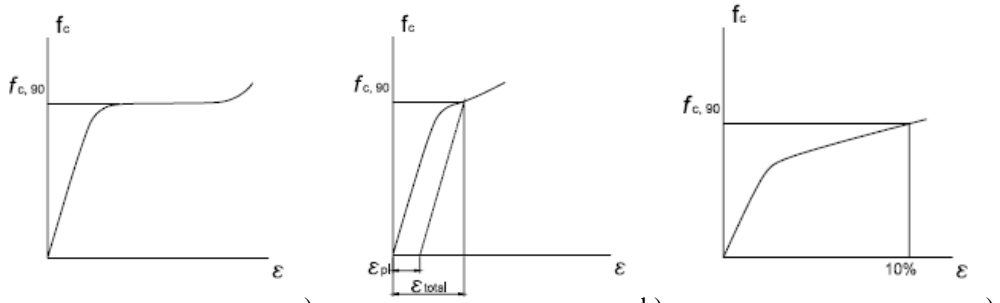

a) b) c)

Figure 6.40. Compression tests perpendicular to grain – Criteria for definition of strength ($f_{c,90}$): a) Pronounced plastic stage; b) Deformation criteria based on the plastic deformation (ε_{pl}); c) Excessive deformation, with imposed value of global deformation (10%).

On the experimental stress-strain diagrams for radial and tangential compression, a conventional proportional stress ($f_{c,90}$) has been defined by the residual specific strain of 1%, according to plastic deformation criteria (Fig. 6.40b). This proportional limit corresponds to the point where the stress-strain curve deviates from the tangential straight line, on which, between 10% and 40% of $f_{c,90}$ the modulus of elasticity ($E_{c,90}$) has been evaluated (Tables 6.9 and 6.10).

By a first analysis of results, the following main observations can be made:

- The peak compressive stress ($f_{c,0}$) exhibited by the clear specimens tested along the grain, is quite homogeneous (CV = 14.27%), with a high average value of about 60 N/mm^2;
- The average values of perpendicular compression strength in radial and tangential directions are very similar, equal to about 5.5 N/mm^2, despite the different observed failure modes. This value, as expected, is eleven times smaller that the same one obtained in parallel direction.

Table 6.8. Compression tests parallel to grain on specimens type DF-C_L: experimental results.

Specimen type DF-C_L	**$E_{c,0}$ [N/mm^2]**	**$f_{c,0}$ [N/mm^2]**	**Origin element**	**$E_{c,0}$ [N/mm^2]**	**$f_{c,0}$ [N/mm^2]**
DF-C_L1-2A	5911	67.41			
DF-C_L2-2A	5892	63.02	2A	6602	64.67
DF-C_L3-2A	8003	63.59			
DF-C_L4-2B	6200	63.13			
DF-C_L5-2B	6375	68.73	2B	7034	67.30
DF-C_L6-2B	8527	70.05			
DF-C_L7-3A	5225	53.46			
DF-C_L8-3A	5912	51.96	3A	5848	54.16
DF-C_L9-3A	6406	57.08			
DF-C_L10-3B	7278	52.51			
DF-C_L11-3B	5389	49.82	3B	6084	50.84
DF-C_L12-3B	5586	50.20			
DF-C_L13-4A	5197	57.80			
DF-C_L14-4A	5792	53.76	4A	5932	57.24
DF-C_L15-4A	6806	60.15			
DF-C_L16-4B	6899	57.64			
DF-C_L17-4B	7639	58.21	4B	7254	56.68
DF-C_L18-4B	7224	54.19			
DF-C_L19-15A	6893	63.11			
DF-C_L20-15A	7665	61.82	15A	7113	62.43
DF-C_L21-15A	6780	62.36			
DF-C_L22-16A	9045	75.74			
DF-C_L23-16A	7556	74.07	16A	7919	74.27
DF-C_L24-16A	7155	73.01			
DF-C_L25-16B	7944	69.64			
DF-C_L26-16B	7679	69.03	16B	7977	69.72
DF-C_L27-16B	8309	70.49			
DF-C_L28-17A	4966	48.25			
DF-C_L29-17A	4438	46.43	17A	4316	46.15
DF-C_L30-17A	3542	43.77			
DF-C_L31-19A	6433	52.55			
DF-C_L32-19A	5987	60.76	19A	6025	55.29
DF-C_L33-19A	5656	52.56			
min	3542	43.77			
average	6555	59.89			
max	9045	75.74			
5-percentile	4169	45.63			
SD	1234	8.55			
CV [%]	18.82	14.27			

Table 6.9. Compression tests perpendicular to grain on specimens type DF-C_{rad}: experimental results.

Specimen type DF-C_{rad}	**$E_{c,90\ rad}$ [N/mm^2]**	**$f_{c,90\ rad}$ [N/mm^2]**	**Origin element**	**$E_{c,90\ rad}$ [N/mm^2]**	**$f_{c,90\ rad}$ [N/mm^2]**
DF-C_{rad}1-2A	612	5.96	2A	578	5.80
DF-C_{rad}2-2A	544	5.63			
DF-C_{rad}3-2B	705	6.69	2B	764	6.50
DF-C_{rad}4-2B	823	6.32			
DF-C_{rad}5-3A	526	5.54	3A	529	5.76
DF-C_{rad}6-3A	532	5.97			
DF-C_{rad}7-3B	521	6.14	3B	495	6.04
DF-C_{rad}8-3B	469	5.94			
DF-C_{rad}9-4A	573	4.71	4A	543	4.51
DF-C_{rad}10-4A	513	4.32			
DF-C_{rad}11-4B	545	5.19	4B	504	4.84
DF-C_{rad}12-4B	463	4.49			
DF-C_{rad}13-15A	628	6.20	15A	611	5.85
DF-C_{rad}14-15A	595	5.51			
DF-C_{rad}15-16A	468	4.51	16A	476	4.94
DF-C_{rad}16-16A	483	5.37			
DF-C_{rad}17-16B	624	5.78	16B	584	5.65
DF-C_{rad}18-16B	544	5.52			
DF-C_{rad}19-17A	392	4.21	17A	365	4.35
DF-C_{rad}20-17A	338	4.50			
DF-C_{rad}21-19A	366	3.95	19A	549	4.40
DF-C_{rad}22-19A	731	4.84			
min	338	3.95			
average	545	5.33			
max	823	6.69			
5-percentile	343	3.99			
SD	116	0.78			
CV [%]	21.21	14.60			

Table 6.10. Compression tests perpendicular to grain on specimens type DF-C_{tg}: experimental results.

Specimen type DF-C_{rad}	**$E_{c,90\ tg}$ [N/mm^2]**	**$f_{c,90\ tg}$ [N/mm^2]**	**Origin element**	**$E_{c,90\ tg}$ [N/mm^2]**	**$f_{c,90\ tg}$ [N/mm^2]**
DF-C_{tg}1-2A	590	8.81	2A	568	8.88
DF-C_{tg}2-2A	547	8.94			
DF-C_{tg}3-2B	843	10.64	2B	847	10.95
DF-C_{tg}4-2B	850	11.25			
DF-C_{tg}5-3A	504	4.46	3A	408	5.13
DF-C_{tg}6-3A	313	5.80			
DF-C_{tg}7-3B	426	4.64	3B	497	4.54
DF-C_{tg}8-3B	567	4.44			
DF-C_{tg}9-4A	400	4.07	4A	468	4.07
DF-C_{tg}10-4A	535	4.07			
DF-C_{tg}11-4B	323	3.71	4B	333	3.64
DF-C_{tg}12-4B	343	3.57			
DF-C_{tg}13-15A	513	6.52	15A	516	6.47
DF-C_{tg}14-15A	518	6.42			
DF-C_{tg}15-16A	493	5.28	16A	440	5.17
DF-C_{tg}16-16A	387	5.07			
DF-C_{tg}17-16B	469	5.58	16B	400	5.68
DF-C_{tg}18-16B	330	5.78			
DF-C_{tg}19-17A	274	3.53	17A	237	3.35
DF-C_{tg}20-17A	200	3.18			
DF-C_{tg}21-19A	381	3.90	19A	382	3.90
DF-C_{tg}22-19A	382	3.89			
min	200	3.18			
average	463	5.62			
max	850	11.25			
5-percentile	211	3.23			
SD	161	2.32			
CV [%]	34.78	41.27			

6.5 MECHANICAL BEHAVIOUR IN COMPRESSION OF OLD CHESTNUT TIMBER

6.5.1 *Parallel to grain*

The mechanical characteristics of tested old chestnut timber under compression parallel to grain has been analyzed by comparing the experimental results obtained by destructive tests carried out on the following three groups of specimens:

- *Structural elements in actual dimensions* (S_A-C; n=14), characterized by macroscopic defects, like knots, slope of grain and longitudinal cracks, and damaged superficial wooden layers, with irregular cross-section shape ($D_{mean}\approx15$ cm; $L\approx90$ cm; $L\approx6D_{mean}$);
- *Structural elements in small dimensions* (S_S-C; n=20), with superficial defects and square cross-section (b=5 cm; L=30 cm; L=6b);
- *Defect-free specimens* (DF-C; n_{tot}=77), free from faults and with square cross-section ($2\times2\times4$ cm^3).

The specimens had standard dimensions, according to UNI EN 408 and UNI ISO Italian codes.

The comparison is represented in Figure 6.41 by means of stress ($\sigma_{c,0}$) – strain ($\varepsilon_{c,0}$) average curves (Fig. 6.41a) and both average and 5-percentile values of compression strength ($f_{c,0}$; Fig. 6.41b) and modulus of elasticity ($E_{c,0}$; Fig. 6.41c). As shown, the three specimens typologies exhibit different responses especially in terms of stress carrying capacity, being the stiffness properties nearly similar each other.

Three levels of compression average strength can be defined: 1) 24 N/mm^2 for structural elements in actual dimensions; 2) 44 N/mm^2 for structural elements in small dimensions; 3) 60 N/mm^2 for defect-free specimens. Therefore, it is possible to assume that the presence of natural defects, irregularities and wood degradations, typical of ancient timber members, drastically reduce the compression strength of chestnut timber elements in actual sizes, of about three times as respect the same mechanical property of small specimens, made of clear wood. Furthermore, defects not only affect the

strength performance of structural material but also its mechanical behaviour. In fact, while the stress-strain curve of clear wood shows, beyond the linear range, a plastic branch with evident softening highlighting a ductile behaviour of the material, the same curves of the structural elements, in both actual and small dimensions, reveal a brittle response, characterized by a abrupt reduction of strength after the peak load reached during the tests (Fig. 6.41a).

Therefore, with a natural material like wood, so depending of the existence of faults, the mechanical evaluation can not use clear specimens. The attention has to be moved towards the experimental investigation of the mechanical evaluation of wood elements having structural dimensions and presenting the natural defects recognize to this material.

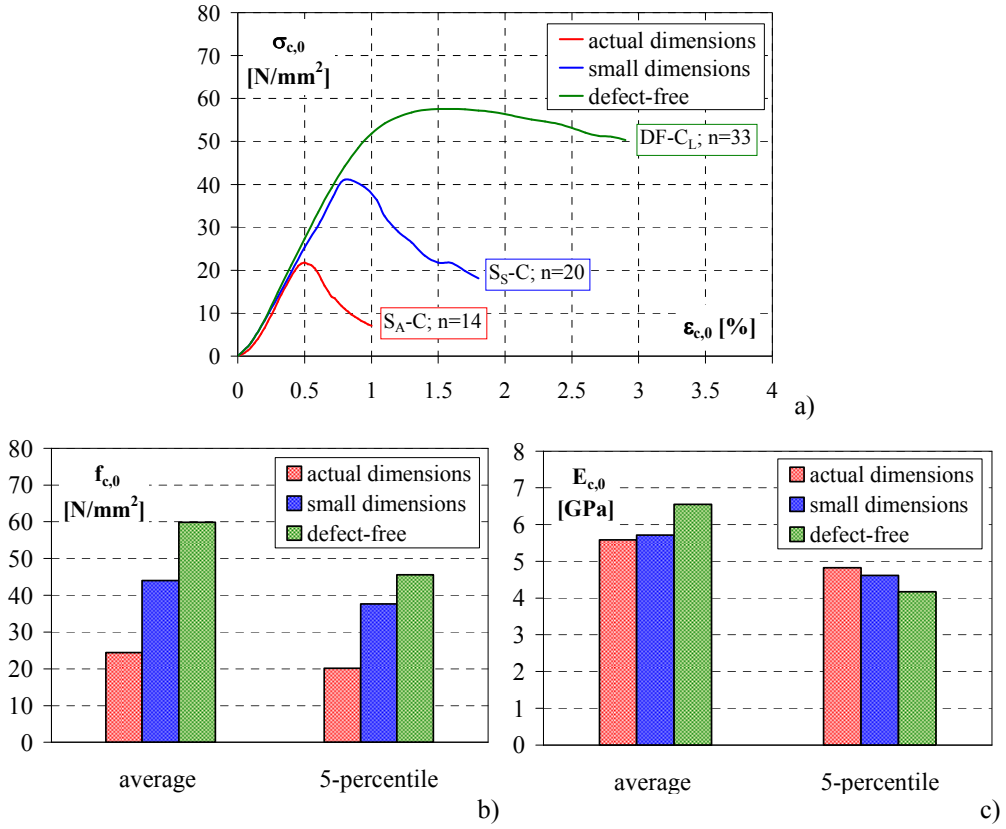

Figure 6.41. Mechanical behaviour in compression parallel to grain of old chestnut timber – Comparison between specimens type S_A-C, S_S-C and DF-C_L: a) Average $\sigma_{c,0}$-$\varepsilon_{c,0}$ curves; b) Strength ($f_{c,0}$); c) Modulus of elasticity ($E_{c,0}$).

In Figure 6.42 the strength and stiffness features of structural and defect-free specimens are compared with reference to the results obtained by the samples extracted from the same origin element. Therefore, the values given in Tables 6.2, 6.4 and 6.8 are considered.

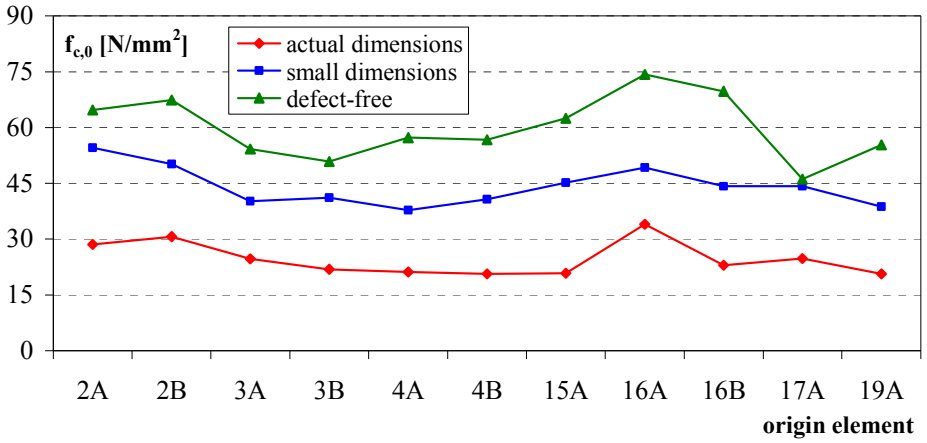

a)

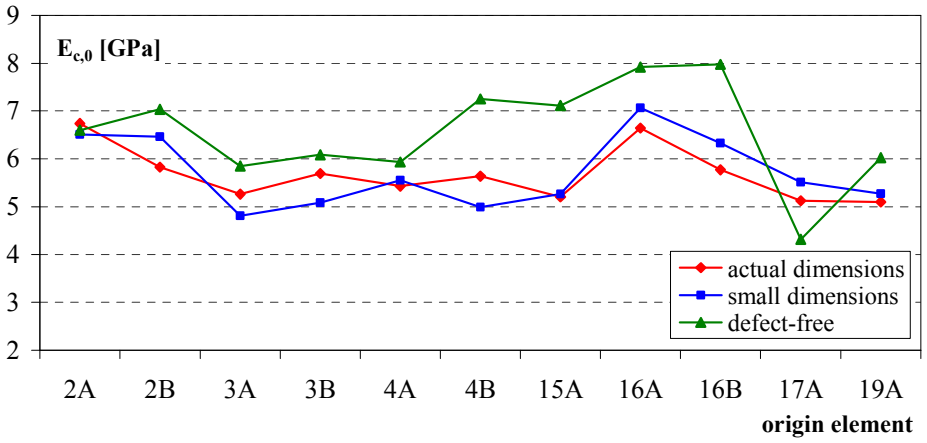

b)

Figure 6.42. Mechanical behaviour in compression parallel to grain of old chestnut timber – Comparison between specimens type S_A-C, S_S-C and DF-C_L extracted by the same origin element: a) Compression strength ($f_{c,0}$); b) Modulus of elasticity ($E_{c,0}$).

In Table 6.11 the experimental results in compression parallel to grain (average, 5-percentile and variation coefficient) are reported for each group of specimens, comparing the same ones with the values reported in European and Italian codes. In particular, the characteristic values of UNI 111035-2 for chestnut wood and of EN 338 for D30 hardwood strength class, together with the admissible compression stress of UNI 11119 for the third category class are considered. It is possible to observe that:

- The strength values of the specimens in actual dimensions (S_A-C) are affected by higher variability, due to the presence of natural defects (Fig. 6.43a);
- Good agreement is provided by comparing the experimental 5-percentile value of specimens type S_A-C (20.13 N/mm^2) and the characteristic values assumed by UNI 11035-2 (22 N/mm^2) and EN 338 (D30; 23 N/mm^2; Fig. 6.43b);
- Comparing the admissible strength of UNI 11119-III (7 N/mm^2) with the average and 5-percentile results of laboratory tests, the obtained safety coefficients are greater than 3, 5 and 6.5 for actual (S_A-C), small (S_S-C) and defect-free (DF-C_L) specimens, respectively (Fig. 6.43b).

Table 6.11. Mechanical behaviour in compression parallel to grain of old chestnut timber: comparison between experimental strength and standard values [N/mm^2].

	experimental results			*UNI*	*EN 338*	*UNI*
Specimen		$\mathbf{f_{c,0}}$		*11035-2*	*D30*	*11119-III*
type	**average**	**5-perc.**	**CV [%]**	$\mathbf{f_{c,0,k}}$	$\mathbf{f_{c,0,k}}$	$\boldsymbol{\sigma_{c,0\ adm}}$
S_A-C (n=14)	24.40	20.13	17.21			
S_S-C (n=20)	44.05	37.67	11.98	22	23	7
DF-C_L (n=33)	59.89	45.63	14.27			

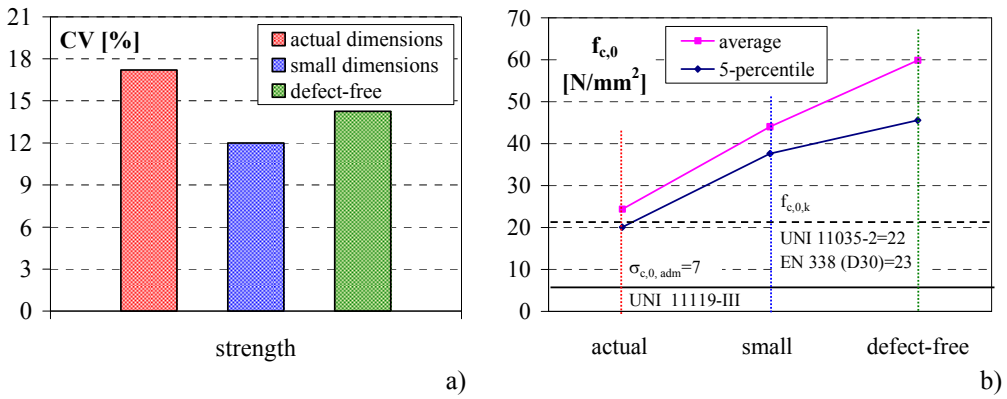

Figure 6.43. Mechanical behaviour in compression parallel to grain of old chestnut timber – Compression strength ($f_{c,0}$): a) Coefficients of variation (CV); b) Comparison of experimental strength with standard values.

6.5.2 *Perpendicular to grain*

The mechanical characterization of old chestnut wood in compression perpendicular to the grain has been carried out by analyzing and comparing the experimental results of tests on the following three groups of defect-free specimens: 1) DF-C_L (n=33) for tests parallel to grain; 2) DF-C_{rad} (n=22) for transverse radial tests; 3) DF-C_{tg} (n=22) for transverse tangential tests. All specimens had standard dimensions (2×2×4 cm^2) according to UNI ISO 3787 and 3132 Italian codes.

The comparison between the mechanical behaviour in compression parallel and perpendicular to the grain is shown in Figure 6.44, where the stress (σ_c) – strain (ε_c) average curves of specimens type DF-C_L and DF-C_{tg} are depicted (Fig. 6.44a) and both average and 5-percentile values of compression strength (f_c; Fig. 6.44b) and modulus of elasticity (E_c; Fig. 6.44c) are represented for longitudinal, radial and tangential specimens. These comparisons are also shown in Figure 6.45, where the tests results given in Tables 6.8, 6.9 and 6.10 are plotted for the samples belonged to the same structural element.

Understanding how the stress-strain relationships in transverse compression are significantly influenced by the anatomy of wood, the tested specimens show very low compressive stiffness and strength when loaded perpendicular to the grain.

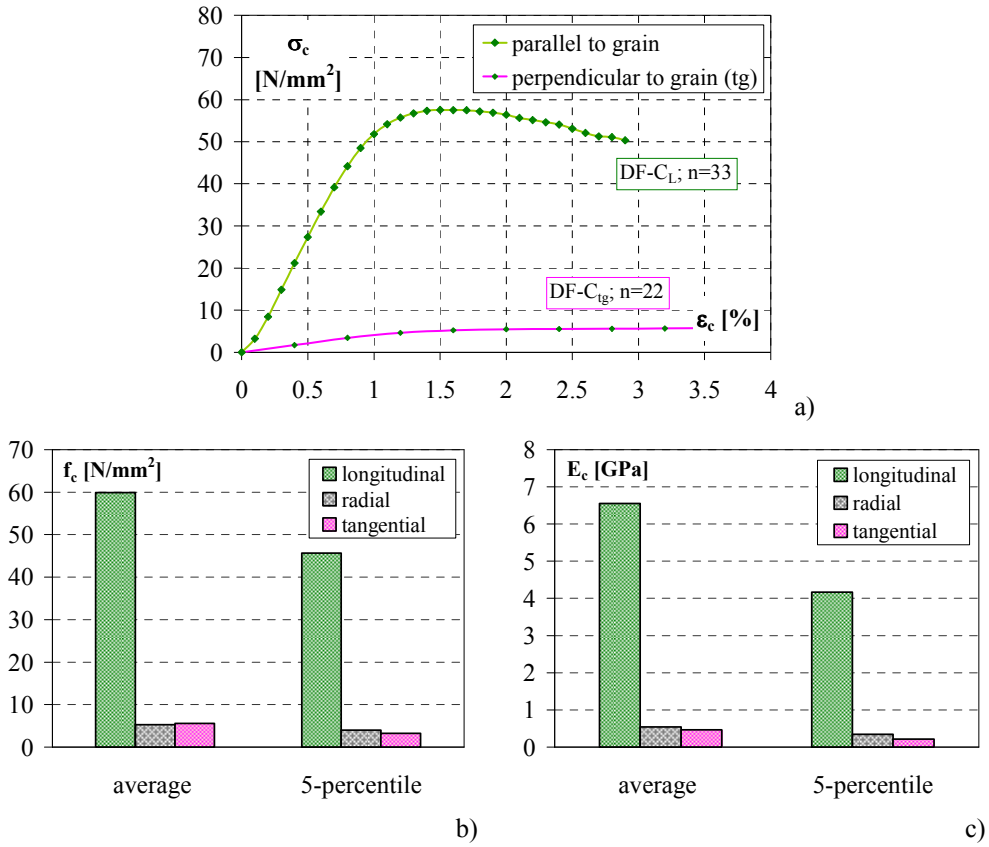

Figure 6.44. Mechanical behaviour in compression perpendicular to grain of old chestnut timber – Comparison between specimens type DF-C_L and DF-C_{tg}: a) Average σ_c-ε_c curves; b) Strength (f_c); c) Modulus of elasticity (E_c).

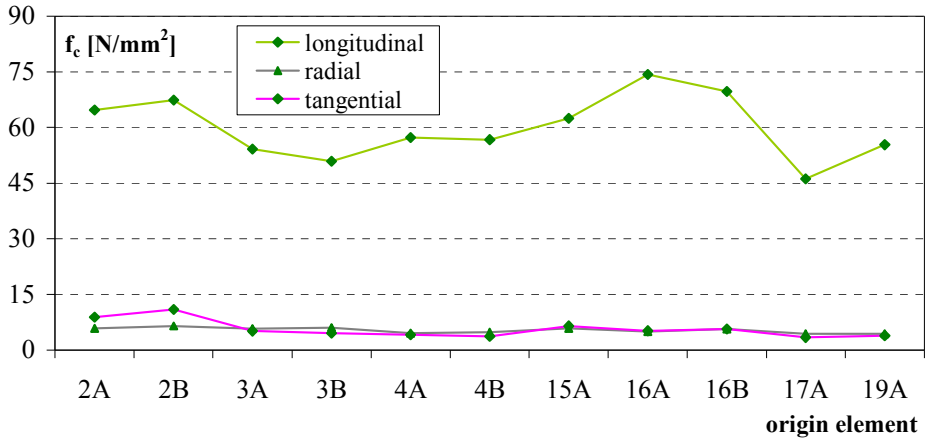

a)

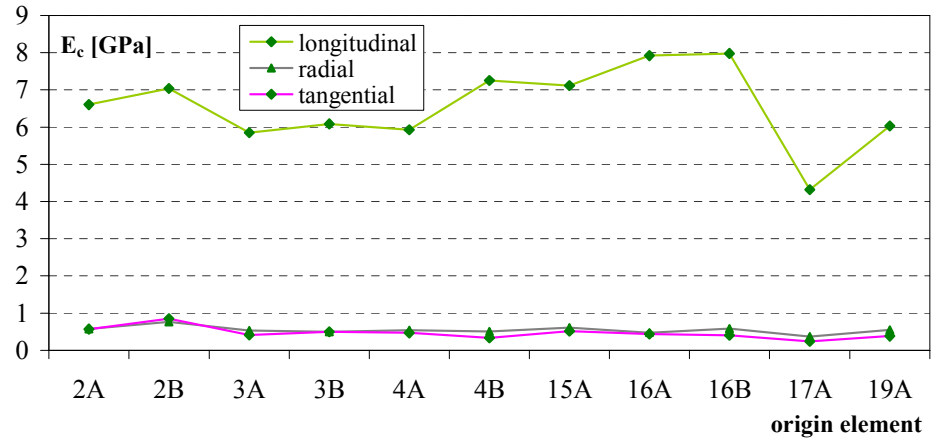

b)

Figure 6.45. Mechanical behaviour in compression perpendicular to grain of old chestnut timber – Comparison between specimens type DF-C_L, DF-C_{rad} and DF-C_{tg} extracted by the same origin element: a) Compression strength (f_c); b) Modulus of elasticity (E_c).

Analyzing the experimental results given in Tables 6.12 to 6.15, where they are also compared with the mechanical properties assumed by European (EN 338, D30) and Italian codes (UNI 11035-2 and UNI 11119-III), the following main observations can be made:

- Similar responses are provided by both stiffness and strength properties in radial and tangential perpendicular direction; whereas the tangential tests are affected by higher coefficients of variation (CV; Tables 6.12 and 6.13);
- 5-percentile strength results ($f_{c,90}$) are comparable with UNI 11035-2 value (Table 6.12);
- Comparing the admissible strength of UNI 11119-III code with the average and 5-percentile results of laboratory tests (Table 6.12), the obtained safety coefficients are equal to about 2.7 and 1.8, respectively;
- The mean modulus of elasticity provided by UNI 11035-2 and EN 338 is about 1.4 times than the experimental value (Table 6.13);
- The $f_{c,0}/f_{c,90}$ ratio by laboratory tests is significantly higher than the same one by European and Italian codes (Table 6.14); whereas, the experimental ratio $E_{c,0}/E_{c,90}$ is similar with the standard one (Table 6.15).

Table 6.12. Mechanical behaviour in compression perpendicular to grain of old chestnut timber: comparison between experimental strength and standard values [N/mm^2].

	experimental results			*UNI*	*EN 338*	*UNI*
Specimen	**$f_{c,90}$**			*11035-2*	*D30*	*11119-III*
type	**average**	**5-perc.**	**CV [%]**	**$f_{c,90,k}$**	**$f_{c,90,k}$**	**$\sigma_{c,90\ adm}$**
DF-C_{rad} (n=22)	5.33	3.99	14.60	3.8	8	2
DF-C_{tg} (n=22)	5.62	3.23	41.27			

Table 6.13. Mechanical behaviour in compression perpendicular to grain of old chestnut timber: comparison between experimental modulus of elasticity and standard values [N/mm^2].

	experimental results		*UNI*	*EN 338*
Specimen	**$E_{c,90}$**		*11035-2*	*D30*
type	**average**	**CV [%]**	**$E_{c,90\ mean}$**	**$E_{c,90\ mean}$**
DF-C_{rad} (n=22)	545	21.21	730	640
DF-C_{tg} (n=22)	463	34.78		

Table 6.14. Mechanical behaviour in compression perpendicular to grain of old chestnut timber: comparison between experimental ratio $f_{c,0}/f_{c,90}$ and standard one.

Specimen type	*experimental results* $f_{c,0}/f_{c,90}$ average	5-perc.	*UNI 11035-2* $f_{c,0,k}/f_{c,90,k}$	*EN 338 D30* $f_{c,0,k}/f_{c,90,k}$	*UNI 11119-III* $\sigma_{c,0}/\sigma_{c,90\ adm}$
DF-C_{rad} (n=22)	11.23	11.43	5.79	2.87	3.50
DF-C_{tg} (n=22)	10.66	14.11			

Table 6.15. Mechanical behaviour in compression perpendicular to grain of old chestnut timber: comparison between experimental ratio $E_{c,0}/E_{c,90}$ and standard one.

Specimen type	*experimental results* $E_{c,0}/E_{c,90}$ average	*UNI 11035-2* $E_0/E_{90,\ mean}$	*EN 338 D30* $E_0/E_{90,\ mean}$
DF-C_{rad} (n=22)	12.02	15.07	15.63
DF-C_{tg} (n=22)	14.15		

Chapter 7
Destructive tests in bending (DT)

7.1 GENERAL

Structural timber displays considerable strength variability between and within members, which makes it difficult to evaluate its reliability and to design timber elements and system in a rational way.

In particular, for bending stress condition, most of today's engineering design methods for timber are based on elementary theory of structures assuming homogeneous material. In reality, due to the presence of various defects in the wood, the variation in strength along a timber beam results in a strength which is dependent on the length of the element, depth of the section and the type of loading, i.e. the moment distribution of the beam. Apart from dimensions and type of loading, the strength is also dependent on climate conditions and the duration of load. One way of describing the variability phenomena and its effects on, for example, the strength of a timber beam is proposed in a model introduced by Riberholt et al. (1979). It is assumed that timber is composed of localized weak zones connected by segments of clear wood, and that failure is primarily initiated in these weak zones. The weak zones correspond to knots or groups of knots, which are distributed along the length at random (Fig. 7.1).

Furthermore, the laboratory results achieved in any assessment of mechanical properties are function of the testing method adopted. Therefore, a standardization of the test procedure is required. Moreover, with the adoption

of limit state design and with the development of both visual and machine stress grading, attention will be increasingly focused on the determination and monitoring of the strength properties and variability of structural grades of timber. EN 408 European Standard specified laboratory methods for the determination of some physical and mechanical features in structural size.

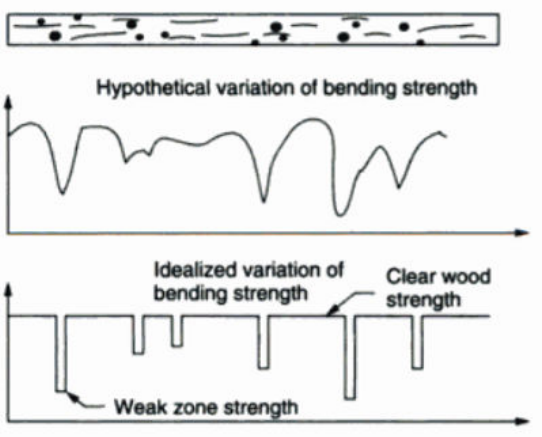

Figure 7.1. Modelling of bending strength variation (Riberholt *et al*., 1979).

The phase of the whole experimental activity, which concerns the evaluation of the local and overall structural behaviour in bending of full-scale timber elements, is described in this chapter. The tested beams, in old chestnut wood (*Castanea sativa* Mill.), were the strut elements of timber roofing trusses of an ancient masonry building of Naples, dismantled in a recent consolidation intervention.

In a preliminary step, the visual inspection was carried out in order to have an exhaustive geometrical survey of the elements and to assess their conservation state, detecting location and extent of defects and alterations. Ring shakes, large isolated knots or knots groups have surveyed on the lateral surface of the specimens. Because the knots position respect to the loading direction influences significantly the impact of these defects kind on the bending performance, their location as respect to the tensile side as well as the position relative to the middle of the specimen was recorded.

According to UNI EN 408, the main purposes of testing investigations were the determination of the load-displacement curves, the stiffness

properties, such as local and global modulus of elasticity, flexural strength, together with the evaluation of relevant failure mechanisms under bending stress state. In this chapter, the main geometrical characteristics of the specimens, testing equipment and set-up are described. The experimental results are discussed and statistically analyzed.

7.2 CHARACTERISTICS OF THE SPECIMENS

Static bending tests were performed on ten selected beams in actual dimensions, labelled as specimens type S_A-B. The used test arrangement was in agreement with European testing standard EN 408 which specifies a four-points loading scheme with two load-points acting in the third of the span, equal to 18 times the board depth (Fig. 7.2).

The evaluation of the local modulus of elasticity in bending is based on the deformations measured over a central gauge length of 5 times the depth of the section. Three points, A, B and C are located at the neutral axis, within the test span, so that the deformation of point B is measured relative to points A and C. Using the deformation value measured at the centre of the span, point D, and at the centre of the compression or tension side, it is possible calculate the so-called global modulus of elasticity in bending. The bending strength is obtained with the continuation of the tests up to the failure.

In Table 7.1, according to the standard static scheme (Fig. 7.2), the main geometric characteristics of the specimens are summarized, together with wood density values (ρ).

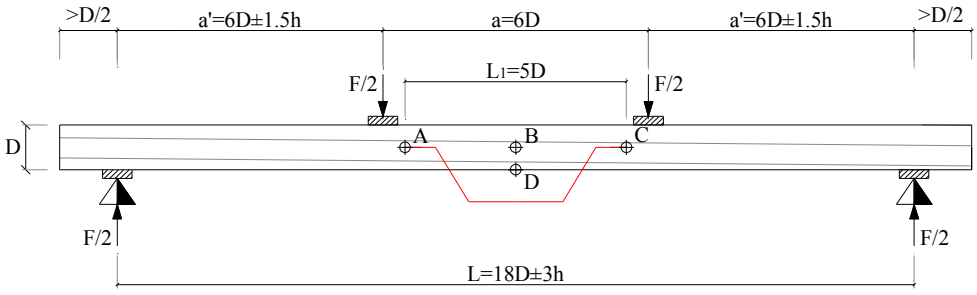

Figure 7.2. Bending tests on specimens type S_A-B – Characteristics of the specimens: test arrangement (UNI EN 408).

The wood density of the beams was determined in a simple way weighing and measuring the dimensions of undamaged end parts of the samples, cut after the destructive tests.

In the testing standard EN 408, it is stated that the test pieces shall be conditioned at 20°C and 65 % relative humidity, which corresponds to a moisture content (MC) of 12 %. It is worth to noticing that, the structural timber in the present investigations had a MC of about 11-12 % at testing.

Table 7.1. Bending tests on specimens type S_A-B: geometric characteristics (D_{mean}, L_{beam}, L_{span}, a, a') and wood density (ρ).

Specimen type S_A-B	**D_{mean} [cm]**	**L_{beam} (≥19 D_{mean}) [cm]**	**L_{span} (≈18 D_{mean}) [cm]**	**a [cm]**	**a' [cm]**	**ρ [kg/m^3]**
B1-1	15.6	340	300	100	100	526
B2-5	16.7	401	300	100	100	638
B3-7	15.6	393	300	100	100	574
B4-8	15.5	302	270	90	90	614
B5-12	15.2	297	248	100	78	604
B6-13	15.1	302	270	90	90	622
B7-21	15.8	332	300	100	100	634
B8-24	13.8	315	270	90	90	554
B9-25	14.8	309	270	90	90	605
B10-27	14.3	278	246	90	78	627

7.3 TESTING EQUIPMENT AND SET-UP

The Mohr Federhaff AG testing machine was used with an hydraulic actuator having a loading capacity of 5000 kN, predisposed for force controlled tests (Fig. 7.3a). The testing equipment was constituted of the following tools: a loading cell HBM of 740 kN, displacement transducers (LVDT) with accuracy of 1×10^{-3}, an acquisition system (HBM-Spider 8) and a Personal Computer for data recording by means of the software Catman (v. 6.2).

According to the four-points static scheme, characterized by a constant bending moment zone and a maximum shear-to-bending moment ratio, the tested beams were supported by means of semi-cylindrical hinges, fixed to a test bed, and loaded with two symmetric concentrated forces, applied by

interposing a rigid steel profile between the actuator and the test specimen (Fig. 7.3b). In all tests the worst defects were randomly placed in the compression or tension zone.

During the tests 5 LVDTs were used (Fig. 7.4). Three traducers (LVDT 1, 2, 3) were placed on the specimen at the neutral axis, one on the mid-span section (LVDT1) and two near the loading points (LVDT 2,3), in order to measure the relative displacements at the central gauge length. The transducers LVDT 4, 5 measured the deflections at the mid-span of the beam, at the centre of the tension side edge, and the loading-actuator displacements, respectively.

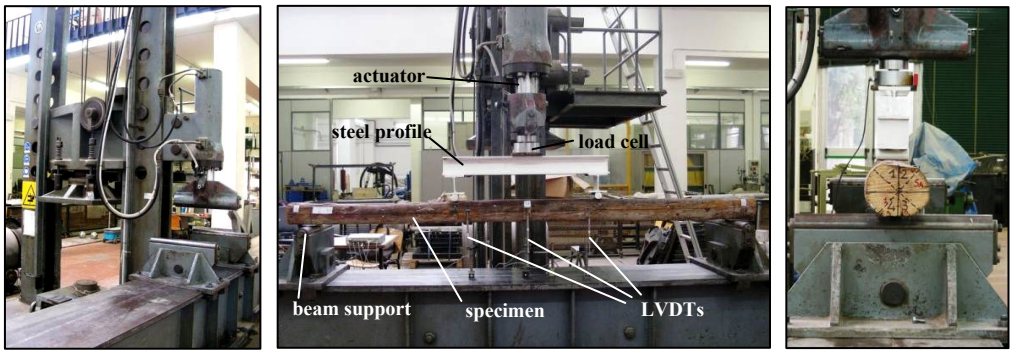

a) b)

Figure 7.3. Bending tests on specimens type S_A-B – Testing equipment and set-up: a) Mohr Federhaff AG machine of 5000 kN capacity; b) Specimen arrangement.

7.4 ELASTIC CYCLES

Three cycles in elastic ranges, equal to 3-6-9 kN, were carried out using a quasi-static loading procedure and limiting the maximum applied force within the conventional branch (0.4 F_{max}). The characteristic value in bending (UNI 11035-2), the standard static scheme and a specimen with mean dimensional sizes were considered for the determination of the expected failure load (F_{max}), as it is shown in Figure 7.5.

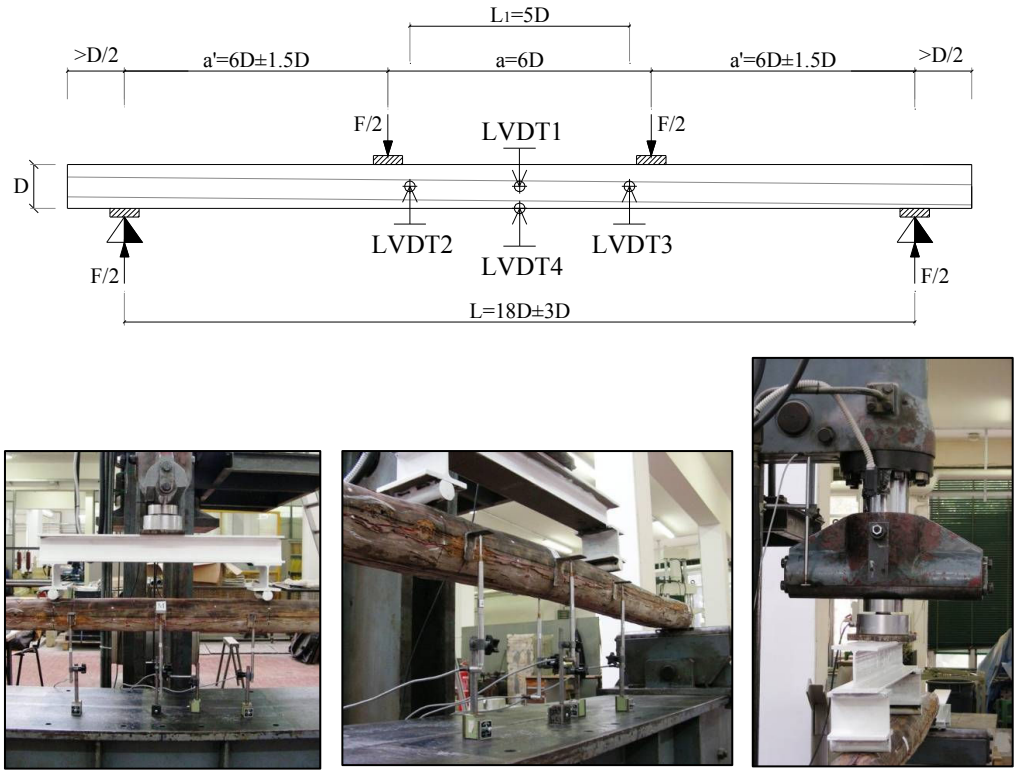

Figure 7.4. Bending tests on specimens type S_A-B – Testing equipment and set-up: displacement transducers (LVDTs) positioning.

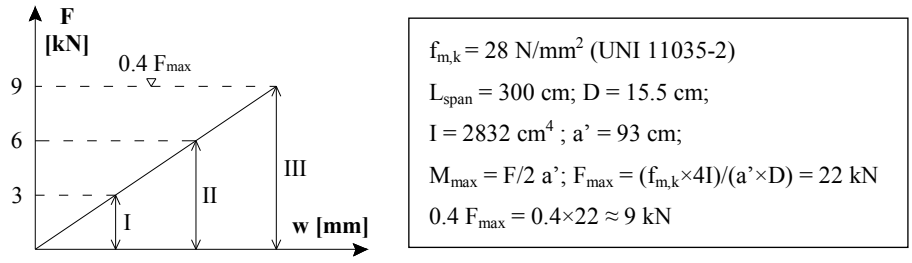

Figure 7.5. Bending tests on specimens type S_A-B – Elastic cycles: load ranges.

The relative displacements (w; LVDT 1, 2, 3) at the central gauge length (L_1) and the corresponding applied load (F) have been fitted in (F-w) curves in order to evaluate the local modulus of elasticity ($E_{m,l}$), as follow:

$$E_{m,l} = \frac{aL_1^2}{16I}\frac{\Delta F}{\Delta w}$$

where ΔF is the load increment on the straight-line portion and Δw is the increment of displacement corresponding; I is the second moment of area; a is the distance between a loading position and the nearest support; L_1 is the gauge length.

In the other hand, the deflection values at the mid-span of the specimen (w; LVDT 4) have been related to the actuator force (F) aiming at obtaining (F-w) diagrams and calculating the global elasticity modulus, given by:

$$E_{m,g} = \frac{23L^3}{1296I}\frac{\Delta F}{\Delta w}$$

where L is the length of the beam span.

As example, typical F-w curves are shown in Figure 7.6, with reference to the specimen S_A-B9-25.

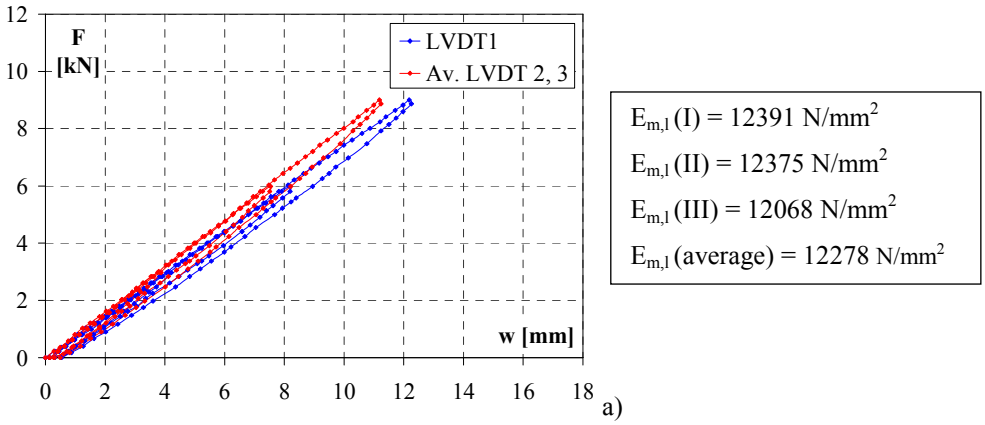

Figure 7.6. Bending tests on specimens type S_A-B – Elastic cycles – Typical F-w curves: a) Local modulus of elasticity ($E_{m,l}$); b) Global modulus of elasticity ($E_{m,g}$) (specimen S_A-B9-25). (continues)

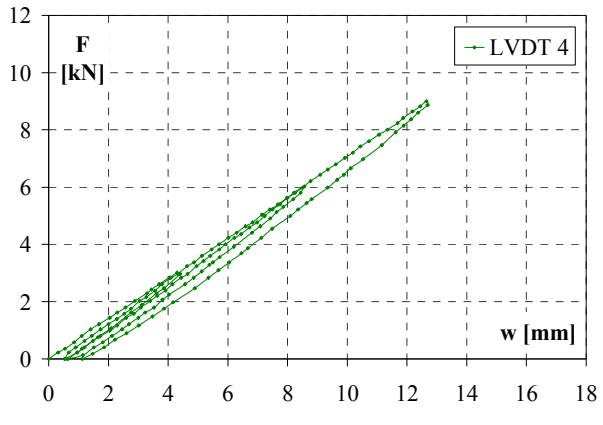

b)

$E_{m,g}$ (I) = 10307 N/mm^2
$E_{m,g}$ (II) = 11036 N/mm^2
$E_{m,g}$ (III) = 11011 N/mm^2
$E_{m,g}$ (average) = 11023 N/mm^2

Figure 7.6. Bending tests on specimens type S_A-B – Elastic cycles – Typical F-w curves: a) Local modulus of elasticity ($E_{m,l}$); b) Global modulus of elasticity ($E_{m,g}$) (specimen S_A-B9-25).

7.5 FAILURE CYCLES

After the elastic cycles, the specimens were tested in bending up to the failure. The test procedure consisted in several loading-reloading cycles, reaching the maximum force within 300±120 sec, according to UNI EN 408, and then reducing it up to the third of the reached peak load. Destructive tests results are provided in terms of applied actuator force (F) versus loading-actuator displacement (w; LVDT 5).

Figures 7.7 to 7.10 show the F-w curves for all tested beams in actual sizes.

On the conventional linear branch of the first loading cycle, ranging from 10% to 40% of the reached maximum load, the global modulus of elasticity has been calculated as:

$$E_{m,g} = \frac{23L^3}{1296I}\frac{(F_{40\%} - F_{10\%})}{(w_{40\%} - w_{10\%})}$$

Moreover, the ultimate bending strength has been evaluated by:

$$f_m = \frac{aF_{max}^{3}}{2W}$$

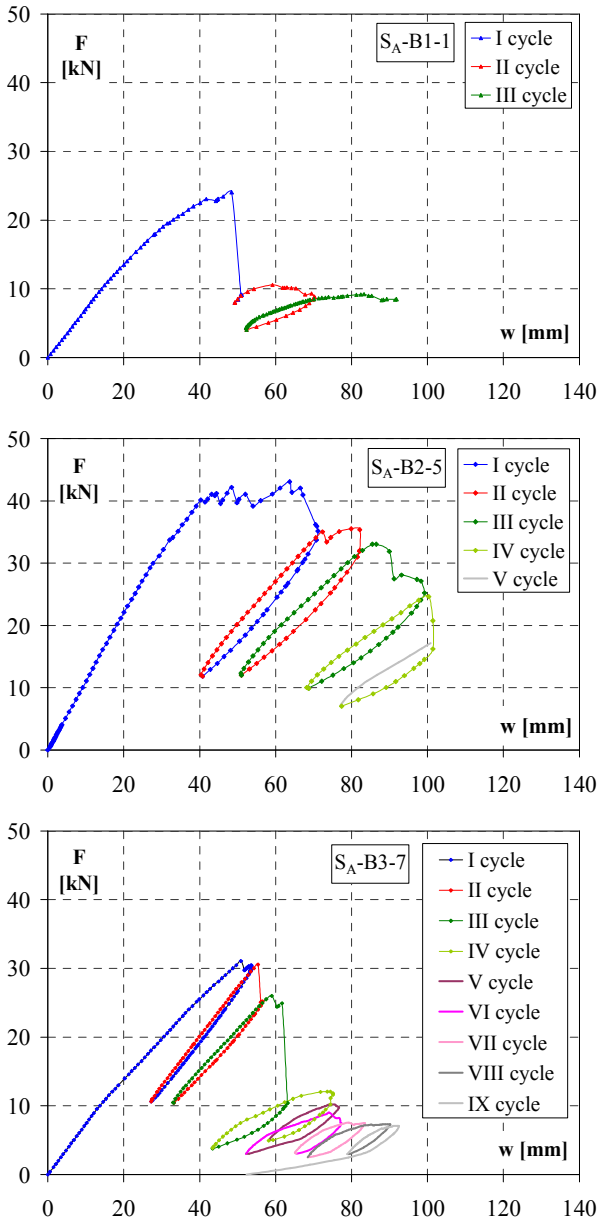

Figure 7.7. Bending tests on specimens type S_A-B – Failure cycles: F-w curves (specimens S_A-B1-1, S_A-B2-5 and S_A-B3-7).

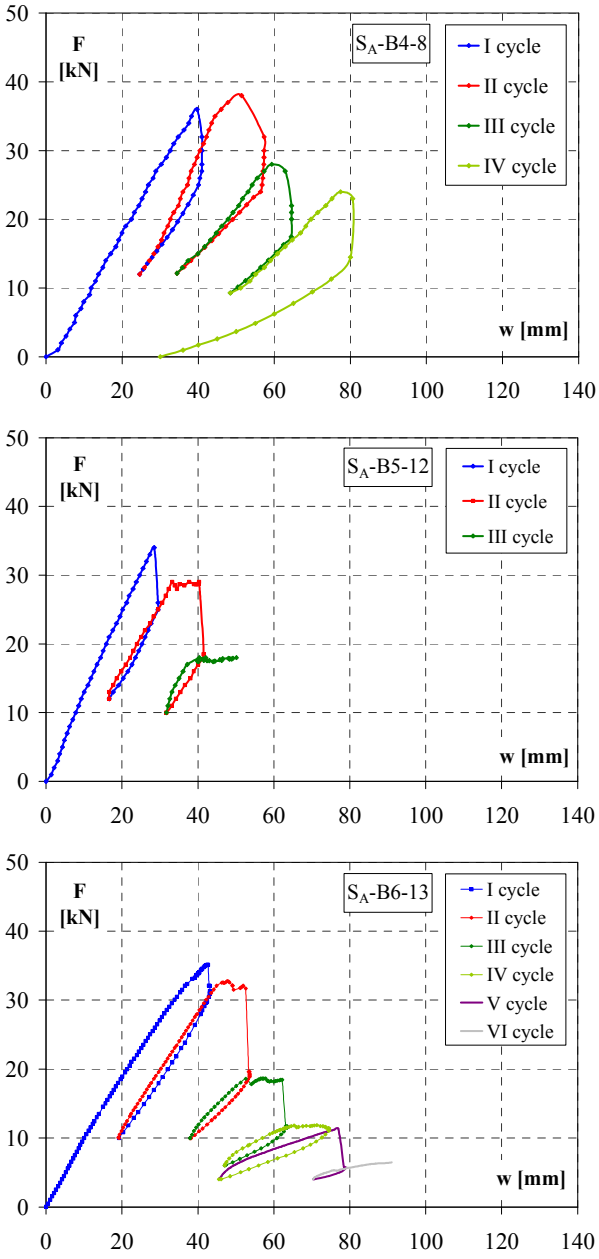

Figure 7.8. Bending tests on specimens type S_A-B – Failure cycles: F-w curves (specimens S_A-B4-8, S_A-B5-12 and S_A-B6-13).

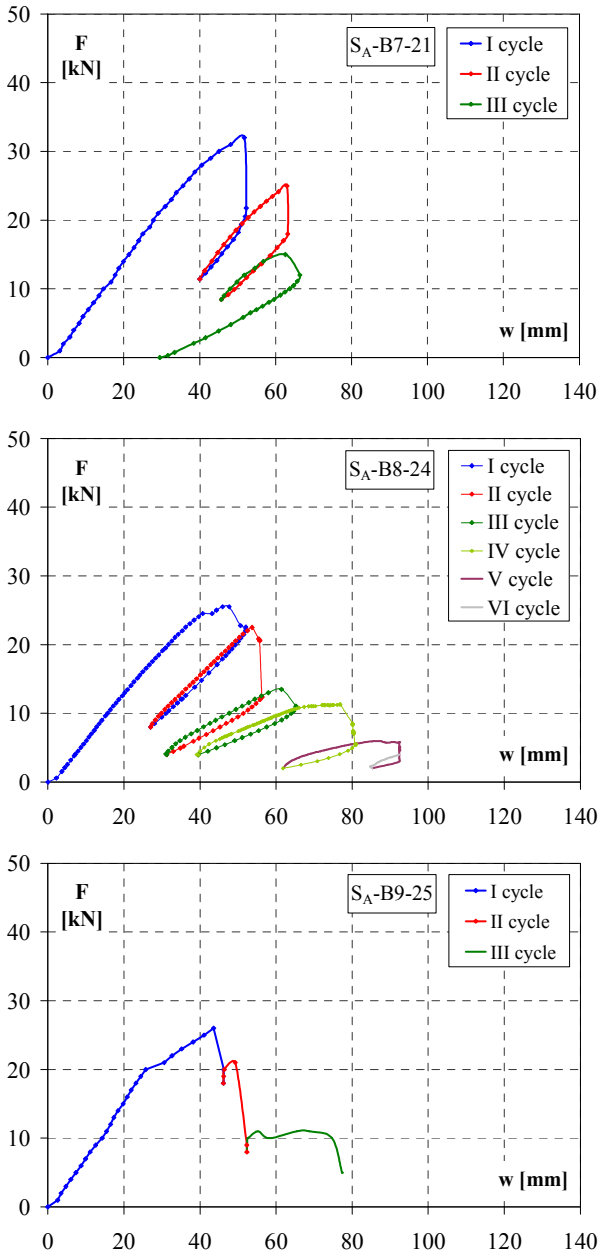

Figure 7.9. Bending tests on specimens type S_A-B – Failure cycles: F-w curves (specimens S_A-B7-21, S_A-B8-24 and S_A-B9-25).

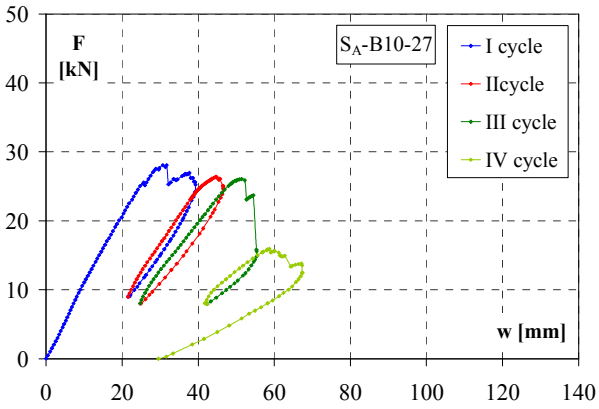

Figure 7.10. Bending tests on specimens type S_A-B – Failure cycles: F-w curves (specimen S_A-B10-27).

The F-w curves of the succeeding failure cycles have been enveloped aiming at evaluating the global behaviour in bending of the tested beams, as it is given in Figure 7.11. It is generally observed that the initial growing branch presents a linear behaviour up to the maximum applied load. Furthermore, after the second or third cycle, an evident reduction of strength occurs, together with an important actuator displacements.

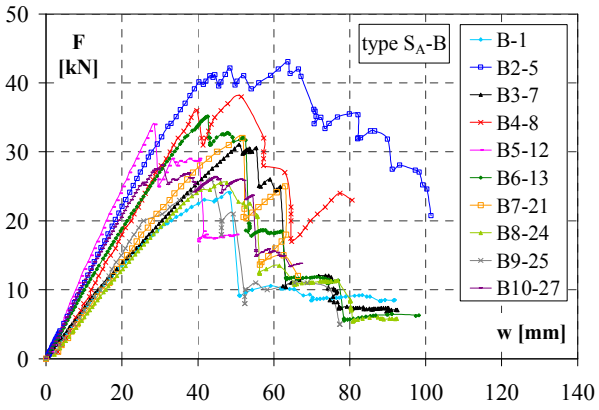

Figure 7.11. Bending tests on specimens type S_A-B – Failure cycles: F-w envelope curves.

Typical failure modes observed during the tests are shown in Figure 7.12. For almost all the specimens the failure mechanism was triggered around large knots located at the central zone and at the tensile edge of the beam cross-section. Therefore the presence of knots did not allow the development of the plastic behaviour in the compression side with consequent rupture at the tension one, manifested by tearing of the more stressed fibres (Fig. 7.12a). In any case an evident buckling the compressed fibres was manifested, followed by the propagation of slip phenomena (Fig. 7.12b).

a)

b)

Figure 7.12. Bending tests on specimens type S_A-B – Failure cycles – Typical collapse mechanism: a) Rupture at the tension side of the beams; b) Buckling mechanism at the compression side.

7.6 RESULTS AND DISCUSSION

In Table 7.2 the bending tests results are given in terms of local modulus of elasticity ($E_{m,l}$), global modulus of elasticity ($E_{m,g}$) calculated in both elastic range and in the first failure cycle, and maximum flexural strength (f_m) reached in the first three destructive cycles. The basic statistic of the measured mechanic properties are reported too, including minimum (min) or 5-percentile, average and maximum (max) values, standard deviation (SD) and coefficient of variation (CV).

Table 7.2. Bending tests on specimens type S_A-B: experimental results [N/mm^2].

	Elastic cycles		**Failure cycles**			
Specimen			**I cycle**		**II cycle**	**III cycle**
type S_A-B	**$E_{m,l}$**	**$E_{m,g}$**	**$E_{m,g}$**	**f_m**	**f_m**	**f_m**
B1-1	11257	10885	10993	32.2	14.2	12.3
B2-5	15291	15374	15336	46.9	38.7	36.0
B3-7	11029	11465	11409	42.0	41.3	35.2
B4-8	12683	12912	12842	44.4	46.9	34.6
B5-12	12162	13910	14188	38.3	31.0	19.2
B6-13	11023	12509	12710	46.7	43.5	24.5
B7-21	12647	13577	12202	40.4	32.5	19.5
B8-24	13120	13146	13187	44.9	39.6	23.7
B9-25	12278	11023	9403	36.6	29.5	15.4
B10-27	13858	13685	14448	38.5	36.2	35.7
min (5-per.)	11023	10885	9403	32.23	14.20	12.30
average	15291	12849	12672	41.09	35.34	25.61
max	12535	15374	15336	46.91	46.90	36.00
SD	1338	1416	1769	4.78	9.27	9.11
CV [%]	8.75	11.02	13.96	11.63	26.24	35.58

It can be stated the agreeable homogeneity provided by the bending behaviour in terms of both stiffness and strength. In fact $E_{m,l}$ presents a CV equal to 8.75 %, while $E_{m,g}$ shows a CV of 11.02 % and 13.96 %, respectively in elastic and failure cycles. A pleasant coefficient of variance is also provided by the ultimate bending strength (f_m, I cycle), equal to 11.63 % (Fig. 7.13a). Besides, it is possible to notice that the values of the global modulus of elasticity in elastic and failure cycles are very similar each other.

Furthermore, the mean ratio between $E_{m,l}$ and $E_{m,g}$ in elastic field is nearly equal to one for each specimen, contrary to the theoretical behaviour, which assumes the first value always higher than the second one, as no shear

deformation is taken into account for the evaluation of the local modulus of elasticity. Probably, the experimental results were influenced by the variability of the beams cross-section dimension through out their length.

The reduction of the load bearing capacity in bending, after the peak load reached during the tests, is emphasized by the strong values of strength variation coefficients in both second and third failure cycle (Fig. 7.13b).

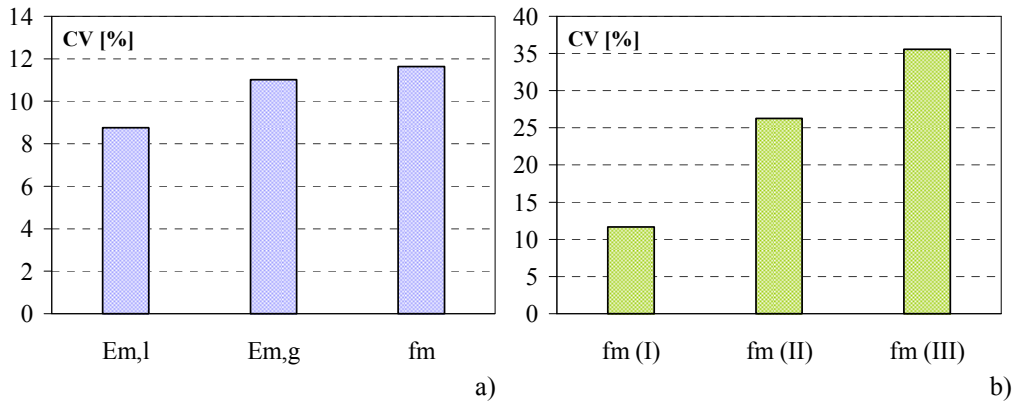

Figure 7.13. Bending tests on specimens type S_A-B – Experimental results – Variation coefficients (CV): a) Stiffness and strength properties; b) Bending strength in first (I), second (II) and third (III) failure cycles.

Finally, the experimental results have been examined in relation with the mechanical properties assumed by the European and Italian codes. In particular, the values of UNI 111035-2 for chestnut wood, EN 338 for D30 hardwood strength class and UNI 11119 for the third category class are considered. The following main conclusions are given:

- Good agreement is provided by comparing the experimental minimum (5-percentile) value of strength (32 N/mm^2) and the characteristic values assumed by UNI 11035-2 (28 N/mm^2) and EN 338 (D30; 30 N/mm^2; Table 7.3) standards;
- Comparing the admissible bending strength of UNI 11119-III (8 N/mm^2) with the average and 5-percentile results of laboratory tests, the obtained safety coefficients are equal to about 5 and 4, respectively (Table 7.3);

- The average value of the global modulus of elasticity obtained by the tests is about higher of 22 % than the mean value assumed by UNI 11035-2 and EN 339 (D30) and of 60 % than the same one reported in UNI 11119 for the third category class (Table 7.4).

Table 7.3. Bending tests on specimens type S_A-B – Experimental results: comparison between experimental strength and standard values [N/mm^2].

experimental results f_m			*UNI 11035-2*	*EN 338 D30*	*UNI 11119-III*
min (5-per.)	**average**	**max**	$f_{m,k}$	$f_{m,k}$	$\sigma_{m\ adm}$
32.23	41.09	46.91	28	30	8

Table 7.4. Bending tests on specimens type S_A-B – Experimental results: comparison between experimental global modulus of elasticity and standard values [N/mm^2].

experimental results $E_{m,g}$			*UNI 11035-2*	*EN 338 D30*	*UNI 11119-III*
min (5-per.)	**average**	**max**	$E_{0,mean}$	$E_{0,mean}$	E_f
10885	12849	15374	11000	10000	8000

Chapter 8
NDT-DT correlations for the mechanical characterization of timber

8.1 GENERAL

In the last phase of the whole research activity the experimental results of non-destructive (NDT) investigations and destructive (DT) tests have been analyzed by means of statistical methods aiming at providing a methodological process for *in situ* mechanical identification of ancient timber elements and structures, using combined non-destructive techniques.

Therefore, on the basis of NDT and DT parameters (Table 8.1), the following correlations have been examined by means of linear regression approach:

- *Correlations between NDT parameters*, relating the longitudinal and transversal measures by ultrasonic, sclerometric and resistographic tests;
- *Correlations between DT parameters*, for the definition of the mechanical behaviour in compression and bending of old chestnut timber;
- *NDT-DT correlations*, for non-destructive estimation of density, modulus of elasticity and strength of the material.

Table 8.1. NDT and DT parameters.

NDT parameters		**DT parameters**	
SWS:	ultrasonic stress wave speed [m/s]	ρ:	density [kg/m^3]
E_{dyn}:	dynamic modulus of elasticity [N/mm^2]	E_c:	modulus of elasticity in compression [N/mm^2]
PD:	sclerometric penetration depth [mm]	f_c:	compression strength [N/mm^2]
A_m:	resistographic mean amplitude [%]	E_m:	modulus of elasticity in bending [N/mm^2]
		f_m:	bending strength [N/mm^2]

Regression analysis is one of the most widely used statistical tools because it provides easy methods for establishing a functional relationship among response or dependent variables *(Y)* and predictors or independent variables *(X_1, X_2,...., X_k)*. Generally, the linear regression model can be explained as follow:

$$Y_i = \beta_0 + \beta_1 X_1 + \beta_2 X_2 + ... + \beta_k X_k + \varepsilon_i$$

where β_0, β_1,..., β_k, called the regression parameters or coefficients, are unknown constants to be determined from the data; ε is the random error, which accounts for the failure of the model to fit the data exactly, representing the discrepancy in the approximation.

The parameters can be determined by means of the most commonly used method, called the *least square error* (LSE). Therefore, in simple linear regression, when one single predictor is involved in the model, the estimated equation represents a line; whereas in multiple analysis, when *k* predictors variables are considered, the regression function represents a plane in cases of two predictors or a hyperplane in cases of more than two predictors.

The quality of the fit in both simple and multiple regression can be assessed directly from the examination of the scatter plots of *Y* versus X_i, and evaluated formally by means of *goodness-of-fit index*, R^2, which is a summary measure to judge the fit of the linear model to a given body of data. R^2 is known as the coefficient of determination because it represents the correlation between the dependent variable and the predicted variable explained by all the

predictors. Note that $0 \leq R^2 \leq 1$, high values of the coefficient indicate a strong linear relationship between the variables involved in the model. It is worth noticing that, for simple regression, R^2 is the square of the Pearson correlation coefficient, which is as a measure of the strength of linear dependence between two variables, giving a value between +1 and −1 inclusive.

Usually, a quantity related to R^2, known as adjusted R-square, is also used for judging the goodness of fit and comparing models having different number of observations *n* and/or of predictor variables *k*. It is defined as:

$$R^2_{adj} = 1 - \frac{n-1}{n-k-1}\left[1 - R^2\right]$$

A large value of R^2 does not necessarily mean that the model adequately fits and describes the data. Therefore, a more detailed analysis is needed, based on statistical inference regarding the regression coefficients. A more formal way of measuring the usefulness of linear fit is to conduct appropriate tests of hypothesis for both individual regression parameters, such as *Student's t-test*, and all predictor variables, such as F-test or ANOVA (ANalysis Of VAriance).

In this chapter correlations based on NDT and DT parameters are statistically analyzed taking into account the theoretical criteria of the linear regression. Scatter plots among the variables, together with the fitted lines or planes are reported, the estimated regression equations are given and the quality of the correlations are defined by the identification of coefficient of determination ranges (R^2; Table 8.2). In particular, for the prediction of timber physical and mechanical properties, combined NDT-DT methods are examined by means of the software SPSS v. 17., based on both simple and multiple linear regression model.

Table 8.2. Coefficient of determination (R^2) ranges.

Range	Correlation
$0.0<R^2<0.1$	low
$0.1<R^2<0.2$	moderate
$0.2<R^2<0.4$	medium
$0.4<R^2<0.6$	good
$0.6<R^2<1.0$	high

8.2 CORRELATIONS BETWEEN NDT PARAMETERS

In the first phase of data elaboration, non-destructive parameters have been correlated each other by means of simple linear regression model, aiming at evaluating the relationships between parameters of different NDT methods (ultrasonic, sclerometric and resistographic) and among longitudinal and transversal measures.

Including in the model all NDT test results, the obtained coefficients of determination (R^2) are provided in Tables 8.3 to 8.5, for the structural elements in actual dimensions (S_A-C + S_A-B), small sizes (S_S-C + S_S-NDT) and both groups (S_A + S_S), respectively.

Table 8.3. Correlations between NDT parameters – Coefficients of determination (R^2) for specimens type S_A-C + S_A-B (n=24).

	SWS_L	PD_L	$A_{m,L}$	SWS_T	PD_T	$A_{m,T}$
SWS_L	1.000	0.018	0.004	0.036	0.007	0.055
PD_L		1.000	0.115	0.016	0.703	0.083
$A_{m,L}$			1.000	0.011	0.264	0.535
SWS_T				1.000	0.020	0.042
PD_T					1.000	0.125
$A_{m,T}$						1.000

Table 8.4. Correlations between NDT parameters – Coefficients of determination (R^2) for specimens type S_S-C + S_S-NDT (n=36).

	PD_L	$A_{m,L}$	PD_T	$A_{m,T}$
PD_L	1.000	0.188	0.450	0.330
$A_{m,L}$		1.000	0.442	0.376
PD_T			1.000	0.498
$A_{m,T}$				1.000

Table 8.5. Correlations between NDT parameters – Coefficients of determination (R^2) for specimens type S_A + S_S (n=60).

	PD_L	$A_{m,L}$	PD_T	$A_{m,T}$
PD_L	1.000	0.235	0.295	0.261
$A_{m,L}$		1.000	0.061	0.474
PD_T			1.000	0.159
$A_{m,T}$				1.000

Moderate inverse relationships have been found between sclerometric and resistographic variables in both parallel (R^2=0.24; Fig. 8.1a) and perpendicular (R^2=0.16; Fig. 8.1b) to grain direction. Like it was expected, the drilling resistance is lower when wood quality, evaluated by hardness testing method, is in worst condition. For longitudinal measurements (Fig. 8.1a) the regression lines of two specimens groups are nearly overlapped; therefore a medium correlation is provided by the single group of elements. Different response were obtained by transversal analysis, as, on the lateral surface of the specimens in actual sizes, higher values of penetration depth were recorded, due to the poor conservation state of the more superficial layers of wood.

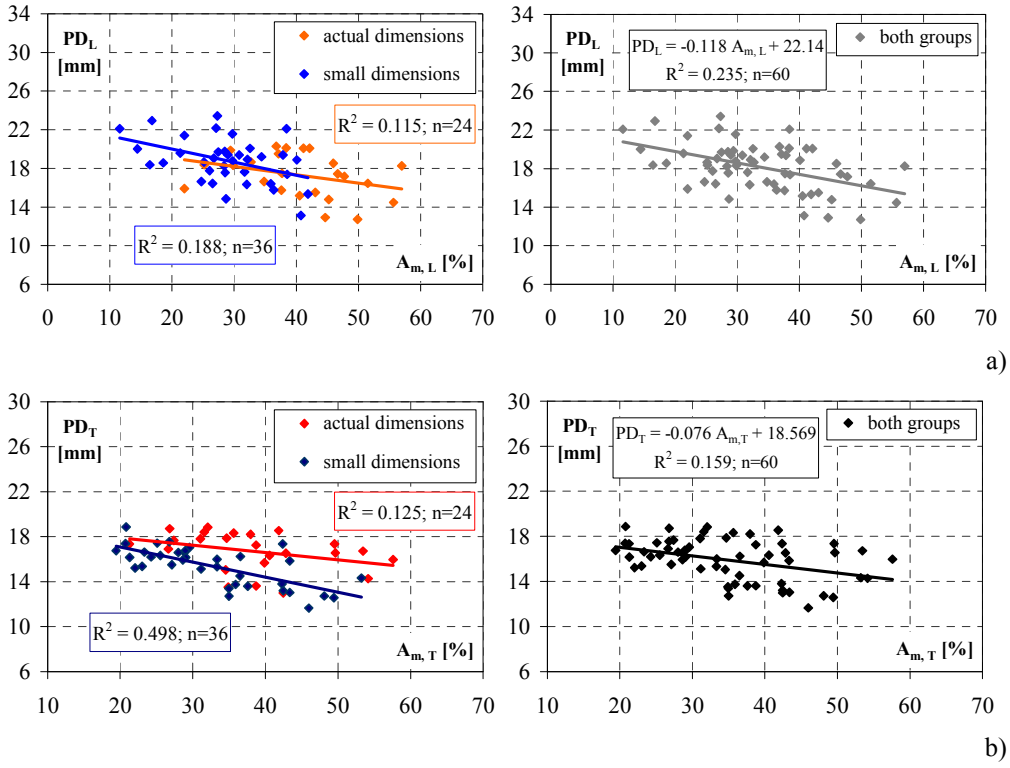

Figure 8.1. Correlations between NDT parameters – Penetration depth (PD) vs mean amplitude (A_m) a) Longitudinal; b) Transversal.

Generally, *in situ* investigations allow only perpendicular to grain measurements on the accessible external faces of the timber members.

Therefore, the acquaintance of a probable relation between longitudinal and transversal NDT parameters seems to be extremely important.

By means of ultrasonic investigations, discordance among axial and transverse stress wave speed (SWS) was observed, according to the orthotropic behaviour of wood. In fact the longitudinal velocity is about three times the same one in transversal direction for all specimens, but no linear agreements is found between these ultrasonic properties. Instead, as the sclerometric and resistographic results seem independent by the tests orientation, medium and good longitudinal-transversal correlations are provided by penetration depth (R^2=0.30; Fig. 8.2a) and mean amplitude (R^2=0.47; Fig. 8.2b) respectively, when the results of all samples are analyzed.

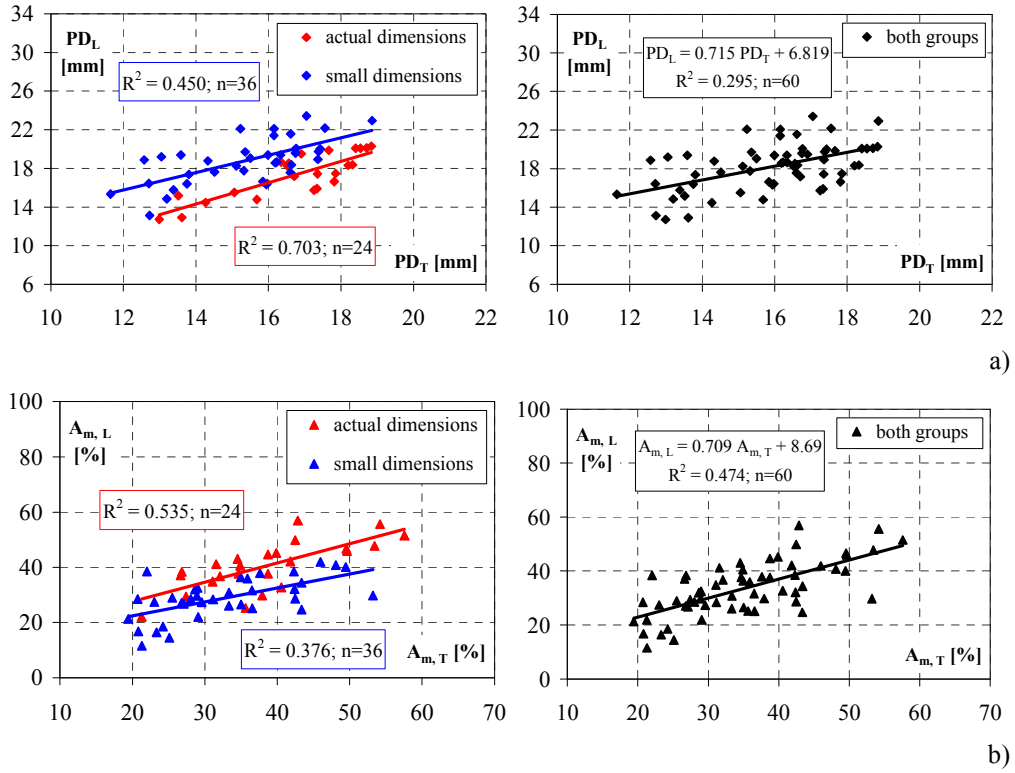

Figure 8.2. Correlations between NDT parameters – Longitudinal (L) vs Transversal (T): a) Penetration depth (PD); b) Mean amplitude (A_m).

8.3 CORRELATIONS BETWEEN DT PARAMETERS

8.3.1 *Compression tests*

8.3.1.1 Parallel to grain

In this section, concerning the experimental results by destructive tests in parallel compression, the relationships among physical, stiffness and strength properties are studied. The statistical analysis emphasizes that a linear correlation between density (ρ), modulus of elasticity ($E_{c,0}$) and strength ($f_{c,0}$) seems adequate to represent the test results. In fact, good and high coefficients of determination (R^2) have been achieved for each group of both structural and defect-free specimens, given in Table 8.6. The corresponding scatter plots and fitted lines are represented in Figure 8.3.

As a result of many years of investigation and observation regarding to the physical-mechanical characterization of wood, density appears one of the main factor that influence the material behaviour. Accordingly, the correlations presented in Figure 8.3a show that the higher the density, the greater the modulus of elasticity of wood and timber specimens. Figure 8.3b leads to the same conclusion, but referred to the compression strength, which is strongly related with wood density. Furthermore, Figure 8.3c shows good relationships between the axial stress and the modulus of elasticity.

Table 8.6. Correlations between DT parameters – Compression tests parallel to grain: coefficients of determination (R^2) for all groups of specimens.

	actual dimensions S_A-C (n=14)			*small dimensions* S_S-C (n=20)			*defect-free* DF-C_L (n=33)		
	ρ	**$E_{c,0}$**	**$f_{c,0}$**	**ρ**	**$E_{c,0}$**	**$f_{c,0}$**	**ρ**	**$E_{c,0}$**	**$f_{c,0}$**
ρ	1	0.435	0.517	1	0.670	0.592	1	0.468	0.829
$E_{c,0}$		1	0.547		1	0.476		1	0.581
$f_{c,0}$			1			1			1

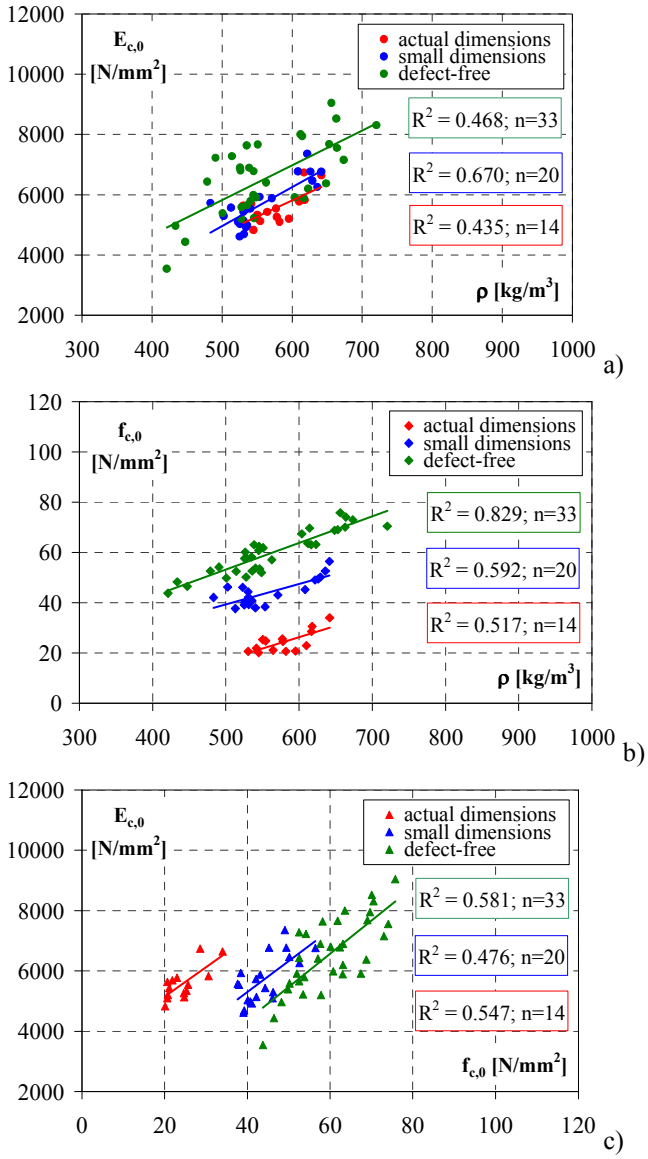

Figure 8.3. Correlations between DT parameters – Compression tests parallel to grain: a) Modulus of elasticity ($E_{c,0}$) vs density (ρ); b) Strength ($f_{c,0}$) vs density (ρ); c) Modulus of elasticity ($E_{c,0}$) vs strength ($f_{c,0}$).

It is important to observe that, for all DT correlations, the experimental regression lines, obtained for both the samples in actual and small dimensions and the defect-free specimens (Fig. 8.3), are perfectly parallel each other, as the similar slope of the estimated regression equations confirm (Table 8.7).

The comparison between the results in terms of adjusted coefficients of determination (R^2_{adj}; Table 8.7), emphasizes that for $f_{c,0}$ *vs* ρ relations, the results improve when the defectiveness of the material is negligible. In fact the defect-free sample provide the highest R^2_{adj}, equal to about 0.80 (Fig. 8.4). Therefore, the presence of faults, their location and kind, grain inclination and geometrical anomalies, influence to great extent timber behaviour in compression parallel to grain.

Table 8.7. Correlations between DT parameters – Compression tests parallel to grain: adjusted coefficients of determination (R^2_{adj}) and linear regression equations.

Specimens type	**$E_{c,0}$ vs ρ**	**$f_{c,0}$ vs ρ**	**$E_{c,0}$ vs $f_{c,0}$**
actual dimensions S_A-C (n=14)	$E_{c,0}$=-663.06+10.787 ρ (R^2_{adj}=0.388)	$f_{c,0}$=-27.659+0.09 ρ (R^2_{adj}=0.477)	$E_{c,0}$= 3220.4+96.767 $f_{c,0}$ (R^2_{adj}=0.509)
small dimensions S_S-C (n=20)	$E_{c,0}$=-1526.4+12.972 ρ (R^2_{adj}=0.652)	$f_{c,0}$=-1.406+0.08 ρ (R^2_{adj}=0.569)	$E_{c,0}$= 1166.5+103.21 $f_{c,0}$ (R^2_{adj}=0.447)
defect-free DF-C_L (n=33)	$E_{c,0}$=75.156+11.504 ρ (R^2_{adj}=0.451)	$E_{c,0}$= 0.168+0.106 ρ (R^2_{adj}=0.823)	$E_{c,0}$=-33.456+110.01 $f_{c,0}$ (R^2_{adj}=0.567)

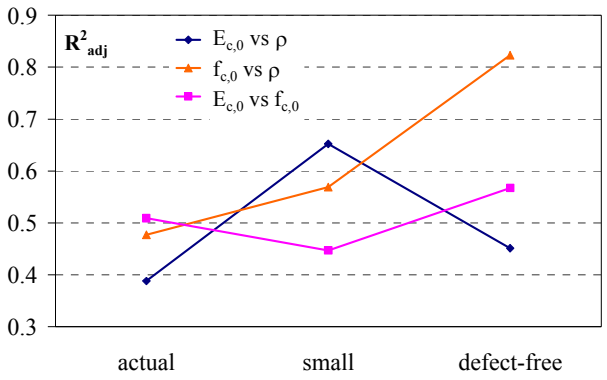

Figure 8.4. Correlations between DT parameters – Compression tests parallel to grain: comparison between R^2_{adj} values of actual, small and defect-free samples.

8.3.1.2 Perpendicular to grain

From studies aiming to characterize the physical and mechanical properties of wood when loaded in transverse compression, it is frequent to adopt a non-linear relation between strength ($f_{c,90}$) and density (ρ), given by:

$$f_{c,90} \approx (\rho)^{\alpha}$$

where α is a constant ranging between 1.5 and 2.3. This value depends on growth rings orientation, specimen dimensions and criteria for definition failure. In absence of more information, α value of a equal to 1.7 is recommended (Gehri, 1998).

EN 384 standard proposes the following characteristic strength value in compression normal to grain for softwood:

$$f_{c,90,k} = 0.015 \cdot \rho_k$$

Concerning the obtained experimental results, in Figure 8.5 the relationships between DT parameters by compression tests perpendicular to grain on clear elements, in both radial (specimens type DF-C_{rad}) and tangential direction (specimens type DF-C_{tg}), are illustrated. The $E_{c,90}$ *vs* ρ and $f_{c,90}$ *vs* ρ correlations (Fig. 8.5a, b), appear to be of exponential type, while for $E_{c,90}$ *vs* $f_{c,90}$ linear agreement is found. Furthermore, medium and good R^2-values are provided when all perpendicular tests results, in both radial and tangential orientation, are involved in the regression model.

8.3.2 *Bending tests*

The experimental mechanical proprieties by bending tests on full-scale beams have been correlated each other, according to simple linear regression model. The DT parameters used in the analysis are the wood density (ρ), local ($E_{m,l}$) and global ($E_{m,g}$) modulus of elasticity and flexural strength (f_m). The statistical results are presented in Table 8.8 and in Figure 8.6.

Generally, the results show moderate and medium correlations (Fig. 8.6a, b, c), apart for the relation between the local and global modulus of elasticity, which provide a good linear agreement (R^2=0.63; Fig. 8.6d).

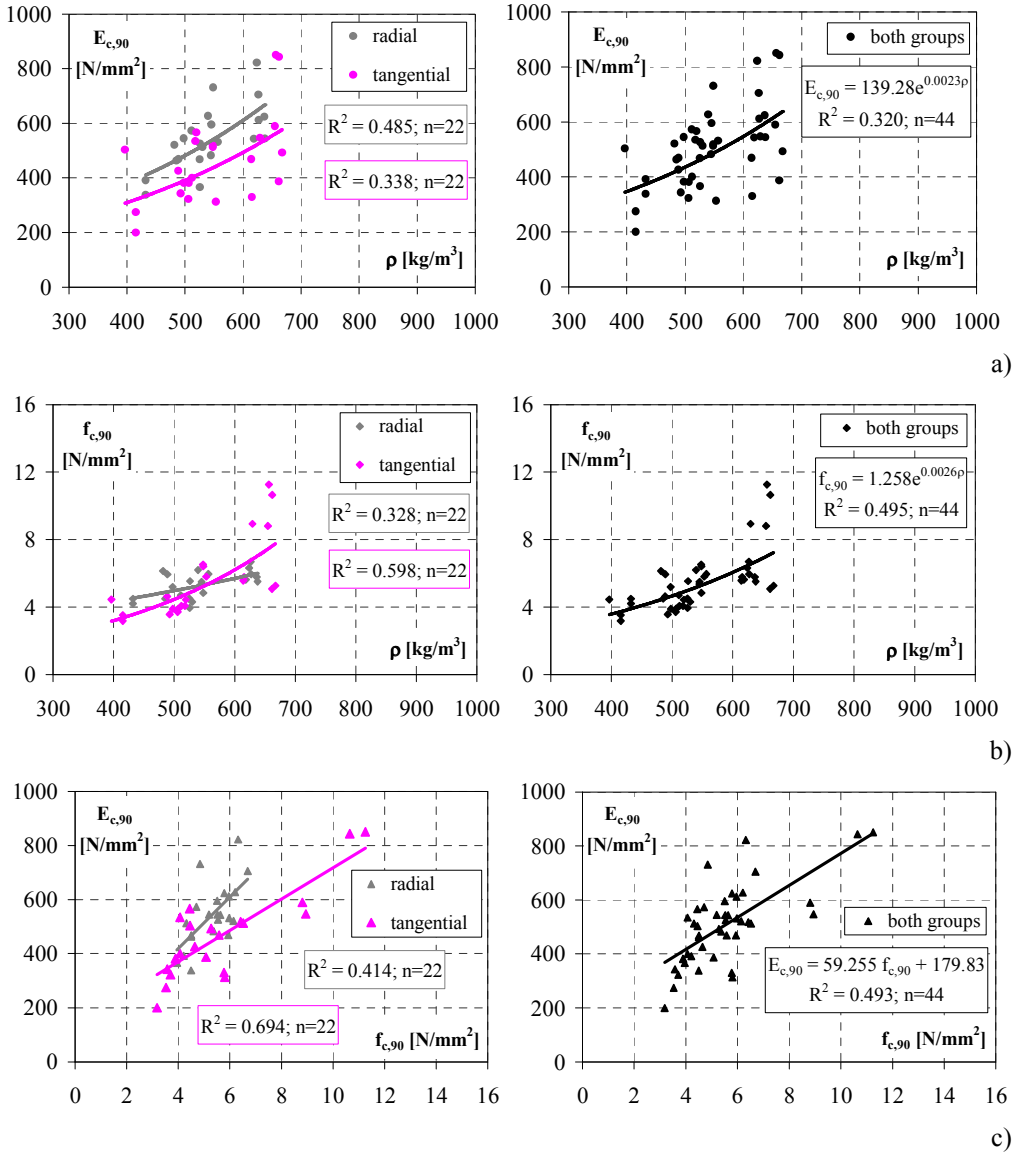

Figure 8.5. Correlations between DT parameters – Compression tests perpendicular to grain: a) Modulus of elasticity ($E_{c,90}$) vs density (ρ); b) Strength ($f_{c,90}$) vs density (ρ); c) Modulus of elasticity ($E_{c,00}$) vs strength ($f_{c,90}$).

Table 8.8. Correlations between DT parameters – Bending tests: coefficients of determination (R^2)

	ρ	$E_{m,l}$	$E_{m,g}$	f_m
ρ	1.000	0.241	0.408	0.207
$E_{m,l}$		1.000	0.628	0.108
$E_{m,g}$			1.000	0.291
f_m				1.000

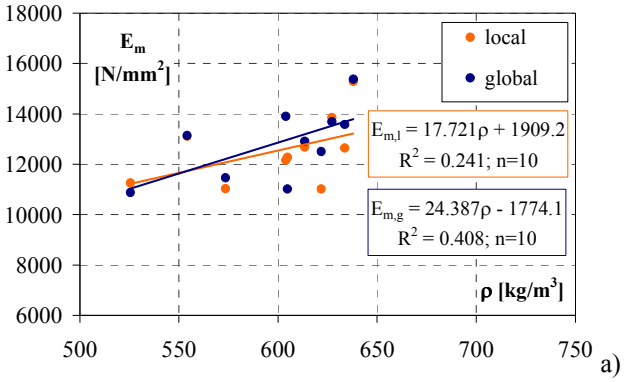

a)

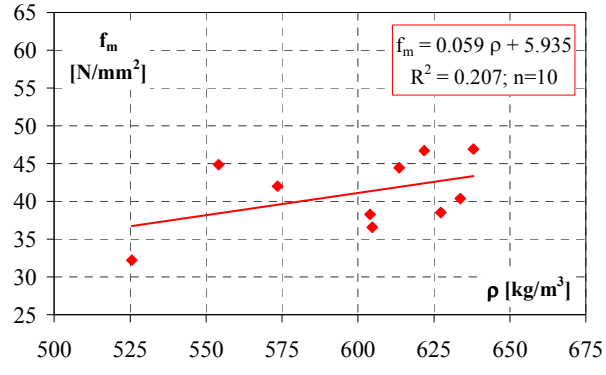

b)

Figure 8.6. Correlations between DT parameters – Bending tests: a) Modulus of elasticity (E_m) vs density (ρ); b) Strength (f_m) vs density (ρ); c) Modulus of elasticity (E_m) vs strength (f_m); d) Global modulus ($E_{m,g}$) vs Local modulus ($E_{m,l}$). (continues)

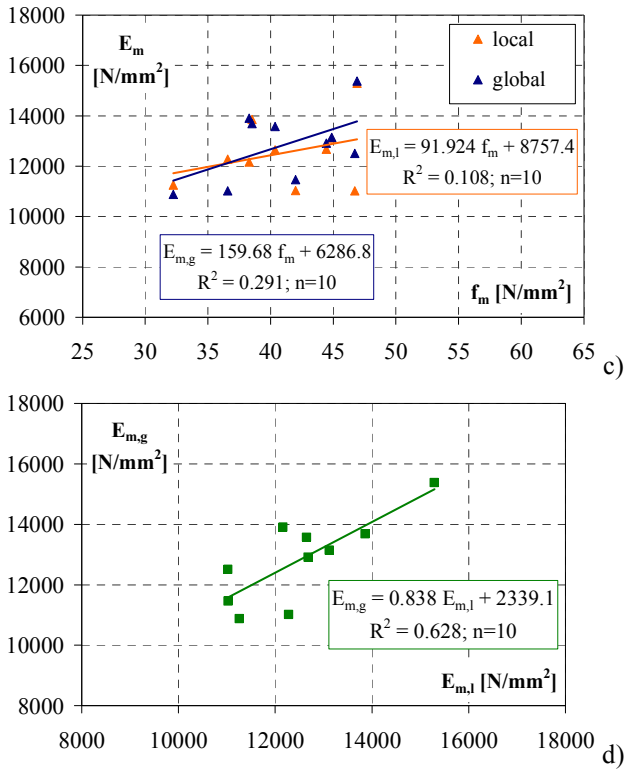

Figure 8.6. Correlations between DT parameters – Bending tests: a) Modulus of elasticity (E_m) vs density (ρ); b) Strength (f_m) vs density (ρ); c) Modulus of elasticity (E_m) vs strength (f_m); d) Global modulus ($E_{m,g}$) vs Local modulus ($E_{m,l}$).

8.4 NDT-DT CORRELATIONS

8.4.1 *Estimation of wood density*

8.4.1.1 Simple methods

Firstly, aiming at evaluating the efficiency on NDT techniques as useful supplement for mechanical characterization of timber, the correlations between ultrasonic, sclerometric and resistographic parameters with wood

density (ρ) have been examined. The R^2-coefficients are given in Table 8.9 and the results are plotted in Figures 8.7.

Relating the wood density with drill-resistance (A_m), the regression lines of elements in both actual and small dimensions are quite coincident and good correlations have been found for both specimens groups in longitudinal (R^2=0.55) and transversal (R^2=0.52) measurements (Fig. 8.8a, b).

On the other hand, when the pin penetration depth (PD) is correlated with density, different responses are provided by the two kinds of samples (Fig. 8.7). Taking in mind that the transversal sclerometric technique is influenced by the conservation state of the superficial wooden layers, the statistical results confirm that, for the elements in actual sizes, often damaged and affected by macroscopic defects on their lateral surface, ρ *vs* PD_T relation is characterized by larger scatters in the results (R^2=0.30; Fig. 8.7b). At the contrary, for the small specimens, almost free from faults, the same analysis shows high agreement between density values and transversal sclerometric parameters (R^2=0.80; Fig. 8.7b). Therefore, when both groups of samples are considered, medium relationship is found (R^2=0.33). Test hammer method in parallel to grain direction also provides medium correlations for both two tested samples and all specimens (R^2=0.38; Fig. 8.7a).

Table 8.9. NDT-DT correlations – Estimation of wood density by simple methods: coefficients of determination (R^2).

Specimens	**Ultrasonic [m/s]**		**Sclerometric [mm]**		**Resistographic [%]**	
type	SWS_L	SWS_T	PD_L	PD_T	$A_{m,L}$	$A_{m,T}$
actual dimensions S_A-C + S_A-B (n=24)	0.000	0.020	0.242	0.300	0.669	0.426
small dimensions S_S-C + S_S-NDT (n=36)	-	-	0.388	0.810	0.508	0.526
both groups S_A + S_S (n=60)	-	-	0.383	0.331	0.554	0.518

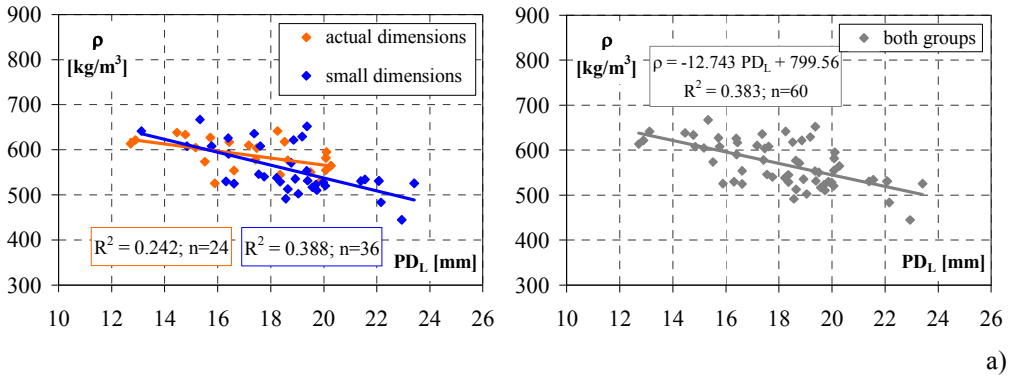

Figure 8.7. NDT-DT correlations – Estimation of wood density by sclerometric method – Density (ρ) vs penetration depth (PD): a) Longitudinal; b) Transversal.

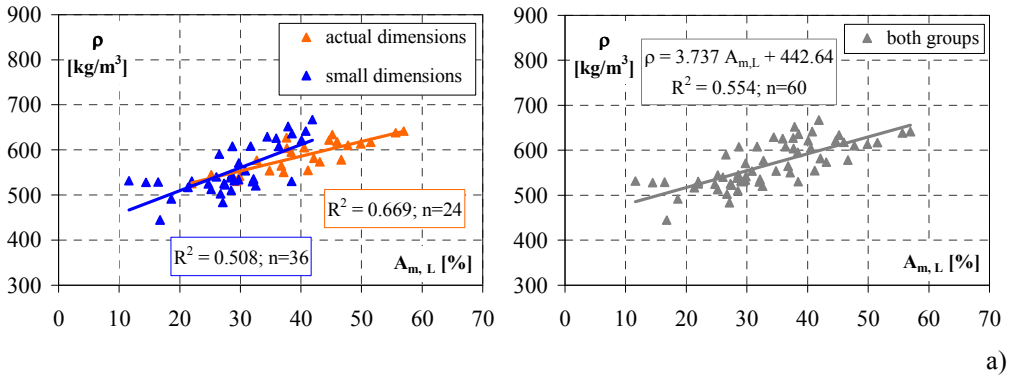

Figure 8.8. NDT-DT correlations – Estimation of wood density by resistographic method – Density (ρ) vs mean amplitude (A_m): a) Longitudinal; b) Transversal. (continues)

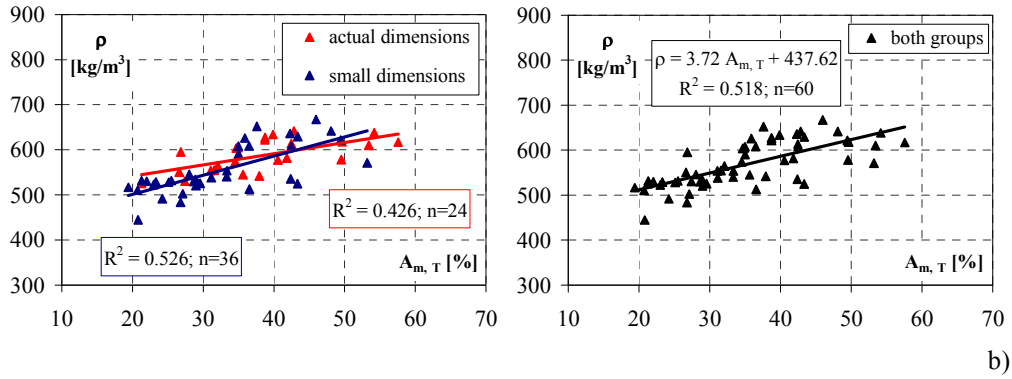

b)

Figure 8.8. NDT-DT correlations – Estimation of wood density by resistographic method – Density (ρ) vs mean amplitude (A_m): a) Longitudinal; b) Transversal.

8.4.1.2 Combined methods

In order to study which combined NDT parameters that can be used for prediction of wood density, multiple liner regression analysis has been carried out, summarized in Table 8.10 in form of R^2-coefficients.

It appears that, including in the model the sclerometric and resistographic variables of all structural elements (n=60), the combination of pin penetration depth (PD) and drilling resistance (A_m) provides strong correlations with wood density, being R^2 equal to about 0.80 for both parallel and transverse methods. These results are represented in Figure 8.8 where the 3D scatter plots together with regression fitted planes are depicted.

With regards to the elements in actual dimensions (n=24), adding in the model also the stress wave speed (SWS), obtained by both direct and indirect ultrasonic tests, high regression-coefficients have been found too (R^2=0.72-0.73).

Table 8.10. NDT-DT correlations – Estimation of wood density by combined methods: coefficients of determination (R^2).

Sclerometric + Resistographic (n=60)		**Ultrasonic + Sclerometric + Resistographic** (n=24)	
$PD_L + A_{m,L}$	$PD_T + A_{m,T}$	$SWS_L + PD_L + A_{m,L}$	$SWS_T + PD_T + A_{m,T}$
0.801	0.785	0.721	0.731

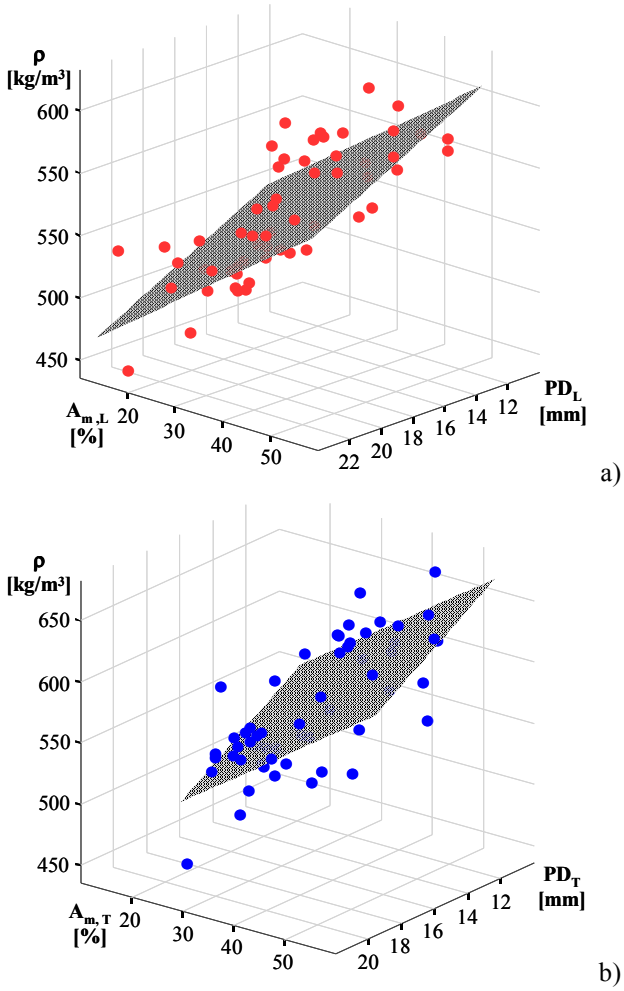

Figure 8.8. NDT-DT correlations – Estimation of wood density – Sclerometric and resistographic combined methods: a) Longitudinal; b) Transversal.

For non-destructive prediction of wood density, all useful models are summarized in Table 8.11. The involved NDT parameters and the corresponding linear regression functions are also given. In addition, the obtained adjusted regression-coefficients (R^2_{adj}) are compared in Figure 8.9. It is worth noticing that similar values have been obtained by means of longitudinal and transversal tests.

Table 8.11. NDT-DT correlations – Estimation of wood density by combined methods: adjusted coefficients of determination (R^2_{adj}) and linear regression equations.

Longitudinal tests			
Model	**NDT parameters**	**R^2_{adj}**	**Linear regression equations**
R_L	$A_{m,\,L}$	0.546	$\rho = 442.64 + 3.737\ A_{m,\,L}$
$S_L + R_L$	$PD_L + A_{m,\,L}$	0.628	$\rho = 596.483 - 6.949\ PD_L + 2.916\ A_{m,\,L}$
$U_L + S_L + R_L$	$SWS_L + PD_L + A_{m,\,L}$	0.680	$\rho = 539.894 - 0.031\ SWS_L - 3.819\ PD_L + 2.959\ A_{m,\,L}$
Transversal tests			
Model	**NDT parameters**	**R^2_{adj}**	**Linear regression equations**
R_T	$A_{m,\,T}$	0.509	$\rho = 437.62 + 3.72\ A_{m,\,T}$
$S_T + R_T$	$PD_T + A_{m,\,T}$	0.603	$\rho = 609.774 - 9.271\ PD_T + 3.014\ A_{m,\,T}$
$U_T + S_T + R_T$	$SWS_L + PD_T + A_{m,\,T}$	0.675	$\rho = 830.66 - 0.118\ SWS_T - 8.027\ PD_T + 2.213\ A_{m,\,T}$

(*) U: ultrasonic [m/sec]; S: sclerometric [mm]; R: resistographic [%]

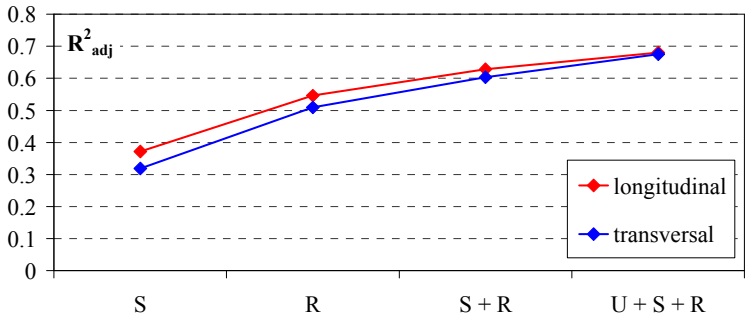

Figure 8.9. NDT-DT correlations – Estimation of wood density by combined methods: comparison between R^2_{adj} values.

On the basis of the statistical results, the following simple and combined techniques could be taken in practical applications for a quick and quantitative estimation of wood density:

- R: resistographic ($R^2_{adj} \approx 0.52$);
- S+R: sclerometric with resistographic ($R^2_{adj} \approx 0.60$);
- U+S+R: all non-destructive techniques, including ultrasonic investigations ($R^2_{adj} \approx 0.68$).

8.4.2 *Prediction of modulus of elasticity in compression parallel to grain*

8.4.2.1 Simple methods

Statistical analysis to quantify the agreements of NDT parameters with modulus of elasticity by destructive tests in compression parallel to grain is provided in Table 8.12 and in Figures 8.10 and 8.11. Two samples are considered, structural elements in actual (n=14) and small dimensions (n=20), and simple linear regression model is used.

R^2-values are low for the relationships with ultrasonic stress wave speed (SWS); whereas, reasonable correlations have been found with both sclerometric and resistographic variables. In particular, transversal wood test hammer measures (PD_T; $R^2 \approx 0.60$; Fig. 8.10b) and longitudinal microdrilling values ($A_{m,\ L}$; $R^2 \approx 0.45$; Fig. 8.11a) appear the most adequate for a quick prediction of stiffness properties of the material. Nearly similar R^2-values are provided by the two groups of specimens.

Table 8.12. NDT-DT correlations – Prediction of modulus of elasticity in compression parallel to grain by simple methods: coefficients of determination (R^2).

Specimens type	**Ultrasonic [m/s]**		**Sclerometric [mm]**		**Resistographic [%]**	
	SWS_L	SWS_T	PD_L	PD_T	$A_{m,\ L}$	$A_{m,\ T}$
actual dimensions S_A-C (n=14)	0.030	0.034	0.323	0.506	0.421	0.303
small dimensions S_S-C (n=20)	-	-	0.218	0.656	0.493	0.292

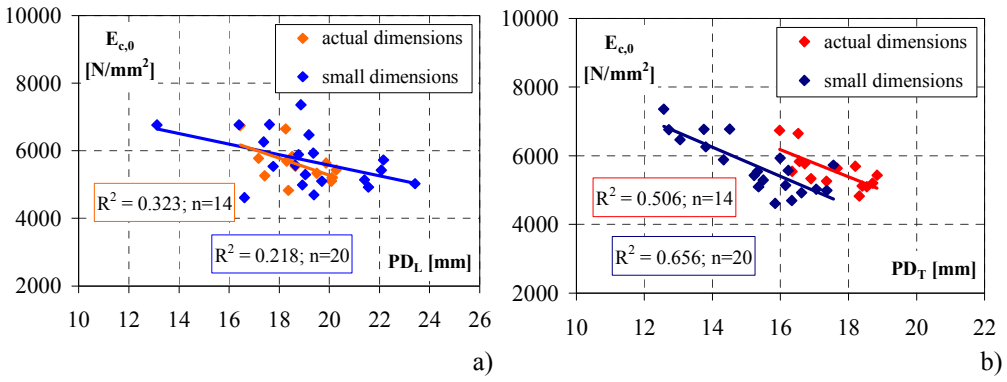

Figure 8.10. NDT-DT correlations – Prediction of modulus of elasticity in compression parallel to grain – Sclerometric method: a) Longitudinal; b) Transversal.

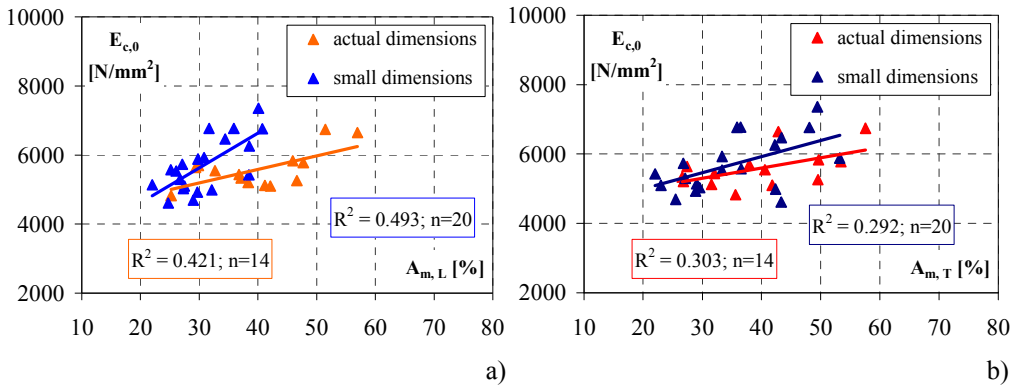

Figure 8.11. NDT-DT correlations – Prediction of modulus of elasticity in compression parallel to grain – Resistographic method: a) Longitudinal; b) Transversal.

8.4.2.2 Combined methods

The multiple linear regression analysis has been shown that the combined sclerometric-resistographic method provides moderate scatter in the results than the simple wood hardness and drill-resistance methods. In fact, by using the combination of transversal sclerometric parameters (PD_T) and longitudinal resistographic ones ($A_{m,L}$), good and high agreements with parallel modulus of elasticity in compression ($E_{c,0}$) have been found for full-scale elements (R^2=0.61; n=14) and small specimens (R^2=0.69; n=20), respectively (Table 8.13).

For both simple and combined non-destructive techniques, in Table 8.14 the R^2_{adj}-values and the linear regression equations are presented. Furthermore, the Figure 8.12 shows the comparison in terms of R^2_{adj}-values between the two groups of samples.

Table 8.13. NDT-DT correlations – Prediction of modulus of elasticity in compression parallel to grain by combined methods: coefficients of determination (R^2).

Specimens type	**Sclerometric + Resistographic** $PD_T + A_{m,L}$
actual dimensions S_A-C (n=14)	0.614
small dimensions S_S-C (n=20)	0.689

Table 8.14. NDT-DT correlations – Prediction of modulus of elasticity in compression parallel to grain by combined methods: adjusted coefficients of determination (R^2_{adj}) and linear regression equations.

Structural elements in actual dimensions (S_A-C)			
Model	**NDT parameters**	**R^2_{adj}**	**Linear regression equations**
S_T	PD_T	0.465	$E_{c,0} = 12462.497 - 393.121\ PD_T$
R_L	$A_{m,\,L}$	0.373	$E_{c,0} = 4008.489 + 39.222\ A_{m,\,L}$
$S_T + R_L$	$PD_T + A_{m,\,L}$	0.544	$E_{c,0} = 9615.763 - 283.612\ PD_T + 23.186\ A_{m,\,L}$
Structural elements in small dimensions (S_S-C)			
Model	**NDT parameters**	**R^2_{adj}**	**Linear regression equations**
S_T	PD_T	0.637	$E_{c,0} = 12209.099 - 425.588\ PD_T$
R_L	$A_{m,\,L}$	0.465	$E_{c,0} = 2592.945 + 101.000\ A_{m,\,L}$
$S_T + R_L$	$PD_T + A_{m,\,L}$	0.653	$E_{c,0} = 9586.742 - 329.74\ PD_T + 37.301\ A_{m,\,L}$

(*) S: sclerometric [mm]; R: resistographic [%]

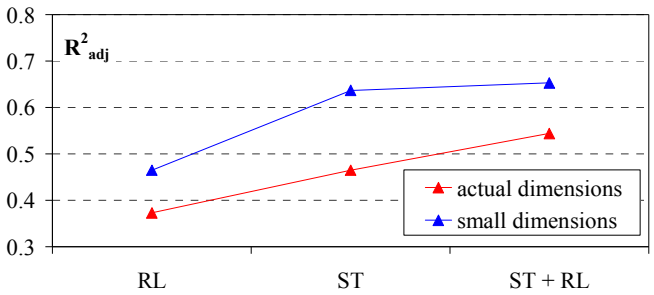

Figure 8.12. NDT-DT correlations – Prediction of modulus of elasticity in compression parallel to grain by combined methods: comparison between R^2_{adj} values.

8.4.2.3 Static vs dynamic modulus

The ultrasonic investigations by direct method on the specimens in actual sizes, tested in compression (type S_A-C; n=14), have allowed the determination of the dynamic modulus of elasticity, according to the theoretical relationship for homogeneous and isotropic material, given by:

$$E_{dyn} = SWS^2 \cdot \rho$$

where SWS is the stress wave speed and ρ is the measured density of the elements.

Therefore, the linear regression between static ($E_{c,0}$) and dynamic (E_{dyn}) moduli has been examined. Medium and moderate correlations have been obtained for longitudinal (R^2=0.25; Fig. 8.13a) and transversal (R^2=0.18; Fig. 8.13b) dynamic modulus, respectively.

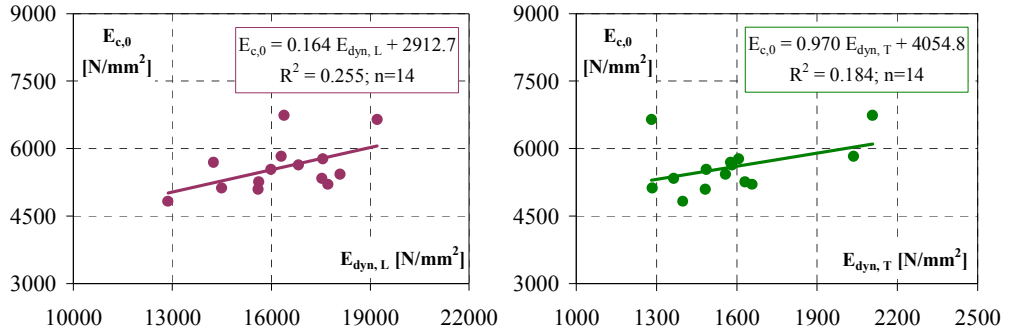

Figure 8.13. NDT-DT correlations – Prediction of modulus of elasticity in compression parallel to grain – Dynamic modulus (E_{dyn}): a) Longitudinal; b) Transversal.

8.4.3 *Prediction of modulus of elasticity in bending*

8.4.3.1 Simple methods

In order to predict the stiffness properties in bending, the local ($E_{m,l}$) and global ($E_{m,g}$) moduli of elasticity, which were obtained by elastic cycles on full-scale timber beams (specimens type S_A-B; n=10), have been correlated with the NDT parameters. The results have been analyzed through the statistical coefficients of determinations (R^2; Table 8.15).

Generally, medium relationships have been found using ultrasonic method (Fig. 8.14). The observed trend is that the higher the stress wave speed in longitudinal direction (SWS_L), the greater the local and global modulus of elasticity (E_m; Fig. 8.14a). Whereas, inverse relationships are provided by the ultrasonic velocity in direct method perpendicular to grain (SWS_T; Fig. 8.14b).

The correlations with the pin penetration depth (PD) show very large scatter in the results, while reasonable linear agreements are found between the modulus of elasticity and drilling-resistance (A_m, Fig. 8.15), especially for longitudinal resistographic measures (R^2 varies in the range 0.48-0.56; Fig 8.15b).

Table 8.15. NDT-DT correlations – Prediction of modulus of elasticity in bending by simple methods: coefficients of determination (R^2).

Specimens type	**Ultrasonic [m/s]**		**Sclerometric [mm]**		**Resistographic [%]**	
S_A-B (n=10)	SWS_L	SWS_T	PD_L	PD_T	$A_{m,L}$	$A_{m,T}$
Local	0.481	0.249	0.000	0.000	0.216	0.475
Global	0.155	0.334	0.000	0.013	0.327	0.564

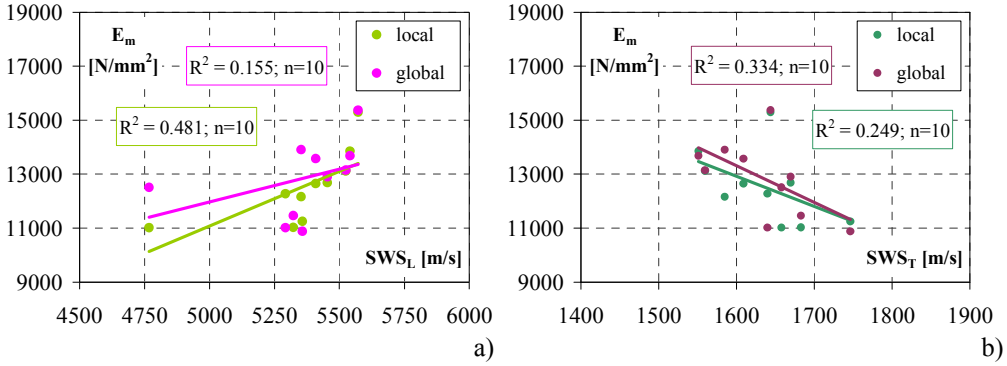

Figure 8.14. NDT-DT correlations – Prediction of modulus of elasticity in bending – Ultrasonic method: a) Longitudinal; b) Transversal.

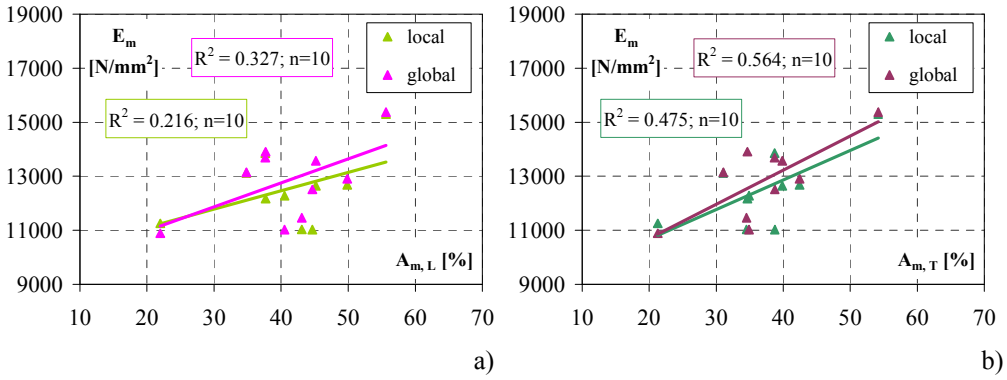

Figure 8.15. NDT-DT correlations – Prediction of modulus of elasticity in bending – Resistographic method: a) Longitudinal; b) Transversal.

8.4.3.2 Combined methods

By multiple regression model among the ultrasonic (SWS) and resistographic parameters (A_m), high R^2-values have been obtained for the estimation of local elasticity modulus in bending, as shown in Table 8.16.

Table 8.16. NDT-DT correlations – Prediction of modulus of elasticity in bending by combined methods: coefficients of determination (R^2).

Specimens type	**Ultrasonic + Resistographic**	
S_A-B (n=10)	$SWS_L + A_{m,L}$	$SWS_L + A_{m,T}$
Local	0.684	0.820

Both simple and combined models are summarized in Table 8.17, including the adjusted coefficients of determination (R^2_{adj}) and the linear regression equations, whereas the Figure 8.16 illustrates the comparison of statistical results.

Table 8.17. NDT-DT correlations – Prediction of modulus of elasticity in bending by combined methods: adjusted coefficients of determination (R^2_{adj}) and linear regression equations.

Model	**NDT parameters**	**R^2_{adj}**	**Linear regression equations**
U_L	SWS_L	0.416	$E_{m,l} = -9149.488 + 4.046\ SWS_L$
R_T	$A_{m,T}$	0.410	$E_{m,l} = 8475.564 + 109.589\ A_{m,T}$
$U_L + R_L$	$SWS_L + A_{m,L}$	0.593	$E_{m,l} = -11578.7 + 3.993\ SWS_L + 66.01\ A_{m,L}$
$U_L + R_T$	$SWS_L + A_{m,T}$	0.768	$E_{m,l} = -9552.914 + 3.473\ SWS_L + 93.842\ A_{m,T}$

(*) U: ultrasonic [m/s]; R: resistographic [%]

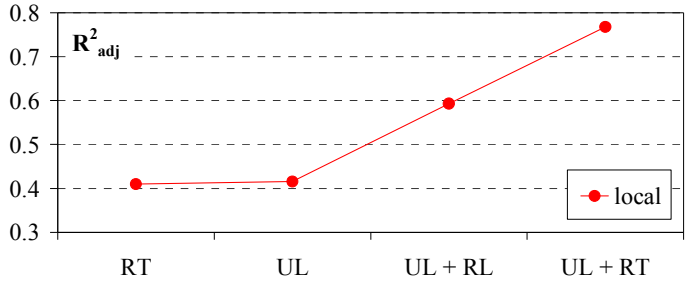

Figure 8.16. NDT-DT correlations – Prediction of modulus of elasticity in bending by combined methods: comparison between R^2_{adj} values.

8.4.3.3 Static vs dynamic modulus

As shown in Figure 8.17 the stiffness mechanical properties in bending could be allowed by means of dynamic modulus of elasticity, obtained by means of ultrasonic direct method in parallel to grain direction ($E_{dyn,\,L}$).

Strong linear agreement is provided with the local elasticity modulus ($E_{m,l}$), as the high R^2-coefficient emphasizes, equal to 0.76 (Fig. 8.17a). Good correlation has been also found between static global modulus ($E_{m,g}$) and dynamic one (R^2=0.51; Fig. 8.17b).

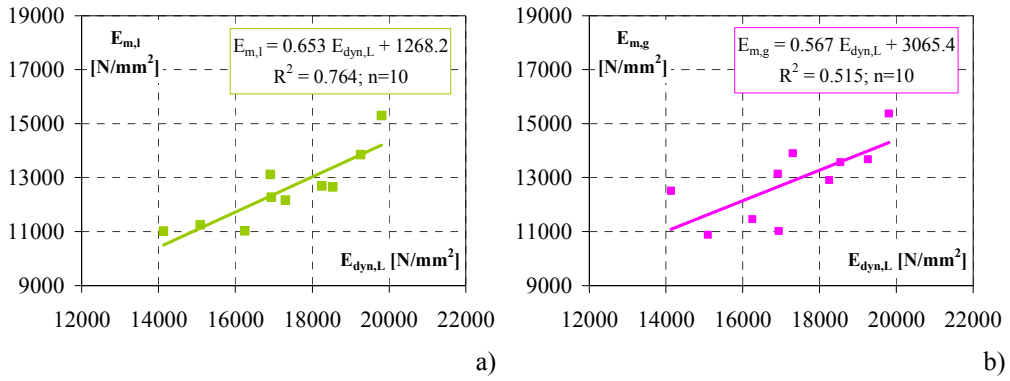

Figure 8.17. NDT-DT correlations – Prediction of modulus of elasticity in bending – Ultrasonic method: a) Local ($E_{m,l}$); b) Global ($E_{m,g}$).

8.4.4 *Prediction of compression strength parallel to grain*

8.4.4.1 Simple methods

The statistical R^2-values among the NDT parameters and ultimate compressive stress parallel to grain ($f_{c,0}$) show the effectiveness of sclerometric and resistographic simple methods in the prediction of strength properties (Table 8.18), according to the results previously achieved for the modulus of elasticity by destructive tests.

The depth to which the pin penetrates into the wood (PD) is inversely proportional to the compression strength of each specimen (Fig. 8.18); while,

there is a growing correlation between the mean amplitude of drilling penetrations (A_m) and strength (Fig. 8.19), as expected.

No relevant difference in terms of R^2-values can be pointed between the two groups of structural elements in actual (S_A-C; n=14) and small sizes (S_S-C; n=20), unless the higher strength values of the small specimens than the actual ones (Figs. 8.18 and 8.19), as a consequence of the less or more influence of natural defects on the mechanical behaviour of timber.

Table 8.18. NDT-DT correlations – Prediction of compression strength parallel to grain by simple methods: coefficients of determination (R^2).

Specimens type	**Ultrasonic [m/s]**		**Sclerometric [mm]**		**Resistographic [%]**	
	SWS_L	SWS_T	PD_L	PD_T	$A_{m,L}$	$A_{m,T}$
actual dimensions S_A-C (n=14)	0.000	0.012	0.188	0.564	0.540	0.231
small dimensions S_S-C (n=20)	-	-	0.246	0.645	0.565	0.143

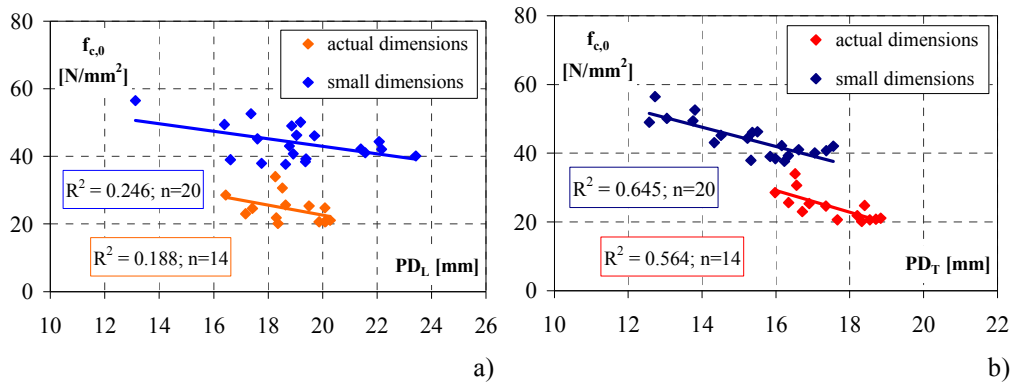

Figure 8.18. NDT-DT correlations – Prediction of compression strength parallel to grain – Sclerometric method: a) Longitudinal; b) Transversal.

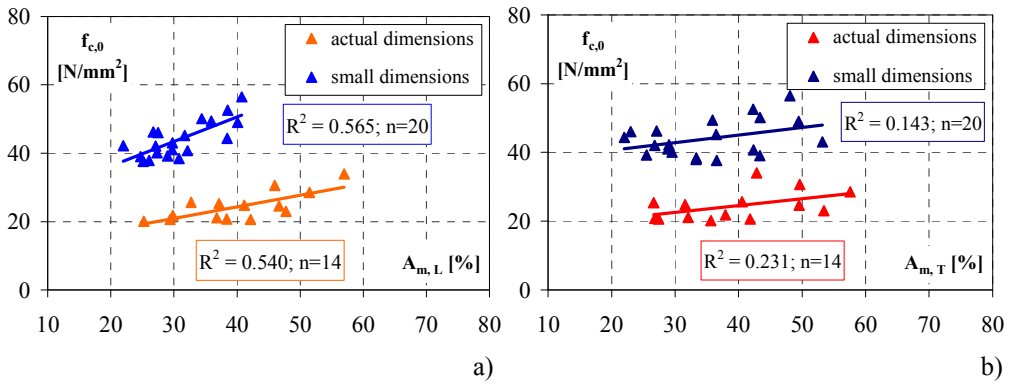

Figure 8.19. NDT-DT correlations – Prediction of compression strength parallel to grain – Resistographic method: a) Longitudinal; b) Transversal.

8.4.4.2 Combined methods

The statistical results of NDT-$f_{c,0}$ simple correlations emphasize that the transversal sclerometric parameters (Fig. 8.18b) and the longitudinal resistographic ones (Fig. 8.19a) may be used as single predictors for a fast estimation of the compression strength. Therefore, they have been combined each other by multiple linear regression, obtaining high R^2 values (Table 8.19) for both actual elements (R^2=0.73) and small specimens (R^2=0.71).

Table 8.19. NDT-DT correlations – Prediction of compression strength parallel to grain by combined methods: coefficients of determination (R^2).

Specimens type	**Sclerometric + Resistographic** $PD_T + A_{m,L}$
actual dimensions S_A-C (n=14)	0.728
small dimensions S_S-C (n=20)	0.712

The estimated regression functions of both simple and combined models are given in Table 8.20, and the corresponding R^2_{adj}-values are represented in Figure 8.20.

Table 8.20. NDT-DT correlations – Prediction of compression strength parallel to grain by combined methods: adjusted coefficients of determination (R^2_{adj}) and linear regression equations.

Structural elements in actual dimensions (S_A-C)			
Model	**NDT parameters**	**R^2_{adj}**	**Linear regression equations**
S_T	PD_T	0.528	$f_{c,0} = 79.926 - 3.172\ PD_T$
R_L	$A_{m,\,L}$	0.501	$f_{c,0} = 10.787 + 0.339\ A_{m,\,L}$
$S_T + R_L$	$PD_T + A_{m,\,L}$	0.679	$f_{c,0} = 53.112 - 2.141\ PD_T + 0.218\ A_{m,\,L}$
Structural elements in small dimensions (S_S-C)			
Model	**NDT parameters**	**R^2_{adj}**	**Linear regression equations**
S_T	PD_T	0.625	$f_{c,0} = 87.093 - 2.820\ PD_T$
R_L	$A_{m,\,L}$	0.540	$f_{c,0} = 21.736 + 0.722\ A_{m,\,L}$
$S_T + R_L$	$PD_T + A_{m,\,L}$	0.678	$f_{c,0} = 62.251 - 1.907\ PD_T + 0.353\ A_{m,\,L}$

(*) S: sclerometric [mm]; R: resistographic [%]

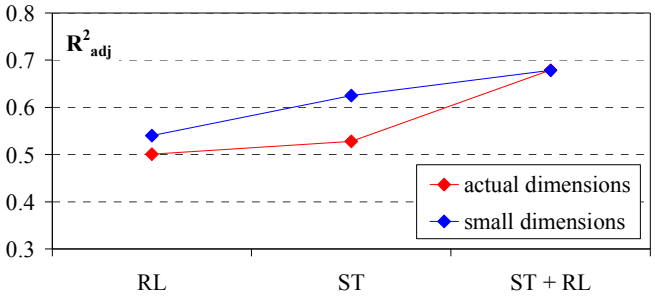

Figure 8.20. NDT-DT correlations – Prediction of compression strength parallel to grain by combined methods: comparison between R^2_{adj} values.

8.4.5 *Prediction of bending strength*

8.4.5.1 Simple methods

Concerning the relationships between NDT variables and bending strength (f_m), very low R^2-values have been found with ultrasonic properties (SWS; Table 8.21). Whereas, the correlation with pin penetration depth (PD) and drill-resistance (A_m) show reasonable scatter in the results (Fig. 8.21).

In particular, the statistical analysis shows that only the simple method based on resistographic measurements is adequate for a non-destructive prediction of bending strength, as the good R^2-coefficients among mean

amplitude and bending strength confirm, equal to 0.58 and 0.49 for longitudinal and transversal measurements, respectively (Fig. 8.21b).

The corresponding R^2_{adj} and the linear fitted equations are provided in Table 8.22.

Table 8.21. NDT-DT correlations – Prediction of bending strength by simple methods: coefficients of determination (R^2).

Specimens type	**Ultrasonic [m/s]**		**Sclerometric [mm]**		**Resistographic [%]**	
	SWS_L	SWS_T	PD_L	PD_T	$A_{m,L}$	$A_{m,T}$
actual dimensions S_A-B (n=10)	0.019	0.050	0.268	0.196	0.581	0.485

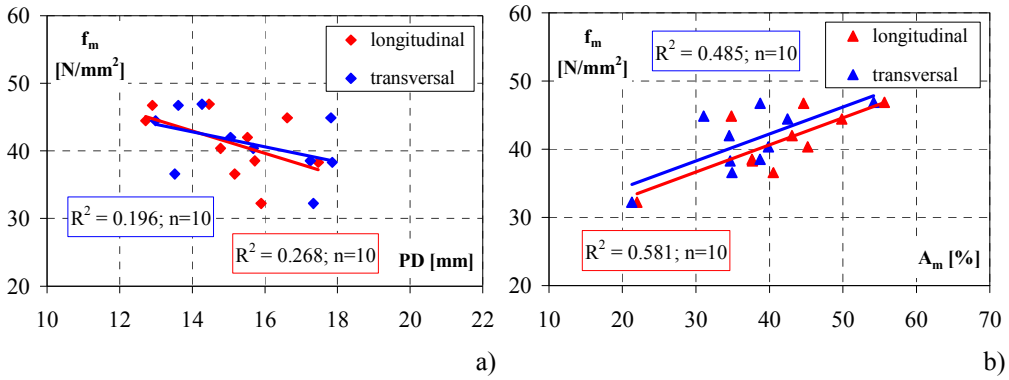

Figure 8.21. NDT-DT correlations – Prediction of bending strength: a) Sclerometric method; b) Resistographic method.

Table 8.22. NDT-DT correlations – Prediction of bending strength by resistographic method: adjusted coefficients of determination (R^2_{adj}) and linear regression equations.

Model	**NDT parameters**	**R^2_{adj}**	**Linear regression equations**
R_L	$A_{m,L}$	0.529	$f_m = 24.684 + 0.399\ A_{m,L}$
R_T	$A_{m,T}$	0.421	$f_m = 26.436 + 0.396\ A_{m,T}$

(*) R: resistographic [%]

Conclusive remarks

The structural and architectural restoration of historical buildings has the aim of studying, interpreting, preserving, rehabilitating safety and service conditions. In the last decades, many research activities concerning the protection and retrofitting of historical building have been financially supported by public administrations and a great increment of the number of interventions of existing structure is underlined. This owes the natural ageing of construction materials, the increasing environmental aggression, the lack of maintenance, the design and execution inaccuracy, the need to provide either the structural upgrading, because of changed boundary conditions, or the post-earthquake repairing. The problem is particularly felt in case of timber structure. In fact, timber is a material used since a very long time in both monumental constructions and historical buildings, particularly for realizing the floor slabs and roofing structures. The knowledge of the construction typologies and technologies used in the past for the realization ancient timber structures is an important starting point for the structural identification, aimed at evaluating of the strength and stiffness capacity and to the definition of appropriate retrofitting or upgrading interventions. In fact, it is necessary to know the static function of each element, how they are connected each other, in order to assess their contribution to the behaviour of the whole system.

In this thesis, the ancient timber roofing structures of the Royal Palace of Naples, which cover the halls of the Historical Apartment, are selected as studies case for exemplifying a proposal methodology of analysis. It is

developed through the following phases: 1) geometrical survey, including the identification of the structural scheme by means of *in situ* inspections; 2) failure diagnosis, for the evaluation of material defects and deterioration degrees, together with the mechanical properties of old timber elements by means of visual grading; 3) structural modelling, for the definition of geometrical, mechanical and loading model; 4) numerical analysis, for the evaluation of the structure capability, carried out according to the current codes; 5) identification of the appropriate retrofitting intervention among the possible ones, whose design has been subjected to the achievement of predetermined objectives, as maximise the retention of original material, considering reversible remedial solutions, based on mixed technologies.

The comprehensive study is a demonstration that the analysis of ancient structures made of wood is a very complex matter, for several inherent difficulties to be faced for both the material and the structural behaviour characterization. Preliminary diagnostic inspections are needed to evidence any damage and decay situations of timber, to find and eliminate their causes and, at the same time, to characterize the structure as respect to the mechanical properties, for determining the strength and stiffness capacities. However further to the complications related to the irregularity and variability of properties of timber, for their own nature, the survey operations in the case of monumental buildings are gotten worse due to the inaccessibility of structures, which is also related to the need of preservation of the inestimable value assets, such as frescoes, canvases, etc., that cannot be removed. For this reasons some approximations based on sensible assumptions should be made on the safe side in order to face and give a solution to structural problems aiming at the safeguarding of the artistic and cultural heritage.

In many rehabilitation interventions the substitution of the horizontal old timber structures with new systems and floors is often proposed. This approach is not accepted for historical building which need the conservation of the existing structures. Therefore, to recover and strengthen the wooden floors specific intervention are required. The wood-concrete composite system represents a reliable solution for the upgrading of the existing floor slab,

which consists of a concrete thin slab connected to the timber beams by means of connectors, like screws, nails, and studs. A reversible and innovative connection system has been proposed for the consolidation of ancient timber floor structures (Mazzolani *et al.*, 2005). It is composed by two parts, bolted together at ad hoc folded wings, rounding the timber beam with the interposition of a rubber layers. The function of the connector is held by the superior wings of the device.

In the present thesis, monotonic push-out tests on the single connector, concerning circular shaped configurations, are presented focusing on aspects influencing the system failure mechanism and the connection performance. The devices with rubber-steel simple contact shows an excessive slip at the rubber-steel interface, together with a relevant rotation of collar parts when they are connected each other around the timber stock by means of two bolts, one at each couple of wings. Therefore, the effect of the bolts tightening increment is examined using both higher bolt grades and two bolts per wing, instead of one. In this way, other two system types have been investigated, characterized by chemical and mechanical blocking of the rubber to the steel collar. The experimental results evidence that the increment of the initial stiffness and strength corresponds to the same one of the total bolts tightening. On the other hand, this connection types exhibit a non-linear shear force-relative slip relationship even for low value of the applied load, due to the deformation extent of the rubber layers depending on the contact irregularities at the rubber-wood interface. Therefore the influence of shape and defects on the system performance is worth to be deeply investigated. The optimum collar connector characterization is needed in order to catch the appropriate design data.

Bending test on full-scale composite floor, realized by two timber beams with circular cross-section and r.c. slab lightened by polystyrene blocks and cast on layer of wooden planks, is also presented. The test results show the global and local behaviour of the system, emphasizing the effectiveness of the proposed technique in terms of both flexural stiffness and strength. In particular, the comparison between the experimental and the only timber beams behaviour shows that the improvement percentage due to the r.c.-timber connection by means of the innovative device is equal to 53 % for the initial stiffness and 119 % for the maximum resistance. The obtained results

represent an experimental support for further theoretical and numerical investigations.

In the field of restoration of historical constructions, visual inspections, instrumental non-destructive testing and monitoring have an important role for diagnosis, structural analysis and retrofitting.

In the case of ancient timber structures, the notable variability of the material turns the identification of physical and mechanical properties hard to get. However they represent a fundamental action to evaluate structural efficiency and safety and also to design restoration interventions. Strength properties of structural timber are usually determined by direct testing of timber elements according to a standardised methodology, and strength is defined on the element level rather than on the base material level. The assessment of the mechanical properties of the existing timber members becomes difficult as it is usually not possible to remove large samples from an ancient structure for direct testing, as it would be advisable. Therefore, some type of non-destructive evaluation of strength (or grading) is required to guarantee the safety of the structure. Historically, the most common method is visual grading of each timber element. Nowadays, a number of different non-destructive technique (NDT) have an own special interest due to the fact that their application does not affect the present structural integrity and safety of the structure.

The problem of non-destructive tests is exactly the lack of standardization, besides the most part of non destructive test is useful to determine physical but not mechanical characteristics, so each method has to be compared or combined to obtain reliable results. Furthermore, safety assessment of ancient timber structures is usually not addressed by the current codes, which are conceptually oriented to new constructions. The Italian code UNI 11119 establishes procedures for the structural grade of timber elements, based on visual inspection, providing the admissible mechanical properties for three categories, which are defined on the basis of defects characteristics of the element. As several experimental investigations show, comparing this values with laboratory test results, high safety coefficient are generally obtained.

Consequently, the structural capacity of the material seems significantly underestimated taking into account only the degradation visible on the structural elements surfaces, according to the current codes. Therefore, the design requirements of existing systems need to be re-defined. The uncertainty about the mechanical properties and the structural behaviour could be reduced by means of non-destructive evaluation.

In this context a wide experimental campaign has developed on old chestnut structural elements and defect-free specimens aiming at providing a methodology for *in situ* mechanical characterization of ancient timber members and structures using Non Destructive Testing (NDT) techniques. The following non-destructive methods were used: hygrometric tests to estimate wood moisture content, ultrasonic investigations as an approach to determine stress wave properties, wood hammer tests to assess material hardness and superficial consistence, resistographic measurements to detect internal defects and density variations. Furthermore destructive tests (DT), in compression and in bending, were performed in order to assess stiffness and strength properties, post-elastic behaviour and collapse mechanisms of the timber elements. After the analysis of the experimental results, including data processing and interpretation, statistical relationships between both NDT and DT parameters, together with NDT-DT correlations have been provided for the mechanical identification of timber, based on linear regression model

On the basis of experimental investigations, the following conclusions can be drawn.

Non-destructive tests (NDT)

- Laboratory tests are the more reliable way to identify the characteristics of the material and play an important role in the calibration of non-destructive tests.
- NDT methods represent an useful supplements to the traditional visual grading, allowing to detect internal defects and critical zone, which are not visible on the external faces of the elements.
- By means of ultrasonic investigations, discordance among dynamic properties in axial and transverse direction has been observed, according to the orthotropic behaviour of wood. In fact, for all specimens, the

longitudinal velocity is about three times the same one in transversal direction..

- The sclerometric technique, based on wood test hammer system, is particularly influenced by the conservation state of superficial wooden layers.
- In the whole experimental campaign, the resistographic measurements showed great efficiency and reliability, having widespread applications in finding internal defects and anomalies, estimating the density variations, analyzing annual ring structures, measuring real dimensions of the transversal section, evaluating the residual area observed in the graphic profiles. However the resistographic tests, performed in both parallel and perpendicular to grain direction on specimens in actual dimensions, are characterized by greater variability in terms of coefficients of variation, due to the presence of internal hollow areas or more resistant parts which influence the local measures of the drilling-resistance.

Destructive tests in compression (DT)

- The destructive tests in compression parallel to the grain show that the mechanical characterization of the material by means of tests on clear specimens is inadequate to have a reliable and complete information on the structural behaviour of timber elements. In fact, important difference appears between the strength values of structural elements in actual dimensions and defect-free specimens, due to the presence of natural defects which drastically reduce of about three times the strength capacity of the chestnut timber.
- Good agreement is provided by comparing the experimental 5-percentile value of the parallel compression strength ($f_{c,0}$) of structural specimens (20.13 N/mm^2) and the characteristic values assumed by UNI 11035-2 (22 N/mm^2) and EN 338 (D30; 23 N/mm^2).
- Comparing the admissible strength in parallel direction of UNI 11119-III (7 N/mm^2) with the average and 5-percentile results of laboratory tests, the obtained safety coefficients are greater than 3.
- The mechanical characterization of clear chestnut wood in compression perpendicular to grain has been performed in radial and tangential direction, taking into account the orientation of the annual rings with

respect to the direction of the applied load. In particular the stress-strain relationships in radial compression are significantly influenced by the anatomy of wood.

- The average values of clear wood strength in perpendicular radial and tangential directions ($f_{c,90}$) are very similar, equal to about 5.5 N/mm^2, despite the different observed failure modes. This value, as expected, is eleven times smaller that the same one obtained in parallel direction.
- 5-percentile strength results ($f_{c,90}$) are comparable with UNI 11035-2 value.
- The $f_{c,0}/f_{c,90}$ ratio by laboratory tests is significantly higher than the same one by European (EN 338, D30) and Italian codes (UNI 11035-2); whereas, the same experimental ratio in terms of modulus of elasticity $E_{c,0}/E_{c,90}$ is similar with the standards.

Destructive tests in bending (DT)

- The bending tests emphasize that slope of grain, large knots or groups of knots, which reduce the element cross section, cause a strong reduction of strength (f_m) if located in tension side of the beams. Therefore, their presence does not only involve a reduction of the service and load bearing capacity of the element, but should be taken into account by considering a more detailed geometry of the member in the structural analysis.
- Good agreement is provided by comparing the experimental minimum (5-percentile) value of strength (32 N/mm^2) and the characteristic values assumed by UNI 11035-2 (28 N/mm^2) and EN 338 (D30; 30 N/mm^2) standards.
- Comparing the admissible bending strength of UNI 11119-III (8 N/mm^2) with the average and 5-percentile results of laboratory tests, the obtained safety coefficients are equal to about 5 and 4, respectively.
- The average value of the global modulus of elasticity obtained by the tests is about higher of 22 % than the mean value assumed by UNI 11035-2 and EN 339 (D30) and of 60 % than the same one reported in UNI 11119 for the third category class.

NDT-DT correlations for the mechanical characterization of timber

- Correlations between NDT parameters
  - Moderate inverse relationships have been found between sclerometric and resistographic variables in both parallel (R^2=0.24) and perpendicular (R^2=0.16) to grain direction.
  - As the sclerometric and resistographic results seem independent by the tests orientation, medium and good longitudinal-transversal correlations are provided by penetration depth (R^2=0.30) and mean drilling-resistance (R^2=0.47) respectively.
- Correlation between DT parameters

  Compression tests parallel to grain:
  - The statistical analysis emphasizes that a linear correlation between wood density (ρ), modulus of elasticity ($E_{c,0}$) and strength ($f_{c,0}$) appears adequate to represent the test results. In particular, density appears one of the main factor that influence the material behaviour.
  - The comparison between the results in terms of adjusted coefficients of determination (R^2_{adj}), shows that for $f_{c,0}$ *vs* ρ relations, the results improve when the defectiveness of the material is negligible. In fact the defect-free sample provide the highest R^2_{adj}, equal to about 0.80. This result confirm that the presence of faults, their location and kind, grain inclination and geometrical anomalies, influence to great extent timber behaviour in compression parallel to grain.

  Compression tests perpendicular to grain:
  - The relationships between DT parameters by radial and tangential tests on clear elements show that the $E_{c,90}$ *vs* ρ and $f_{c,90}$ *vs* ρ correlations appears to be of exponential type, while for $E_{c,90}$ *vs* $f_{c,90}$ linear agreement is found. Medium and good R^2-values are provided when all perpendicular tests results, in both radial and tangential orientation, are involved in the regression model.

  Bending tests:
  - Generally, the DT results show moderate and medium correlations, apart for the relation between the local and global modulus of elasticity, which provide a good linear agreement (R^2=0.63).

- NDT-DT correlations:

  Estimation of wood density:

  - The statistical analysis show that correlating the NDT parameters with wood density, medium and good agreements exist, respectively, for sclerometric (S) and resistographic (R) methods. While no relevant correlations have been found between ultrasonic (U) parameters and density.
  - The multiple linear regression analysis show that the following simple and combined methods, in both longitudinal and transversal direction, could be taken in practical applications for a quick and quantitative estimation of wood density:
    R: $R^2_{adj} \approx 0.52$;
    S+R: $R^2_{adj} \approx 0.60$;
    U+S+R: $R^2_{adj} \approx 0.68$.

  Prediction of modulus of elasticity

  - By using the combination of transversal sclerometric parameters and longitudinal resistographic ones, good and high agreements with parallel modulus of elasticity in compression have been found for full-scale elements ($R^2_{adj}=0.54$) and small specimens ($R^2_{adj}=0.65$), respectively.
  - By multiple regression model among the ultrasonic stress wave speed and drill-resistance, high R^2_{adj}-values have been obtained for the estimation of local elasticity modulus in bending, R^2_{adj} being equal to 0.59 and 0.77 for longitudinal and transversal tests, respectively.
  - Strong linear agreement is provided by the relationship between the local elasticity modulus and the longitudinal dynamic modulus, as the high R^2-coefficient emphasizes, equal to 0.76.

  Prediction of strength

  - The transversal sclerometric parameters and the longitudinal resistographic ones may be used as single predictors for a fast estimation of the compression strength parallel to grain; therefore, their combination provide high R^2_{adj}-values, equal to 0.68.
  - The simple method based on resistographic measurements is nearly adequate for a non-destructive prediction of bending strength, as the good R^2_{adj}-coefficients confirm, equal to 0.53 and 0.42 for longitudinal and transversal measurements, respectively.

In conclusion, the reasonable relationships achieved between non destructive and destructive parameters, show a great efficiency and reliability of NDT techniques as practical application for diagnosis, assessment and mechanical identification of timber members, leading to the appraisal of the timber structures integrity.

The experimental campaign is still going on by extending the investigations on large samples of both structural and defect-free specimens, aiming at establishing reliable NDT-DT correlations, based on statistical analysis and evaluation.

References

AA. VV. (2002). *Apa engineered wood handbook*. McGraw-Hill Book co. Editor.

Aghayere, A., Vigil, J. (2007). *Structural wood design*. Wiley & Sons Ltd. Editor.

Bertolini, C., Brunetti, M., Cavallaio, P. & Macchioni N. (1998). A non destructive diagnostic method on ancient timer structures: some practical application examples. *Proceedings of 5 th World Conference on Timber Engineering*. Montreux. Presses Polytechniques et Universitaires Romandes, Vol. I, 456-565.

Blass, H. Gorlacher, R. (2004). Compression perpendicular to the grain. *Proceedings of the 8th World Conference of Timber Engineering WCTE 2004*. Finland, Vol. II: pp. 435-440.

Bodig, J. (1963). The peculiarity of compression of conifers in radial direction. *Forest Products Journal*. 13: pp. 438-446.

Bodig, J. (1965). The effect of anatomy on the initial stress-strain relationship in transverse compression. *Forest Products Journal*. 14: pp. 197-202.

Bodig, J., Jayne, B.A. (1993). Mechanics of wood and wood composite. *Krieger Publishing Company*: 712 pp.

Bonamini, G., Noferi, M., Togni, M., Uzielli L. (2001). Ispezione e diagnosi in situ delle strutture. *L'Edilizia*, Vol. 2.

Bonamini, G., Noferi, M., Togni, M., Uzielli, L. (2001). Il manuale del legno strutturale – Vol I – Ispezione e diagnosi in opera. Rome, Italy, Mancosu editor.

Branco, J., Cruz, P., Dias, S. (2005). Old timber beams – Diagnosis and reinforcement. *Proceedings of the International Conference The Conservation of Historic Wooden Structures*. Florence, Italy. Vol I: pp. 417-422.

Branco, J., Varum, H.; Cruz, P. (2006). Structural grades of timber by bending and compression tests. *Materials science forum*. Vol. 514-16 (2), pp. 1663-1667.

Calderoni, B., De Matteis, G., Giubileo C., Mazzolani, F.M. (2006). Experimental correlation between destructive and non-destructive tests on ancient timber elements. *5th International Conference on Structural Analysis of Historical Constructions "SACH 2006"*. New Delhi, India, 6-8 November 2006 – (Editors C. Modena, P.B. Lourenco, P. Roca & S. Agrawal): 351-358 (ISBN 1403-93157-7).

Calderoni, B., De Matteis, G., Giubileo C., Mazzolani, F.M. (2006). Flexural and shear behaviour of ancient wooden beams: Experimental and theoretical evaluation. *Engineering Structures,* 28, pp. 729-744, Elsevier ltd (ISSN 0141-0296).

Ceccotti, A., Togni, M. (1996). NDT on ancient timber beams: assessment of strength/stiffness properties combining visual and instrumental methods. *Proceedings of the 10th International Symposium of Non-destructive Testing of Wood*. Lausanne, Switzerland: pp. 379-388.

Ceraldi, C., Mormone, V., Ermolli, E. (2001). Resistographic inspection of ancient timber structures for the evaluation of mechanical characteristics. *Materials and Structures*. Rilem, Vol. 34: pp. 59-64.

CNR-DT 206 (2007): Istruzioni per la progettazione, esecuzione e controllo delle strutture in legno.

De Matteis, G., Giubileo, C., Calderoni, B., Mazzolani, F.M. (2005). Analisi sperimentale di travi in legno di castagno antico mediante prove di rottura a taglio e a flessione. *L'Edilizia*. n. 141, De Lettera Editor, Milano, Italy.

EN 1991-1 (2002): Actions on structures. Part 1: General actions. Densities, self-weight, imposed loads for buildings.

EN 1995-1 (2004): Eurocode 5. Design of Timber Structures. Part 1: General – Common rules and rules for buildings.

EN 1998-1 (2004): Eurocode 8. Design of structures for earthquake resistance. Part 1: General rules, seismic actions and rules for buildings.

Faggiano, B., Marzo, A., Grippa, M.R., Mazzolani, F.M. (2008). Analysis of wooden roofing structures in monumental buildings. *Proceedings of the 10th world conference on timber engineering WCTE 2008*, Miyazaky, Japan, June2-5, 2008.

Faggiano, B., Grippa, M.R., Marzo, A., Mazzolani, F.M. (2009). Combined non-destructive and destructive tests for the mechanical characterization of old structural timber elements. *3rd International Conference on Advances in Experimental Structural Engineering.* San Francisco, United States, 15-16 October, 2009.

Faggiano, B., Grippa, M.R., Marzo, A. (2009). Experimental evaluation of the mechanical properties of wood by means of non-destructive compared techniques for the characterization of existing wooden structures. *PRIN 2006 "Diagnosis techniques and totally removable low invasive strengthening methods for the structural rehabilitation and the seismic improvement of historical timber structures"* (in Italian)

Faggiano, B., Grippa, M.R., Marzo, A., Mazzolani, F.M. (2009). Mechanical identification by NDT of old chestnut structural timber. *Proceedings of the First International Conference PROHITECH09 "Protection of Historical Buildings".* Rome, Italy, 22-24 June 2009 - (F.M. Mazzolani Editor): Vol. 1, 295-300.

Faggiano, B., Marzo, A., Formisano, A., Mazzolani, F.M. (2009). Innovative steel connections for a composite wood-steel-concrete floor: a numerical

investigation, Published in *Computer & Structures* (Elsevier – K. J. Bathe and B.H.V. Topping editors, ISSN 0045-7949), January 2009.

Feio, A.O.,. Lourenco, P.B., Machado, J.S. (2004). Compressive behaviour and NDT correlations for chestnut wood. *Proceeding of the 4th International Seminar SAHC 2004*. Padova, Italy, 10-13 November 2004.

Feio, A.O. (2005). *Inspection and Diagnosis of Historical Timber Structures: NDT Correlations and Structural Behaviour*. PhD Thesis. University of Minho, Department of Civil Engineering, Portugal.

Gehri, E. (1998). Load introduction and load transfer perpendicular to grain. *Proceedings of the 5th World Conference on Timber Engineering*. Montreux, Switzerland. Vol. I: 213-223 pp.

Gelfi, P., Giuriani, E., Marini, A. (1998). Behavoiur of stud shear connectors in the composed wood-concrete beams: theoretical modelling and experimental comparisons. *Proceedings of the 3rd Italian Workshop on the Composed Structures*. 29-30 October, 1998, Ancona, Italy (in Italian).

Giordano, G. (1986). *Tecnologia del legno*. Torino, Italy, UTET Editor.

Giordano, G. (1989). *Tecnica delle costruzioni in legno (Wooden structure engineering)*. Hoepli Editor, Milano, Italy.

Giubileo, C. (2005). *Experimental and Theoretical Analysis of the Structural Behaviour of Ancient Timber Structures*. PhD Thesis. University of Naples "Federico II", Department of Structural Engineering (DIST), Naples, Italy.

Kasal, B., Anthony R.W. (2004). Advances in in-situ evaluation of timber structures. *In Progress in Structural Engineering and Materials*. John Wiley & Sons, Vol. 6.

Kunesh, R.H. (1968). Strength and elastic properties of wood in transverse compression. *Forest Products Journal*. 18 (1): pp- 65-72.

Macchioni, N., Piazza, M. (2009). Italian standardisation activity in the field of diagnosis and restoration of ancient timber structures. *Proceedings of the First International Conference PROHITECH09 "Protection of Historical*

Buildings". Rome, Italy, 22-24 June 2009 - (F.M. Mazzolani Editor). Vol. 1, 349-353.

Madsen, B. (1991). Length effects in timber. *Proceedings of 1991 International Timber Engineering Conference*. London, UK, 1991.

Marzo, A., Grippa, M.R., Faggiano, B., Mazzolani, F.M. (2009). Push-out tests on steel collar connections for composite timber-concrete beams. *Proceedings of the First International Conference PROHITECH09 "Protection of Historical Buildings"*. Rome, Italy, 22-24 June 2009 - (F.M. Mazzolani Editor). Vol. 1, 355-360.

Mazzolani, F.M., Faggiano, B., Marzo, A. (2004). Methodology for the analysis of complex historical wooden structures: a study case. *Proceedings of the IV International Seminar SAHC 2004*. Padova, Italy, pp. 945-955.

Mazzolani, F.M., Faggiano, B., Marzo, A. (2005). Retrofitting of complex wooden structures by means of mixed reversible technologies: a study case. *Proceedings of COST C12 Final conference*. Innsbruck, Austria, pp. 587-597.

Mazzolani, F.M., Faggiano, B., Marzo, A. (2006). Analysis of roofing structures in monumental buildings. *Proceeding of the V International Seminar SAHC 2006*. New Delhi, India. Lorenço, Roca, Modena, Agrawal (editors), Macmillan India Ltd Publisher, 2006, ISBN 972 8692 27 7, CD ROM, Vol. 1 "Timber structures", paper n. 19, pp. 471-478.

Mazzolani, F.M., Faggiano, B., Marzo, A., Guglielmo, E., Calicchio, D. (2008). Identification of existing wooden structures by ND methods: the Diplomatic Hall of the Royal Palace of Naples. *Proceeding of the National Congress DIACOMAST*. Caserta, Italy (in Italian)

Mazzolani, F.M., Faggiano, B., Marzo, A. & Grippa, M.R. (2009). The Diplomatic Hall of the Royal Palace of Naples: diagnosis, analysis and retrofitting of the timber structures. *Proceedings of the First International Conference PROHITECH09 "Protection of Historical Buildings"*. Rome, Italy, 22-24 June 2009 - (F.M. Mazzolani Editor). Vol. 1, 367-373.

Migliore, M.R. & Ramundo, F. (2003). Evaluation of mechanical properties of timber trusses by non-destructive tests. *Proceedings of XXXII IAHS World Conference*. Trento, Italy.

Migliore, M.R. & Ramundo, F. (2004). Identification of the mechanical properties of timber structures by combined non-destructive tests. *Proceedings of International Seminar on Structural Analysis of Historical Constructions SAHC*. Padova, Italy.

Migliore, M.R. & Ramundo, F. (2009). Experimental testing for the identification of mechanical characteristics of ancient timber elements. *Proceedings of the First International Conference PROHITECH09 "Protection of Historical Buildings"*. Rome, Italy, 22-24 June 2009 - (F.M. Mazzolani Editor). Vol. 1, 375-380.

Munafo', P., Antonucci, R. (1994) Use of methods for determining the mechanical properties of antique wood. *Proceedings of the 3th International Conference on Inspection, Appraisal, Repairs e Maintenance of Buildings and Structures*. Bangkok, pp. 1-8.

OPCM 3431 (2005). Norme tecniche per il progetto, la valutazione e l'adeguamento sismico degli edifici.

Parisi, M., Piazza, M. (1999). Mechanics of plan and retrofitted traditional timber connections. *Journal of Structural Engineering*. Vol. 126 (12): pp. 1395-1403.

Parisi, M., Piazza, M. (2007). Restoration and strengthening of timber structures: principles, criteria and examples. *Practice Periodical on Structural Design and Construction*. Vol. 12, No. 4, November 2007, pp. 177-185.

Piazza, M., Baldassino, N. & Zanon, P. (1996). In situ evaluation of the mechanical properties of timber structural elements. *Proceedings of the X Symposium on NDT of Wood*. Lausanne, Switzerland.

Piazza, M. & del Senno, M. (2001). Proposals and criteria for the preliminary evaluation, the design and the execution of works on ancient load bearing timber structures. In C. Bertolini Cestari (ed), *Wooden Handwork/Wooden Carpentry: European Restoration Sites*. Paris: Elsevier.

Piazza, M. & del Senno, M. (2002). Applicabilità di indagini strumentali. *L'Edilizia* n.4, Milano, Italy.

Piazza, M., Tomasi, R., Modena, R. (2005). *Strutture in legno*. Hoepli Editor, Milano, Italy.

Quagliarini, E., D'Orazio, M. (2005). *Recupero e conservazione di volte in "camorcanna".* Alinea Editor, Firenze, Italy.

Raczkowski, J., Lutomski, K., Molinski, W., Wos R. (1999). Detection of early stages of wood decay by acoustic emission technique. *Wood Science and Technology*, Vol. 33, Springer Verlag.

Renn, R.J., Kim, J.B. (1999). Non-destructive evaluation (NDE) of the stiffness and strength of in situ timber structural members. *In Proceedings of the 1st Rilem Symposium on Timber Engineering.* Stockholm, Sweden.

Ronca P., Gubana A. (1998). Mechanical characterisation of wood structures by means of an in-situ penetration test. *In Construction and Building Materials*. Elsevier, Vol. 12.

Ross, R., Pellerin, R., Volny, N,. Salsig, W., Falk, R. (1999). Inspection of timber bridge using stress wave timing non-destructive evaluation tools – A guide for use and interpretation. *General Technical Report FPL-GTR-114. Madison, WI: U.S. Department of Agriculture, Forest Service, Forest Products Laboratory:* 15 pp.

Ross, R., Hunt, M. (2000). Stress wave timing non-destructive evaluation tools for inspecting historic structures – A guide for use and interpretation. *General Technical Report FPL-GTR-119. Madison, WI: U.S. Department of Agriculture, Forest Service, Forest Products Laboratory:* 16 pp.

Tabarsa, T. and Chui, Y.H. (2000). Stress-strain response of wood under radial compression. Part I. Test method and influences of cellular properties. *Wood and Fiber Science*. 32 (2): pp. 144-152.

Tampone, G. (1996). *Il restauro delle strutture di legno*. Milan, Italy, Hoepli editor.

Tampone, G. (2001). Acquaintance of the ancient timber structures. *Historical constructions. Possibilities of numerical and experimental techniques*. Lourenco P.B. & Roca P. editors.

Thelandersson S. L. H. (2003). *Timber Engineering*. Wilwy & Sons LTD. Editor.

Turrini, G., Piazza, M. (1983). A technique for stiffness and strength upgrading of wooden floor. Recuperare. Vol. 5, pp. 224-237 (in Italian).

UNI 11035-1 (2003). Legno strutturale. Classificazione a vista di legnami italiani secondo la resistenza meccanica: Terminologia e misurazione delle caratteristiche.

UNI 11035-2 (2003). Legno strutturale. Regole per la classificazione a vista secondo la resistenza e i valori caratteristici per tipi di legname strutturale italiani.

UNI 11118 (2004). Beni culturali. Manufatti lignei. Criteri per l'identificazione delle specie legnose.

UNI 11119 (2004). Beni culturali. Manufatti lignei. Strutture portanti degli edifici. Ispezioni in situ per la diagnosi degli elementi in opera.

UNI 11130 (2004). Beni culturali. Manufatti lignei. Terminologia del degradamento del legno.

UNI 11138 (2004). Beni culturali. Manufatti lignei. Strutture portanti degli edifici. Criteri per la valutazione preventiva, la progettazione e l'esecuzione di interventi.

UNI 11141 (2004). Beni culturali. Manufatti lignei. Linee guida per la datazione dendrocronologia del legno.

UNI 11161 (2005). Beni culturali. Manufatti lignei. Linee guida per la conservazione, il restauro e la manutenzione.

UNI EN 1912 (2002). Legno strutturale. Classi di resistenza. Assegnazione delle categorie visuali e delle specie.

UNI EN 1990 (2004). Eurocodice. Criteri generali di progettazione strutturale.

UNI EN 1993-1 (2004). Progettazione delle struttura di acciaio. Parte 1: Regole generali e regole per gli edifici.

UNI EN 1994-1 (2004). Progettazione delle strutture composte acciaio-calcestruzzo. Parte 1: Regole generali e regole per gli edifici.

UNI EN 335-1 (1993). Durabilità del legno e dei prodotti a base di legno – Definizione delle classi di rischio di attacco biologico. Generalità.

UNI EN 335-2 (1993). Durabilità del legno e dei prodotti a base di legno – Definizione delle classi di rischio di attacco biologico. Applicazione al legno massiccio.

Wilson, EL. (1998). Three dimensional static and dynamic analysis of structures. *Computers & Structures Inc*., 1998. Berkeley, California (USA).

UNI EN 338 (1997). Legno strutturale. Classi di resistenza.

UNI EN 384 (1997). Legno strutturale. Determinazione dei valori caratteristici delle proprietà meccani-che e della massa volumica.

UNI EN 408 (2004). Strutture di legno. Legno massiccio e legno lamellare incollato. Determinazione di alcune proprietà fisiche e meccaniche.

UNI EN 518 (1997). Legno strutturale. Classificazione. Requisiti per le norme di classificazione a vista secondo la resistenza.

UNI EN 519 (1997). Legno strutturale. Classificazione. Requisiti per il legno classificato a macchina secondo la resistenza e per le macchine classificatrici.

UNI EN 12504 (2001). Prove sul calcestruzzo nelle strutture. Prove non distruttive. Determinazione dell'indice sclerometrico.

UNI ISO 3132 (1985). Legno. Determinazione della resistenza a compressione perpendicolare alla fibratura.

UNI ISO 3787 (1985). Legno. Metodi di prova. Determinazione della resistenza a compressione parallela alla fibratura.

Uzielli, L. (1992). Evaluation of timber elements bearing capacity. *L'Edilizia*. 12, 753-762.

Wood Handbook (1999). *Forest Service Agricultural Handbook*. U.S.D.A.